

https://dspace.org/

A spatial model to determine the location and extent of sodic sites in the Shingwedzi and Ripape river catchments of the Kruger National Park using remote sensing classification techniques and satellite imagery

Kleyn, Linda Gail

2012-02-01
http://hdl.handle.net/10539/11222

Downloaded from a DSpace repository. https://dspace.org/

A SPATIAL MODEL TO DETERMINE THE LOCATION AND EXTENT OF SODIC SITES IN THE SHINGWEDZI AND RIPAPE RIVER CATCHMENTS OF THE KRUGER NATIONAL PARK USING REMOTE SENSING CLASSIFICATION TECHNIQUES AND SATELLITE IMAGERY

Linda Gail Kleyn

A dissertation submitted to the Faculty of Science,
University of the Witwatersrand,
in partial fulfilment of the requirements for the degree of Master of Science

25 February 2011

DECLARATION

I declare that this dissertation is my own, unaided work. It is being submitted for the Degree of Master of Science in the University of the Witwatersrand, Johannesburg. It has not been submitted before for any degree or examination in any other University.



_____

Linda Gail Kleyn

8th of September 2011, Johannesburg, South Africa

Supervisor:
Dr Barend F N Erasmus

Committee:
Prof Mary Scholes
Prof Kevin Rogers
Prof Dave Mycock

ABSTRACT

Sodic soils are salt-affected soils which are high in sodium in relation to magnesium and calcium. Commonly called sodic sites in the Kruger National Park (KNP), these patches exhibit unique functional characteristics due to the high levels of sodium which cause surface crusting, cracking and the dispersion of clay particles. The aim of this study is to use satellite imagery to map sodic sites in the KNP at different spatial and spectral scales, giving the best option for a repeatable, semi-automated classification. The resultant map of sodic sites for the KNP will be used as a management tool and for future research projects.

A field test for sodicity was necessary to collect sufficient ground truth samples for robust accuracy assessment of the image classification. Sodic soils are identified by measuring EC, pH and SAR which are highly variable within site and between testing methods, and therefore not useful for rapid ground truth classification of sodic soils in the field. The sodium level at which clay particle dispersion takes place varies between soils, but is measurable in the field using the Emerson dispersion test. Laboratory tested sodic soil sites from previous research re-tested in this study showed positive results for dispersion of clay particles in water. The physical properties of sodic sites described in the literature and observed in the field were applied to classify sodic sites in the KNP in the field using a decision tree, together with results from the dispersion test and the observed presence of the grass species *Sporobolus iocladus*.

Landsat 7 and SPOT 5 imagery cover the whole park, with ASTER, CAO hyperspectral, LiDAR and black and white orthophotos available for selected areas. The topography elements of crest and footslope were derived from the STRM 90m digital elevation model (DEM). Image preprocessing to top of atmosphere reflectance was performed where necessary and visual enhancement techniques and transformations were applied to derive the normalised difference vegetation index (NDVI) and other indices. Spectral signatures were checked against spectral signature libraries, and the class separation was tested using the cluster analysis of spectral signatures. MODIS NDVI averages placed the imagery in phenological context.

Object-based image analysis using eCognition was applied to classify the sodic sites of the Shingwedzi and Ripape River catchments. The input imagery was segmented into

ecologically meaningful patches and classification accuracy was assessed using the field samples collected using the decision tree to identify four classes: sodic sites (bare and woody), river sand, riverine vegetation and savanna areas. Comparison of the accuracy assessments for the Shingwedzi study site showed that the Landsat 7 and SPOT 5 classification algorithms gave an overall kappa index accuracy of 89% and 78% respectively, and a sodic site kappa index of 90% and 89%. Validation results using the ground truth samples gave an overall kappa index accuracy of 61% for Landsat 7 and 52% for SPOT 5, with a sodic site kappa index of 49% and 39% respectively. The classification algorithms were applied to the Ripape study site for Landsat 7 and SPOT 5 with repeatable results for the SPOT 5 imagery of 88% overall kappa index and 81-93% kappa index for sodic sites using similar seasonal imagery in the wet to early dry season. The Landsat 7 classification algorithm was applied to the entire KNP based on the repeatability results of 56% overall kappa index and 60% sodic site kappa index for the Ripape site. The quest for a repeatable algorithm to classify sodic sites from satellite imagery has been met by the SPOT 5 imagery using scenes acquired at similar seasonal stages. The late wet season or early dry season imagery was used to apply the classification algorithm with the best success. Changes in size or shape of sodic sites over time requires very high resolution imagery and further studies to understand where the edge of sodic sites are detected from imagery, and how the phenology of the vegetation growing on these sites affects detecting any change in size of the sodic site.

ACKNOWLEDGEMENTS

If it had not been for a chance meeting between myself and Dr Rina Grant of Scientific Services in the Kruger National Park, I would not have been exposed to the fascinating world of sodic sites. Thanks Rina.

If it had not been for Dr Barend Erasmus's foresight to purchase exciting new software and his enthusiasm to see it being used, I would not have had the means to enter the world of digital numbers and come out with a usable product and career. Thanks Barend for your constant encouragement, enthusiasm and big picture vision. I could not have done any of this without your support.

If it had not been for Dr Izak Smit from Scientific Services in Kruger National Park, I would have not had access to the digital imagery used for this project and his enthusiasm for the possibilities of using remote sensing to classify sodic sites. Thanks Izak. And thanks to your team at the GIS Laboratory.

If it had not been for the Rangers from Scientific Services in the Kruger National Park who accompanied onto many sodic sites in the Shingwedzi region, I would not have been here to tell this tale. Thanks for keeping me safe from rampant young elephant bulls on exposed sodic sites.

If it had not been for Dr Francesca Parini, I would have not had got that first draft done while Barend was recuperating. Thanks Fran. And thanks to the students in the Lab who kept me young and enthusiastic.

If it had not been for Wolfgang Lück and Dr Melanie Lück-Vogel who ran a remote sensing course at CSIR Satellite Application Centre, I would not have had the tools to achieve the results of this work. Thanks Wolfgang and Melanie.

If it had not been for the support and patience of my family, I would not have had the space to achieve anything. Thanks Rick, Philippa and Megan. You can all stop asking: "Are you there yet?"

TABLE OF CONTENTS

LIST OF FIGURES viii
LIST OF TABLES xiii
LIST OF APPENDICES xv

CHAPTER 1: INTRODUCTION 1

1. PROBLEM STATEMENT 1

2. OBJECTIVES 3

3. LITERATURE REVIEW 3
3.1 Sodic soils and sodic sites 3
3.1.1 Distribution of salt-affected soils 3
3.1.2 Chemical properties of sodic soils 4
3.1.3 Physical properties of sodic soils 8
3.1.4 Development sequence of sodic soil formation 11
3.1.5 Erosion of sodic soils 12
3.1.6 Vegetation on saline and sodic soils 13
3.1.7 Sodic sites as nutrient hot spots 15
3.1.8 Sodic site area dynamics 17
3.2 Remote Sensing as a tool for mapping sodic sites 17
3.2.1 Properties of sodic sites detected in digital imagery: bare soils 20
3.2.2 Properties of sodic sites detected in digital imagery: vegetation 22
3.3 Ground truth samples and classification accuracy assessment 23
3.3.1 Sampling design 25
3.3.2 Response design (class selection) 27
3.3.3 Analysis (error matrix) 28
3.4 Image normalisation and pre-processing 30
3.4.1 Normalisation of input imagery 30
3.4.2 Spectral signatures 31
3.5 Classification 32
3.5.1 Visual Interpretation 32
3.5.2 Digital Image Analysis 33
3.5.3 Vegetation Indices 35
3.5.4 Image Transformations 39

4. STUDY SITE 39

CHAPTER 2: IDENTIFICATION OF SODIC SITES USING FIELD TESTS 41

1. INTRODUCTION 41

2. METHODS 44
2.1 Study Site 45

2.2 Data collection of ground truth sample sodic sites *46*
2.2.1 Geo-referenced laboratory tested sodic soils 46
2.2.2 Geo-referenced sodic sites visually assessed by previous researchers 46
2.2.3 Sample site selection for the current project 47
2.3 Aerial visibility of sodic sites *48*
2.4 Visible characteristics of sodicity in the field *48*
2.4.1 Bare soils 49
2.4.2 Vegetation identified on sodic sites 52
2.4.3 Herbivores on sodic sites 54
2.4.4 Visual Classification Sample Sites 54
2.5 Field tests for chemical and physical soil properties *55*
2.5.1 Soil chemistry 55
2.5.2 Soil physical properties 56
2.6 Analysis of results *58*

3. RESULTS 59
3.1 Aerial visibility *59*
3.2 Field tests: chemical and physical soil properties *61*
3.2.1 Electrical conductivity and pH 61
3.2.2 Turbidity, slaking and dispersion 63
3.3 Field tests: observation of visible characteristics of sodicity *68*

4. DISCUSSION AND CONCLUSION 72

CHAPTER 3: CLASSIFICATION OF SODIC SITES 75

1. INTRODUCTION 75

2. METHODS 77
2.1 Study site *78*
2.2 Data Input *78*
2.2.1 Satellite and Airborne Imagery 78
2.2.2 Image normalisation and pre-processing 82
2.2.3 Additional layers (derivatives and ancillary data) 83
2.3 Pre-classification imagery assessment *84*
2.3.1 Spectral signature investigation 84
2.3.2 Class separation 85
2.3.3 Seasonal context of imagery 85
2.4 Object-based image analysis (OBIA): Classification of sodic sites *86*
2.4.1 Class selection and decision tree outline for classification of sodic sites 87
2.4.2 Data input layers 88
2.4.3 Segmentation 89
2.4.4 Classification methodology 90
2.4.5 Accuracy assessment 91

3. RESULTS 93
3.1 Pre-classification imagery assessment *93*
3.1.1 Spectral signatures 93
3.1.2 Class separation 95
3.1.3 Seasonal context of imagery 100

3.3 Object-based classification *107*
3.3.1 Segmentation 107
3.3.2 Classification algorithm development for Shingwedzi training site 110
3.3.3 Shingwedzi study site classification algorithm applied to Ripape study site 124
3.3.4 CAO Hyperspectral and LiDAR imagery for sodic size change classification 129
3.3.5 Classification of KNP 132

4. DISCUSSION 133
4.1 Imagery selection *133*
4.1.1 Spatial resolution 133
4.1.2 Spectral signature separation 135
4.1.3 Geometric accuracy 135
4.1.4 Seasonal effects 135
4.2 Classifcation methods *137*
4.2.1 Object-based classification 137
4.2.2 Repeatable classification methodologies 140
4.3 Accuracy assessment *140*
4.4 Change detection *140*

5. CONCLUSION 141

CHAPTER 4: SPATIAL MODELLING OF SODIC SITES IN THE KRUGER NATIONAL PARK - CONCLUSION 143

1. THE SODIC TERMINOLOGY DEBATE 143

2. DECISION TREE DEVELOPED FOR IN FIELD IDENTIFICATION OF SODIC SITES 144

3. SODIC SITES AND HETEROGENEITY IN THE LANDSCAPE 144

4. DYNAMIC PROPERTIES OF SODIC SITE EXTENT 145

5. POSITION IN THE LANDSCAPE 146

6. INFLUENCE OF GEOLOGY ON CLASSIFICATION OF SODIC SITES 146

7. EROSION AND DEGRADATION OF SODIC SITES 147

8. GROUND TRUTH SAMPLING 147

9. ACCURACY ASSESSMENT 149

10. CLASSIFICATION RESULTS AND SODIC SITE VARIABLITY 150

11. FUTURE RESEARCH IDEAS 151

LIST OF FIGURES

Figure 1: Diagram illustrating the standard classification of normal, saline, saline-sodic and sodic soils in relation to soil pH, EC, SAR and ESP for Northern hemisphere soils based on plant reaction to salinity and sodicity (Brady and Weil, 2001). 6
Figure 2: Nine levels of salinity and sodicity based on levels of dispersion showing flocculated soils (very saline sodic or non-sodic soils), mechanically dispersive soils (saline non-sodic, sodic or very sodic soils) and spontaneously dispersive soils (non-saline non-sodic, sodic or very sodic soils) (Levy, 1999; Qadir and Schubert, 2002). 8
Figure 3: Example of an error matrix showing the difference between producers accuracy (how well the landscape can be mapped) and the users accuracy (how reliable the classification map is to the user) (Jenness and Wynne, 2007). 28
Figure 4: Typical spectral signatures of water, soil, dry and green grass for the visible and infra-red wavelengths (Sanderson, 2008). 32
Figure 5: Soil line concept demonstrating the observed linear relationship between red (R) and near-infra-red (NIR) reflectance or image intensity of bare soil. The soil line extends from darker soils with low R and NIR image intensity (Point A) to an upper region of bright soils with high R and NIR image intensity (Point B). Point C represents a pure vegetation pixel and Point D represents a partially vegetated pixel (Fox and Sabbagh, 2002). 38
Figure 6: The KNP study area showing the Shingwedzi River catchment study site and the Ripape River study site on the south western boundary. 40
Figure 7: All the known sodic sites recorded for the KNP by previous research projects. Square points indicate laboratory tested sodic soils. Circles indicate sodic sites that do not have published soil chemistry results and were identified through observation of visible sodic characteristics. 45
Figure 8: Decision tree for classification of sodic sites from other vegetation types based on the characteristics of sodic soils described in the literature. 50
Figure 9: Sodic site near Ripape River during the dry season after heavy utilisation by herbivores. 51
Figure 10: Sodic site near the Ripape River of the KNP during the wet season showing herbaceous cover prior to grazing by herbivores 52
Figure 11: *Sporobolus ioclados* (Pan dropseed) (van Oudtshoorn and van Wyk, 1999). 53
Figure 12: *Sporobolus nitens* (Curley-leaved dropseed) (van Oudtshoorn and van Wyk, 1999). 53
Figure 13: *Tragus berteronianus* (Carrot-seed grass) (van Oudtshoorn and van Wyk, 1999). 54
Figure 14: Sample sites in the Shingwedzi River catchment identified using the visual assessment decision tree 55
Figure 15: Estimating turbidity using spatula visibility showing non-sodic soil on the left, moderately sodic soil in the centre and strongly sodic soil on the right (Rengasamy and Bourne, 1997). 56
Figure 16: Example of a soil crust sample of the exposed B horizon used for the slaking and dispersion test. 57
Figure 17: Slaking of the soil crust sample with no dispersion (a) and slaking and dispersion showing the cloudy water surrounding the collapsed soil aggregate (b). 58

Figure 18: Aerial photograph taken during November 2006 showing the difference between sodic sites found on granite and basalt geologies and the variation in size, vegetation cover and relationship to rivers and drainage lines. 60
Figure 19: Electrical conductivity (EC) and pH values for sodic sites, savanna and riverine bush sample sites identified using the land cover decision tree for visual classification of sodic sites in KNP. 62
Figure 20: Examples of turbidity test results showing variation of results for 3 samples from the same sodic site and the difference between unstirred (a) and stirred (b) samples. The fourth test in (a) on the right was a combination of the 3 samples on the left. 63
Figure 21: Slaking and dispersion test results sorted by decreasing slaking..... 64
Figure 22: Slaking and dispersion test results sorted by decreasing dispersion..... 66
Figure 23: The result of the cluster analysis by geology and dispersion soil test only, giving good separation between sodic sites on granite from other classes and confusion between sodic sites and savannas on the basalts. 67
Figure 24: Percentage bare soil, woody and grass cover for both training and randomly selected sites to illustrate the importance of bare soil area as the initial criteria for defining a sodic site. 69
Figure 25: The result of the cluster analysis by geology, dispersion soil test, topography, bare soil percentage and the presence of *Sporobolus ioclados*, giving 6 major clusters. 71
Figure 26: Shingwedzi River catchment study site and Ripape River catchment study site showing available digital imagery coverage per site 79
Figure 27: Comparison of the different sensor spatial resolutions and bandwidths of digital imagery selected for the project (yellow, purple and turquoise represent the non-visible bands). The CAO hyperspectral imagery consists of 72 bands which fall within the ultra-violet, visible and near infra-red bands (Appendix VI for detailed band widths). 81
Figure 28: MODIS NDVI 250m imagery showing the SPOT 5 scene for the Shingwedzi study site area within the KNP boundary as a yellow polygon. The mean NDVI for this polygon over each 16-day composite for 9 years was used to calculate a phenology cycle graph. 86
Figure 29: Hierarchy of classes for image classification based on the vegetation cover and topographic location as applied in the classification algorithm work flow. 87
Figure 30: Example of the accuracy assessment produced by eCognition software showing the number of classified pixels per class and accuracy values. 92
Figure 31: Spectral profile for Landsat 7 ETM+ image (north KNP) dated 21 May 2001 plotted from 10 typical sample sites per class. 94
Figure 32: Spectral profile for SPOT 5 image (north KNP) dated 5 October 2005 plotted from 5 typical sample sites per class. 94
Figure 33: Unsupervised classification of Landsat 7 ETM+ north KNP image dated 21 May 2001 (a) based on 75 classes, grouped into 5 classes (b) using the average spectral signatures (c). 96
Figure 34: Unsupervised classification of Landsat 7 ETM+ southern KNP image dated 30 May 2001 (a) based on 75 classes, grouped into 5 classes (b) using the average spectral signatures (c). 97
Figure 35: Unsupervised classification of SPOT 5 northern KNP image dated 5 October 2005 (a) based on 75 classes, grouped into 5 classes (b) using the average spectral signatures (c). 98
Figure 36: Average spectral profile of the 75 classes determined by an unsupervised classification over all 72 bands using Erdas Imagine 9.2. Blue = sodic; Green = vegetation; Yellow = dry grassland; Brown = bare soil; Purple = shadow. 99

Figure 37: Class 75 (red) of the unsupervised classification image shown in grayscale using Erdas Imagine 9.2 Grouping Tool. 99
Figure 38: Classes 75 (red), 73 and 72 (turquoise) and 64 (blue), of the unsupervised classification of the hyperspectral imagery using Erdas Imagine 9.2 Grouping Tool. 100
Figure 39: Shingwedzi Study Site MODIS NDVI average for the area of KNP covered by each image over 9 years, depicting the acquisition date of each image as a vertical line. 102
Figure 40: Ripape Study Site MODIS NDVI average for the area of KNP covered by each image over 9 years, depicting the acquisition date of each image as a vertical line 103
Figure 41: Mean NDVI for each Landsat 7 ETM+ imagery polygon indicating the acquisition date of the Landsat 7 ETM+ images (solid vertical lines). 105
Figure 42: Mean NDVI for each SPOT 5 imagery polygon indicating the acquisition date of the SPOT5 images (solid vertical lines) and the anniversary date of the southern SPOT 5 106
Figure 43: Segmentation of Landsat 7 imagery using chessboard segmentation and the KNP Boundary thematic layer (a) and multispectral segmentation of the visible and infra-red bands at scale parameter of 10 (b), 5 (c) and 3 (d). 108
Figure 44: Segmentation of CAO hyperspectral imagery using multispectral segmentation of the visible and infra-red bands at scale parameter of 20 (a), 50 (b), 100 (c) and 200 (d). 109
Figure 45: SPOT 5 panchromatic imagery segmentation (a) overlayed on ASTER multi-spectral imagery for the same river bed showing the pixel misalignment due to a georeferencing shift of approximately 40m. 110
Figure 46: Summary of the classification algorithm work flow applied to all multi-spectral imagery at all study sites. 110
Figure 47: Geology (a) and topography classification (b) showing drainage lines as unclassified and crests as out of the area of interest (AOI) for the Shingwedzi study site using Landsat 7 imagery. 111
Figure 48: Landsat 7 ETM + (21 May 2001) false colour image (a) (RGB = Band 4:3:2) and classification (b) of the Shingwedzi study site showing the classes Water (blue), River Sand (yellow), Riverine vegetation (dark green), Savanna (light green) and Sodic sites (red) 112
Figure 49: Landsat 7 ETM+ (21 May 2001) classified sodic sites (red) showing the main Shingwedzi catchment rivers (blue) and tributaries (light blue). Area of sodic sites = 15.36 km^2 out of 1316.97 km^2 total area = 1.16 % cover. 113
Figure 50: SPOT 5 (5 October 2005) false colour image (a) (RGB = Band 4:3:2) and Classification (b) of the Shingwedzi study site showing four classes: River Sand (yellow), Riverine vegetation (dark green), Savanna (light green) and Sodic sites (red). 116
Figure 51: SPOT 5 (5 October 2005) classified sodic sites (red) showing the main Shingwedzi catchment rivers (blue) and tributaries (light blue). Area of sodic sites = 9.28 km^2 out of 1202.86 km^2 total area = 0.77 % cover. 117
Figure 52: SPOT 5 (12 April 2008) false colour image (a) (RGB = Band 4:3:2) and Classification (b) of the Shingwedzi study site showing four classes: Water (blue), River Sand (yellow), Riverine vegetation (dark green), Savanna (light green) and Sodic sites (red). 119
Figure 53: SPOT 5 (12 April 2008) classified sodic sites (green) showing the main Shingwedzi catchment rivers (blue) and tributaries (light blue). Area of sodic sites = 26.74 km^2 out of 935.85 km^2 total area = 2.86 % cover. 120
Figure 54: ASTER (29 June 2006) false colour image (a) (RGB = Band 4:3:2) and Classification (b) of the Shingwedzi study site showing four classes: River

Sand (yellow), Riverine vegetation (dark green), Savanna (light green) and Sodic sites (red).....121
Figure 55: ASTER (29 June 2006) classified sodic sites (red) showing the main Shingwedzi catchment rivers (blue) and tributaries (light blue). Area of sodic sites = 12.03 km^2 out of 1296.6 km^2 total area 0.93 % cover.....122
Figure 56: Landsat 7 ETM + (30 May 2001) false colour image (a) (RGB = Band 4:3:2) and Classification (b) of the Ripape study site showing four classes: River Sand (yellow), Riverine vegetation (dark green), Savanna (light green) and Sodic sites (red).....124
Figure 57: Landsat 7 ETM+ (30 May 2001) classified sodic sites (red) showing the Ripape catchment rivers and tributaries (blue). Area of sodic sites = 0.46 km^2 out of 100.12 km^2 total area = 0.46 % cover. 125
Figure 58: SPOT 5 (26 March 2006) false colour image (a) (RGB = Band 4:3:2) and Classification (b) of the Ripape study site showing four classes: River Sand (yellow), Riverine vegetation (dark green), Savanna (light green) and Sodic sites (red).....126
Figure 59: SPOT 5 (26 March 2006) classified sodic sites (green) showing the main Ripape catchment rivers (blue) and tributaries (light blue). Area of sodic sites = 1.44 km^2 out of 79.81 km^2 total area = 1.8 % cover.....126
Figure 60: SPOT 5 (12 May 2006**)** false colour image (a) (RGB = Band 4:3:2) and Classification (b) of the Ripape study site showing four classes: River Sand (yellow), Riverine vegetation (dark green), Savanna (light green) and Sodic sites (red).....127
Figure 61: SPOT 5 (12 May 2006) classified sodic sites (green) showing the main Ripape catchment rivers (blue) and tributaries (light blue). Area of sodic sites = 1.495 km2 out of 100.13 km2 total area = 1.49 % cover.....128
Figure 62: CAO Hyperspectral imagery (25 April 2008) false colour image (a) (RGB = Band 60:45:20) and classification of sodic sites (b) (turquoise) of a subset of the Ripape study site.....130
Figure 63: CAO Hyperspectral imagery (25 April 2008) classified by object heights from LiDAR imagery for a subset of the Ripape study site showing ground, grass, bush and tree heights and the sodic core area from the spectral signature clustering result (Class 75 = top blue signature of Figure 38).....131
Figure 64: Landsat 7 ETM+ (21 and 30 May 2001) classified sodic sites (black) for the area of the KNP covered by the two images (Path/row: 169/076 and 168/077).....132
Figure 65: Spatial resolution comparison between the Landsat 7 ETM+ 30m multi-spectral (21 May 2001) and SPOT 5 10m multi-spectral (12 April 2008) late wet season to early dry season object-based classification of sodic sites. 134
Figure 66: SPOT5 wet and dry season imagery for the Shingwedzi study site where the classification of sodic sites is an underestimation due to the difficulty in separating sodic sites from other bare soils in the dry season. The wet season classification of sodic sites gives a much higher percentage cover because there is less spectral confusion between bare soils. 136
Figure 67: Comparison between the Landsat 7 (21 May 2001) object-based classification and the pixel-based classification of Matthys and Wessels (2001).....138
Figure 68: Comparison between the SPOT 5 (12 April 2008) object-based classification and the pixel-based classification of Matthys and Wessels (2001).....139
Figure 69: Time line of the Landsat missions showing the currently operational Landsat 5 and 7 satellites and the planned Landsat Data Continuity Mission (LDCM) to be launched in 2012.....161

Figure 70: The new Landsat LDCM satellite's OLI sensor bands compared to Landsat 7 bands created by L.Rocchio and J.Barsi 162
Figure 71: Comparison of Spectral Bands between ASTER and Landsat 7 ETM+ showing percentage reflectance per wavelength. 164
Figure 72: Spectral sensitivities for the four multi-spectral and panchormaitc bands for SPOT 5 166

LIST OF TABLES

Table 1: Slaking and dispersion classes for the Emerson Aggregate test 9
Table 2: Spontaneous dispersion classes (Vance, McKenzie and Tisdall, 2002). 10
Table 3: Number of sample sites collated and collected by the current project for the Shingwedzi study site, showing the tests applied, the geology of each site and sampling method used. 47
Table 4: Summary of acquisition dates for satellite and airborne imagery available for the Shingwedzi and Ripape River catchment study sites, and full KNP coverage. 82
Table 5: Spectral signature descriptions based on the relative value of reflectance values for each band (adapted from Baraldi *et al*., 2006) 84
Table 6: Input imagery and themeatic layers for processing in eCogntion (Definiens Version 5) software. 89
Table 7: Summary of satellite and airborne imagery available for the Shingwedzi River and Ripape River catchment study sites showing acquisition dates and seasonal context..... 101
Table 8: Results of the multi-spectral satellite imagery segmentation parameter selection for Landsat 7, ASTER, SPOT 5 and CAO hyperspectral imagery. 107
Table 9: Error matrix of random visually assessed samples (reference class) compared to the classification result (user class) for the Shingwedzi study site based on number of pixels. 114
Table 10: Error matrix of ground truth samples (reference class) compared to the classification result (user class) for the Shingwedzi study site based on pixel numbers. 114
Table 11: Error matrix of random visually assessed samples (reference class) compared to the classification result (user class) for the Shingwedzi study site based on pixel numbers..... 117
Table 12: Error matrix of ground truth samples (reference class) compared to the classification result (user class) for the Shingwedzi study site based on pixel numbers. 118
Table 13: Error matrix of random visually assessed samples (reference class) compared to the classification result (user class) for the Shingwedzi study site based on pixel numbers. 120
Table 14: Error matrix of ground truth samples (reference class) compared to the classification result (user class) for the Shingwedzi study site based on pixel numbers. 120
Table 15: Error matrix of random visually assessed samples (reference class) compared to the classification result (user class) for the Shingwedzi study site based on pixel numbers..... 122
Table 16: Error matrix of random ground truth samples (reference class) compared to the classification result (user class) for the Shingwedzi study site based on pixel numbers. 122
Table 17: Summary of accuracy assessment results for all imagery classification algorithms for the Shingwedzi study site where the first value is for random visually assessed samples and the value in bold is based on the stratified random ground truth data. 123
Table 18: Error matrix of ground truth samples (reference class) compared to the classification result (user class) for the Ripape study site based on pixel numbers. 125

Table 19: Error matrix of ground truth samples (reference class) compared to the classification result (user class) for the Ripape study site based on pixel numbers. 127
Table 20: Error matrix of ground truth samples (reference class) compared to the classification result (user class) for the Ripape study site based on pixel numbers. 127
Table 21: Summary of accuracy assessment results for Landsat 7 and SPOT 5 imagery classification algorithms developed on the Shingwedzi study site and applied to the Ripape study site for random visually assessed samples 129
Table 22: Landsat 7 ETM+ bands and band widths 162
Table 23: ASTER band and band widths 165
Table 24: Spectral Bands and band widths for SPOT 5 satellite imagery 167
Table 25: The CAO Alpha System design specifications (Asner *et al*., 2007) 168
Table 26: Spectral bands and band widths for CAO Hyperspectral data giving Landsat equivalent names for common wavelegths for comparison. 169
Table 27: Gain coefficients for ASTER images (Thorne, Biffar and Takashima, 1999) 173
Table 28: Landsat ESUN values for the conversion from spectral radiance to reflectance (Chander and Markham, 2003) 174
Table 29: ASTER ESUN values for the conversion from spectral radiance to reflectance (Smith) 174
Table 30: SPOT 5 ESUN values for the conversion from spectral radiance to reflectance 175

LIST OF APPENDICES

APPENDIX I: Published laboratory chemical analyses of sodic soils in the Shingwedzi and Ripape River catchments of the KNP 160
APPENDIX II: Landsat 7 ETM+ 161
APPENDIX III: Advanced Airborne Thermal Emission and Reflections Radiometer (ASTER) 164
APPENDIX IV: SPOT 5 166
APPENDIX V: Carnegie Airborne Observatory (CAO) Hyperspectral images and waveform LiDAR data 168
APPENDIX VI: Orthorectified aerial photographs 170
APPENDIX VII: Shuttle Radar Topography Mission (SRTM) 90 m digital elevation model (DEM) 170
APPENDIX VIII: Moderate Resolution Imaging Spectroradiometer (MODIS) 170
APPENDIX IX: Radiometric normalisation: pre-processing methods for conversion from DN to reflectance values for Landsat 7 ETM+, ASTER and SPOT 5 imagery. 171
APPENDIX X: Classification algorithm process tree for object-based image analysis of Landsat 7 and SPOT 5 imagery using eCongnition (Definiens Professional V 5). 176

CHAPTER 1

INTRODUCTION

1. PROBLEM STATEMENT

Approximately 32% of South Africa's surface area is covered by salt-affected soils derived through soil pedogenesis, and most of these soils are saline-sodic (deVilliers, Nell, Barnard and Henning, 2003). The salt-affected soils of the Kruger National Park (KNP) form distinct patches in the landscape, visible as bare soil areas with restricted vegetation cover, at the foot of a slope or catena (Dye and Walker, 1980).

Sodic soils are salt-affected soils which are high in sodium in relation to magnesium and calcium (Qadir and Schubert, 2002). The high levels of sodium cause surface crusting, cracking and the dispersion of clay particles (Emerson, 1967). Commonly called sodic sites in the KNP, these salt-affected patches exhibit unique functional characteristics which will be used to produce a functional, rather than chemical definition of sodic sites for identification in the field.

Grant and Scholes (2006) found that sodic sites are nutrient hot spots with higher quality forage than the surrounding hill crests. In the KNP these areas are considered key resource areas for herbivores and in spite of their small size, make a disproportionately important contribution to the available high quality forage. The presence of sodic sites may affect seasonal animal movement patterns in an enclosed, managed ecosystem such as the KNP, and may also determine the number of animals that can be supported (Grant and Scholes, 2006). The KNP collects census data of animal numbers and location, but does not have information on the location, extent or changes in size of salt-affected patches or sodic sites.

The dispersion of the clay particles of sodic soils are seen as erosion and degradation. Chappell (1992) recorded the erosion of sodic sites in the Ripape River catchment and an

accurate map of the location and extent of these patches will be a useful management tool.

The park is approximately 2 million hectares in extent, so remote sensing is the only practical option to map sodic areas for the whole park. Sodic sites are visible on black and white aerial photographs as light grey areas near rivers and hence, aerial photographs have been used to measure the possible increase or decrease in sodic site size over time on selected sample sites (Chappell, 1992; Khomo and Rogers, 2005).

Previous classification of sodic sites in the Shingwedzi River catchment applied pixel-based classification to medium resolution Landsat 7 ETM+ imagery (Mathys and Wessels, 2001). The major shortcoming of pixel-based classification methods is that the pixels are not seen as an ecologically representative object and cannot be placed in context of the surrounding environment using spatial relationships or topology. This study will consider object-based image analysis (de Kok, 2006; Hajek, 2006) for more accurate classification of Landsat 7 ETM+, ASTER and SPOT 5 imagery using repeatable, statistically robust sampling and classification methods (Foody, 2002).

The aim of this study is to use satellite imagery to map salt-affected bare soil patches in the KNP at different spatial and spectral scales, giving the best option for a repeatable, semi-automated classification. In order to accurately validate the classification, many sample sodic sites must be identified in the field, based on sites of known soil chemistry. A field test for sodicity is necessary to collect sufficient ground truth samples for robust accuracy assessment. The resultant map of sodic sites for the KNP will be used as a management tool and for future research projects.

The functional characteristics of sodic soils are investigated in Chapter 1. The methods chapters are divided into two sections: the identification of sodic sites in the field (Chapter 2) followed by the object-based classification methods applied to digital imagery to classify sodic sites (Chapter 3). The link between the two chapters is the accuracy assessment of the classification where the ground truth samples from Chapter 2 are used to validate the image classification methods in Chapter 3. The resultant maps of sodic sites are validated using the ground truth samples to assess the best method for a repeatable, semi-automated classification of sodic sites for KNP. Chapter 4 concludes with the impact of the spatial modelling of sodic sites on management and spatial

relationships of sodic sites in the landscape at different scales based on the results of sodic site classification.

A working understanding of the principles and application of remote sensing techniques is assumed for this study and further background information can be obtained from remote sensing text books and publications (Campbell, 2002; Lillesand, Kiefer and Chipman, 2004; Jensen, 2006).

2. OBJECTIVES

2.1 Develop and apply a rapid assessment field method to test for sodic soils, and to develop a functional definition of sodic sites for identification in the KNP based on visual characteristics of sodic soils rather than the chemistry of sodic soils.

2.2 Produce a validated map of the sodic sites in the Kruger National Park using this functional definition of sodic sites from digital imagery at different resolutions and spectral band widths through the application of object-based classification and image analysis algorithms.

2.3 Compare the accuracies of predicting sodic sites using different spatial resolutions, band widths, scales and additional datasets, for semi-automated and repeatable methodologies, and to relate the results to the spatial relationships between sodic sites and the surrounding landscape at different scales.

3. LITERATURE REVIEW

3.1 Sodic soils and sodic sites

3.1.1 Distribution of salt-affected soils

Salt-affected soils are a worldwide phenomenon covering 380-995 Mha (7%) of the Earth's surface (Bui, Krogh, Lavado, Nachtergaele, Toth and Ftizpatrick, 1998; Yu and Meixner, 2007) and are divided into two categories. Saline soils are high in neutral soluble salts, which adversely affect plant growth, while sodic soils have a high sodium concentration, which causes alkali hydrolysis, and are often termed 'alkali soils' (Abrol, Yadav and Massoud, 1988). Saline-sodic soils have both a high level of all salts and high

concentration of sodium. These soil chemistry definitions are described in detail in Section 3.1.2.

The soil structure of sodic soils is affected due to the high concentrations of sodium in relation to magnesium and calcium, which indirectly affects plant growth through the development of an impervious layer. Sodic soils are found where the climate shows great seasonal variance, as occurs in arid to semi-arid regions (Bui *et al*., 1998) . Of the salt-affected soils worldwide, 62% are saline-sodic or sodic (Yu and Meixner, 2007). Approximately 32% of South Africa's surface area is covered by salt-affected soils derived through soil pedogenesis (de Villiers *et al*., 2003).

Secondary salinisation, due to human intervention (irrigation), is common in Australia and other arid or semi-arid countries where the use of saline irrigation water increases the levels of salts in the soil (Pannell and Ewing, 2004). Secondary sodicity occurs when irrigation water is high in sodium (Qadir and Schubert, 2002) . There is no evidence of secondary sodicity in South Africa (de Villiers *et al*., 2003). The sodic soils found in South Africa are largely derived through natural pedogenesis from sodium rich parent material and fall into the saline-sodic category. The KNP geology is dominated by igneous rock including rhyolite, granite, basalts and gabbros (Venter, Scholes and Eckhardt, 2003). The granite and rhyolite parent material is higher in sodium, potassium and aluminium than the basalts and gabbros (Pidwirny, 2006).

Sodic soils have been investigated in the Nylsvley Nature Reserve in Limpopo province (Scholes and Walker, 1993) and in the KNP in the Mpumalanga province of South Africa (Barichievy, 2005; Chappell, 1992; Khomo and Rogers, 2005; Levick, 2008; Saah, 2004; Teren, 2004; Venter, 1990). Sodicity affects soils in other southern African countries and has been documented in Botswana (McCarthy and Ellery, 1994) and Zimbabwe (Dye and Walker, 1980). The majority of these studies have been soil chemistry investigations on a limited number of sodic soil sites at the footslope of a catena.

3.1.2 Chemical properties of sodic soils

Saline soils are high in soluble salts such as calcium, magnesium and potassium and therefore have a high cation exchange capacity (CEC), whereas sodic soils are high in sodium relative to the other divalent salts calcium and magnesium (Qadir and Schubert, 2002). The surfaces of clay particles in saline or sodic soils are negatively charged, and

are neutralized by exchangeable cations including calcium (Ca^{2+}), magnesium (Mg^{2+}), sodium (Na^{+}) and potassium (K^{+}). The CEC is the total negative electric charge per mass of soil and is measured in a laboratory based on calcium (Ca^{2+}), magnesium (Mg^{2+}), sodium (Na^{+}), potassium (K^{+}) hydrogen (H^{+}) and aluminium (Al^{3+}) concentrations (van de Graaff and Patterson, 2001).

Soil salinity is measured by the electrical conductivity (EC) expressed as deciSiemans per metre (dS/m) where 1 dS/m = 1 mS/cm = 1000 μS/cm (van de Graaff and Patterson, 2001). A soil saturated paste is the standard laboratory preparation method used to measure soil salinity and is expressed as the saturated extract equivalent (EC_{se} or $EC_{e)}$. Water is removed from a saturated soil sample using a centrifuge and the EC is measured. Most levels of EC expressed in tables and figures use the $EC_{se.}$ Soil suspension methods used to estimate EC include a 1:1 soil-water ratio paste extract (Zhang, Schroder, Pittman, Wang and Payton, 2005), a 1:1 or 1:5 soil-water solution or suspension expressed as $EC_{1:1}$ and $EC_{1:5}$ respectively. $EC_{1:1}$ measured using a 1:1 soil-water suspension is converted to the saturated extract equivalent (EC_{se}) readings by multiplying by a conversion factor of 2.2 (Dobermann and Fairhurst, 2008), but the factor is dependant on the clay percentage of the soil. All EC readings should be converted to this standard version for comparison, and EC values are meaningless if the methods used are not reported (van de Graaff and Patterson, 2001). Field tests are normally done using the soil suspension method and laboratory analyses use the saturated paste extracts.

Levels of salinity for water and their effects on plants are different to levels of soil salinity, and the different terminology and EC cut-off values may lead to confusion. The readings obtained when measuring EC from a soil sample are affected by the method used to prepare the soil sample and the interpretation of salinity measures is complicated by the variability within sample sites, seasonal effects of rainfall and the soil type (sand, loam or clay). Representative soil samples are required and the methods used to determine EC must be carefully recorded.

The sodicity of the soil is measured by the Exchangeable Sodium Percentage (ESP), which is the percentage of Na^{+} relative to the Cation Exchange Capacity (CEC), or the Sodium Adsorption Ratio (SAR) which is expressed as a ratio of Na^{+} to the presence of $Ca^{2+}$and Mg^{2+} as follows:

$$SAR = Na^{+} / [(Ca^{2+} + Mg^{2+}) / 2]^{0.5} \quad [1]$$

Both EC and SAR are measured using a soil saturated paste (Abrol, Yadav, and Massoud, 1988). These laboratory analyses may overestimate levels of available sodium and the true electrical conductivity (Qadir and Schubert, 2002) as the formula assumes that calcium and magnesium occur in equal proportions.

Soils are spatially heterogeneous and samples taken from the same sites give highly variable results. Teren (2004) found that sodic sites in the KNP had lower levels of sodium in the soils under trees (average SAR = 2.41 mmol/l and EC = 1.6 dS/m) than the surrounding bare patches (average SAR = 34.24mmol/l and EC = 9.3 dS/m), and that the levels of sodicity varied within the bare areas. Sodicity did not decrease from the centre to the edge of the sodic site as expected, but was heterogeneous within the sodic site (Qadir and Schubert, 2002). In the Northern hemisphere, a soil is considered to be sodic when the EC is lower than 4 dS/m, the ESP value is higher than 15 or the SAR value is over 13, and the pH is above 8.5 (Brady and Weil, 2001) as illustrated in Figure 1.

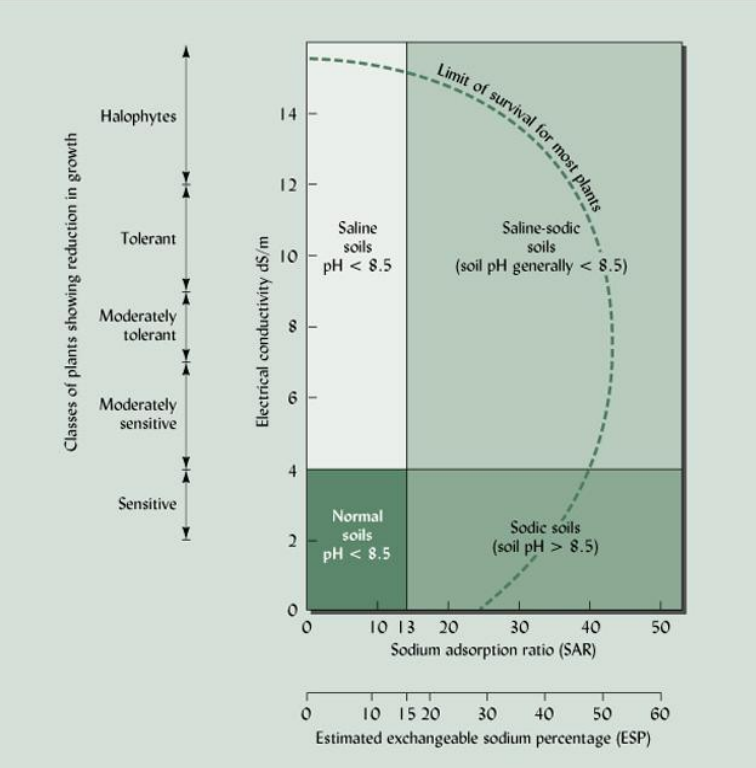


Figure 1: Diagram illustrating the standard classification of normal, saline, saline-sodic and sodic soils in relation to soil pH, EC, SAR and ESP for Northern hemisphere soils based on plant reaction to salinity and sodicity (Brady and Weil, 2001).

Soils with an EC over 4 dS/m and a pH less than 8.5 are considered saline-sodic. Soil pH is the measure of hydrogen ion concentration in solution and is expressed as an acidity or alkalinity level (Slattery, Conyers and Aitken, 1999). The pH ranges for soils are between 3.4 and 10, with a range from 5 to 7 common in humid regions and 6.5 to 9 in arid regions. pH is a good indicator of soil chemical properties and is easily measured in the field using an air-dried soil to water ratio of 1:1 and a hand-held pH meter. Low pH levels (below a pH of 5) affect plant growth due to nutrient imbalances and high pH levels of over 8 indicate the presence of sodium and magnesium and the resultant effects of clay dispersion on plant growth (Qadir and Schubert, 2002). Most sodic soils have a pH over 7, except in cases where aluminium (Al^{3+}) is present where the pH is less than 6.

The cut-off level of 4 dS/m for electrical conductivity is linked to the level of salinity at which crops are affected and not to the level at which the physical properties of soil degrade or disperse (Qadir and Schubert, 2002). However, there is no unanimous definition of the dispersion potential of a sodic soil based on pH, ESP or SAR, and EC (Levy, 1999; Qadir and Schubert, 2002). Dispersion is a characterisitic of high sodium in the soil and is discussed in more detail later in this chapter. Australian soils have been found to disperse at an ESP of 6 (Quirk, 2001), which is used as a cut-off for sodic versus non-sodic soils in that country, lower than the northern hemisphere standard ESP cut-off of 15. A proposal that sodicity be divided into three levels: ESP < 6 = non-sodic, ESP 6-15 = sodic, ESP > 15 = very sodic is based on the dispersive or flocculated character of illite type soils (Levy, 1999; Qadir and Schubert, 2002). The three sodicity levels are combined with three salinity levels: non-saline (0-4 dS/m), saline (4-8 dS/m) and very saline (>8 dS/m), giving nine categories (Figure 2). This shows that different soil types and climatic conditions will affect the cut-off levels to define a sodic soil.

South Africa uses the standard definition for sodic soils as EC < 4dS/m, ESP > 15 and pH > 8.5 (Figure 1), but divides saline-sodic soils into two groups: alkaline saline-sodic if pH > 8.5 and non-alkaline saline-sodic when pH < 8.5 (de Villiers *et al*. 2003). Chappell (1992) found low SAR values in the soils in the Ripape River catchment area of the Kruger National Park and concluded that it was the presence of dispersed clay that affected permeability rather than the sodium ion concentration. This conclusion is probably based on the classical levels of sodium used to define sodic soils in the literature

at the time, and indicates that measuring the sodium ion concentration level does not show when clay dispersion will take place.

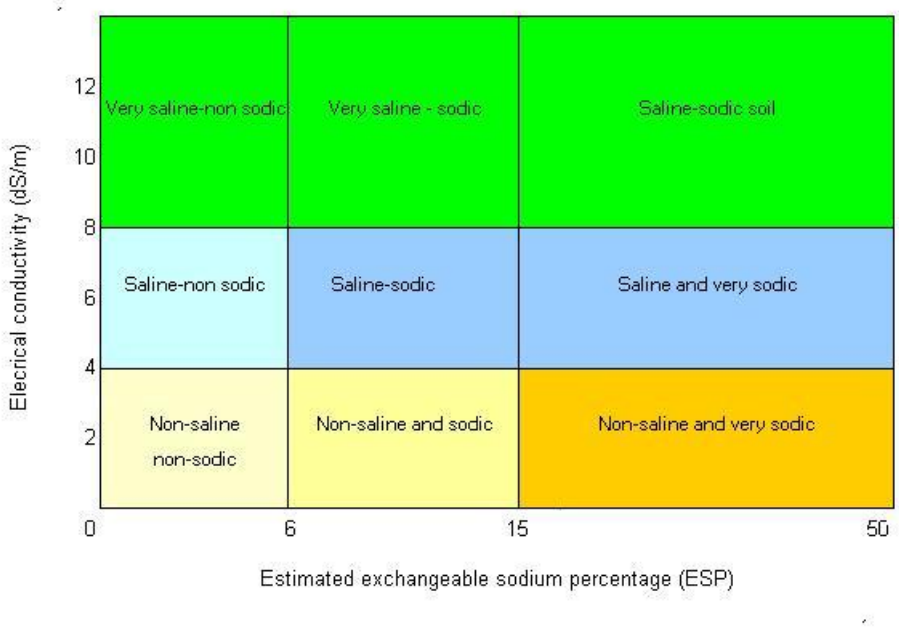


Figure 2: Nine levels of salinity and sodicity based on levels of dispersion showing flocculated soils (very saline sodic or non-sodic soils), mechanically dispersive soils (saline non-sodic, sodic or very sodic soils) and spontaneously dispersive soils (non-saline non-sodic, sodic or very sodic soils) (Levy, 1999; Qadir and Schubert, 2002).

3.1.3 Physical properties of sodic soils

The chemical composition of sodic soils causes changes in structural properties due to physical processes. Clay particles swell, separate (disperse or deflocculate) and become suspended in water, in the presence of high sodium levels (Vance, McKenzie and Tisdall, 2002).

The deflocculation of clay particles occurs when sodium cations are adsorbed by the clay platelets causing swelling and dispersion, and is more pronounced at a higher pH (McBride, 1999). Deflocculated clay particles in the soil give rise to a decreased permeability and hydraulic conductivity of the soil typical of the B-horizon of sodic soils. An increased SAR, and resulting deflocculated clay particles, creates an impermeable soil layer and increases runoff (Leske and Buckley, 2003). Therefore, sodic soils show physical properties of crusting, cracking and water logging (restricted water infiltration) which adversely affects plant growth (Mills and Fey, 2004). These areas are easily

identified in the KNP as bare patches with little to no vegetation cover for most of the year.

Slaking occurs where soil macro-aggregates are broken down to micro-aggregates when exposed to moisture. The loss of soil structure contributes to hard setting or crusting of the small particles on the surface upon subsequent drying. Crusting of the top layer of the soil and cracking and swelling is visible. The lateral movement of water below the crust, through the B-horizon, causes tunnelling or piping which eventually collapses and forms gulley erosion (Chappell, 1992; Barre, Biggs and Sharp, 2004; Raine and Loch, 2003).

As there is no single sodium level applicable to all soils at which dispersion occurs, the Emerson dispersion test was devised to determine dispersion potential (Emerson, 1967). This is a measure of when sodic soils exhibit sodic behaviour. Dispersion of clay particles can therefore be used as a measure of sodicity in the soil as a substitute for laboratory analyses for SAR or ESP, as not all soils that exhibit physical sodic soil behaviour fit the sodic soil chemical specifications and thresholds (Levy, 1999). Emerson (1967) devised a simple field test to classify soil aggregates based on their coherence in water. Air-dried aggregates were immersed in water and classified according to the time it took for macro-aggregates to collapse into micro-aggregates (slaking) and for clay particles to be dispersed into the water which became turbid. Wet, remoulded aggregates and the suspension of aggregates in water were also used to test for slaking and dispersion. The Emerson Aggregate test distinguishes eight aggregate classes using the three techniques described above and depicted in Table 1.

Table 1: Slaking and dispersion classes for the Emerson Aggregate test

Class	**Slaking Result**	**Dispersion Result**
1	Slakes	Complete Dispersion
2	Slakes	Some Dispersion
3	Slakes	Some Dispersion after remoulding
4	Slakes	No Dispersion (Carbonate or Gypsum present)
5	Slakes	Dispersion in shaken suspension
6	Slakes	Flocculates in shaken suspension
7	No slaking	Swells in water
8	No slaking	Does not swell

The dispersion test described by Emerson (1967) has been modified and adopted to test the relationship between chemical test for sodicity and dispersion classes (Vance, McKenzie and Tisdall, 2002). Small, 1 cm sized, air-dried aggregates are gently immersed in rainwater (saline water is unsuitable) with the soil crust uppermost after immersion, and observed for over 1 minute. The categories applied are illustrated in Table 2 .

Table 2: Spontaneous dispersion classes (Vance, McKenzie and Tisdall, 2002).

Observed behaviour	*Class*	*Observed behaviour*
Not applicable	0	Clear water
Very slight	1	Discoloured water or a thin clay particle cloud present around the soil
Slight	2	A thin line of clay particles begin to accumulated around the edge of aggregate
Moderate	3	A thick line of clay particles begin to accumulated around the edge of aggregate
Severe	4	Whole fragment covered with clay particles

An alternative field test for sodicity is based on the turbidity of the water from a 1:5 soil to water suspension (Rengasamy and Bourne, 1997). 500 ml of water is gently poured into a bottle containing 100g of soil without disturbing the soil. The lid is placed on the bottle which is then gently inverted and returned to its original position to stand for 4 hours undisturbed. The level of sodicity is measured by the cloudiness of the water. Clear or almost clear water is non sodic, partly cloudy water is medium sodicity and very cloudy or opaque water indicates high sodicity The turbidity in the water is due to the dispersion of clays caused by high sodium levels in the soil.

The hydraulic conductivity of the soil is affected by the total of soluble salts in the soil and the salts present in the irrigation or rain water. In semi-arid environments, the effect of high levels of sodium in the soil on hydraulic conductivity is higher with rain water, which has a low EC, than it would be with saline irrigation water (Levy, 1999). Sodic soils in natural environments are therefore more susceptible to clay dispersion and loss of permeability in the soil due to the low EC of rain water.

The soil texture influences the effect of sodium on the soil structure (Rengasamy and Bourne, 1997). Texture describes the proportion of sand, silt and clay in the soil. High

clay soils are more susceptible to sodicity and subsequent dispersion of clays due to the forces of adhesion between the clay particles retaining water and nutrients. The standard ribbon test for texture involves making a ball of soil and water in the palm of the hand up to field capacity and rolling this into a ribbon. The texture classes depend on the feel of the soil when wet and how long the ribbon holds before breaking (Tongway and Hindley, 2005).

3.1.4 Development sequence of sodic soil formation

The theories describing the origins of sodic soils in the landscape are still widely debated and the classical catenal theories do not apply to all sodic soil formation worldwide (Bui *et al*., 1998). Sodium concentrations may increase due to the evapotranspiration of salts by vegetation or due to deposition as sedimentary soil during flooding.

Sodic soils are commonly found on the footslopes of the catena where parent-material contains a high concentration of sodium, such as granite and basalt. Salts leached from the upper slopes of the catena, accumulate in the lower slopes, where they concentrate in the soils (Chappell, 1992; Dye and Walker, 1980; Khomo and Rogers, 2005). The accumulation of salts at the footslope, known as the classical or catenal model of sodic soil formation, is dependant on the presence of water in the form of a perched water table or shallow groundwater rich in salts, low slope gradients and the weathering of sodium rich minerals, such as albite, as a source of sodium (Bui *et al*., 1998). Sodic soils occur at the riparian-upland boundary of the riparian zones in the Kruger National Park (Khomo and Rogers, 2005), on footslopes near rivers (Dye and Walker, 1980) and occasionally on seeplines (Jacobs, Bechtold, Biggs, Grimm, Lorentz, McClain, Naiman, Perikas, Pinay and Scholes, 2007). Sodic soils have been described by Dye and Walker (1980) in Zimbabwe where plant communities adapted to shallow A-horizons and impermeable B-horizons, were identified.

The evapotranspirational model for the origin of sodic soils was described in the Okavango Delta in Botswana, where it was shown that sodic islands developed due to a shallow ground water table and the evapotranspiration of salts by the vegetation to create high levels of sodium in the soils (McCarthy and Ellery, 1994). Khomo and Rogers (2005) suggest that both the catenal and evapotranspirational models may play a part in the formation of sodic sites in the KNP due to the encroachment of sodic sites towards the riparian zone (down hill) and the upland areas respectively, over a 50 year period. In the

Nylsvley Wetland Reserve (Scholes and Walker, 1993), sodic soils are associated with a high water table due to the seasonal flooding of the wetland, and are susceptible to erosion due to the duplex nature of the soils.

Sediment deposited due to flooding may also contribute to the level of salts and nutrients on sodic sites (Jacobs *et al*., 2007) and may replace the eroded A-horizon and encourage vegetation cover, especially grasses.

Despite the debate on how these soils originate, it appears that topography, suitable parent material and variable water dynamics are the primary requirements for the development of sodic soils which form sodic sites in the landscape. The origin of each sodic site may be a combination of the catenal, transpirational and sedimentation theories depending on the topographic position in the landscape.

3.1.5 Erosion of sodic soils

Sodic soils are susceptible to erosion due to their chemical make-up which causes physical and structural weaknesses. These are high clay, duplex soils with an impervious B-horizon which gives rise to a perched water table (Raine and Loch, 2003). The shallow A-horizon is easily eroded, exposing the underlying B-layer. Lateral movement of water causes sub-surface tunnelling and eventual collapse of the B-horizon (Chappell, 1992). This high erosion risk has prompted the need for these sites to be included in a monitoring program to detect degradation changes. Sodic sites are considered degraded when the B-horizon soil is lost due to erosion, and the potential for vegetation to grow on the site is lost.

The erosion of the A-horizon was originally thought to be due to a loss of grass cover and sheet erosion during the heavy storms of the early summer rains. However, Chappell (1992) found that most water movement was shown to occur below the surface. According to Chappell (1992), sheet erosion may be responsible for erosion of the unprotected A-horizon, but it appears that the chemical and structural composition of the soil, which restricts plant growth, contributes more to bare patch formation than water run-off.

Concern was raised regarding the installation of artificial watering points near to these fragile soils in the KNP, and adjoining private parks, which would in turn attract greater

numbers of animals and increase the potential for erosion of sodic soils (Chappell, 1992). Management of animal numbers and position of artificial waterholes and roads may be enough to keep these fragile sodic sites in a relatively stable state.

Bare soils are linked with degradation when they coincide with a loss of vegetation cover, and therefore a loss of functionality or health (Tongway and Hindley, 2005). However, sodic soils are not necessarily less functional or unhealthy as the sodic soils in the KNP have high quality biomass production and are heavily utilised by herbivores (Grant and Scholes, 2006). The degraded image of sodic soils may be due to the literature published in agriculture and the building industry. In agricultural environments, saline and sodic soils negatively affect crop growth and these soils are therefore described as degraded in terms of the requirements for agriculture. In the building industry sodic soils are defined as degraded due to their loss of structure and potential to erode. The link between sodic soils and degradation should not be assumed in the natural environment, unless there is evidence of B-horizon erosion.

3.1.6 Vegetation on saline and sodic soils

Plant growth is stunted by soils that are high in salts with a high electrical conductivity due to the osmotic effects which limit water uptake, which causes plant nutrient imbalances (Qadir and Schubert, 2002). A high pH also affects the availability of essential plant nutrients such as calcium and magnesium (Abrol, Yadav and Massoud 1988). Halophytes are plants which are adapted to thrive in high salt or arid conditions. In sodic soils, plant growth is also stunted by the physical structure of deflocculated clay in the B-horizon, caused by the high level of exchangeable sodium (Dye and Walker, 1980). In saline-sodic soils both the presence of salts and high concentrations of sodium will give rise to halophytic plants as well as those adapted to the adverse conditions created by the physical structure of the sodic soil.

Three dominant tree species were observed by Dye and Walker (1980) on sodic soils on the footslopes throughout the sodium geologies in Zimbabwe: *Colophospermum mopane, Acacia gerarrdii* and *Acacia mellifera*. Although these trees are not found exclusively on sodic soils, they formed large groups, while the remaining species were found as isolated individuals. Mopane has a shallow root system and has the ability to adapt to the lack of water easily available in sodic soils, but will be stunted due to the shallow A-horizon (Dye and Walker, 1980). Different plant communities were observed from the crests to

the footslopes, which linked the variation in woody plant species to soil characteristics and the catenal theory of the origins of sodic soils in Zimbabwe.

In the Kruger National Park, tree species identified on footslopes of granitic based soils where duplex clays occur include *Euclea divinorum*, *Spirostachys africana*, *Acacia welwitschii*, *Acacia grandicornuta*, *Papea capensis* and *Terminalia prunioides* (Venter, Scholes and Eckhardt, 2003). *Colophospermum mopane* and *Salvadora australis* commonly occur in the dry granitic sodic soils of the northern KNP (Teren, 2004). Again, these tree species do not occur exclusively on sodic soils, but sodic sites are identified more accurately using the presence or absence of groups of these woody species.

Grass species commonly found growing on sodic soils include *Sporobolus nitens*, *Sporobolus ioclados*, *Tragus berteronianus* and *Dactyloctenium aegyptium* (Venter, Scholes and Eckhardt, 2003) which are short, creeping lawn grasses with relatively low biomass production. *Tragus berteronianus* is commonly found in disturbed areas and is one of the first grasses to grow in hard or compacted soils (van Oudtshoorn and van Wyk, 1999). Khomo and Rogers (2005) found *Tragus berteronianus* to be the most common grass species on sodic sites on the Phugwane River in the northern KNP, with other species including *Eragrostis trichophora*, *Eragrostis pallens* and *Bothriochloa bladhii* (Khomo, 2003). Siebert, Matthee and van Wyk (2003) found *Sporobolus ioclados* in the brackish footslopes of the Potlake Nature Reserve in Sekhukhuneland, East of the KNP. *Tragus berteronianus* was found in association with *Salvadora australis*, together with *Aristida adscensionis*, *Cenchrus ciliaris*, *Chloris virgata*, *Enneapogon cenchroides* and *E. scoparius* which dominate the grass cover. Khomo (2003) also noted an association between the tree and grass species found on sodic soils as a result of the salt concentration in the soil. *Tragus berteronianus* and *Cenchrus ciliaris* were not found on sodic sites in Kenya where they were only found on non-saline soils (Onkware, 2000) and only *Sporobolus spicatus* and *Cyperus laevigatus* were found to be true halophytes. This may indicate mis-identification of the plant species, or that these grasses are an indicator of low salinity rather than high sodicity, and are therefore able to survive on sodic sites but do not occur as frequently. This discrepancy requires further investigation into the grass species found on sodic soils in the KNP as there are currently no veld condition assessments done on sodic soils.

Of all these grass species, *Sporobolus ioclados* is the only species which grows exclusively on sodic soils and is used as an indicator species (Scholes, M. C. *pers comm*., 2008). The germination of *Sporobolus ioclados* seeds has been observed in highly saline soils in Pakistan (Khan and Gulzarw, 2003). From a herbivory perspective, *Sporobolus ioclados* was rated by Trollope (1989, referenced in Thrash, 1998) on a scale of 1 to 10 as 5 for forage biomass potential and 5 for burning fuel potential. *Panicum maximum* was rated 10 and 6 respectively, and *Tragus berteronianus* was rated 0 for both forage and fire. The higher forage rating indicates that *Sporobolus ioclados* has greater grazing potential than *Tragus berteronianus* and should be managed to be the dominant species on salt-affected patches. The leaf material has high concentrations of sodium in the leaf material (Kroger and Rogers, 2005; Mutanga, 2004) which will attract herbivores.

3.1.7 Sodic sites as nutrient hot spots

Areas dominated by sodic or saline-sodic soils have been described as sodic patches (Venter, Scholes and Eckhardt, 2003; Khomo and Rogers, 2005) or sodic sites (Grant and Scholes, 2006) in research carried out in the KNP. No other collective definition for the phenomenon of sodic soils was found in the literature. Sodic sites have been equated to grazing lawns found in East Africa due to the short, grazing grass found on salt-affected soils and are nutrient rich patches (Grant and Scholes, 2006). Sodic sites can therefore be described as nutrient-rich, fine-scale patches in the landscape that contribute to the ecological heterogeneity of savanna woodlands at different scales.

Ecological management of the ecosystem of the KNP focuses on maintaining the heterogeneity of the system, both spatially and temporally, in an effort to maintain biodiversity (Venter, Scholes and Eckhardt, 2003). Sodic sites in the landscape contribute to heterogeneity at different scales, namely the catchment scale, catenal scale and sodic site scale (Pickett, Cadenasso and Benning, 2003). These patches form transition zones or ecological boundaries between the riparian and upland mosaics (Cadenasso, Pickett, Weathers, Bell, Benning, Carreiro and Dawson 2003; Khomo and Rogers 2005). Grazers and browsers use the available resources at different scales, namely the local feeding patch, habitat and biome scales (Venter, Scholes and Eckhardt, 2003). Herbivores are attracted to watering points, high quality grazing and mineral licks at the sodic site scale, which may influence animal movement between different habitats.

Sodic sites act as both a source and sink for nutrients (Jacobs *et al*., 2007). Clay particles, salts and organic matter accumulate in sodic soils, but are redistributed when clay disperses due to high levels of sodium. Water-logging and water movement through sodic soils create favourable conditions for de-nitrification and a subsequent loss of nitrogen emitted as nitrous oxide (Venter, Scholes and Eckhardt, 2003). Intermittent flooding causes nutrient displacement in the sediment and re-distribution of nutrients from sodic sites into the riparian zone (Jacobs *et al*., 2007).

In the KNP, large numbers of herbivores are more commonly found in the nutrient-rich basaltic areas to the east of the park where forage quantity is high (Naiman, Braack, Grant, Kemp, du Toit and Venter, 2003). However, in the relatively nutrient-poorer granitic areas on the western side of the park, herbivores are often observed utilizing the sodic sites near the rivers (Grant and Scholes, 2006). Herbivores, attracted to sodic sites, utilize the nutrients in the form of forage and minerals and redistribute these nutrients to other parts of the landscape. Sodic sites are nutrient hot spots due to their high forage quality and their ability to sustain herbivores through the dry season (Grant and Scholes, 2006). Research currently being conducted on micro-nutrients in the soils of the Kruger National Park indicates that there are higher Na and Se levels in sodic soils than in the non-sodic soils (Ratnam *et al.*, 2008). High levels of sodium found in the leaves of trees and grasses (Kroger and Rogers, 2005; Mutanga, 2004; Teren, 2004) may attract animals to these high nutrient areas. Sodic sites offer animals other advantages as they appear to be refuges for herbivores against predators, provide wallowing points (Khomo and Rogers, 2005) and may be used as natural mineral licks. The grass species that occur on these high sodium soils are adapted to high rates of herbivory by concentrate grazers, and although these areas appear to be degraded and therefore susceptible to erosion, they are essential heterogeneous patches which have an important function in providing herbivores with essential nutrients. The number of animals supported by the ecosystem may be determined by these high quality forage patches, but the extent of these nutrient hot spots needs to be determined to support this theory (Grant and Scholes, 2006).

These sites need to be studied to inform management decisions regarding animal numbers that can be supported by the ecosystem and detect the early signs of possible degradation of these patches. Mapping the location and extent of sodic sites will assist researchers and managers to quantify the relevance of these patches to the functioning of the ecosystem. Patch dynamics have a spatial context (Venter, Scholes and Eckhardt, 2003) and by

locating sodic sites in the landscape, the function of sodic sites in the ecosystem by providing high nutrient islands in a low nutrient system can be explored. Grant and Scholes (2006) suggest that these nutrient hot spots will become even more important in management decision making for smaller game reserves where the numbers of concentrate grazers cannot be maintained through the dry season due to limited (or no) high nutrient patches.

3.1.8 Sodic site area dynamics

Studies along the Phugwane River in the north of the Kruger National Park, based on the extent of visible bare ground observed from aerial photographs over a 50 year period from 1942 to 1989, have shown that there has been a three-fold increase in the area of sodic sites on the boundary between riparian and upland systems based on the area of visible bare ground (Khomo and Rogers, 2005). Chappell and Brown (1993) also recorded changes in bare area from 0.64 hectares in 1944, to 6.5 hectares in 1965, 9.7 hectares in 1974 and 5.5 hectares in 1985 along the Ripape River, KNP, using aerial photographs from 1944 to 1985. The changes based on the albedo affect of bare soils were attributed to a combination of rainfall and management practices over the 40 year period (Chappell, 1992). Albedo is the ratio of reflectance to incoming irradiance over a wide spectral band width and is related to bare soil (Huete, 2004).

This dynamic aspect of sodic sites, although seen as a natural process of pedogenesis, needs to be monitored, as these sites may indicate changes occurring in the ecosystem. A visual representation of the changes over time will be a useful tool for this purpose, but is not possible until the sodic sites have been mapped so that their dynamic properties can then be monitored. However, it is important to consider that the seasonal state and level of biomass production on the site will influence the area of bare soil visible on aerial photographs and may skew change detection estimations either positively or negatively.

3.2 Remote Sensing as a tool for mapping sodic sites

Remotely sensed data are obtained from satellite sensors, digital sensors mounted on aircraft or from scanned aerial photographs. Natural radiation is produced by the energy from the sun reflecting off the Earth's surface, or from energy absorbed and then re-emitted, as with infrared radiation. This reflected radiation spans the wavelengths of the

electromagnetic spectrum and is recorded by the sensor as an image. Remote sensing is defined by Lillesand, Kiefer and Chapman (2004) as "the science and art of obtaining information about an object, area or phenomenon through the analysis of data acquired by a device that is not in contact with an object, area or phenomenon under investigation".

Researchers in the KNP require a validated map of sodic sites for the entire park to attempt to answer management questions regarding the possible effects of nutritional hot spots on herbivore movements (Grant and Scholes, 2006). KNP is almost 2 million hectares in extent with large areas which are not accessible by road. The recent acquisition of high resolution satellite imagery (SPOT 5) for the entire extent of the KNP, makes remote sensing the only feasible option for the identification of sodic sites throughout the park. Remote sensing analysis is applied to imagery to detect and map sodic sites in the KNP. Digital images are characterised by the area on the ground represented by each pixel (spatial resolution), the number of electromagnetic band widths recorded (spectral resolution) and the time interval between each acquisition (temporal resolution).

Classification of land cover classes using remote sensing techniques has been undertaken from aerial photographs since the early 1920s, by visual interpretation of the black and white image based on knowledge of the scene under scrutiny. Aerial photographs have a very high spatial resolution (under 1m) but the temporal and spectral resolutions are low. Photographs are most commonly panchromatic, represented as black and white from the visible wavelengths, or colour images in the red, green and blue wavelengths (RGB).

The acquisition of multi-spectral satellite imagery from space has increased the possibility of obtaining remotely sensed imagery at a higher temporal resolution (up to every 1 to 2 days) with electromagnetic band widths in the visible and near-infrared (NIR) to shortwave infrared (SWIR) ranges (not visible to the eye). Large areas can be assessed at low to medium resolutions more often, and this allows for the possibility of mapping large areas and detecting changes in the ecosystem over time. Spatial resolution determines the smallest size of objects that can be distinguished in the image. Spectral resolution determines which bands are available to distinguish objects with different spectral properties, eg. SWIR bands are required for the identification of different geological minerals. The time of season when the image is acquired is as important as how often images are acquired (Kerle, Janssen and Huurneman, 2004) as vegetation

phenology changes affect classification results. The scope of the application determines the appropriate spatial, spectral and temporal resolution required, as well as the appropriate seasonal stage of acquisition.

The location and extent of sodic sites has been documented in the northern KNP using remote sensing analysis techniques applied to Landsat 7 ETM+ 15m panchromatic images acquired in May 2000 (Mathys and Wessels, 2001). The result was a land cover map which included a bare soil class using a pixel-based, unsupervised classification. Manual editing of the bare soils land cover class classified the sites close to rivers as "riverbeds" and those away from the rivers as "sodic sites", bearing in mind that locating sodic sites was not the primary objective of this mapping exercise. A total of 337 training sites and 206 validation points for all classes were used, but no accuracy assessment was published for this result. The result was a classification with a "salt and pepper" effect (or noise) of sodic sites, where single pixels were identified in isolation from larger groups of pixels seen as objects called sodic sites.

Object based image classification (described in Section 3.3.2) of the riparian boundary in the Shingwedzi catchment was undertaken using Landsat 7 ETM+ imagery acquired in June 2000, October 2000, May 2001 and September 2001 (Saah, 2004). Sodic sites were identified from bare surfaces using the tasselled cap transformation which calculates three indices namely brightness, greenness and wetness. The bare surface area was estimated at less than 1% of the total area classified in the granites and 1% in the basalts. Of this total bare surface area in the granites, 30% was estimated to be sodic, with 51% sodic in the basalts. The distance from classified bare areas to the nearest river centre line was analysed and 62% of the sodic sites were found within 100-300 m of the river (Saah, 2004).

Four sodic sites were studied on the Ripape River, where satellite imagery and aerial photography from 1944 to 1985 was used to detect possible changes in the size of sodic sites (Chappell, 1992). The size and shape of the sodic sites at the bottom of the catenas were drawn based on the albedo effect of bare soils and a subjective analysis of the changes were depicted using overlaid polygons of the sodic sites. Chappell (1992) recorded changes up the slope to the limit of the duplex soils and along the drainage line in an unconstrained manner. All these previous studies used Landsat imagery, but with higher resolution SPOT 5 imagery currently available, classification of sodic sites is

expected to be more accurate at a smaller scale. Together with high resolution imagery, the object-based classification methods used by Saah (2004) have the potential to improve the classification of sodic sites.

3.2.1 Properties of sodic sites detected in digital imagery: bare soils

In order for the classification of sodic sites from digital imagery to correlate with the definition of a sodic site in the field, each of the properties of sodic sites on the ground is considered as a property detectable from the imagery.

Large scale mapping of salt-affected soils has included ground based laboratory spectral analysis techniques on salt crusts (Howari, Goodell and Miyamoto, 2002) and remote sensing analysis, in combination with geophysical surveys and solute transport models, which define the subsoil salt movement (Farifteh, Farshad and George, 2006). The focus has been on mapping severely saline areas, as the moderate to slightly salt-affected soils are more difficult to identify with less visible salt crusting. Similar problems are encountered when mapping sodic soils, and although the SWIR bands are more sensitive to moderate and slight salinity or sodicity, multispectral imagery has limited success in predicting the spatial distribution of salt-affected soils (Bannari, Guedon, El-Harti, Cherkaoui, El-Ghmari and Saquaque, 2008). Bannari *et al*. (2008) measured a correlation of 52.9% between two SWIR bands and ground reference electrical conductivity (EC), thus showing a low correlation between the level of cations in the soil and the digital data. There is also no relation between recorded reflectance values and pH, which may be due to the variation in EC and pH in the field (Sethi, Dasog, van Lieshout and Salimath, 2006). Strongly saline soils show physical properties of dry surface salt crusts, but the physical structure of cracking and surface crusting of sodic soils may be masked by the colour, brightness or roughness of the soil surface (Bannari *et al*., 2008). Soil moisture, clay percentage and the amount of organic matter will affect the electromagnetic signal recorded by the sensor and cause difficulties with the identification of sodic soils. Therefore, the chemical composition of sodic soils cannot be used to identify sodic sites from digital imagery.

Optical remote sensing is limited to the surface of the soil or vegetation and cannot be used to estimate sub-surface or root zone soil moisture. Sodic soils are associated with a perched water table and reduced hydraulic conductivity resulting in high soil moisture content. Synthetic Aperture Radar (SAR) is used to measure surface soil moisture and a

significant correlation was found between SAR backscatter and the NIR band for dry, bare soils based on surface roughness (Moran, Hymer, Qi and Kerr, 2002), excluding vegetated areas. Both optical and SAR imagery are used together to measure soil moisture in sparsely vegetated areas, defined as those areas with a normalised difference vegetation index (NDVI) value of less than 0.45, using radar imagery from both wet and dry seasons (Wang, Qi, Moran and Marsett, 2004). Radar imagery was not available for this project.

As sodic soils are formed at the footslope of a catena near drainage lines or floodplains, the elevation of these sites and their relation to rivers (Saah, 2004) is determined digitally using a digital elevation model (DEM) and the known river system. The landscape was divided into hill crests and valley bottoms using a digital terrain model (DTM) or DEM. The resolution of the DTMs may vary according to the method of acquisition and are more accurate in less mountainous regions such as the KNP. Bare soil patches found on digital images which do not occur on the foot slopes of the catena will need to be investigated as they may not be sodic sites.

Erosion of sodic sites is linked with degradation (Chappell, 1992) identified from digital imagery based on the albedo effect of bare soil. Land degradation in the rural north eastern region of South Africa was measured using this National Land Cover classification and NDVI (Wessels, Prince, Frost and van Zyl, 2004). Semi-arid vegetation classes in the Great Fish River basin were mapped from Landsat TM imagery with greater accuracy when a textural index was included to discriminate between disturbed or undisturbed rangeland (Tanser and Palmer, 2000). In soil erosion research, the location of gullies was investigated using remote sensing in Kwa-Zulu Natal. The results showed that using Landsat TM and SPOT 5 panchromatic imagery together with vegetation indices, it was difficult to distinguish gullies from other soil features at a reasonable accuracy due to the variability of the vegetation component of gullies. The inclusion of Support Vector Machine classification algorithm assisted semi-automated classification, but that higher resolution imagery would be preferred (Taruvinga, 2008) . The albedo effect, textural indices and NDVI are used together with medium and high resolution multi-spectral and panchromatic imagery to detect the bare soils associated with sodic sites.

3.2.2 Properties of sodic sites detected in digital imagery: vegetation

Vegetation responses to salinity are used as in indicator for the presence of salt-affected soils in agricultural crops (Eldiery, Garcia and Reich, 2005), but cannot be applied in a natural environment with a heterogeneous mix of plant species as the changes in biomass due to salt stress cannot be detected in a way that shows a causal effect. However, plant growth in heterogeneous vegetation may be adversely affected by the levels of sodium in the soil and this reduced vegetation cover is measured as the percentage bare soil. Bare soil patches are visible as high intensity or bright pixels and are used to separate bare areas from senescent or vegetated areas in very high resolution imagery (Laliberte, Rango and Fredrickson, 2006).

The seasonal changes in sodic sites from bare patches to grass covered sites during the wet season are used to determine which bare patches are truly sodic sites using the NDVI to measure the quantity of biomass (Wessels *et al.*, 2004). Sodic sites are heavily grazed in the wet season showing a faster decline in grass cover than the surrounding areas, and the change to bare soil during the dry season should be detectable before the surrounding areas are grazed. If multi-temporal imagery at a high spatial resolution is available (5-15m), the change in vegetation cover is used to determine which bare areas show sodic behaviour.

It has been established that the vegetation present on sodic soils differs from the surrounding areas in terms of tree density, grass cover and plant species. Although remote sensing is used to measure vegetation cover from high resolution imagery, it is more difficult to identify plant species. Very high resolution hyperspectral imagery and known plant species spectral signatures are necessary to identify plant species (Skidmore, Mutanga, Schmidt and Ferwerda, 2005).

Vegetation in southern Africa has been classified at the biome scale and vegetation types or plant community scale using remote sensing techniques and examples are listed below. The effect of phenology on vegetation classification in different biomes was investigated over the whole of South Africa and found that vegetation types can be grouped according to their responses to the environment (Hoare and Frost, 2004). Multi-scale remote sensing of the spatial dynamics of the savanna in the Kruger Park from 1972 to 2002 was to be investigated using Landsat TM and the soil adjusted vegetation index (SAVI), but this work has not been completed to date (Mathew, Aplin and Field, 2005). Fynbos plant

communities were mapped using Landsat TM in the De Hoop Nature Reserve with a view to detect plant community changes (Kotze and Fairall, 2006). Mapping of vegetation in southern Africa is limited to medium resolution imagery and higher spatial resolution imagery available for this project will improve results based a more detailed discrimantion of vegetation patches.

Single plant species identification remains a challenge and is dependant on the resolution of the imagery. A study for the detection of alien invasion species in KwaZulu-Natal found that high resolution black and white aerial photography was the most cost-effective and accurate solution, while Landsat TM satellite imagery was the least accurate as the coarse resolution made it difficult to detect alien species (Rowlinson, Summerton and Ahmed, 1999). Mapping plant species distribution has been attempted using hyperspectral imagery in the Kruger National Park (Skidmore *et al.*, 2005). A review of the use of remote sensing in rangeland monitoring concluded that costs are prohibitive and that the spectral library available for local plant species is limited (Palmer and Fortescue, 2003). In other southern African countries, remote sensing has been used in vegetation studies. In Zimbabwe, changes in spatial heterogeneity were measured looking at the increase in arable fields using Landsat TM and NDVI for monitoring change (Murwira and Skidmore, 2006). The identification of tree species in the Kalahari was made using high resolution airborne imagery and object-based classification methods for an upscaling transpiration study (Kimani, Hussin, Lubczynski, Chavarro and Obakeng, 2007). Individual species classification will be beyond the scope of this project.

The pattern of the nutrient hot spot patches will be detected on the imagery from the vegetation cover and bare soil areas and not from the nutrients. The impact of animals on sodic sites evident from tracks, wallows and middens cannot be detected from imagery, but the effects of grazing may be detected from percentage cover change on sodic areas.

3.3 Ground truth samples and classification accuracy assessment

The advantage of using digital imagery to classify vegetation is the large areas that can be covered, but the accuracy of these results depends on the resolution of the imagery and the detail of ground truthing of vegetation types (Lillesand, Kiefer and Chipman, 2004).

If the land cover classes are difficult to define in the field, these classes will not be accurately identified spectrally in the image. Classification of land cover in the field has a high time and manpower cost which is reduced using digital imagery. However, ground truth sampling is still necessary for accuracy assessment purposes and the time and effort spent in the field is constantly weighed against the purpose of the classification and level of accuracy required.

A land cover classification is a model of the ecosystem and with every model, bias and errors occur. In the ideal world vegetation classes are crisp and unambiguous, but in complex ecosystems most boundaries are not unambiguous and the ecological continuum is better described by fuzzy logic (Rocchini and Ricotta, 2007). Some land cover classes may in fact be transitions, or ecotones, between two classes, and fuzzy classification algorithms have been applied to improve classification results (Benz, Hofmann, Willhauck, Lingenfelder and Heynen, 2004). Classes of vegetation types are derived at different scales from biomes through to vegetation types and associations. Field samples measure species diversity and abundance, and vegetation classes are grouped using statistical methods including regression, ordination, principle component analysis and neural networks. Representative field samples must be as homogenous as possible, while representing the heterogeneity of the area. The larger the patch size of the field sample, the higher the accuracy of the classification (Smith, Wickham, Stehman and Yang, 2002). Bare sodic sites in the KNP appear as crisp, unambiguous classes if the soil chemistry clearly distinguishes them from the surrounding areas and the larger sodic sites will be classified more accurately. The surrounding woody vegetation found on sodic soils will be the ambiguous class, which may confuse the edge of the sodic site with other non-sodic savanna vegetation. The rest of the land cover classes are not required for the classification of sodic sites which will simplify the sample design compared to a complete land cover classification.

A classification is not complete until the accuracy of the result has been assessed (Congalton, 1991). The value of a map is determined by the accuracy of the classification, but map accuracy is difficult to measure and express (Foody, 2002). Not all applications require the same level of accuracy (Wulder, Franklin, White, Linke and Magnussen, 2006) as users have different requirements for the map or model. The map producer must weigh up the effort required to highlight inaccuracies in a map as apposed to spending time on improving the classification analysis. A map is a model and will

contain errors and some loss of information. Implications of the error must be understood when linking with other data sets for analysis (Foody, 2002). Statistically, accuracy combines bias and precision and a map is accurate if it represents an unbiased representation of reality.

Accuracy assessment is only as good as the data collected for the test site and will incorporate errors in test data including spatial mis-registration, photo interpretation errors or changes in land cover between dates of image acquisition and field data collection. Errors accumulate through including remote sensing classifications with spatial layers of a geographic information system (GIS) (Congalton, 1991). The standard reporting convention is the error matrix, including producer and user accuracies, referred to as the descriptive technique, and Kappa statistics referred to as the analytical techniques. Accuracy assessment and sampling methods must be fully reported so that users can determine how suitable the map is for their particular needs (Foody, 2002; Janssen and van der Wel, 1994; Verbyla and Hammond, 1996)

The three components to accuracy assessment are the sampling design, the response design (classes) and the analysis (Stehman and Czaplewski, 1998) as discussed in detail in Sections 3.3.1 to 3.3.3.

3.3.1 Sampling design

Accuracy assessment measures the correspondence between the ground truth data (or field samples) and the classification, and not with reality. Ground truth data are field samples identified on the ground and are just another classification based on subjective interpretations, which contain error. Ground truth data may contribute more to the error than the classification of the image. In the absence of ground based data, remotely sensed data obtained by visual interpretation and expert knowledge is used as reference data. The level of accuracy of ground truth data depends on the level of detail required by the classification and influences the difficulty of obtaining field samples.

The error matrix, which is discussed in more detail later, must be representative of the entire classified image so the field data sampling design must fully represent the whole map (Congalton, 1991) and not focus on the large, homogenous areas (Foody, 2002). There may be many training areas within a test area and this gives a first approximation of overall accuracy or classification. The classification method used on the test area is

then used to classify the rest of scene. The sample unit may be a point or an area such as a pixel, cluster of pixels or polygons (objects) (Congalton and Greene, 2008) and must be defined before the sampling and response design is completed (Stehman and Czaplewski, 1998). The comparison between the map and the samples will be made on this basis.

The sampling method used for reference data collection has the most effect on how the error matrix will be interpreted, based on the bias or error introduced (Verbyla and Hammond, 1996). There are five sampling methods suitable for reference data, namely: simple random sampling; systematic sampling, stratified random sampling, cluster sampling and stratified, systematic, unaligned sampling (Congalton and Greene, 2008). Kappa analysis assumes a multinomial sampling model and only simple random sampling truly satisfies this assumption (Congalton, 1991), however simple random sampling is not always practically possible and may under sample small, yet important classes. To avoid bias introduced into the error matrix causing under or over estimation of the true accuracy, a combination of random and systematic sampling is recommended (Congalton, 1991): use systematic sampling to collect training data, and random sampling for the validation accuracy assessment (Lillesand, Kiefer and Chipman, 2004), preferably before classification and during the same time frame. Stratified random sampling after classification may require two trips to the field, one for training and one for accuracy assessment or validation. This may have temporal implications between time of training and validation during different seasons and may be different to the image. If both sets of data are collected at the same time, periodicity errors may occur due to autocorrelation in systematic sampling. Autocorrelation affects the assumption of sample independence, but may be avoided by an increase in the sample size and avoidance of a regular grid (Wei and Chen, 2004).

The training or validation sample size should include as few samples as possible, but enough so that any statistical analysis is valid. Traditional thinking on sample size cannot apply to images due to the large number of pixels, clusters or polygons. A balance between statistically sound and what is practically possible must be reached. A minimum of 50 samples per class is generally used, with more samples for more important or variable classes (Congalton and Greene, 2008). If there are more than 12 classes or 500 000 hectares, then 75 to 100 samples would improve the result (Congalton, 1991).

3.3.2 Response design (class selection)

The sampling design determines where the samples are located, but each sample must be classified according to a classification scheme which is determined by the objectives of the study. The classes should be as unambiguous as possible and include every area to be classified. Usually crisp, non-overlapping entities are assigned to a single class, which are mutually exclusive (Foody, 2002). Classes should be logically explained as opposed to artificial classes (tree species vs cover classes), which is not always possible to avoid.

When crisp, unambiguous membership is applied to unique and mixed classes, the degree to which the class is mixed cannot be determined. Fuzzy classifiers can be used to overcome this problem, particularly in an environment of continuums and transitions found in vegetation ecology. Fuzzy logic allows for partial and multiple class membership and helps to deal with the vagueness and uncertainty in complex systems. A crisp set of results is either 0 or 1, whereas a fuzzy set of results is a membership function between 0 and 1 defined as a mathematical function (Jindal and Josan, 2007). Fuzzy logic and object-based classification techniques have been used to map different soils based on brightness, which may be applicable to mapping sodic soils (Brodsky and Boruvka, 2006).

Rocchini and Ricotta (2007) propose using hierarchical classification schemes for environmental management as information derived from such classification must apply at different scales for different decision making levels. The classification of sodic sites occurs at the middle hierarchy, where the super-object is the catchment and the sub-object may be the bare area, grassed area and treed area, as an example.

Fuzzy hierarchical classification fits with the 'ecological continuum' theory. Due to the high degree of complexity in ecological systems, fuzzy set theory fits better than crisp classification. There are problems with assessing accuracy of classification if fuzzy logic is used. Fritz and See (2004) use a fuzzy confusion matrix which includes results from a questionnaire completed by experts on the difficulty in differentiating different cover classes. This is then combined with the classical error matrix and the areas of uncertainty are then mapped. Mapping one class, such as sodic sites, makes the accuracy assessment simpler than land cover classification of all classes, however some other general classes are also required for accuracy assessment using the error matrix where overall accuracy is measured (discussed in detail in the next section).

3.3.3 Analysis (error matrix)

The error matrix is a square matrix with the same number of rows and columns as classes. Classification is tested against the actual ground truth samples (training set or reference data). Errors of commission, where the incorrect prediction is made, and errors of omission, where the correct prediction fails, are reflected per class. Overall accuracy is calculated using all samples and all classes (Figure 3).

Producer accuracies are calculated per class to show how well the sample sites are classified, which is of more interest to the person producing the classification. The user accuracies show the probability that a pixel classified in a class represents the class on the ground as represented by the ground truth samples, and is of more interest to the person using the classification in the field.

Good results indicate that homogenous training areas were selected, classes are spectrally separable and the classification applied works well for training areas. It says nothing about the performance of the classification for the rest of the image. The overall accuracy of training areas is not the overall accuracy of the scene (Lillesand, Kiefer and Chipman, 2004). Poor user accuracies will show which classes are being confused and does not give a correct or incorrect answer (Congalton, 1991). Both the producers and users accuracies must be considered for each class to assess the accuracy of the classification.

		Reference Data			
		Deciduous Forest	Coniferous Forest	Grassland	Total
Classification Data	Deciduous Forest	60	22	4	86
	Coniferous Forest	2	30	3	35
	Grassland	1	4	10	15
	Total	63	56	17	136

Overall Accuracy: $\frac{100}{136} = 73.5\%$

Category	Producer's Accuracy	User's Accuracy
Deciduous Forest	$\frac{60}{63} = 95.2\%$	$\frac{60}{86} = 69.8\%$
Coniferous Forest	$\frac{30}{56} = 53.6\%$	$\frac{30}{35} = 85.7\%$
Grassland	$\frac{10}{17} = 58.8\%$	$\frac{10}{15} = 66.7\%$

Figure 3: Example of an error matrix showing the difference between producers accuracy (how well the landscape was mapped) and the users accuracy (how reliable the classification map is to the user) (Jenness and Wynne, 2007).

The typical expected target accuracies of a classification using remotely sensed data are 85% overall accuracy with no class below 70% (Thomlinson, Bolstad and Cohen, 1999) and with a relatively even level of accuracy for all classes. This target accuracy was reviewed by Wulder *et al*. (2006) and found to be unrealistic as many regional land cover classifications, using medium resolution imagery, result in user and producer accuracies between 50% and 70%. The level of accuracy required depends on the purpose of the map and the usefulness of the classification should not depend on meeting artificial criteria (Wulder *et al*., 2006). Any changes in the area of sodic sites will require a high degree of accuracy to detect real changes rather than artefacts from seasonal effects.

Image data are binomially or multi-nominally distributed, therefore normal theory statistics which are applied to normally distributed data cannot be used for image analysis (Congalton, 1991), and discrete multivariate analysis is preferred. The Kappa coefficient (Jenness and Wynne, 2007) allows for a variance term to be calculated, compensates for chance agreement and allows comparisons to be made using the significant difference.

$$\hat{K} = \frac{N\sum_{i=1}^{r} x_{ii} - \sum_{i=1}^{r}(x_{i+} * x_{+i})}{N^2 - \sum_{i=1}^{r}(x_{i+} * x_{+i})} \qquad [2]$$

where r is the number of rows in the confusion (error) matrix
x_{ii} is the number of observations in row i and column i
(on the major diagonal)
x_{i+} is the total observations in row i
x_{+1} is the total of observations in column i
N is the total number of observations included in the matrix.

Definiens Professional (eCognition) produces the Kappa statistic as well as the other statistics in the software's accuracy assessment algorithm. Accuracy assessment is used for the comparison between classification product, and the overall and individual class accuracies are interpreted according to the requirements of the classification. Many zeros in a matrix occur when the classification is exceptionally good or when there are too few samples. The error matrix result will assist to refine the classification and is thus part of an iterative process of classification and accuracy assessment.

3.4 Image normalisation and pre-processing

Before the classification of sodic sites is implemented, the imagery must be radiometrcially and geometrically corrected (see Appendix IX) and pre-processed to ensure that the imagery has been normalised. This is especially important for comparisons between imagery acquired by different sensors on different dates with specific sun geometry at the time of acquisition. All indices are calculated using radiometrically corrected reflectance values described in detail in Appendix IX.

3.4.1 Normalisation of input imagery

Satellite-sun geometry must be taken into account to convert radiance to top of atmosphere (TOA) reflectance, and the atmospheric effects need to be calculated to obtain top of canopy (TOC) or "at surface" reflectance values characteristic of the surface type under investigation (Wei and Chen, 2004), also known as first order normalisation.

Further radiometric pre-processing (atmospheric correction) of the image may be considered for the comparison of quantitative values, such as vegetation indices, between other images, or for change detection (Song, Woodcock, Seto, Lenney and Macomber, 2000). It is possible to obtain imagery that has been processed to this level for land cover change detection, but there are cost implications. For clear and near cloud free imagery, the first order normalization of imagery reduces relative noise between multi-temporal imagery and gives a more consistent result for land cover classification (Huang, Yang, Hoomer and Zylstra, 2002). Further improvement can be made by atmospheric correction which takes the distorting effect of aerosols in the atmosphere into account. These particles and gases cause absorption, reflectance, scattering and fluorescence (Kerle, Janssen and Huurneman, 2004) and their effects are dependant on wavelength. The blue and green bands in the visible electromagnetic range are affected by aerosols, more than the red and near infra-red bands.

Vegetation indices are highly correlated to vegetation cover and are expressed as ratios using the reflectance value at the canopy or surface (Karnieli, Kaufman, Rener and Wald, 2001). If the image has not been converted to reflectance values then these indices may not be compared to other values obtained using reflectance values. Thus, radiometric calibrations are made to avoid measuring non-real differences. For classification methods using vegetation indices to be used on different scenes it is necessary to apply radiometric

corrections. If training data are obtained from the same image, then atmospheric correction is not necessary as the data are in the same relative scale (Song *et al*., 2001). If spectral signatures are used to classify objects across images from different acquisition dates or sensors, then atmospheric correction should be taken into account.

It is important to understand the pre-processing of imagery before analysis can begin and the terminology used before embarking on analysis of the data. Confusion in terminology is illustrated in the paper by Yuksel, Akay and Gundogan (2008) where conclusions are reached based on "surface reflectance" when no atmospheric correction was made.

3.4.2 Spectral signatures

Satellite sensors record the electromagnetic radiation from the earth at the satellite for each band as a relative radiation intensity or digital number (DN). The unit of spectral radiance (L) is the rate of transfer of energy (Watts) recorded at a sensor, per square metre on the ground, for one steradian[1], per unit wavelength measured ($W/m^2/sr/\mu m$) (Geosystems, 2006). The solar energy, or irradiance, passes through the atmosphere and strikes an object in the atmosphere or on the surface of the earth. Five possible interactions take place: the energy may be transmitted, absorbed, reflected, scattered or emitted. Multi-spectral sensors are designed to record reflected energy of the visible and near-infrared wavelengths, and the emitted energy of the thermal range. The sensor records raw solar energy values which are converted to radiance at the sensor using pre-launch calibrations[2]. Reflectance is the ratio of reflected energy to the solar energy and is calculated from the radiance value and expressed as a percentage. The unique manner in which objects absorb, reflect, scatter or emit solar energy at different wavelengths determines that object's spectral signature (Figure 4).

Once imagery has been normalised (converted from digital numbers to TOA reflectance or TOC reflectance) the spectral signatures of vegetation, bare soils and water should be comparable to spectral signatures of spectral libraries supplied by the USGS[3] or some software packages. Well calibrated normalised imagery will give a more repeatable classification (Baraldi, Puzzolo, Blonda, Bruzzone and Tarantino, 2006).

[1] steradian: unit of measure equal to the solid angle subtended at the centre of a sphere by an area on the surface of the sphere that is equal to the radius squared
[2] Landsat 7 Science Data Users Handbook: http://landsathandbook.gsfc.nasa.gov/handbook.html
[3] United States Geological Survey (USGS)

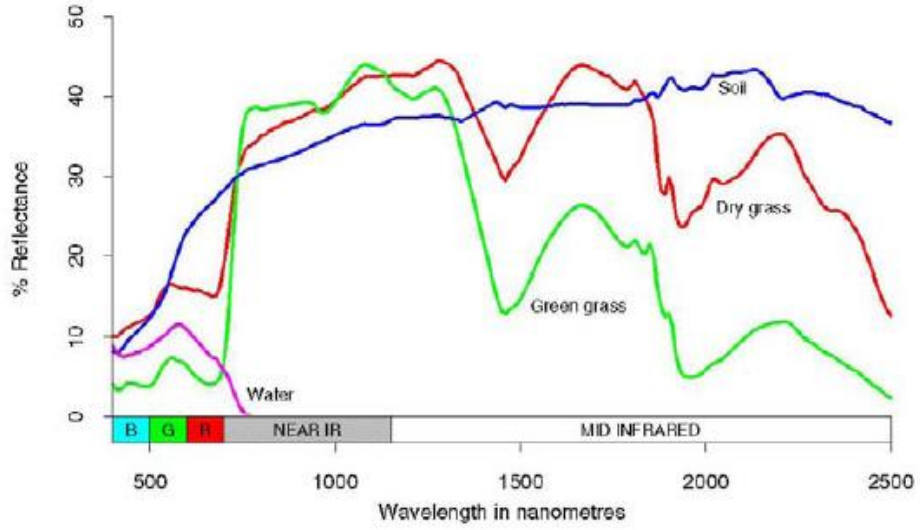


Figure 4: Typical spectral signatures of water, soil, dry and green grass for the visible and infra-red wavelengths (Sanderson, 2008).

3.5 Classification

Classification of imagery into land cover classes such as sodic sites can be interpreted visually based on knowledge about the area or using image analysis techniques based on spectral signatures, texture and structural qualities.

3.5.1 Visual Interpretation

Visual classification and interpretation by the human eye is still the first and most common method applied to digital imagery. The visual classification and interpretation of aerial photographs is based on colour, tone, size, shape, texture, shadow, pattern, height, association and knowledge of temporal change and phenology of the project area (Lillesand, Kiefer and Chipman, 2004). Additional information such as topography, geology and soils assist with accurate classification. It is this ability of the human brain to see and interpret imagery based on knowledge, which is emulated by the software Definiens Professional (eCognition) for digital imagery classification.

Colour image visualisation methods are applied to imagery to assist with visual interpretation without changing the values of the pixel data. These methods include stretching, filtering, true and false colour composites of the visible and near-infrared layers (Lillesand, Kiefer and Chipman, 2004).

Other visual enhancement techniques include transformations and fusion of images. Pan-sharpening is the fusion of higher resolution panchromatic imagery and lower resolution multi-spectral (MSS) images to produce a higher resolution multi-spectral image for large scale applications (Zhang, 2004). The fusion of images may cause colour distortion problems and different fusion methods are applicable for mapping, visualisation applications or digital image classification, which requires spectral integrity of the data. The adaptive image fusion (AIF) method maintains spectral information sufficiently well for multi-spectral digital classification (Steinnocher, 1999).

Visual interpretation may be useful for locating sodic sites in the orthorectified aerial photographs supplied by KNP. Different operators use differing interpretations so automated methods are preferable for a repeatable result. Bare soils have a high reflectance, or albedo effect, but soil moisture and soil type or geology affect reflectance and must be taken into account when visual classification is used for sodic soils (French, Schmugge, Ritchie, Hsu, Jacob and Ogawa, 2008).

3.5.2 Digital Image Analysis

Digital image analysis is the numerical processing and analysis of imagery using various classification methods including unsupervised and supervised pixel classifications, or object-oriented image analysis (Lillesand, Kiefer, and Chipman, 2004) . Unsupervised classification is a statistical grouping of pixels according to their spectral characteristics using Iterative Self-Organising Data Analysis Technique (ISODATA). Supervised classification is a pixel-based method where typical samples of each class are selected and the classification follows these pixels to classify the whole image. The pixel-based classification method results in a "salt-and-pepper" effect due to the spatial heterogeneity of reflectance properties.

A pixel is described by its value, size and position. An object is a collection of pixels which have similar spectral homogeneity or heterogeneity and are described by their value, size, position, shape and context, or topology (de Kok, Buck, Schneider and Ammer, 2000). Spatial patterns or patches as seen in landscape ecology and environmental applications at different scales are more closely represented by objects than pixels (Blaschke and Hay, 2001). Pixel-based clustering encounters problems with

high standard deviation from the spectral mean, but object-based clustering can deal with heterogeneity both spatially and spectrally (Manakos, Schneider and Ammer, 2000).

Objects can be hierarchically classed and described in terms of super- and sub-objects, particularly useful for describing ecological patches in the landscape at different scales in terms of spatially nested patches (Pickett, Cadenasso and Benning, 2003). The most basic object is the pixel with super-objects at levels above the pixel (Definiens Version 5, 2006). The hierarchy level can be related to classification at different scales. The process of grouping pixels into objects is called segmentation which attempts to replicate the visual interpretation of an image by the human eye and brain (Schiewe, 2002). The method of segmentation used by Definiens Professional (eCognition) is the Fractal Net Evolution Approach (Baatz and Schäpe, 2000). Pixels are merged based on spectral and spatial heterogeneity or homogeneity. User defined parameters are required to segment at different scales, as attributes of the image such as texture, colour and form, are scale dependent (Blaschke and Hay, 2001). The application of this segmentation technique provided by Definiens Professional (eCognition) is a process of trial-and-error for the selection of the scale parameter. A segmentation optimiser was tested to use the objects of interest to train the segmentation process thereby improving the efficiency of the segmentation process (Zhang and Maxwell, 2006). This technique has not yet been implemented in the current software.

The problems of segmentation at different scales may be improved by using texture as well as colour intensity, as texture becomes important at different scales (Corcoran and Winstanley, 2006). Height information provided by LiDAR imagery will further improve segmentation into meaningful objects with different height classes per object (Asner, Knapp, Kennedy-Bowdoin, Jones, Martin, Boardman and Field, 2007; Lucas, Lee, Armston, Breyer, Bunting and Carreiras, 2008) but LiDAR images are limited to small areas and are not readily available for the KNP.

Pixel-based classifications work sufficiently well for broad scale, regional land cover classifications using medium resolution imagery, eg. Landsat or ASTER. With the increase in resolution from 30 m to 1m and below, object-based classification, including topographic ancillary data, was found to be more robust than pixel-based classification of vegetation alliances and eliminated the salt and pepper effect seen with pixel based classification (Yu, Gong, Clinton, Biging, Kelly and Schirokauer, 2006).

Detailed vegetation studies to plant species level require very high spatial and spectral resolution imagery to accurately classify to species level (Kimani *et al.*, 2007). This research found that accuracy was dependant on the sample size, sampling quality, the classification framework and the heterogeneity of the vegetation, and that the ground-truth classification methods based on ecological features may not always be comparable due to the statistical methods used for image classification.

Change detection of shrublands using object-based analysis and very high resolution airborne multispectral imagery found that object-based standard nearest neighbour mean and standard deviation of the red and NIR bands, and NDVI gave the best result (Stow, Hamada, Coulter and Anguelova, 2008). Images of near-anniversary dates were selected providing that precipitation prior to the acquisition was similar.

The development of object-based image analysis has created a number of commercially available software options including Definiens Professional and ESRI Feature Analyst to name only two. Definiens Professional was found to give more accurate results for the classification of tree species than Feature Analyst (Kimani *et al.*, 2007) and has the ability to automate the analysis using sequential processing automation (de Kok, 2006; Hajek, 2008). Expert knowledge about the spectral and spatial characteristics of the classes are included in this automated process and the class hierarchy classified using a step-by-step, repeatable process.

The use of object-based classification illustrating Definiens Professional's ability to segment and classify using the class hierarchy (Hajek, 2006) will be adapted to classify sodic sites from medium to high resolution imagery.

3.5.3 Vegetation Indices

Vegetation mapping and changes in vegetation patterns have been recorded using the unique reflectance properties of green vegetation in the visible and near-infrared wavelengths (VNIR). Energy in the red band is absorbed due to photosynthetic activity of plants and reflected in the NIR band due to leaf structure (Lillesand, Kiefer and Chipman, 2004). This difference in the two bands in highly productive plants is called the red edge. Vegetation indices based on the red and NIR bands are used to differentiate vegetation classes and account for the soils spectral interference and atmospheric effects.

Vegetation indices include slope-based, distance-based and orthogonal transformations (Eastman, 2003).

The most common slope-based vegetation index is the normalised difference vegetation index (NDVI) which is a simple arithmetic expression of the relationship between the red and NIR bands known as the red edge (Tucker, 1979). The NDVI is expressed as follows:

$$NDVI = (\rho NIR - \rho Red) / (\rho NIR + \rho Red) \quad [3]$$

where ρRed = spectral reflectance in the red wavelength expressed between 0 and 1

ρNIR = spectral reflectance in near infra-red wavelength expressed between 0 and 1

The result is a value between -1 and +1 where negative NDVI values represent non-vegetated areas (cloud, snow, water or bare surfaces) and positive NDVI values indicate varying densities of green vegetation below 0.3 for sparse vegetation and over 0.6 for dense vegetation. In practice, these values are only a guideline and the actual thresholds for different classes vary for each image. Water bodies may be deep and clear, partially silted, or contain algal growth or water plants which will affect the NDVI value. The sum of the NDVI under the curve from leaf-on to leaf-off indicates plant biomass production, but does not distinguish between grasses and woody plants. The stage of phenology of the plant during the growing season will determine the amount of photosynthetic material present and influence the NDVI value. The NDVI value will saturate to 1 in very dense forest areas which is less relevant in the semi-arid savannas of the KNP. The NDVI ratio reduces topographic, illumination and atmospheric affects (Eastman, 2003) and remains the standard measure of vegetative cover.

Bare soils are classified as the absence of vegetation using the NDVI. The vegetation fraction in forest is measured using the Forest Canopy Density (FCD) model which incorporates the NDVI, bare soil index and shadow index.

The Bare Soil Index (BI) was described using the short wave infra-red band of Landsat imagery (Jamalabad and Abkar, 2004) as follows:

$$BI = ([[(\rho SWIR_{1.6} + \rho\ Red) - (\rho NIR + \rho Blue)] / [(\rho SWIR_{1.6} + \rho Red) + (\rho NIR + \rho Blue)]] * 100) + 100 \quad [4]$$

where ρBlue = spectral reflectance in the blue wavelength (TM1)
ρRed = spectral reflectance in the red wavelength (TM3)
ρNIR = spectral reflectance in near infra-red wavelength (TM4)
$\rho SWIR_{1.6}$ = spectral reflectance in short wave infra-red wavelength including the 1.6 μm wavelength (TM5)

The fractional cover of trees, grass and bare soil in savanna ecosystems have been estimated using NDVI and the different ways trees and grass respond to rainfall at the regional scale (Scanlon, Albertson, Caylor and Williams, 2002). The differences in the rate of green-up for grasses and trees was found to be useful to distinguish between trees and grass at the landscape scale (Archibald and Scholes, 2007), but how the tree/grass ratio ultimately influences NDVI is still a matter of debate.

Sparse vegetation in arid or semi-arid environments will have pixels of bare soil and vegetation, or mixed pixels including both vegetated and non-vegetated signals. The soil line is the regression of bare soil pixels expressed in feature space using the red and NIR bands (Figure 5). The slope and intercept of this line are used in distance-based indices. Distance-based vegetation indices include the brightness effect of the bare soil background, which the NDVI does not take into account. Dark soils have the lowest Red and NIR values with bright soils with the highest Red and NIR values (Fox and Sabbagh, 2002). Soil moisture also influences the determination of the soil line.

The perpendicular vegetation index (PVI) was the first distance-based index used to include the soil line:

$$PVI = (NIR - bRed + a) / (b^2 + 1)^{0.5} \quad [5]$$

where a = the intercept of the soil line
B = the slope of the soil line
Red = reflectance in the red band
NIR = reflectance in the near infra-red band

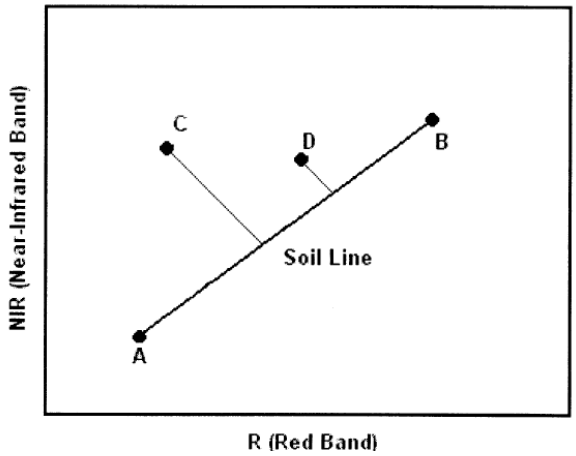


Figure 5: Soil line concept demonstrating the observed linear relationship between red (R) and near-infra-red (NIR) reflectance or image intensity of bare soil. The soil line extends from darker soils with low R and NIR image intensity (Point A) to an upper region of bright soils with high R and NIR image intensity (Point B). Point C represents a pure vegetation pixel and Point D represents a partially vegetated pixel (Fox and Sabbagh, 2002).

The soil adjusted vegetation index (SAVI) (Huete, 1988) and the transformed soil adjusted vegetation index (TSAVI) are an improvement on the use of the soil line and its associated assumption of a parallel increase in vegetation cover to the soil line (Fox and Sabbagh, 2002). Although the process of defining the soil line for each image can be automated (Fox, Sabbagh, Searcy and Yang, 2004) using an iterative process, the distance-based vegetation indices have not been widely adopted. This may be due to the difficulty in calculation of the slope and intercept of the soil line and there has been no significant evidence of an improvement of the value obtained from the simple NDVI formula (Fox, *et* al., 2004). The modified soil adjusted vegetation index (MSAVI) (Qi, Chehbouni, Huete, Kerr and Sorooshian, 1994) attempted to simplify the calculation of the constants and using induction, $MSAVI_2$ was devised as follows:

$$MASVI_2 = [\, 2\,NIR + 1 - (\,(\,2\,NIR + 1\,)^2 - 8\,(NIR - Red)\,)^{0.5}\,]\,/\,2 \qquad [6]$$

where Red = reflectance in the red band
NIR = reflectance in the near infra-red band

The soil adjusted vegetation indices are more important in crop biomass production estimation than the estimation of vegetation cover in natural environments, where accurate production is not measured to the same accuracy. As the NDVI will be used primarily to measure the absence of vegetation (bare soil) for the classification of sodic soils, only the NDVI and BI will be included in the classification algorithm.

3.5.4 Image Transformations

The reflectance values of the different bands in digital imagery are often highly correlated for objects (eg. blue and green bands) and therefore duplicate information is contained in other bands but may not contribute to the identification of the object. The principal components analysis (PCA) and tasselled cap transformation reduce the correlated bands to a set of new uncorrelated bands, one of which is a green index. The PCA orthogonal transformation is used for data compaction and noise removal and is used to pick up environmental trends from multi-temporal imagery (Wessels *et al.*, 2004). The first principal component has the highest variation and is typically the albedo effect (bare soil index). The second principal component has the next highest variation and represents the variation in vegetation cover (Eastman, 2003).

The tasselled cap transformation was developed for the Landsat MSS, TM and ETM+ sensors, and applied to multi-spectral images to reduce the image to less data without losing information (Crist and Kauth, 1986). The result is a brightness, greenness and wetness layer which together explain 97-99% of the spectral variation and are primarily used in vegetation studies. If near cloud free imagery is used for the application of the tasselled cap transformation, no atmospheric correction is necessary for at-satellite reflectance imagery. The tasselled cap co-efficients are calculated for each Landsat sensor and the Landsat 7 ETM+ co-efficients are based on at-satellite reflectance (Huang, Wylie, Yang, Homer and Zylstra, 2002). Co-efficients for tasselled cap transformation are not readily available for ASTER or SPOT 5 imagery.

4. STUDY SITE

The Kruger National Park is situated in the lowveld region of the north eastern part of South Africa in the savanna biome (Figure 6).

The geology of the park is divided down the centre of the park by the granitic soils in the west and the basaltic clays in the east (Venter, Scholes and Eckhardt, 2003). The mean annual rainfall ranges from 300-500 mm/year in the northern arid bushveld zone to 500-700mm/year in the central and southern lowveld bushveld zone. The two savanna types found in the Kruger National Park are the broad-leaved and fine-leaved savannas which cover 75% and 25% of the park respectively (Venter, Scholes and Eckhardt, 2003) with

different tree species occurring in each. The vegetation types are largely determined by the soils and climatic conditions and are described by Venter (1990) using land types, land units and land elements. Sodic sites fall into the land element scale.

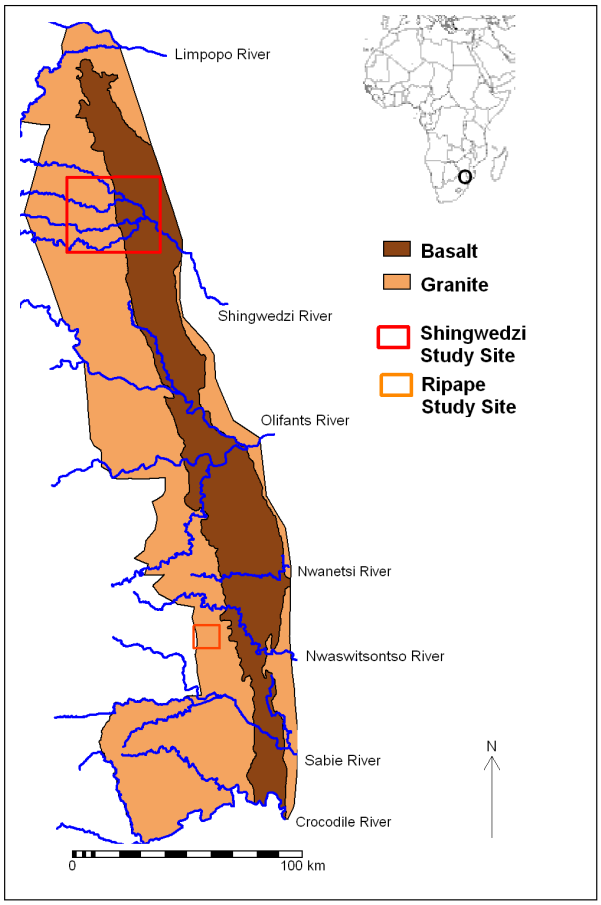


Figure 6: The KNP study area showing the Shingwedzi River catchment study site and the Ripape River study site on the south western boundary.

Two study sites were selected for describing and locating sodic sites: the Shingwedzi river catchment including the tributaries Mphongolo, Phugwane, Bububu and Nkulumbeni in the north of the KNP, and the Ripape River on the western border of the park in the south of the KNP (Figure 6). The Shingwedzi River catchment was selected because the majority of previous research on sodic soils was carried out on the Shingwedzi River and its tributaries. The Ripape River is a tributary to the Nwaswitsontso River and was selected as a study site based on the sodic sites along the Ripape River which were studied by Chappell (1992).

CHAPTER 2

IDENTIFICATION OF SODIC SITES USING FIELD TESTS

1. INTRODUCTION

Researchers in the Kruger National Park (KNP) require a validated map of sodic sites for the entire park to attempt to answer management questions regarding the possible effects of nutritional hot spots on herbivore movements (Grant and Scholes, 2006). The KNP is two million hectares in extent, with large areas which are inaccessible by road. Remote sensing image analysis is the only feasible option for the identification of sodic sites throughout the park.

Classification of digital imagery requires ground truth samples for robust statistical validation of the product (Congalton, 1991). Samples of known sodic sites, and other land cover types, must be identified in the field to assess the accuracy of the image-based classification. The land cover classes selected for field samples should be crisp, non-overlapping and mutually exclusive (Foody, 2002). The sampling design for training data may be systematic, but must be random or stratified random for validation samples (Congalton and Greene, 2008). For a balance to be achieved between statistically sound and what is practically possible, a minimum of 50 samples per class is generally used. It is therefore necessary to use in-field, rapid assessment methods to identify sodic sites on the ground. Sodic site ground truth samples must also be visible on digital imagery for accurate image classification.

The importance of sodic sites in the KNP is that the soils are a source and sink of nutrients (Jacobs *et al*., 2007) known as nutrient hot-spots hot spots due to their high forage quality and their ability to sustain herbivores through the dry season (Grant and Scholes, 2006). Sodic sites are patches of sodic soil identified by an elevated sodium level relative to other divalent salts: calcium and magnesium (Qadir and Schubert, 2002). Saline soils are high in soluble salts including calcium, magnesium and potassium and have a high cation exchange capacity (CEC). Soil salinity is measured by the electrical

conductivity (EC) expressed in deciSiemans per metre (dS/m) (van de Graaff and Patterson, 2001). Soil sodicity is measured by the Exchangeable Sodium Percentage (ESP) which is the percentage of sodium (Na^+) relative to the CEC, or the Sodium Adsorption Ratio (SAR), expressed as a ratio of Na^+ to the presence of $Ca^{2+}$and Mg^{2+} as follows (Qadir and Schubert, 2002) :

$$SAR = Na^+ / \ [(Ca^{2+} + Mg^{2+}) / 2]^{0.5} \qquad [7]$$

Both EC and SAR are measured using a soil saturated paste or extract (EC_{se}) (Abrol, Yadav and Massoud, 1988).

A soil is considered to be sodic when the EC is lower than 4 dS/m, the ESP value is higher than 15 or the SAR value is over 13, with a pH above 8.5 (de Villiers *et al*., 2003). Soils with an EC over 4 dS/m and a pH less than 8.5 are considered saline-sodic. The cut-off level of 4 dS/m for electrical conductivity is linked to the level of salinity at which crops are affected and not to the level at which the physical properties of soil degrade or disperse (Qadir and Schubert, 2002). Australian soils have been found to disperse at an ESP of 6 (Quirk, 2001), which is used as a cut-off for sodic versus non-sodic soils in that country, lower that the northern hemisphere standard ESP cut-off of 15. South Africa uses the standard definition for sodic soils as EC < 4dS/m, ESP > 15 and pH > 8.5, but divides saline-sodic soils into two groups: alkaline saline-sodic if pH > 8.5 and non-alkaline saline-sodic when pH < 8.5 (de Villiers *et al*. 2003).

The chemical composition of sodic soils causes changes in structural properties due to physical processes. Slaking occurs where macro-aggregates are broken down to micro-aggregates in the presence of water, and contributes to hard setting or crusting of the small particles on the surface or the top layer of the soil. Clay particles swell, separate (disperse or deflocculate) and become suspended in water, in the presence of high levels of sodium (Vance, McKenzie and Tisdall, 2002). The deflocculation of clay particles occurs when sodium cations are adsorbed by the clay platelets causing swelling and dispersion, and is more pronounced at a higher pH (McBride, 1999). As there is no single sodium level applicable to all soils at which dispersion occurs, the Emerson slaking and dispersion test was devised to determine dispersion potential (Emerson, 1967), a measure of when sodic soils exhibit sodic behaviour. The dispersion test described by Emerson (1967) was modified and adopted to test the relationship between the chemical test for sodicity and dispersion classes (Vance, McKenzie and Tisdall, 2002).

Previous studies of sodic sites in KNP have been restricted to a fine scale chemical investigation of the soils at four sites in the Ripape River catchment (Chappell, 1992) and five sites in the Shingwedzi River catchment (Khomo, 2003; Barichievy, 2005; Teren, 2004). Soil samples were taken by these researchers, from different depths in the soil profile, along transects down catenas, and under and between trees. The soil samples were analysed in a laboratory for salinity, sodicity and other minerals. Venter (1990) analysed over 370 samples of all soils throughout the park, 31 of which were sodic or saline-sodic soils based on the ESP value greater than 6 dS/m.

The chemical and physical properties of sodic soils cause visible characteristics of sodicity in the field. Plant growth is stunted by soils that are high in salts with a high electrical conductivity due to the osmotic effects which limit water uptake, which in turn, causes plant nutrient imbalances (Qadir and Schubert, 2002). Bare soils which show crusting and cracking of the B-horizon are typical characteristics of high sodium levels (Mills and Fey, 2004). Sodic soils are susceptible to erosion due to their chemical make-up which causes physical and structural weaknesses. These are high clay, duplex soils with an impervious B-horizon which gives rise to a perched water table (Raine and Loch, 2003). The shallow A-horizon is eroded, and the underlying B-layer is exposed. Lateral movement of water causes sub-surface tunnelling and eventual collapse of the B-horizon (Chappell, 1992). Sodic soils are commonly found on the footslopes of the catena where parent-material contains a high concentration of sodium, such as granite and basalt. Salts leached from the upper slopes of the catena, accumulate in the lower slopes, where they concentrate in the soils (Chappell, 1992; Dye and Walker, 1980; Khomo and Rogers, 2005).

In the KNP, tree species identified on footslopes of granitic based soils where duplex clays occur include *Euclea divinorum*, *Spirostachys africana*, *Acacia welwitschii*, *Acacia grandicornuta*, *Papea capensis* and *Terminalia prunioides* (Venter, Scholes and Eckhardt, 2003). *Colophospermum mopane* and *Salvadora australis* commonly occur in the dry granitic sodic soils of the northern KNP (Teren, 2004). These tree species do not occur exclusively on sodic soils, but sodic sites can be identified more accurately using the presence or absence of groups of these woody species. Grass species commonly found growing on sodic soils include *Sporobolus nitens*, *Sporobolus ioclados*, *Tragus berteronianus* and *Dactyloctenium aegyptium* (Venter, Scholes and Eckhardt, 2003) which are short, creeping lawn grasses with relatively low biomass production.

In the KNP, large numbers of herbivores are more commonly found in the nutrient-rich basaltic areas to the east of the park where forage quantity is high (Naiman et al., 2003). However, in the relatively nutrient-poorer granitic areas on the western side of the park, herbivores are often observed utilizing the sodic sites near the rivers (Grant and Scholes, 2006). Herbivores, attracted to sodic sites, utilize the nutrients in the form of forage and minerals and redistribute these nutrients to other parts of the landscape. Sodic sites are nutrient hot spots due to their high forage quality and their ability to sustain herbivores through the dry season (Grant and Scholes, 2006). Sodic sites offer animals other advantages as they appear to be refuges for herbivores against predators, provide wallowing points (Khomo and Rogers, 2005) and may be used as natural mineral licks. The grass species that occur on these high sodium soils are adapted to high rates of herbivory by concentrate grazers, and although these areas appear to be degraded and therefore susceptible to erosion, they are essential heterogeneous patches which have an important function in providing herbivores with essential nutrients. The number of animals supported by the ecosystem may be determined by these high quality forage patches, but the extent of these nutrient hot spots needs to be determined to support this theory (Grant and Scholes, 2006).

The objective for this study is to develop a method to identify sodic sites in the field using a functional definition of sodic sites for the KNP, based on visual characteristics of sodic soils rather than the chemistry of sodic soils alone, and to apply this rapid assessment field method to test for sodic soils.

2. METHODS

The sodic sites which were identified using soil chemistry by previous researchers are identified in the field and used to confirm the visual characteristics of sodicity in the field and on imagery. Visually assessed sodic sites from previous researchers were included in the additional ground truth sample sites for the development of a decision tree for rapid in field assessment of sodic sites. The decision tree is then tested on the known sodic soils and based on the results, used for classification of sodic sites and other classes to be included in the image analysis classification.

2.1 Study Site

The Kruger National Park is situated in the lowveld region of the north eastern part of South Africa in the savanna biome (Figure 6). The geology of the park is divided down the centre of the park by the granitic soils in the west and the basaltic clays in the east (Venter, Scholes and Eckhardt, 2003).

Two study sites were selected for describing and locating sodic sites: the Shingwedzi river catchment including the tributaries Mphongolo, Phugwane, Bububu and Nkulumbeni in the north of the KNP, and the Ripape River on the western border of the park in the south of the KNP (Figure 7). The Shingwedzi River catchment was selected because the majority of previous research on sodic soils was carried out on the Shingwedzi River and its tributaries (Figure 7). The Ripape River is a tributary to the Nwaswitsontso River and was selected as a study site based on the sodic sites along the Ripape River which were studied by Chappell (1992).

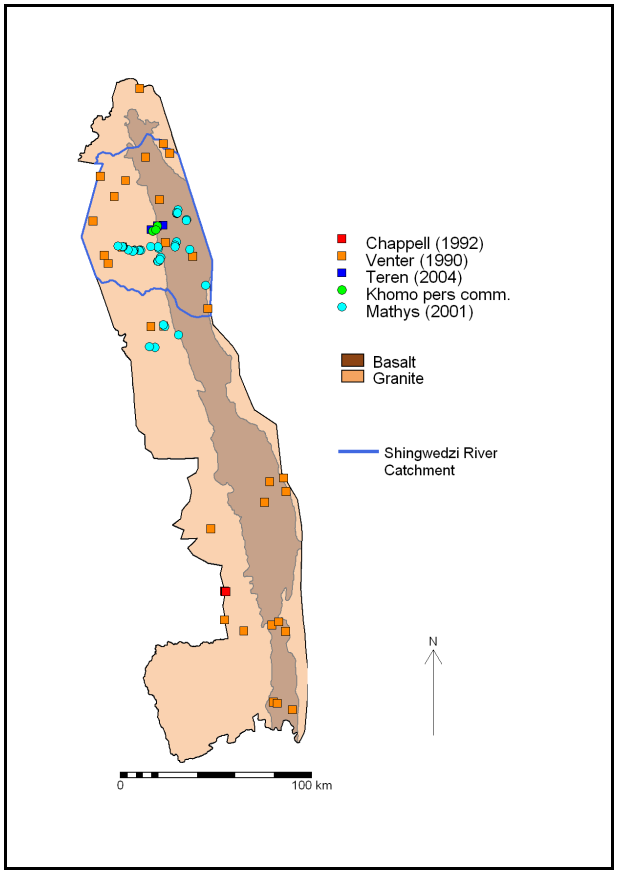


Figure 7: All the known sodic sites recorded for the KNP by previous research projects. Square points indicate laboratory tested sodic soils. Circles indicate sodic sites that do not have published soil chemistry results and were identified through observation of visible sodic characteristics.

2.2 Data collection of ground truth sample sodic sites

2.2.1 Geo-referenced laboratory tested sodic soils

Venter (1993) recorded 370 soil sample analyses, for all horizons, throughout the KNP. Nineteen of these A and B horizon soil samples from thirteen sodic sites in the Shingwedzi River catchment were interpreted by this project as sodic. The interpretation was based on a level of ESP > 15 (de Villiers *et al*., 2003) and the Australian level of ESP > 6 as a cut-off, as discussed in the literature (Vance, McKenzie and Tisdall, 2002). The samples were classified as saline-sodic for EC over 4 dS/m. All the saline-sodic samples were A horizon soil samples, although not all A horizon samples were saline-sodic (see Appendix I for analysis summary). In this project, only samples from the B horizons were used to compare with field sampling of the top crust of B horizons on bare patches.

Teren (2004) tested for sodicity under and between trees on three sites along the Phugwane River. The results shown for soil samples taken between trees in the 0-20cm depth range were included as sodic soils for this project. EC and pH results from 10 samples on each of the three sites, and the SAR for one site calculated from nine soil samples of the bare soil between trees, are included in Appendix I for reference.

Khomo (2005) georeferenced five sample sodic sites on the banks of the Phugwane and Shingwedzi Rivers where soil samples were analysed using laboratory based techniques for EC, pH and SAR. However, these results are unpublished but the sodic sites have been included with the laboratory tested sodic sites by this project.

Chappell (1992) surveyed four transects in the Ripape River catchment from the crest to the footslope or sodic site. Two of the sites reported a SAR value for the B horizon over 13 (de Villiers *et al*., 2003) and were included in this study, while two sites were well below this value (see Appendix I) and were therefore excluded as sodic sites.

2.2.2 Geo-referenced sodic sites visually assessed by previous researchers

Mathys (2001) recorded 40 sample sodic sites in the Shingwedzi River catchment during a survey to map sodic sites in the northern plains (Figure 7). Percentage bare ground, dominant woody species, soil texture and slope where recorded and a visual classification of sodic or non-sodic sites was made.

2.2.3 Sample site selection for the current project

Although the primary objective of this project is to identify sodic sites from digital imagery, it is necessary to differentiate bare sodic areas from other bare and vegetated areas both on the ground and from imagery. Additional classes were identified (savanna, riverine bush and river sand) and their topographic location (footslope vs crest) was determined.

The Shingwedzi study area was stratified by parent material (geology), topography (footslopes) and easy access by road for maximum coverage. The 100 training sample sites for this project were selected systematically using the geographically located sites from previous research researchers (Venter, 1990; Mathys and Wessels, 2001; Khomo, 2003; Teren, 2004), aerial photographs and satellite imagery to assist with identification of visible sodic sites (Table 3). This systematic sampling was undertaken during March and October 2007, which covered the wet and dry season of that year.

For robust verification of the classification of sodic sites on imagery, a set of 50 random ground truth samples was collected for all classes. The random stratified sampling for validation was undertaken during April 2008, the end of the wet season of that year (Table 3). A random sample grid was drawn up for the Shingwedzi River catchment and samples within 100 m of the roads were selected for assessment and in-field classification.

Table 3: Number of sample sites collated and collected by the current project for the Shingwedzi study site, showing the tests applied, the geology of each site and sampling method used.

Class	Field Samples	Geology		Sampling method		Field tests per class			
		Granite	Basalt	Training	Random	% Cover	EC/ pH	Slake/ Dispersion	Visual observation only
Sodic	91	56	35	81	10	53	25	43	35
River Sand	2	2	0	0	2	2	0	2	2
Riverine Bush	7	7	0	3	4	4	4	3	3
Savanna	50	31	19	16	34	34	30	27	16
TOTAL	150	96	54	100	50	93	59	75	56

2.3 Aerial visibility of sodic sites

For sodic sites to be successfully identified on digital imagery, these sites must be visible to the eye. The sodic sites identified by previous researchers (Venter, 1990; Chappell, 1992; Mathys and Wessels, 2001; Khomo, 2003; Teren, 2004), were each located on aerial photography and satellite images to confirm their visibility.

An aerial survey was carried out to assess the visibility of sodic sites from an aerial platform and to observe the heterogeneity between and within sodic sites on different geologies. The aerial survey was flown in November 2006, heading north from Skukuza to the Nwaswitsonto and Ripape rivers near Talamati Rest Camp, where Chappell (1992) had researched sodic sites. From the Ripape River, the flight continued east to the basalt soils along the Rietpan firebreak road south of Satara, south along the Sabie River towards Lower Sabie rest camp, west along the Nwaswitshaka River towards Pretoriuskop, and back to Skukuza flying over the Skukuza flux tower. This aerial survey covered the granitic and basaltic substrates.

To determine whether the geo-referenced laboratory tested sodic soil sites where visible on satellite imagery, these sites were visually assessed against a SPOT 5 panchromatic (black and white) image. Each geo-referenced sodic soil sample was plotted on the imagery and counted as visible on the image if placed within a visibly bright bare patch, and shown to be sodic by chemical analysis. The Venter (1990) sites were accepted as visible if the geo-reference fell within 150m from a visible sodic site. It is not clear whether a GPS unit was used to identify the position of these sites, and if not, this would account for the discrepancy in co-ordinate and the nearest visible sodic site.

2.4 Visible characteristics of sodicity in the field

Sodic sites are described by the soil chemistry, soil physical properties and by visual characteristics of sodicity in the soil. In the field, a rapid assessment technique is required to determine whether a site has the potential to have sodic soil or not. A comprehensive soil chemistry assessment is not possible due to the large number of samples required for the accuracy assessment of remote sensing classification. The rapid

assessment technique interprets the characteristics of sodicity which manifest in the soil structure which affects vegetation growth, and are used to quickly assess a sodic site.

All sites from previous research and the current study were visited and the geographic position was recorded using a GPS (Garmin 12) with an accuracy of 10-15m. The observation date, elevation and the site impression based on size and shape of the sodic patch were recorded. Based on the characteristics of sodicity discussed in the literature, the following visual data was recorded at the sodic patch scale:

- Presence of bare soil and percentage bare cover of the site
- Percentage cover of woody plant species
- Percentage cover of grass plant species
- Site on a footslope (Yes or no)
- Visible erosion of A or B layer (sheet or gulley erosion)
- Visible water table or standing water
- Soil crusting or cracking
- Evidence of animals on the sight (physical presence, middens, wallows, licks)
- Dominant woody and grass species

A decision tree was derived based on the above criteria to assist with identification of the five selected classes in the field (Figure 8).

2.4.1 Bare soils

The most obvious characteristic of sodicity, both on the ground and from an aerial perspective, is bare soil with an exposed B-horizon and signs of crusting and cracking. This is the first branch of the decision tree (Figure 8). If this bare area is found at the footslope of a catena or near a drainage line, then the factors leading to the formation of a sodic soil are likely to be in place. If this bare area is found in the riparian zone or drainage line, the bare soil is assumed to be river sand, and if found on the crest, is a bare crest and included with the general savanna class. If the bare area is on the footslope and not river sand or a bare crest, a number of additional criteria will indicate how strongly the evidence points to sodic soils.

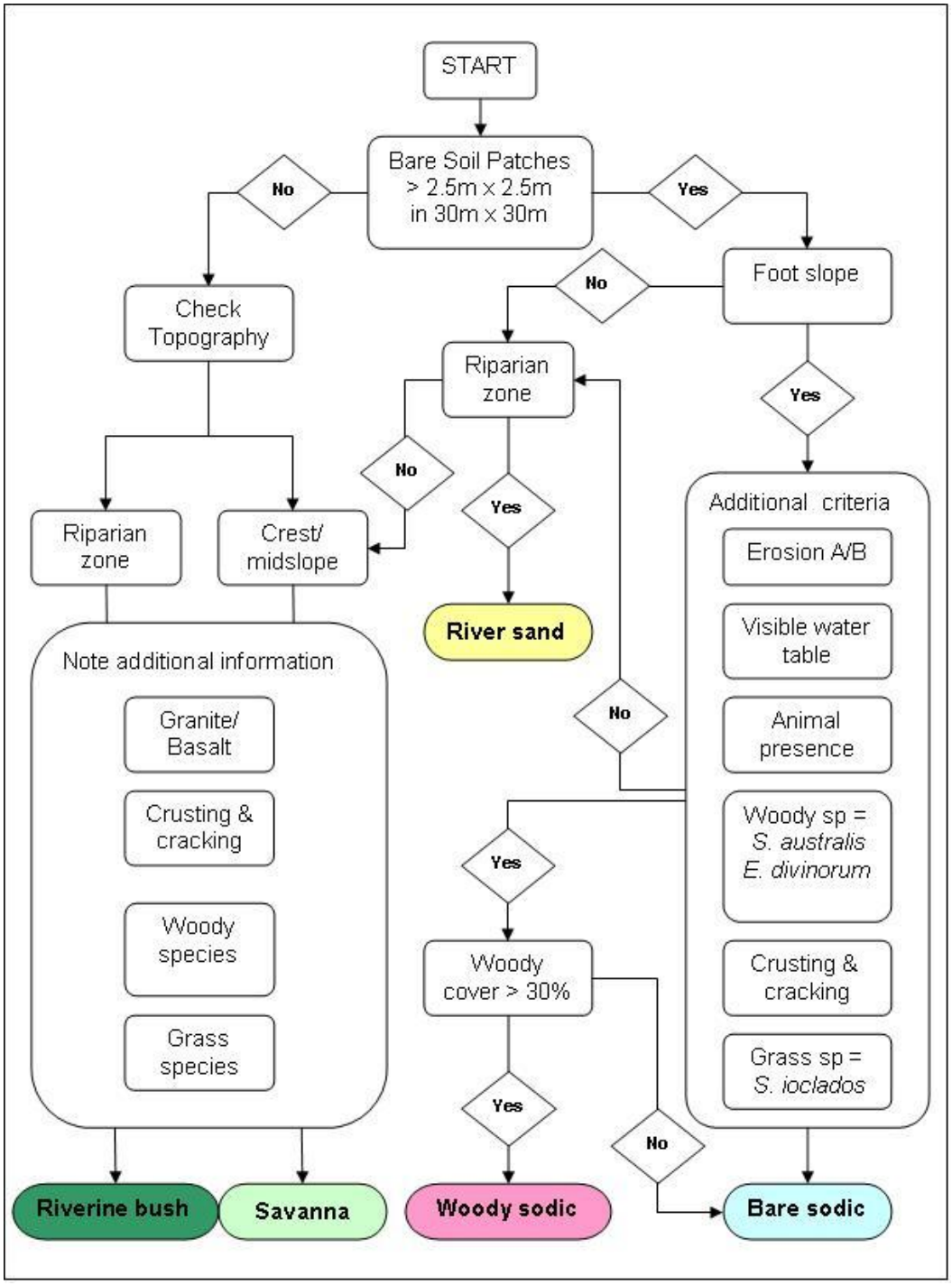


Figure 8: Decision tree for classification of sodic sites from other vegetation types based on the characteristics of sodic soils described in the literature.

Bare sodic sites have lost the thin and often sandy A-horizon due to a loss of vegetation cover. B-horizon erosion may also be visible in the form of tunnel or gulley erosion (Chappell, 1992). The presence of a variable water table and high percentage clay soils will indicate the possibility of a sodic soil. Animal wallows often indicate a high or

variable water table and visible crusting and cracking of the B horizon indicates a high clay content in the soil.

Areas of A-horizon soils may be covered with grass tufts or creeping, stoloniferous grasses. Depending on the season, these grassed areas will appear as heavily grazed lawns (Figure 9) or high quality standing grazing pastures (Figure 10), interspersed with bare patches. Note the bare, crusted sodic area visible during both wet and dry seasons.

The sodic site is expected to be found on a footslope, although this is not always easy to determine in gently sloping landscapes. Footslopes are usually found near drainage lines or rivers and these bare sodic sites are usually close to a drainage line. If the footslope is difficult to determine, and there are no additional criteria present, then the decision tree will identify the site as non-sodic.



Figure 9: Sodic site near Ripape River during the dry season after heavy utilisation by herbivores.



Figure 10: Sodic site near the Ripape River of the KNP during the wet season showing herbaceous cover prior to grazing by herbivores.

2.4.2 Vegetation identified on sodic sites

The vegetation growing on sodic sites is affected by the level of salinity and sodicity in two ways. Salinity affects the nutrient and water availability in the soil. Plant species adapted to salinity are known as halophytes. The physical structure of the soil affects plant root growth and is seen by stunted growth forms of woody plants and even dead tree stumps compared to the same species in the surrounding area. Specific woody species such as *Euclea divinorum* and *Salvadora australis* are commonly found in dense groups on sodic sites, although these woody species may also be found in other vegetation types where they are not the dominant species (Gertenbach, 1983). Woody cover on sodic sites may be sparse, but can also be dense, as found in the Mopani woodlands.

The grass species *Sporobolus ioclados* (Figure 11) is a tufted, stoloniferous perennial grass, adapted to sodicity, grows exclusively on sodic soils (Scholes pers comm.) and is thus an indicator of sodic sites. The inflorescence is a finely branched, open panicle characterised by the centrally whorled branches (van Oudtshoorn and van Wyk, 1999). The leaves are concentrated at the base and are open with a course, thickened edge.



Figure 11: *Sporobolus ioclados* (Pan dropseed) (van Oudtshoorn and van Wyk, 1999).

Other grazing lawn species dominant on sodic sites which may be confused with *Sporobolus ioclados* include *Sporobolus nitens* (Figure 12) and *Tragus berteronianus* (Figure 13). Both these grass species have similar short and wavy leaf blades, which makes identification difficult if there are no visible inflorescences. However, *Sporobolus nitens* is a perennial grass and *Tragus berteronianus* is an annual grass which grows in disturbed areas (van Oudtshoorn and van Wyk, 1999).



Figure 12: *Sporobolus nitens* (Curley-leaved dropseed) (van Oudtshoorn and van Wyk, 1999).

The inflorescence of *Sporobolus ioclados* and *Sporobolus nitens* are similar, but the latter does not have the centrally whorled branches on the panicle over the entire panicle, but rather an alternate configuration after the first whorl. Incorrect identification of *Sporobolus ioclados* may lead to an incorrect identification of sodic sites if used in isolation without looking at the collection of characteristics of sodicity. Correct identification, on the other hand, gives a positive identification of sodic soil, and this a sodic site.



Figure 13: *Tragus berteronianus* (Carrot-seed grass) (van Oudtshoorn and van Wyk, 1999).

2.4.3 Herbivores on sodic sites

Animal activity is often evident on sodic sites in wallows, middens, salt licks and paths and is included in the visible characteristics that contribute to the identification of the sodic site.

2.4.4 Visual Classification Sample Sites

Four classes were identified using this visual classification decision tree: possible sodic sites (woody or bare), river sand, riverine bush and general savanna (crest or midslope). Figure 14 shows the georeferenced sample sites for all classes identified using the decision tree (Figure 8) and listed in Table 3.

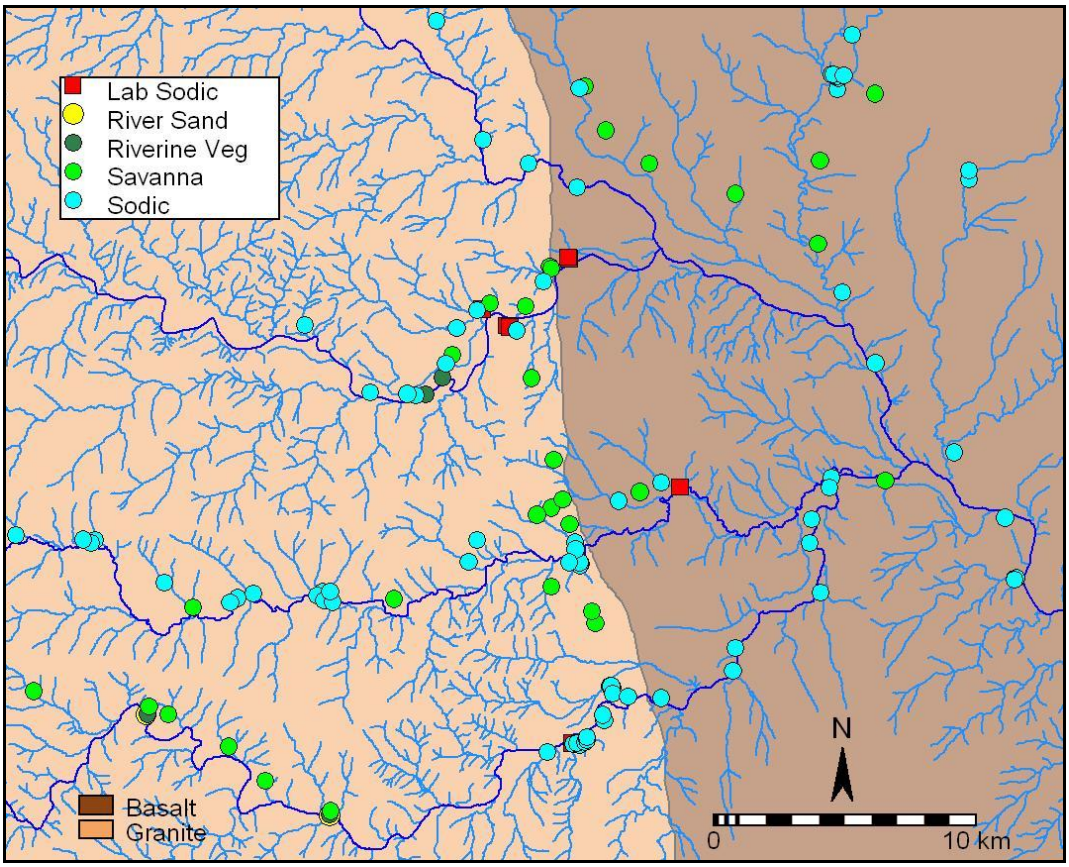


Figure 14: Sample sites in the Shingwedzi River catchment identified using the visual assessment decision tree.

2.5 Field tests for chemical and physical soil properties

Sodic soils express their sodicity as visible characteristics of high sodium, but a rapid assessment soil chemistry test in the field would assist with confirming that the visual characteristics are due to high salts, and in particular, high sodium. There are no in field tests to measure SAR or ESP, but EC, pH and soil physical properties can be tested. Physical soil properties tested include texture, turbidity, slaking and dispersion. If the known sodic soils are identified chemically or physically in the field, then the tests are applied to confirm that a sodic site identified using the decision tree is a sodic soil.

2.5.1 Soil chemistry

Soil samples were taken for each of the training and random sample sites (Table 3). EC and pH were measured using the average of three samples per site. Soil samples were taken from the upper crust of the exposed B-horizon using a flat trowel and analysed once

air-dried (24-48 hours). Electrical conductivity and pH were recorded using the hand held Hanna pH and conductivity meter and the 1:1 soil to water suspension method.

2.5.2 Soil physical properties

The texture class was determined using the ribbon test, where moist soil is rolled into an elongated shape and the percentage clay is estimated according to how flexible the rolled soil is when folded into a horseshoe shape (Thien, 1979).

The turbidity field test for sodicity is based on the turbidity of the water from a 1:5 soil to water suspension (Rengasamy and Bourne, 1997). 500 ml of water is gently poured into a bottle containing 100g of soil without disturbing the soil. The lid is placed on the bottle which is then gently inverted and returned to its original position to stand for 4 hours undisturbed. The level of sodicity is measured by the cloudiness of the water. Clear or almost clear water is non sodic, partly cloudy water is medium sodicity and very cloudy or opaque water indicates high sodicity (Figure 15). The turbidity in the water is due to the dispersion of clays caused by high sodium levels in the soil.



Figure 15: Estimating turbidity using spatula visibility showing non-sodic soil on the left, moderately sodic soil in the centre and strongly sodic soil on the right (Rengasamy and Bourne, 1997).

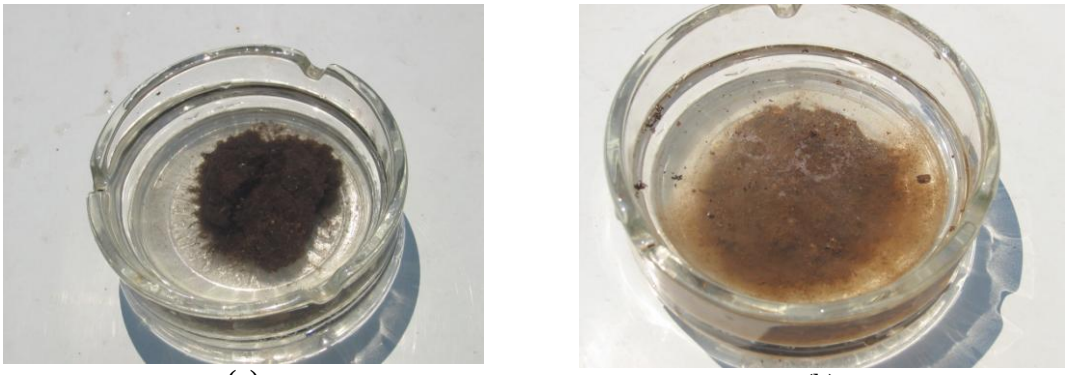
The slaking and dispersion test described by Emerson (1967) has been modified and adapted to test the relationship between chemical test for sodicity and dispersion classes (Vance, McKenzie and Tisdall, 2002). Small, 1 cm sized, air-dried aggregates are gently

immersed in rainwater (saline water is unsuitable) with the soil crust uppermost after immersion, and observed for over 1 minute (Figure 16).



Figure 16: Example of a soil crust sample of the exposed B horizon used for the slaking and dispersion test.

The one-minute slaking and dispersion tests were carried out in the field if soil was dry, as crusts may break during transport. A small aggregate of B-horizon crust about 1-2 cm^2 was gently placed in a container of local water, enough to be submerged. The time for slaking (Figure 17a) and dispersion (Figure 17b) was noted and ranked according to the modified dispersion ratings (Vance, McKenzie and Tisdall, 2002). The results of spontaneous dispersion are scored as follows: none (0); very slight (1); slight (2); moderate (3) and severe (4). Slaking is rated from stable (no disintegration of the aggregate) to unstable (complete disintegration) (Emerson, 1967). If soils were not dry when sampled, the slaking and dispersion tests were only carried out once the soil was air-dried after 48 hours. Wet clay aggregates are quite stable to transport.



(a) (b)

Figure 17: Slaking of the soil crust sample with no dispersion (a) and slaking and moderate dispersion (with a value of 3) showing the cloudy water surrounding the collapsed soil aggregate (b).

2.6 Analysis of results

The results of the chemical field tests of EC and pH will be plotted for each of the visually classified sample sites using the decision tree. EC and pH values are expected to follow the theories of saline and sodic soils described in Chapter 1.

The results from the visually classified sample sites using the decision tree were derived using the attributes collected at each site for soil and vegetation properties. The decision tree, derived from the literature about the visual characteristics of sodic soil, was used to determine the sample class in the field. The attributes noted at each sample site will be statistically clustered using numerical classification or cluster analysis for an objective grouping of the sites. This will test if the decision tree method, including field based soil tests, are reliable to classify sodic sites in the field. The analysis for different combinations of attributes will indicate which of the attributes contribute the most to the in field classification of sodic sites.

The statistical package StatistiXL was used to group sites into a hierarchy of groups using agglomerative grouping based on the similarity of attributes. The output is illustrated as a dendrogram.

3. RESULTS

3.1 Aerial visibility

The aerial survey covered the granitic and basaltic substrate and sodic sites were clearly visible from the air in both geologies, based on the bare areas in relation to drainage lines (Figure 18).



(a) Ripape River sodic sites on granite either side of the drainage line



(b) Rietpan fire break road sites on basalt near drainage line



(c) Sodic sites in drainage line on basalt forming drainage line



d) Sabie River woody sodic sites on basalt with bare soil with small bare patches



(e) Nwatimihri River sodic site south of Skukuza on granite showing road



(f) Large sodic site near Pretoriuskop on granite near river



(g) Near Pretoriuskop fire plots on granite



(h) Near Pretoriuskop fire plots on granite



(i) Small sodic sites near Pretoriuskop on granite



(j) Nwaswitshaka River on granite



(k) Nwaswitshaka River, Skukuza on granite



(l) Near Skukuza flux tower on granite

Figure 18: Aerial photograph taken during November 2006 showing the difference between sodic sites found on granite and basalt geologies and the variation in size, vegetation cover and relationship to rivers and drainage lines.

The sodic sites in the basalts were noted in the drainage lines and were not very different in soil colour from the surrounding area, whereas the sites in the granites showed up in bright contrast to the surrounding areas and were noted next to the drainage lines (Figure 18).

The laboratory tested sodic sites from previous research projects were visually assessed against a SPOT 5 panchromatic image to test whether the sodic sites would be visible on the imagery. Six of Venter's sodic soil sites were on or within 150m of a sodic site, but 2 sites were excluded, as they did not fall into this cut-off distance. All the other sites from previous research corresponded with bright, bare soil near drainage lines and will be used as image classification validation samples on both geologies.

As sodic site samples for this project were selected systematically based on visibility in the field and from imagery, all bare sites were classed as visible on satellite imagery. Sites with over 50% woody cover are more difficult to distinguish from the surrounding savanna sites as the bare soil sodic sites, but these were included as they show the characteristics of sodicity.

3.2 Field tests: chemical and physical soil properties

3.2.1 Electrical conductivity and pH

The electrical conductivity and pH readings were taken at 59 sample sites (Table 3) for all classes to see if the sodic site results would be different from the river sand, riverine bush and savanna classes.

The electrical conductivity readings ($EC_{1:1}$) were converted to a saturated extract equivalent (EC_{se}) using a factor of 2.2 for clay soils (Dobermann and Fairhurst, 2008), which allows for comparisons to be made with other research results. Electrical conductivity and pH results (Figure 19) do not separate the visually identified sodic and savanna samples using the land cover decision tree (Figure 8). Riverine bush appears to have a similar EC on granite to that of sodic sites, but the pH readings vary. From the results the EC and pH readings made in the field were not useful in distinguishing visually sodic from the savanna and riverine bush classes.

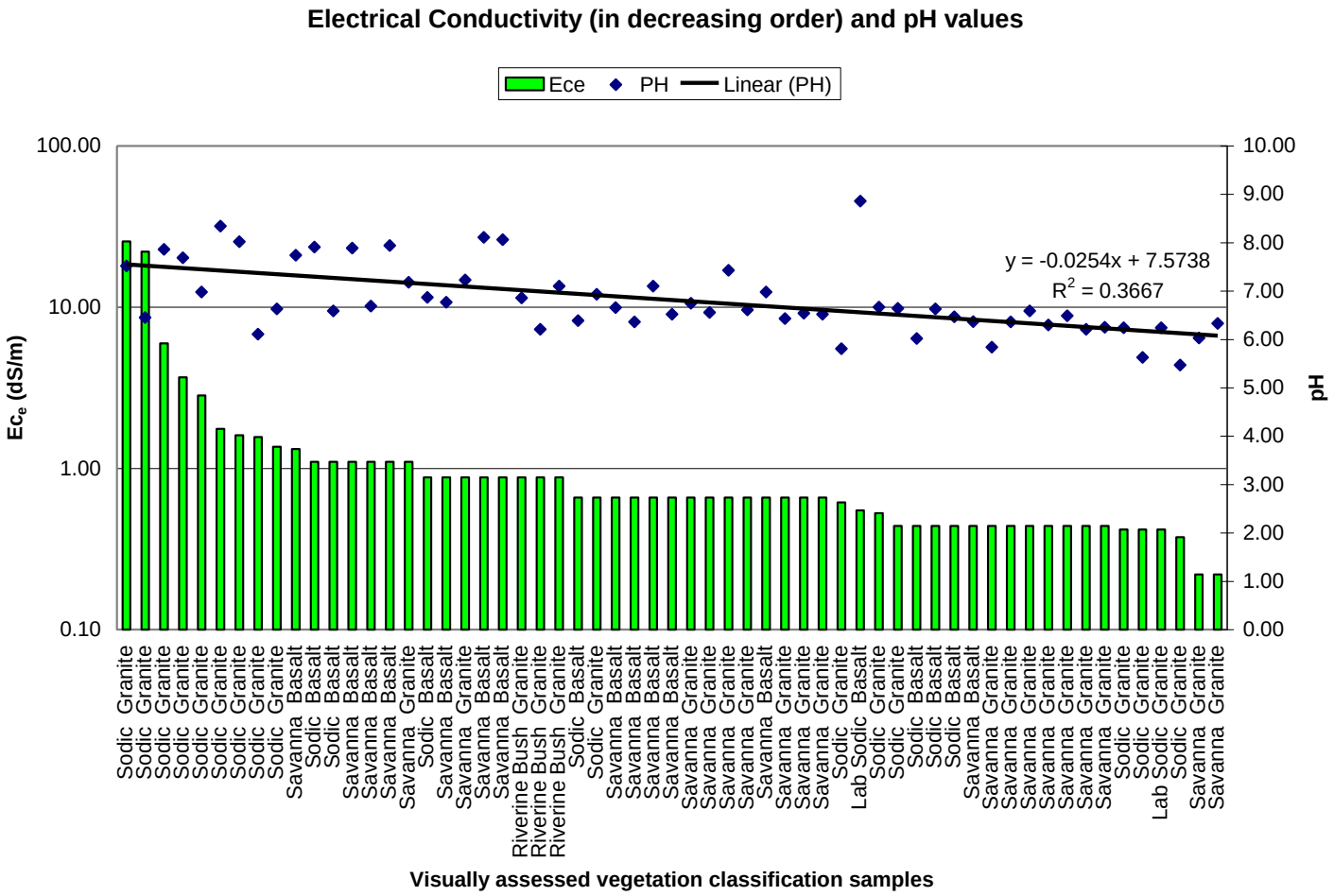


Figure 19: Electrical conductivity (EC) and pH values for sodic sites, savanna and riverine bush sample sites identified using the land cover decision tree for visual classification of sodic sites in KNP.

3.2.2 Turbidity, slaking and dispersion

The turbidity tests (Rengasamy and Bourne, 1997) did not give clear results. The soils swelled very rapidly on wetting and little disturbance or turbidity was observed after gently inverting the container (Figure 20a). The texture class for all samples from sodic sites was medium to high clay, and this high clay content appeared to inhibit the ability of the water to interact with the soil to create any form of turbidity due to dispersion of clay particles. After stirring and resettling after 4 hours, there was only a marginal improvement (Figure 20b). The turbidity test was rejected as a suitable rapid assessment method for dispersion or deflocculation of clays due to the difficulty in assessment and the variability within samples.



(a) (b)

Figure 20: Examples of turbidity test results showing variation of results for 3 samples from the same sodic site and the difference between unstirred (a) and stirred (b) samples. The fourth test in (a) on the right was a combination of the 3 samples on the left.

The slaking and dispersion test was more easily measured on the soil samples than the turbidity test. The slaking and dispersion field test indicates sodicity if the soil crust sample from the B horizon (Figure 16) disperses when in contact with water (Figure 17b).

The slaking and dispersion results from 75 samples (including two river sand samples) were sorted in decreasing slaking class to show the degree of aggregate collapse on wetting (Figure 21). The slaking result reflects the stability of the soil aggregate, but does not indicate the dispersion potential of the clay particles. The dispersion result indicates the presence of sodium in the soil.

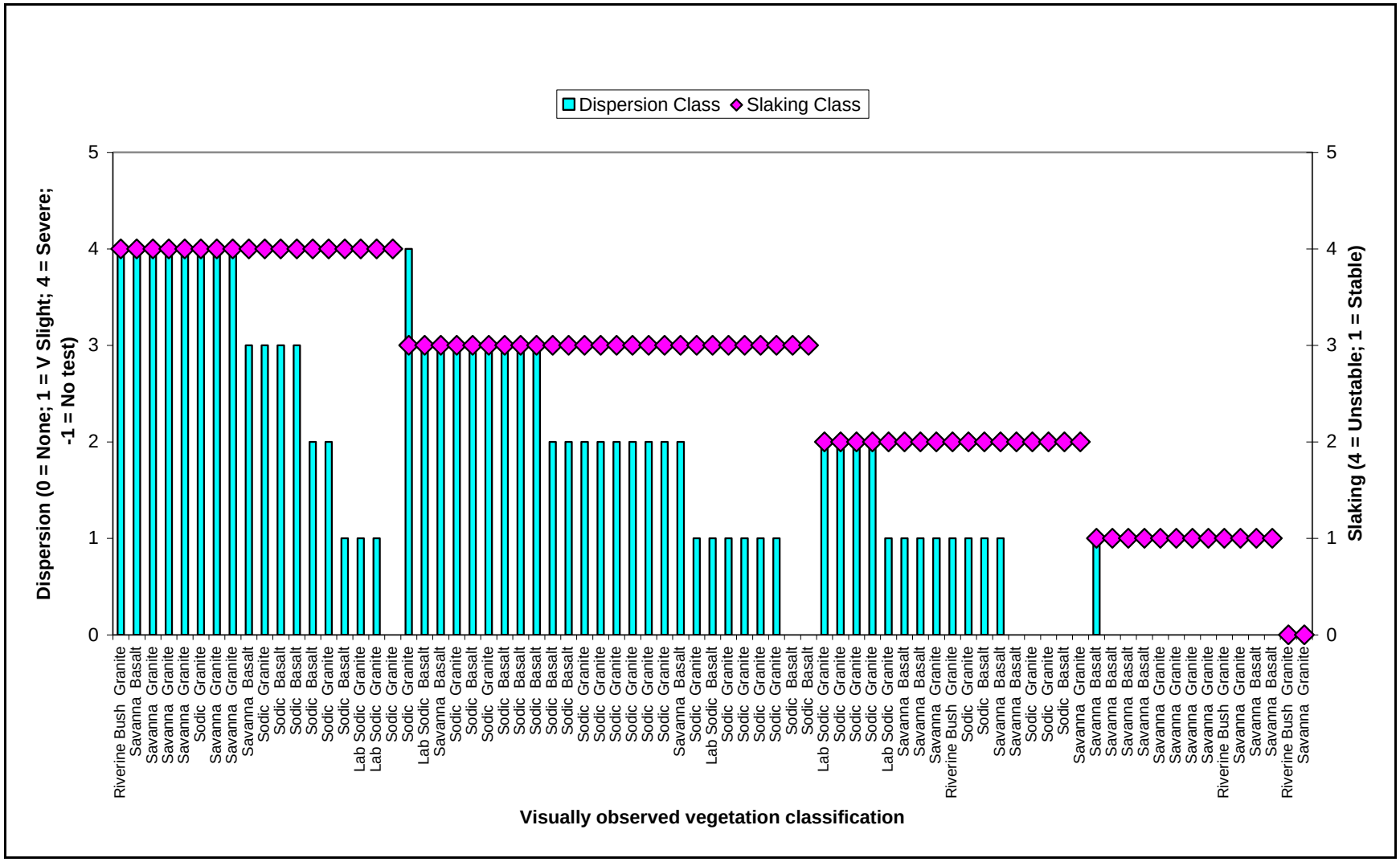


Figure 21: Slaking and dispersion test results sorted by decreasing slaking.

The majority of soil samples (77%) from the visually classified sodic sites were unstable with a value of 3 or 4, including some savanna samples on basalt which were also highly unstable. All six laboratory tested sodic soils sample sites were unstable or very unstable as would be expected on sodic soils. A slaking class of 2 has the most overlap between sodic and non-sodic vegetation types. However, slaking is not confined to soils with high sodium levels and cannot be used to differentiate sodic from non-sodic soils.

When sorted by decreasing dispersion (Figure 22), the results showed a good relationship between high to medium dispersion with sodic sites on granites and basalts. Some sodic sites on granite have only slight dispersion, while there are many savanna sites on basalt which show medium to high dispersion.

All six of the previously studied sodic sites gave positive results of slaking and dispersion for both granite and basalt soils. On this basis, the dispersion test was adopted as a useful indicator of sodic soils for rapid assessment of sodic sites.

A cluster analysis was carried out on all samples where the slaking and dispersion tests were performed (Figure 23) based on the geology and dispersion test results only. No additional criteria were included for the cluster analysis. The results showed that the sodic sites classified using the decision tree criteria were clearly separated from the other classes (savanna, river sand and riverine bush) in the granites.

The cluster analysis grouped the sodic and savanna samples in the granitic areas with two savanna samples grouped with sodic sites, and a similar result for the basaltic areas. The savanna samples have similar dispersion results as sodic sites, but are not visually sodic, possibly due to a high woody component typical of Mopani trees. There are four sodic sites in the basalts grouped with savanna sites, which indicates that their dispersion values were low despite showing visual sodic characteristics and identified as sodic sites from the decision tree.

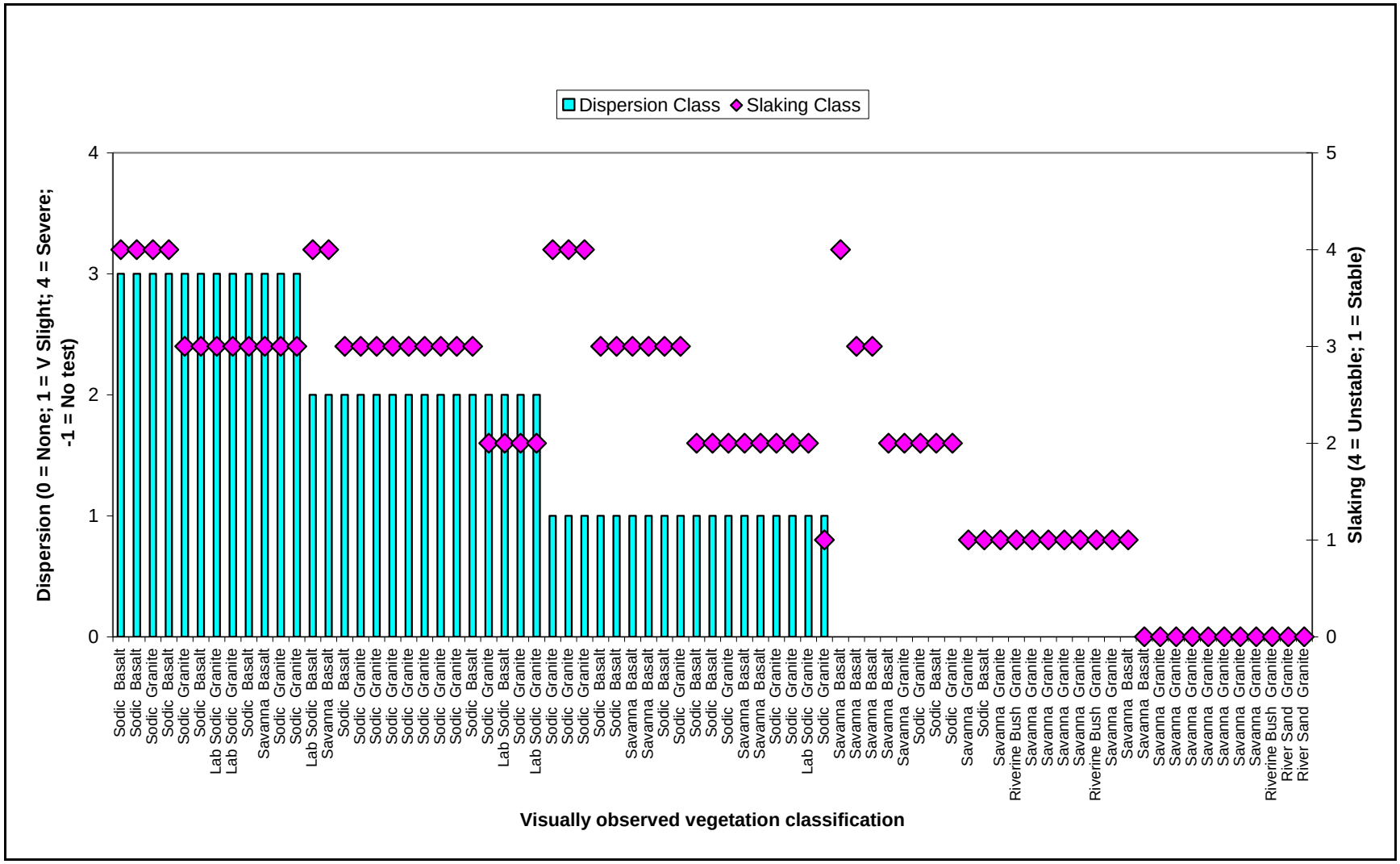


Figure 22: Slaking and dispersion test results sorted by decreasing dispersion

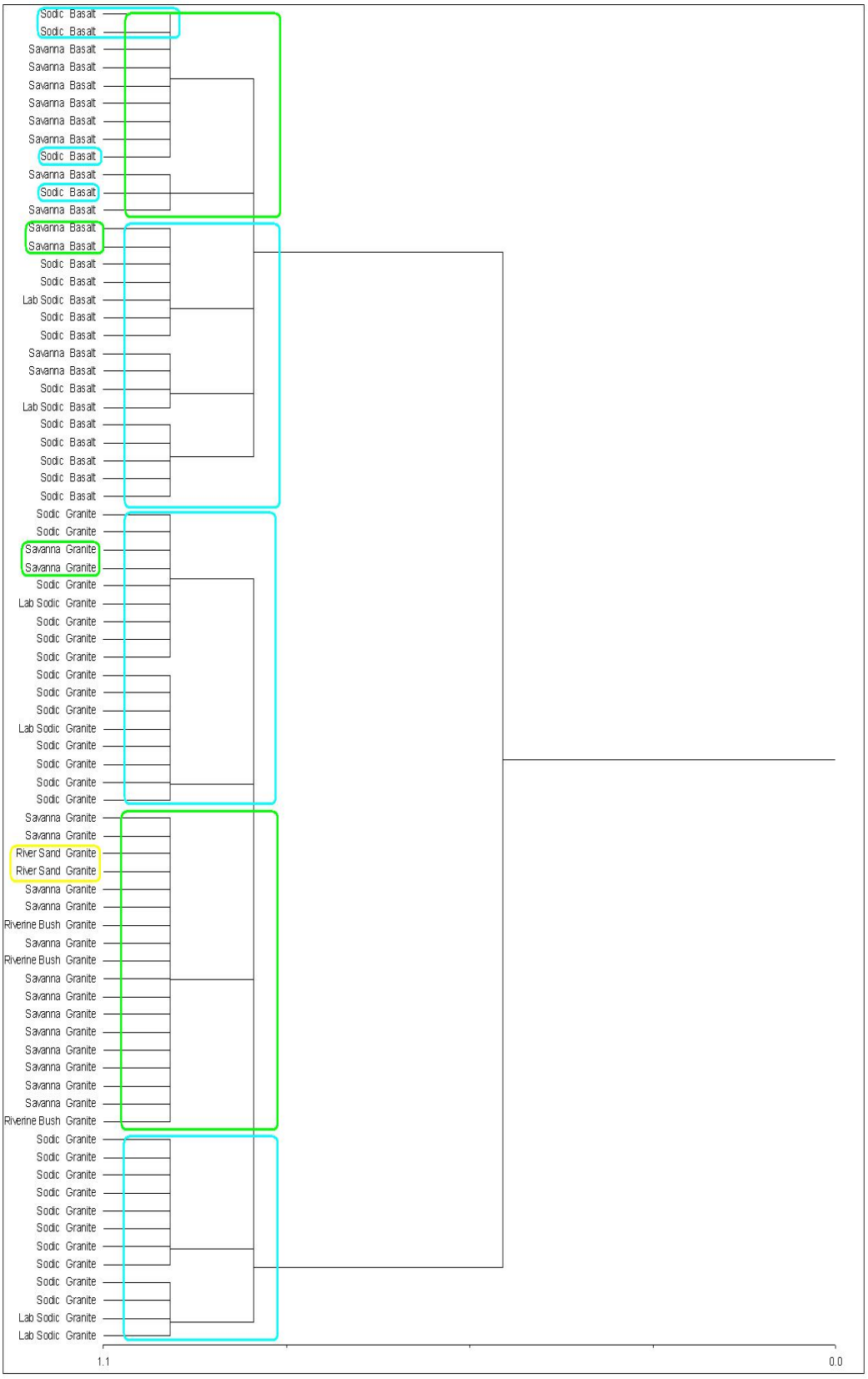


Figure 23: The result of the cluster analysis by geology and dispersion soil test only, giving good separation between sodic sites on granite from other classes and confusion between sodic sites and savannas on the basalts.

3.3 Field tests: observation of visible characteristics of sodicity

The decision tree (Figure 8) was used to classify 150 samples sites into four land cover classes namely: river sand, riverine bush, savanna (on crests or midslopes) and sodic sites (both predominantly bare and woody covered sites). This total included six laboratory tested sodic soils sites from previous research which were identifiable in the field and accessible by road.

The percentage of bare ground is the starting point for the sodic site classification using the land cover decision tree (Figure 8) and the first visual characteristic of sodicity noticed in the field. Figure 24 illustrates the samples sorted by decreasing bare soil percentage. The x-axis gives the result of the class according to the decision tree, and the underlying geology based on the KNP geology division between granites and basalts. The laboratory tested sites are shown with the class name prefix of "Lab". Of the 93 samples sites where percentage bare ground, woody cover and grass cover were recorded, 75 soil crusts were tested for slaking and dispersion of the clay particles.

In Figure 24, the dispersion value of -1 indicates that no slaking and dispersion test was recorded. The presence of the grass species *Sporobolus ioclados* is shown by the green square at the top of the graph.

There is a clear cut-off in bare cover percentage between sodic sites, which have more than 5% bare soils, and the savanna or riverine classes which have less than 5% bare soil coverage. The laboratory tested sodic soil sites classified according to the land cover decision tree are all classified as sodic sites with visible characteristics of sodicity and a spontaneous dispersion class of 3 or 4 (moderate to severe). All sample sites classified sodic based on the presence of *Sporobolus ioclados* had a dispersion value ranging from 1 (very slight) to 4 (severe), while one of the sites with *Sporobolus ioclados* present had a dispersion value of 0 (no dispersion). The geology of this sample was basalt with a very low bare cover percentage which indicates that the dispersion test may not be an effective test for sodicity due to the high clay content of basalt or the grass species was mis-identified. Within the sodic sites, the variability between woody and grass cover is clearly illustrated (Figure 24). The sodic sites in the granites and basalts with less than 30% bare area, but with 50-60% woody cover were dominated by *Colophospermum mopane* and *Salvadora australis.*

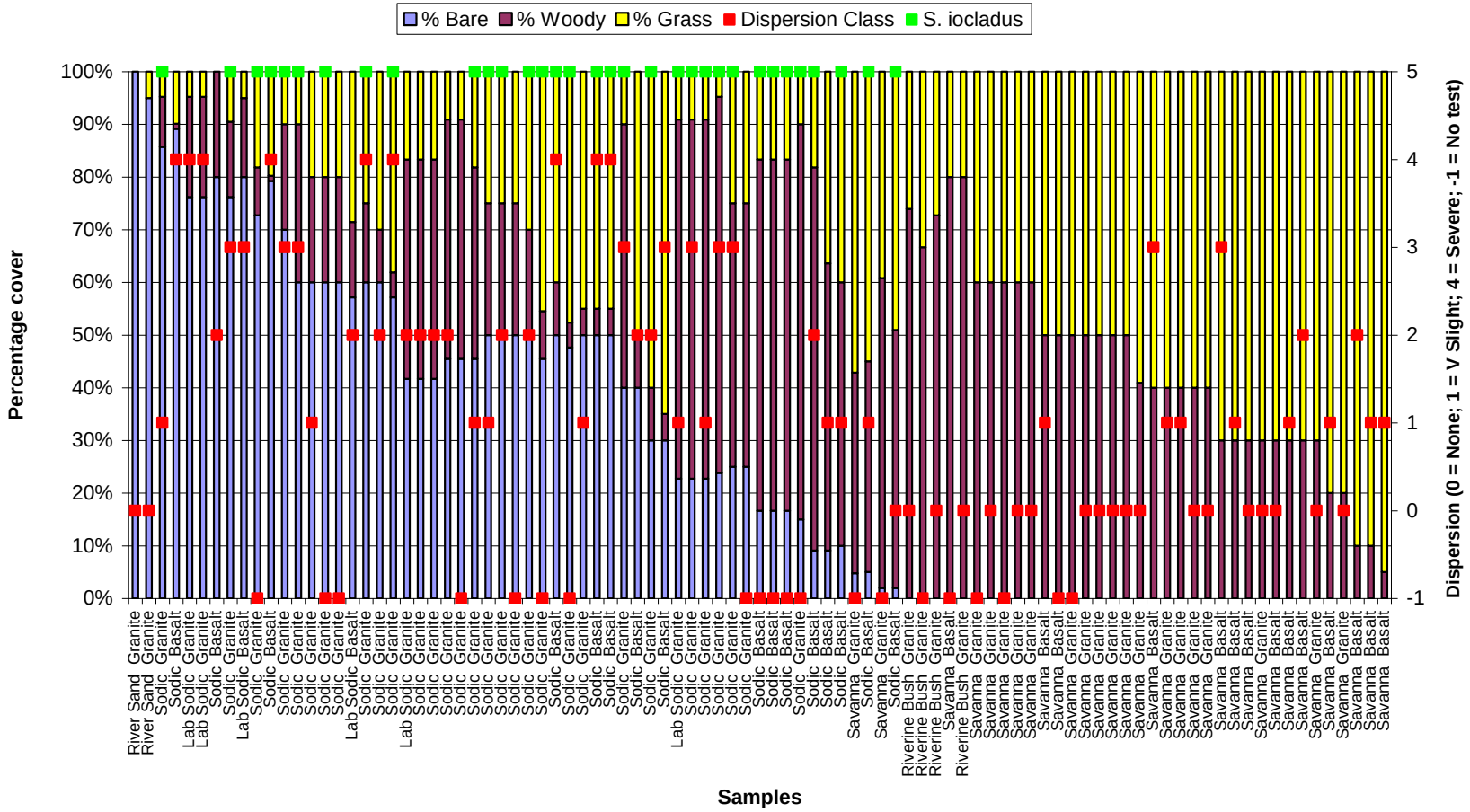


Figure 24: Percentage bare soil, woody and grass cover for both training and randomly selected sites to illustrate the importance of bare soil area as the initial criteria for defining a sodic site.

The visually assessed samples were clustered using a cluster analysis program based on geology, dispersion test, footslope, bare percentage and the presence of *Sporobolus ioclados*. The results show six major clusters where the sodic sites on the granites and the savanna sites on granites were clearly distinguished and were grouped seperately (Figure 25). Some sodic sites on basalt are grouped with the savanna sites on basalt which agrees with the overlap found using the dispersion test on the high clay basalt soils. These are possibly saline soils which do not exhibit sodic behaviour for vegetation. There is some overlap between riverine bush, sodic sites and river sand which is probably due to the topographic definition, as all these classes occur on the footslope. Overall, the cluster analysis result agrees with the results illustrated using the dispersion result and the percentage bare soil (Figure 24).

The sodic sites in the basalt geologies classified using the decision tree are often confused with savanna sites, which may be due to the high clay content. It is possible that basaltic clays disperse at lower levels of sodium than granitic soils without the obvious visible characteristics of sodicity. It appears that additional criteria are therefore more important for accurate assessment of sodic sites on basalt soils than on the granites, where the dispersion test could be enough.

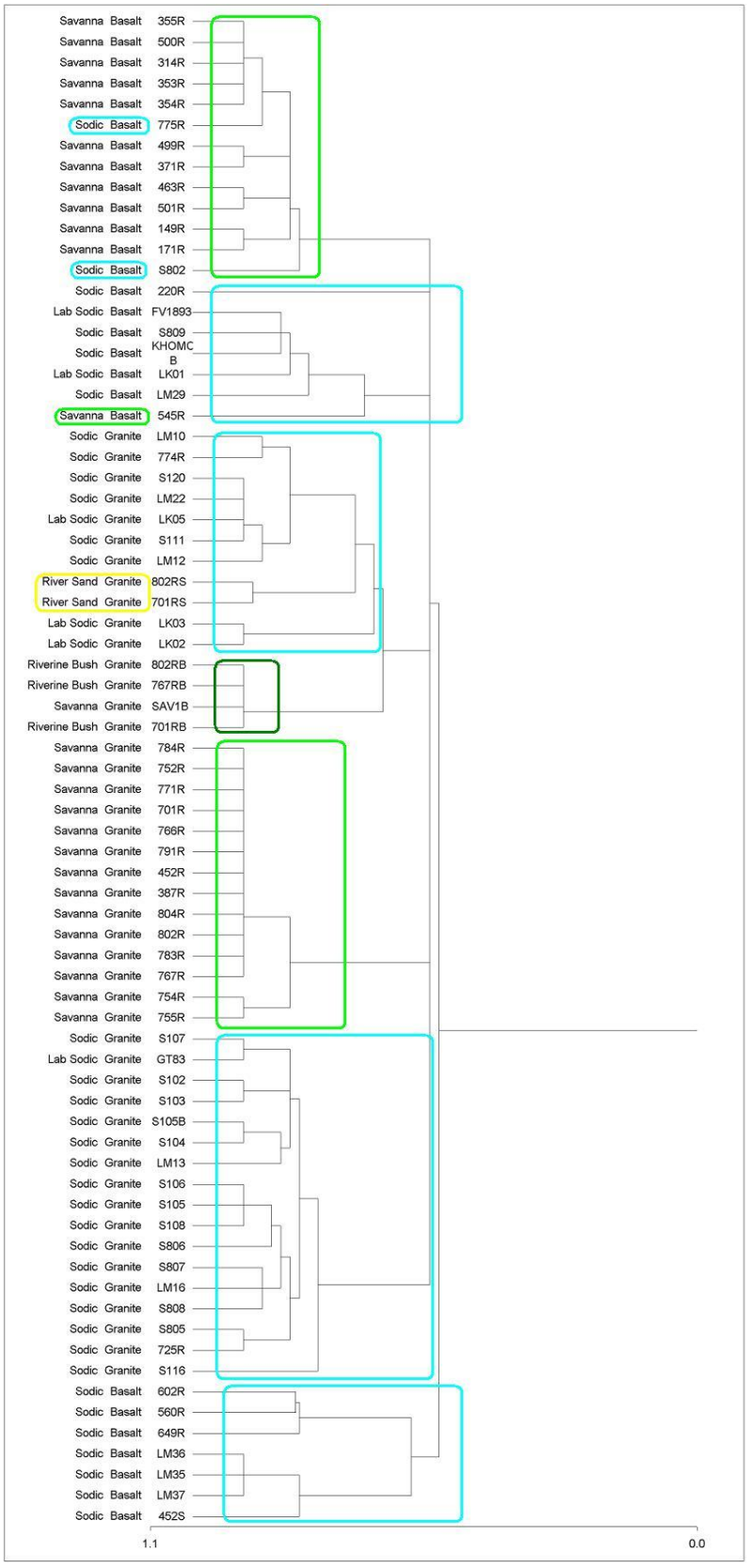


Figure 25: The result of the cluster analysis by geology, dispersion soil test, topography, bare soil percentage and the presence of *Sporobolus ioclados*, giving 6 major clusters.

4. DISCUSSION AND CONCLUSION

A validated map of the sodic sites of the KNP derived using remote sensing image analysis requires ground truth samples for accuracy assessment. There is no escaping the constraints of time, cost and manpower of collecting data over large areas in often inaccessible areas. But, without ground truth data, a classification is not validated (Congalton, 1991) and the user's confidence in the results is limited. Because sodic soils are described by their chemistry, laboratory analysis is expensive and time consuming, and a fast and simple solution is required to collect at least 50 ground truth samples per class.

The Shingwedzi study site was used as the test site for identification of sodic sites in the field as it had more previous data to compare results and logistically the roads in the area allowed for a more comprehensive survey. Validation ground truth samples are therefore only available for accuracy assessment of the Shingwedzi site, and validation samples for the Ripape site will be obtained using random virtual samples directly from the imagery. The visual land cover decision tree (Figure 8) was not tested in the Ripape Study area, but as the substrate is granite, the assumption is made that it would be a suitable test for sodic sites, as for all sites throughout KNP.

Although many of the geo-referenced laboratory tested sodic soil sites from previous research were inaccessible, or inaccurately geo-referenced, there were six sodic sites (three with more than one soil sample) which were confirmed as sodic soils based on soil chemistry. All the six sodic soil sites were classified as sodic according to the visual classification decision tree and the dispersion field test. More of these chemically classified sodic soils would have been desirable for a more convincing result, but based on the results for the sites available, there is no reason to doubt the effectiveness of the dispersion test, especially on granitic soils, to indicate high sodium soils.

Other soil chemistry field tests including the measure for salinity (EC) and soil pH are highly variable within a sodic site and therefore did not assist with the classification of sodic sites without a measure of sodicity. The laboratory tested sodic soils results for pH and EC did not concur with the values for sodic sites in the literature. The recommendation of this research is that texture, pH and EC measurements do not contribute enough to the classification of sodic sites to warrant the time and effort to

perform these tests in the field, although they could be useful to determine whether a soil is sodic or saline sodic based on the EC and pH.

The sample design of the project was based on systematic sampling based on previously researched sites and obviously bare sites along the roads travelled in the study area. Other possible sample sites were identified from imagery and visited to carry out data collection. This is acceptable for training samples, but fails to satisfy the requirement for validation samples, which should be random or stratified random (Congalton and Greene, 2008). As sodic sites cover a small area compared to the other classes, stratification along topography (uplands versus lowlands) would ensure the stratified random selection of sufficient samples. The recommended number of samples per class is 50 but the classes that have less importance in the scope of the project may be less, and the focus class may be more (Congalton, 1991). There were 91 sodic sites samples collected and 50 for the savanna class, but insufficient samples for river sand and riverine vegetation. However, the focus class is well covered and for classification accuracy, the savanna class should be sufficient for detection of confusion between classes. In this project the total of 100 training samples and 50 random testing samples may affect the robustness of the accuracy assessment of the classification, but if enough random virtual samples are collected from the imagery based on local knowledge, this would satisfy the statistical assumptions of the kappa statistic used to compare accuracy. Both error matrix results will be represented in the classification results.

The visibility of sodic sites on the imagery is determined by the geology of the area. Granites soils are light or bright and are clearly visible, whereas basalt soils are darker and often moister and are more difficult to identify on the imagery. The results of the classification of all the sites using the classification decision tree were clearer for the granite samples than for the basalt samples. This is probably due to the high clay percentage in the basalts which will cause dispersion at lower sodium levels than the granites. The implication of this difference in geologies may influence the accuracy of classification on basalts, which is therefore expected to be lower than for granites based on the soil colour.

The visual classification tree was developed to classify sample sites in the field into four classes: riverine bush, savanna, river sand and sodic sites (bare or woody). The ideal class selection requirement for crisp, non-overlapping classes is difficult to define in

environmental systems due to ecotones, and the woody sodic class may be confused with savanna. The criteria for the woody sodic class must therefore include the locality to a bare sodic site for the class to be distinguished from the savanna class.

The first criterion used to define a sodic site is the degree of open ground or bare soil. The topographic position is evaluated to determine if the site is on the crest, mid-slope, foot slope or riparian zone. Additional criteria are evaluated to determine whether the visible characteristics of sodic soils are present. Not all sodic sites will exhibit all the additional criteria. Once the classification result is found, the presence of *Sporobolus ioclados* and a dispersion class of 1 to 4 will confirm the classification of sodic sites. The visual classification of sodic sites including the dispersion test will adequately classify sodic versus non-sodic site. No one characteristic of sodicity is enough to conclusively decide that a site is sodic, but the more characteristics present increases the probability of correctly classifying sodic sites.

The implications of these results for remote sensing image analysis of sodic sites is that the rapid assessment methods to identify sodic sites in the field allow for a 15 minute in field classification including a 1 minute dispersion soil test to confirm the result. The time taken to get from one site to another is still the major restriction on number of samples collected in a day. The robustness of the validation accuracy assessment results will be affected by the sampling design due to the difficulty in collecting random samples in an environment where access to sites is a challenge. The increased number of samples due to ease of visual classification on the ground should compensate for the lack of true random sampling design.

In conclusion, the visual assessment of a site in the KNP using the decision tree developed from the characteristics of sodic soils described in the literature, together with the result of the dispersion test of the soil crust of the B horizon, will give a reliable in field land cover classification into sodic or non-sodic sites on granites, but less reliable on basalts.

CHAPTER 3

CLASSIFICATION OF SODIC SITES

1. INTRODUCTION

Researchers in the KNP require a validated map of sodic sites for the entire park to attempt to answer management questions regarding the possible effects of nutritional hot spots on herbivore movements (Grant and Scholes, 2006). KNP is almost 2 million hectares in extent with large areas which are not accessible by road.

Previous attempts to classify sodic sites in the Shingwedzi River catchment used Landsat ETM+ 30m multispectral and 15m panchromatic imagery. The acquisition of SPOT 5 high resolution satellite imagery for the entire extent of the KNP in 2007 makes remote sensing a feasible option for the identification of sodic sites throughout the park at 10m or 2.5m resolution. Classification of sodic sites is expected to be more accurate at a smaller scale. This project will classify sodic sites at a much higher spatial resolution than before and test the transfer of the classification algorithm to imagery covering the entire KNP. An automated or at least, semi-automated algorithm will be tested.

Pixel-based classification was applied in the northern KNP on Landsat 7 ETM+ 15m panchromatic images acquired in May 2000 (Mathys and Wessels, 2001). Pixels classified as bare which were not near a river or a footslope were manually excluded from the sodic site class. Pixels have no relationship to each other (topology) in pixel based classification and are based only on the spectral properties of the pixel. Object based classification of the riparian boundary in the Shingwedzi catchment was undertaken using Landsat 7 ETM+ imagery acquired in June 2000, October 2000, May 2001 and September 2001 (Saah, 2004). Sodic sites where identified from bare surfaces using the tasselled cap transformation which calculates three indices namely brightness, greenness and wetness. The spatial resolution of Landsat imagery is 30m, so only large sodic sites would be identified and smaller sodic sites should be identified using higher resolution imagery (eg. SPOT 5 10m). The classification accuracy will be assessed using a

validation process so that the resultant map of sodic sites can be used for management decisions and other research questions.

Chemical properties of sodic soils are not detectable from medium to high resolution imagery, but the bare patches with sparse to no vegetation cover are visible on aerial photography and satellite imagery as high intensity or bright pixels and are used to separate bare areas from senescent or vegetated areas in very high resolution imagery (Laliberte, Rango and Fredrickson, 2006) . The normalised difference vegetation index (NDVI) is widely used to map vegetation greenness and soil bareness. Energy in the red band is absorbed due to photosynthetic activity of plants and reflected in the NIR band due to leaf structure (Lillesand, Kiefer and Chipman, 2004). The fractional cover of trees, grass and bare soil in savanna ecosystems have been estimated using NDVI at the regional scale (Scanlon *et al.*, 2002). The NDVI is based on the normalised reflectance value of the imagery and in order for results from different images to be comparable, radiometric correction to top of atmosphere (TOA) or top of canopy (TOC) reflectance is essential. All images used in this study were pre-processed to TOA reflectance values before classification algorithms were applied.

The vegetative cover of sodic sites is dependant on season, rainfall and herbivory. MODIS satellite imagery provides a high temporal record of the normalized difference vegetation index (NDVI) values over large areas and is used as a measure of variability in season phenology for the specific area under study. NDVI time series have been used to analyse time series and ecosystem processes (Lhermitte, Vwebesselt, Jonckheere, Nackaerts, van Aart, Verstraeten and Coppin, 2008) and produce a phenological classification of the vegetation of South Africa at the biome scale (Hoare and Frost, 2004). MODIS NDVI was used in this study to place the imagery in a phenological phase to understand the expected vegetation cover of sodic sites at the time of acquisition. Additional input data was used to determine the topographic position of the bare patches. The SRTM DEM was included to determine the footslopes of catenas, where sodic sites are expected to be found, and the vector river layer assised with the location of the drainage lines.

Four sodic sites were studied on the Ripape River, where satellite imagery and aerial photography from 1944 to 1985 was used to detect possible changes in the size of sodic sites (Chappell, 1992). The classification algorithm developed for the Shingwedzi study

site will be applied to the imagery for the Ripape study site to classify sodic sites in the Ripape River catchment.

The aim of this study is to apply object-based classification techniques to digital imagery that will be repeatable, semi-automated and applicable for the entire KNP. In order for the classification algorithm to be repeatable, the imagery must be suitable in terms of spatial resolution (minimum mapping unit), spectral separation (class separation) and temporal resolution to test the effect of seasonal phenology on the classification of sodic sites. A repeatable algorithm will be used to classify different areas of the KNP as new imagery becomes available.

2. METHODS

Classification methods used for digital image analysis are divided into four basic steps: class selection and collection of ground truth data; selection and further processing or normalization of available imagery to be used in the classification; development of the classification methods and iterative testing of accuracy against training ground truth samples; and finally, validation accuracy assessment of the classification using validation ground truth samples. The methods applied for class selection and ground truth sample collection for validation are described in Chapter 2.

The following steps will be used to classify sodic sites from multi-spectral imagery:

- Selection of imagery for the training study site specifically and imagery for all of the KNP in general
- Assessment and selection of imagery in respect to spatial, spectral and temporal resolution
- Perform pre-processing on imagery to normalise data and create derivative products to improve classification of sodic sites
- Assessment and selection of imagery in terms of class separation using spectral signatures and seasonal effects
- Include derivatives from imagery and other ancillary data (DEM, vector layers etc).
- Apply object-based classification methodologies (iterative process):
    - segmentation and hierarchy of segmentation
    - classification using a process tree suitable for automation

    - accuracy assessment for training
    - re-classify to improve accuracy
- Validation using ground truth samples
- Apply classification methods developed on training site to second study site and all of KNP and accuracy assessments to validate results

2.1 Study site

In order for a methodology to be developed for a repeatable classification of sodic sites over the entire KNP, a smaller test or training area is selected to validate the classification methods. The selection of two study sites in the KNP was based on the areas where previous research had identified sodic sites in the field (Chappell 1992; Khomo 2003; Mathys and Wessels, 2001; Teren, 2004; Venter, 1990) (Figure 26). The second study site is the Ripape River catchment on the western border of the KNP, where four sodic sites on the Ripape River were studied by Chappell (1992).

Ground truth data was collected for the Shingwedzi River catchment study site in the north of KNP (as described in Chapter 2), and was therefore selected as the training area for the classification algorithm for sodic sites. The Ripape study site was not sampled for ground truth validation, as for the Shingwedzi study site, as there were only four laboratory tested sodic sites without georeferences for the exact sites. The classification methods developed in the Shingwedzi training area were applied to the Ripape River study site to test whether the same algorithm developed can be used to identify the four known sodic sites identified by Chappell (1992). The same classification algorithm will be applied to classify sodic sites for the KNP as a whole.

2.2 Data Input

2.2.1 Satellite and Airborne Imagery

The KNP provided this project with Landsat 7 ETM+ (see Appendix II), ASTER (see Appendix III), and SPOT 5 multi-spectral satellite imagery (see Appendix IV), black and white ortho-rectified aerial photographs (see Appendix V), Carnegie Airborne Observatory (CAO) hyperspectral and LiDAR airborne imagery (see Appendix VI). The

digital elevation model (DEM) (see Appendix VII) and MODIS NDVI imagery (see Appendix VIII), were sourced independently. These standard products where not acquired specifically for the classification of sodic sites, but the imagery available was used where applicable.

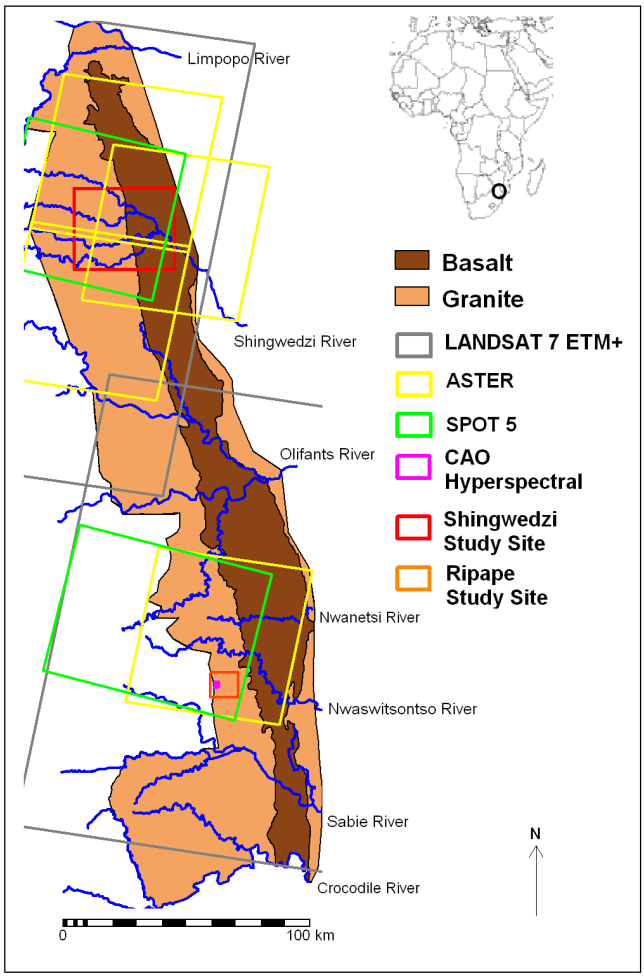


Figure 26: Shingwedzi River catchment study site and Ripape River catchment study site showing available digital imagery coverage per site

Spatial coverage

The multi-spectral satellite imagery available for the KNP falls into two categories: imagery for selected areas of the park and imagery which spatially covers the entire extent of the park. Imagery covering the Shingwedzi River catchment study area includes Landsat 7 ETM+, ASTER and SPOT 5 multi-spectral satellite imagery, and black and

white orthophoto airborne imagery (Figure 26). Imagery covering the Ripape River catchment study area includes Landsat 7 ETM+, ASTER and SPOT 5 multi-spectral imagery and the CAO hyperspectral and LiDAR airborne imagery strip (Figure 26). The CAO LiDAR imagery is the first high resolution height data available for this research area.

Classification of sodic sites for the entire KNP requires a repeatable image analysis algorithm over all the images which cover the KNP. Only the Landsat 7 and SPOT 5 imagery cover the whole KNP. Two Landsat 7 ETM+ images cover over 90% of the KNP which allows for classification of sodic sites over the entire park using the images from path 168 and row 77 and path 169 and row 76 (Figure 26). SPOT 5 imagery is also available for the entire KNP (Figure 26). MODIS NDVI imagery and the SRTM DEM are available for the entire KNP.

Spatial resolution

The spatial resolution for the multi-spectral imagery selected for this project based on spatial coverage includes medium resolution imagery (30 m Landsat 7 ETM+ and 15m ASTER) and high resolution imagery (10 m SPOT 5). Panchromatic imagery for the respective multi-spectral imagery is 15 m Landsat 7 ETM+ and 2.5 m SPOT 5 and is included into the classification algorithm for a higher resolution classification result similar to the results obtained from pan-sharpened imagery. The very high resolution CAO hyperspectral imagery has a spatial resolution of 1.12m, and the black and white aerial photographs a resolution of 0.86m.

Spectral resolution

Spectral resolution refers to the number of bands recorded per sensor and the band width spread from ultra-violet to the longer short-wave infra-red bandwidths. Multi-spectral sensors, including Landsat 7 and ASTER, record in the electromagnetic range from visible to short-wave infra-red wavelengths over 2000nm. SPOT 5 excludes the blue range in the visible wavelengths and the SWIR in the near-infra red bandwidths greater than 2000nm. The CAO hyperspectral imagery records 72 bands in the visible to near-infrared bandwidths, excluding the mid-infrared and short wave infrared ranges. The imagery selected for classification of sodic sites in the KNP showing spatial resolution and spectral bands are summarised in Figure 27.

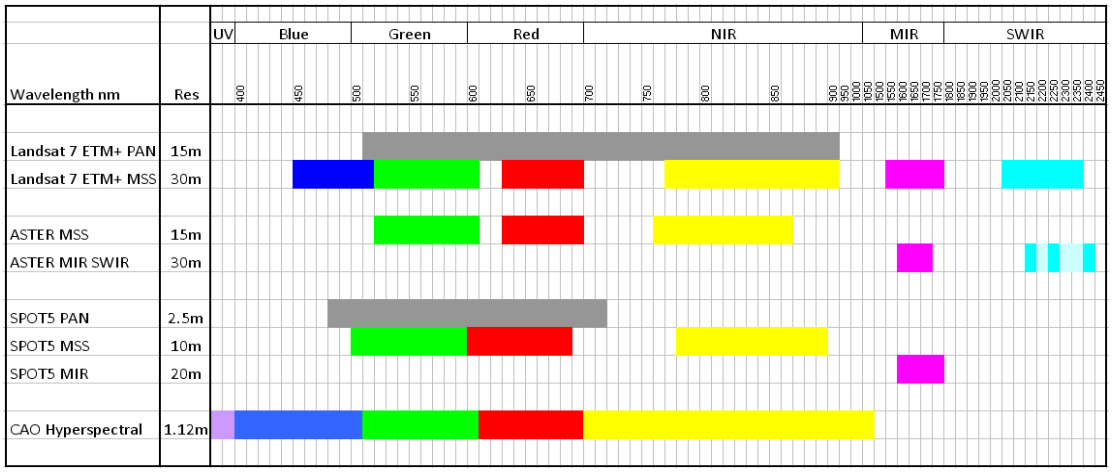


Figure 27: Comparison of the different sensor spatial resolutions and bandwidths of digital imagery selected for the project (yellow, purple and turquoise represent the non-visible bands). The CAO hyperspectral imagery consists of 72 bands which fall within the ultra-violet, visible and near infra-red bands (Appendix VI for detailed band widths).

MODIS NDVI imagery has a 250m spatial resolution and the SRTM DEM with a 90 m resolution is available for full coverage of the KNP.

Temporal resolution and acquisition dates

MODIS NDVI imagery has a very high temporal resolution providing a composite image every 8 or 16 days. The spatial resolution, however, is 1km to 250m, depending on the product, but the high temporal resolution makes it a useful product for phenology studies.

Landsat thematic mapper sensor (Landsat 5 TM) imagery, collected on a systematic basis, is available from 1984 to the present. Landsat 7 ETM+ imagery is available from 1999, when the satellite was launched. On 31 May 2003 the scan line corrector (SLC) on the satellite malfunctioned and since this date all imagery has been supplied as SLC-off mode with areas of missing data seen as stripes across the scenes. The areas between the gaps still provide useful data. All SLC-on archive data (up to 31 May 2003) is now freely available for download from the USGS website. Landsat 7 has a re-visit period of 16 days, and 18 days for Landsat 5, and the sensors record continuously. The KNP has a large number of Landsat images in the archive from both sensors from previous projects.

ASTER imagery is available from 1999 (launch date) with a revisit period of 16 days, only on request, so the archive is dependant on what scenes were requested in the past. The KNP has some imagery from 2005 and 2006 for sections of the park but additional cloud-free scenes could be sourced if available from the imagery supplier. The SPOT 5

imagery is also recorded only on request and the satellite has a revisit period of 26-days. KNP archive has SPOT 5 imagery for each scene in the park from 2005 to 2008, but not all areas of the park were recorded on the same date, or even the same season, however the spatial coverage is an important factor in favour of the SPOT 5 data set. Hyperspectral imagery was acquired for the KNP on airborne platforms during April 2008 and therefore has a low temporal resolution with limited coverage of the KNP.

The satellite and airborne imagery available for this project is summarised in Table 4.

Table 4: Summary of acquisition dates for satellite and airborne imagery available for the Shingwedzi and Ripape River catchment study sites, and full KNP coverage.

Study Site	**Satellite Imagery**			***Airborne Imagery***	
	Landsat 7 ETM+	**ASTER**	**SPOT 5**	**Orthophoto (black and white)**	***CAO Hyperspectral and LiDAR***
Shingwedzi	21/05/2001	01/04/2006 29/06/2006	05/10/2005 12/04/2008	May 2001	-
Ripape	30/05/2001	26/06/2005	26/03/2006 12/05/2006	-	*25/04/2008*
KNP	*USGS archive 1999 to 31 May 2003*	-	*Above plus 16/12/2005 20/09/2005 16/03/2006 11/05/2006 17/05/2006*	-	-

2.2.2 Image normalisation and pre-processing

If a classification algorithm is to be developed on one training study site and then applied to imagery in a different area of the KNP, the input data must be converted to reflectance values based on the angle of the sun at the time of acquisition, called radiometric correction or normalisation. If normalisation is not implemented, any results will be scene specific and not transferable to other scenes if classification is based on spectral signatures.

Geometric and radiometric pre-processing of the satellite imagery was implemented for each sensor based on the level of pre-processing performed by the supplier (see Appendix IX for detailed explanation). The level 1G Landsat 7 ETM+ images, downloaded from the USGS website[4], were pre-processed using Erdas Imagine 9.2 models. The 8-bit scaled digital numbers (DN) were converted to top of atmosphere (TOA) radiance using

[4] http://eros.usgs.gov/#/Find_Data/Products_and_Data_Available/Satellite_Products

the bias and gain values from the metadata file supplied with each image (Appendix IX). The TOA radiance was converted to TOA reflectance using the sun geometry values for each scene. The SPOT 5 imagery was provided as Level 3 orthorectified 8-bit scaled DN images. The imagery was pre-processed to TOA radiance using the bias and gain values supplied in the metadata file with each image, followed by the conversion of radiance to TOA reflectance using the sun geometry factors (Appendix IX). No atmospheric correction was made to the cloud free Landsat or SPOT scenes due to the complexity of implementation and possible additional error greater than the atmospheric effects themselves (Baraldi *et al.*, 2006). The ASTER imagery was Level 2 AST09, atmospherically corrected, surface radiance data. The radiance values were converted to reflectance based on the sun geometry at the time of acquisition (see Appendix IX). The CAO hyperspectral imagery was received in ENVI file format, including a header file, orthorectified, georeferenced and atmospherically corrected. No further pre-processing was performed on this data. MODIS NDVI imagery is atmospherically corrected and no further pre-processing was performed on this data.

Landsat 7 and SPOT 5 imagery panchromatic imagery was pre-processed to TOA reflectance, but not pan-sharpened (pan-merged or fused) with the multi-spectral imagery to avoid any loss of the original multi-spectral values. Definiens Professional is able to include the higher resolution imagery in the classification algorithm by re-sampling the lower resolution imagery to the higher resolution of the panchromatic images.

2.2.3 Additional layers (derivatives and ancillary data)

Derived images were produced for each of the sensors, including NDVI, PCA, tasselled cap (Landsat only) and statistical cluster analysis (unsupervised classification or ISODATA), as additional layers for improved interpretation of the suitability of the imagery and classification of sodic sites. The very high resolution orthorectified black and white aerial photographs over the Shingwedzi River catchment site will be used to visually identify accuracy assessment training samples. Additional vector layers were included for interpretation and visualisation of the classification results including the KNP boundary, main rivers and tributaries, and roads.

2.3 Pre-classification imagery assessment

Normalised imagery is expressed as top of atmosphere (TOA) or top of canopy (TOC) reflectance and well calibrated normalised imagery will give a more repeatable classification (Baraldi *et al*., 2006). To check the result of reflectance calculations the spectral signatures of invariant objects such as deep water, roads or runways should be comparable to standard spectral signatures of spectral libraries supplied by the USGS or some software packages (eg ATCOR Calibration files) (Geosystems, 2006). The spectral signatures can also be used to indicate how well the imagery will distinguish between the classes selected for the classification process.

2.3.1 Spectral signature investigation

To gain an understanding of how clearly the spectral signatures for the selected classes represent the classes to be identified, ten typical samples (pixels) were selected for each of the classes (visible sodic sites, river sand, green dense trees, grassland and water) using the spectral profile tool in Erdas Imagine 9.2. The spectral signatures of visually selected pixels are compared to the relative value of reflectance for each band described in Table 5. The results will indicate whether the radiometric corrections or normalisation resulted in comparable signatures for invariant objects such as deep water, and if not, then the calculation applied may not be correct.

Table 5: Spectral signature descriptions based on the relative value of reflectance values for each band (adapted from Baraldi *et al*., 2006)

Class	***Description of typical spectral signature***
Bare soils	*spectral signatures with low reflectance values in the blue band, increasing in the green, red, NIR and MIR bands, decreasing in the SWIR bands*
Dry grassland or senescent foliage and bare soil	*spectral signatures with lower reflectance values in the red than green bands (or equal), NIR and MIR bands, decreasing in the SWIR bands*
Savanna or green grassland	*spectral signatures with lower reflectance values in the red than green bands (or equal), peaking in the NIR band (red edge) and decreasing in the MIR and SWIR bands*
Green trees or dense foliage	*spectral signatures with lower reflectance values in the red than green bands, peaking in the NIR band (red edge) and decreasing in the MIR and SWIR bands*
Water, shadow or burn scars	*spectral signatures with the highest reflectance values in the blue band, decreasing gradually in the green, red, NIR and MIR bands, decreasing less obviously in the SWIR bands*

2.3.2 Class separation

As described in Table 5, the spectral signatures for water, shadow and burnt vegetation are similar in their relative relationships between the visible and infra-red bands. Although these classes may appear visually separate on the image, spectral properties alone will not be sufficient to separate the classes and ancillary data will be required to improve the classification. To investigate how easily sodic sites will be to classify using spectral properties alone, a statistical clustering of spectral signatures, also called unsupervised classification or the ISODATA algorithm, was performed. Each image was clustered using the ISODATA algorithm (Erdas 9.2) into a maximum of 75 classes and the average spectral signature per class was compared to the spectral signatures of known sodic sites in the image. The grouping tool of Erdas Imagine 9.2 was used to group the 75 classes into five land cover classes based on visual appraisal of the image and the classes used for the spectral investigation described above (Table 5).

2.3.3 Seasonal context of imagery

Sodic sites consist of areas of bare soil where no vegetative growth occurs due to crusting or high levels of sodium, interspersed with vegetated patches where the soil of the A horizon is not eroded. During the wet season these vegetated patches, which could cover a large proportion of the sodic site, may be covered by dense grass stands. Seasonality and the variability in the phenological stages between years must be taken into account when using digital imagery for the classification of sodic sites. As rainfall patterns vary between years, it is not always useful to compare anniversary dates, but rather dates of similar phenological stage in similar seasons with similar rainfall. Classification of vegetation classes for a large area is affected by seasonal variability within the area, and semi-automated classification algorithms must be tested on images from different phenology stages (wet or dry season). The MODIS NDVI 16-day composite imagery allows for a phenological interpretation of the imagery used to classify sodic sites.

Although SPOT 5 imagery is available for the whole of the KNP, the dates of acquisition do not fall within the same season or the same year, and the effect of this seasonal difference on the classification of sodic sites must be assessed if a classification algorithm is to be repeatable for the whole park. To get an overall understanding of the phenological variability between the scenes within the KNP, the MODIS NDVI dataset from February 2000 to May 2008 for KNP (191 layers) was clipped for each Landsat 7 ETM+ and SPOT 5 scene within the KNP boundary, i.e. an area with a similar ecological

management strategy with similar land use (Figure 28). The mean NDVI values for the area of KNP covered by the imagery were plotted for each 16-day composite provided by the MODIS data to produce a phenology cycle graph. The date of acquisition of each image was noted on the NDVI cycle to indicate the season at which the image was acquired and for comparison with the season of acquisition of other images. In this way, classification algorithms can be developed, and tested using accuracy assessment, for different seasonal stages if necessary.

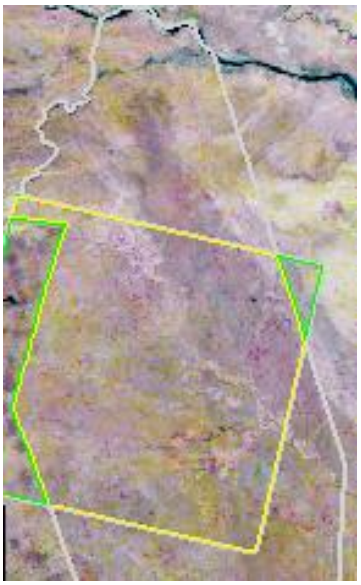


Figure 28: MODIS NDVI 250m imagery showing the SPOT 5 scene for the Shingwedzi study site area within the KNP boundary as a yellow polygon. The mean NDVI for this polygon over each 16-day composite for 9 years was used to calculate a phenology cycle graph.

2.4 Object-based image analysis (OBIA): Classification of sodic sites

Object-based image analysis (OBIA) is a digital image classification technique where pixels are grouped into objects based on homogeneity of the pixels in the input layers selected, and classified according to knowledge of the relationships between objects as neighbours or in a hierarchy of objects. The OBIA for this project was implemented using eCognition (Definiens Developer) software. The three basic stages of OBIA are segmentation into objects, classification into semantic classes and accuracy assessment. This is an iterative process until the required classification accuracy is reached.

The following classification workflow was applied to all imagery at all study sites:

- identify land cover classes
- input multi-spectral, pan chromatic and additional derived raster and thematic layers
- segmentation of layers
- object-based image analysis (classification algorithm development)
- accuracy assessment using visually interpreted samples from imagery
- iterative repetition of segmentation and object-based image analysis
- final validation using field ground truth reference samples
- export results of sodic site classification to vector layer

The classification algorithm developed in the Shingwedzi study site will be applied to the Ripape study site and the whole of KNP for Landsat 7 and SPOT 5 imagery.

2.4.1 Class selection and decision tree outline for classification of sodic sites

The classes selected for the identification of the ground truth samples in Chapter 2 are used for the classification of sodic sites in the object-based image analysis in a class hierarchy (Figure 29). In order for the accuracy assessment to have meaningful overall accuracy results it is necessary to classify a number of general and closely related classes to identify areas of confused classification (hence the confusion matrix).

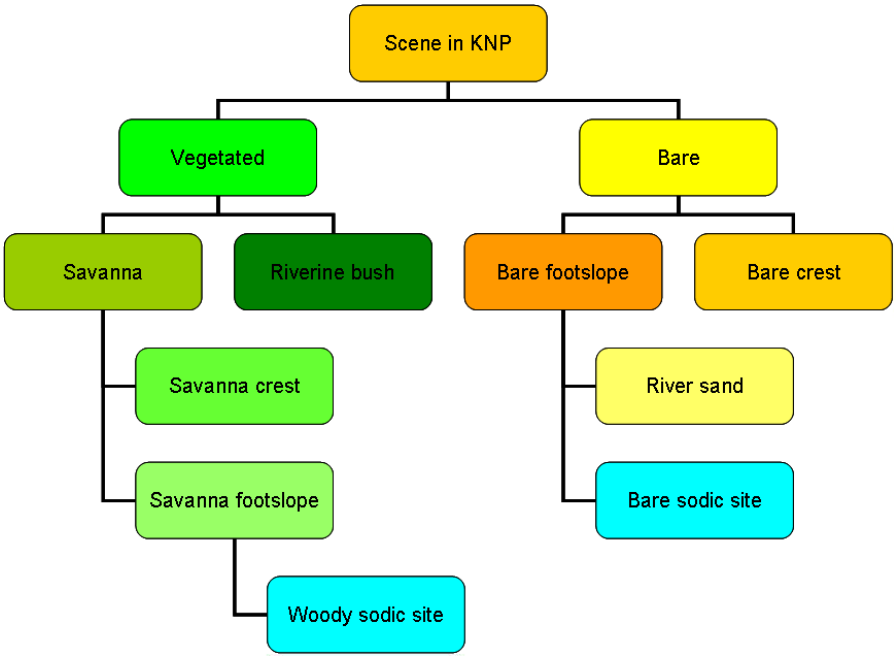


Figure 29: Hierarchy of classes for image classification based on the vegetation cover and topographic location as applied in the classification algorithm work flow.

The class hierarchy used to classify sodic sites is based on vegetation cover and bare soil on the footslopes of catenas. As the primary split in the hierarchy is to detect bare versus vegetated land cover classes, the NDVI and bare soil index are included in the input layers of the object based image analysis (OBIA). The topographic position of bare footslopes and bare crests was determined using a DEM and the vector river layer from the KNP was used to confirm drainage lines and the height of the crest above the drainage line. For the vegetated areas, the variability of woody cover between and within sodic sites requires inclusion of not only bare areas, but the adjacent woody savanna areas that appear different to the mid-slope or uplands savanna areas. Thus, sodic sites can be bare areas, but may also include adjoining vegetated and open woody savanna areas with visible bright soil patches. OBIA allows for objects to be associated with each other either hierarchically or as neighbours. Possible sodic sites are classified as bare soils at footslopes, which are not river sand. Savanna classes found on footslopes with low percentage cover (measured as low NDVI) adjoining sodic patches were included as part of the sodic site (Figure 29). This relationship between objects cannot be determined with pixel-based classification methods.

2.4.2 Data input layers

The pre-processed panchromatic and multispectral images were as image inputs to eCognition software (Table 6). The images are not mosaicked, and no pan-sharpened images were used to ensure that the spectral information is retained in its original form. Pan-sharpening refers to fusion of the high resolution panchromatic band with the multi-spectral bands to create a higher resolution multi-spectral image, but the original pixel values may be lost in some processes, affecting the spectral signature of the pixels or objects.

Additional layers created using Erdas Imagine 9.2 were also inserted including NDVI, principle component analysis (PCA), the tasselled cap transformation brightness, greenness and wetness index layers (available for Landsat only), as well as the cluster analysis (ISODATA) results of the multi-spectral layers. The 90 m SRTM DEM was included and the entire project was subset to the study site. Thematic layers included in the project were the KNP boundary, granite-basalt geology boundaries and the main river layers. The sample site waypoints were included in the Shingwedzi study site to determine which objects to use as samples for validation of the final classification.

Table 6: Input imagery and themeatic layers for processing in eCogntion (Definiens Version 5) software.

Image Layers	**Landsat 7 ETM+**	**ASTER**	**SPOT5**	***CAO Hyperspectral***
Panchromatic	PANir	N/A	PAN	
Multispectral	Blue, Green, Red, NIR, MIR, SWIR	Green, Red, NIR, MIR, SWIR5, SWIR6, SWIR7, SWIR8, SWIR9	Green, Red, NIR, MIR	*72 layers ranging from Ultra-violet to NIR*
Vegetation Index	NDVI	NDVI	NDVI	*NDVI(45-32)*
Principal Component Analysis	PCA1	-	PCA1	
Tasselled Cap	TasCap1, TasCap2, TasCap3	-	-	
Cluster analysis 75 classes	MSSCluster	MSSCLuster	MSSCluster	*MSSCluster*
DEM	DEM90m	DEM90m	DEM90m	*LiDAR DEM, LiDAR DTM. VegHeight*
Thematic Layers				
Vector layers	KNP_Boundary KNP_Rivers KNP_Geology	KNP_Boundary KNP_Rivers KNP_Geology	KNP_Boundary KNP_Rivers KNP_Geology	-
Waypoints (for Shingwedzi study site only)	KNP_Waypoints	KNP_Waypoints	KNP_Waypoints	-
Customized Features				
	MSAVI2, NDBaI, NDMI	*MSAVI2, NDBaI, NDMI*	*MSAVI2, NDBaI, NDMI*	

2.4.3 Segmentation

Segmentation is an iterative process to find meaningful objects for classification. The first segmentation creates a very large object to demarcate the study site within the KNP using the study site polygon and KNP boundary vector layer. The classification is thereby restricted to the area of interest (study site) within the image scene, within the KNP boundary. The scale parameter, compactness and shape/spectral parameter are changed on an iterative basis until the objects represent the actual object to be classified. The smaller the scale parameter the more memory is required for segmentation. Different size or shaped objects are required for different classes and the segmentation for sodic sites used the hierarchical levels to segment the rivers, geology and topography, as well as sodic sites. The scale parameter used varied to give a hierarchical structure based on fine to coarse homogenous areas. Shape to spectral weighting was set at 0.2 giving colour the major weighting over shape for segmentation. The compactness criterion was set to 0.5 as natural objects have highly variable shapes. The higher the compactness weighting, the more compact the objects will be.

The segmentation parameters will be the same for imagery of the same spatial and spectral resolution. The segmentation iterative process will be repeated for each sensor: Landsat 7, ASTER, SPOT 5 and CAO hyperspectral and LiDAR.

2.4.4 Classification methodology

The object-based classification of sodic sites for multi-spectral imagery is processed in four stages based on the segmentation hierarchy and the classes used for the classification of sodic sites (Figure 29) as follows:

a) Classify rivers at the segmentation scale, shape and compactness most suited to river objects (long and thin) so that the objects which overlay with the river vector layer are used to separate river sand from sodic sites.
b) Classify the granite and basalt geologies at the segmentation scale, shape and compactness most suited to geology objects so that the objects which overlay the geology vector layer are used to distinguish between sodic sites in different geologies
c) Classify the topography as crests and foot slopes so that the bare soils on crests are excluded from the classification.
d) Classify sodic sites at the segmentation scale, shape and compactness most suited to large and small sodic sites based on bare soils on footslopes and surrounding vegetation with a different spectral signature to the general savanna.

The area of the imagery within the study site and KNP boundary is classified as the area of interest. The areas in the park with different geologies require different values to determine the drainage lines and crests. The basalt areas are much flatter than the granitic areas and the classic catenas are less obvious both in the field and using a DEM. A different threshold is used to classify crests in the basalts to that used in the granites, and the resulting drainage area was unclassified for further analysis, in the next phase of classification of the land cover classes.

The goal of the first land cover class separation is to separate water from land. Shadows caused by steep topography or cloud have a similar spectral signature to water. There were no obvious shadows in the imagery used for the training classification. The second separation of classes is between bare soil areas and vegetated areas (Figure 29). The bare soil areas were classified using the tasselled cap brightness index (for Landsat only), first principal component analysis (PCA), bare soil index (BSI) and NDVI, as well as the multi-spectral layers (blue, green, red, NIR and SWIR). River sand was classified using

the vector layer of main rivers as most large rivers have banks of river sand which may be confused with sodic areas next to rivers. The areas of no vegetation were classified as sodic areas and adjustments were made to the classification of river sand, sparse vegetation and sodic areas in relation to water and each other. Sparse vegetation is spectrally close to bare soils and separated using slightly higher NDVI values and the tasselled cap Greeness Index (for Landsat only). The remaining vegetation was classified as high biomass vegetation, most often found along riverine areas. Savanna vegetation was treated as a general class for the classification of sodic sites. Sparse vegetation was separated from savannas based on the low level of biomass measured by the NDVI, and the possible contribution of bare soils interspersed with the vegetation. Any objects with a medium NDVI that were classified as bare soils or sparsely vegetated by the other features other than NDVI, were excluded. The topology relationships between classified objects were used in the clean up phase of the classification. All crest areas were classified as general savanna.

The hyperspectral imagery has the benefit of many more spectral bands for classification and LiDAR give the ability to determine the height of objects above the ground. Hyperspectral imagery is only available for the Ripape study site, so can only be tested for a small area, and is not intended for mapping sodic sites in the whole of the KNP. Sodic soil patches are often very bare open areas with few or no trees, and this ground layer will assist in identifying sodic core areas. Tree height classes are calculated from the difference between the elevation model (DEM) and the terrain model (DTM) and classified using the finest scale segmentation. Together with the spectral layers relevant to bares soil, only areas with a vegetation height under 1 m were considered as possible sodic sites. Fine scale classification with the inclusion of height classes could be an option for quantification of sodic site size changes.

2.4.5 Accuracy assessment

The confusion or error matrix expresses the accuracy of the classified objects or how well the ground truth field samples were classified. The error matrix is known as the descriptive analysis of the classification (Figure 30). The kappa statistic is referred to as the analytical analysis of the classification. Visually assessed samples from each image were collected and used for the accuracy assessment for training the classification algorithm. Validation of the final classification in the Shingwedzi study site was performed using the ground truth samples described in Chapter 2. Normally ground truth

samples would be split into training and validation samples, but due to the relatively small number of stratified random samples collected in the field, visually assessed samples were used as training samples, sometimes iteratively, and all the ground truth field samples were used for the validation accuracy assessment.

The error matrix indicates the areas of confusion between classes which require improvement in the classification algorithm. The recommended classification accuracy is over 85% accuracy overall and at least 70% accuracy in each class. In the example (Figure 30), savanna is classified with the best accuracy, but there is major confusion in the riverine vegetation where the majority of samples were classified as savanna and the objects classified as riverine bush were largely sparse vegetation samples. Changes to the grouping of classes, an increase in the number of samples and classification algorithm improvements will all contribute to an improved classification. The results for the Hellden and Short accuracy measures were not used for this study. The kappa index of agreement (KIA) is the accuracy value used to compare accuracy assessments from different classification results, taking into account variance and compensates for chance agreement.

User \ Reference Class	River sand	Savanna	Riverine vegetation	Bare Soil sodic patches	Sparse veg	Sum
Confusion Matrix						
River sand	3	0	2	79	1	85
Savanna	33	2864	126	404	701	4128
Riverine vegetation	1	25	48	8	185	267
Bare Soil sodic patches	0	17	0	705	46	768
Sparse veg	0	138	1	29	42	210
unclassified	0	0	3	0	0	3
Sum	37	3044	180	1225	975	
Accuracy						
Producer	0.08108108108	0.9409	0.2667	0.5755	0.04307692308	
User	0.03529411765	0.6938	0.1798	0.9180	0.2	
Hellden	0.04918032787	0.7987	0.2148	0.7075	0.07088607595	
Short	0.02521008403	0.6648	0.1203	0.5474	0.03674540682	
KIA Per Class	0.06655204311	0.7577	0.2290	0.506	0.004807289454	
Totals						
Overall Accuracy	**0.6706**					
KIA	**0.3883**					

Figure 30: Example of the accuracy assessment produced by eCognition software showing the number of classified pixels per class and accuracy values.

3. RESULTS

3.1 Pre-classification imagery assessment

3.1.1 Spectral signatures

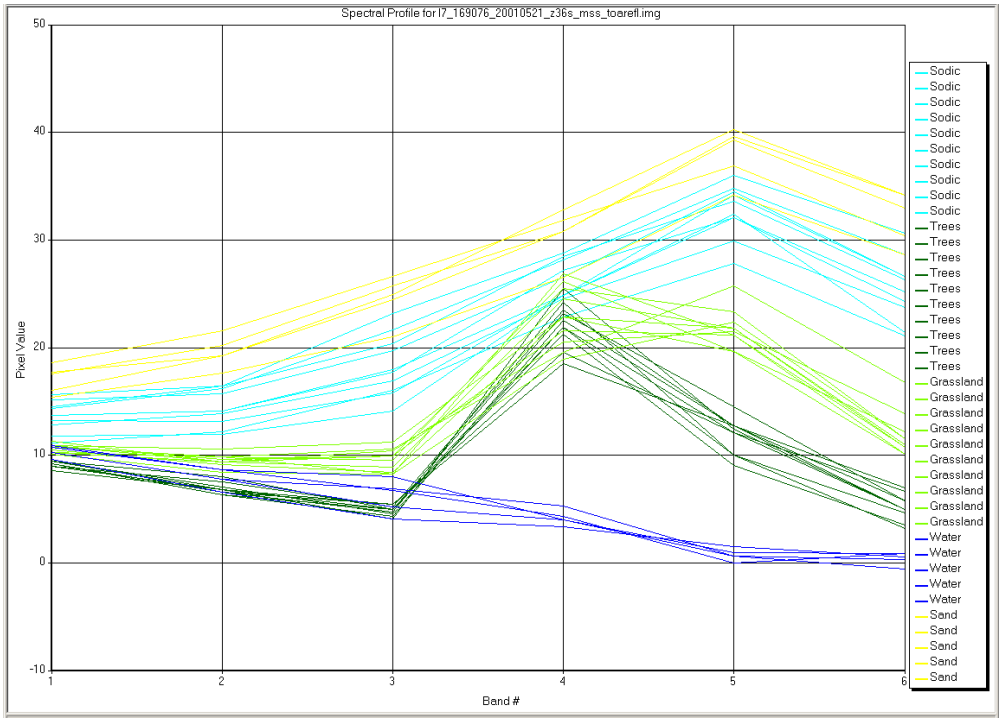
Radiometric correction or normalisation was performed on the Landsat 7 ETM+ and SPOT 5 imagery. The ASTER imagery was received atmospherically corrected, but radiometric correction for the sun geometry was made. These three sensor data sets were checked for spectral signature compliance and the results for water, river sand, sodic sites and vegetation (trees and grassland) are as follows:

a) Water spectral signatures followed the expected relative value of the peak reflectance in the blue band and lowest in the MIR or SWIR bands. The water spectral signature is typical for clear water bodies (no algal growth, reeds or silt).

b) The river sand and sodic site samples show the typical bare soil spectral signature, low in the blue band and steadily increasing reflectance through to the mid-infrared bands (low moisture), and are difficult to differentiate from each other.

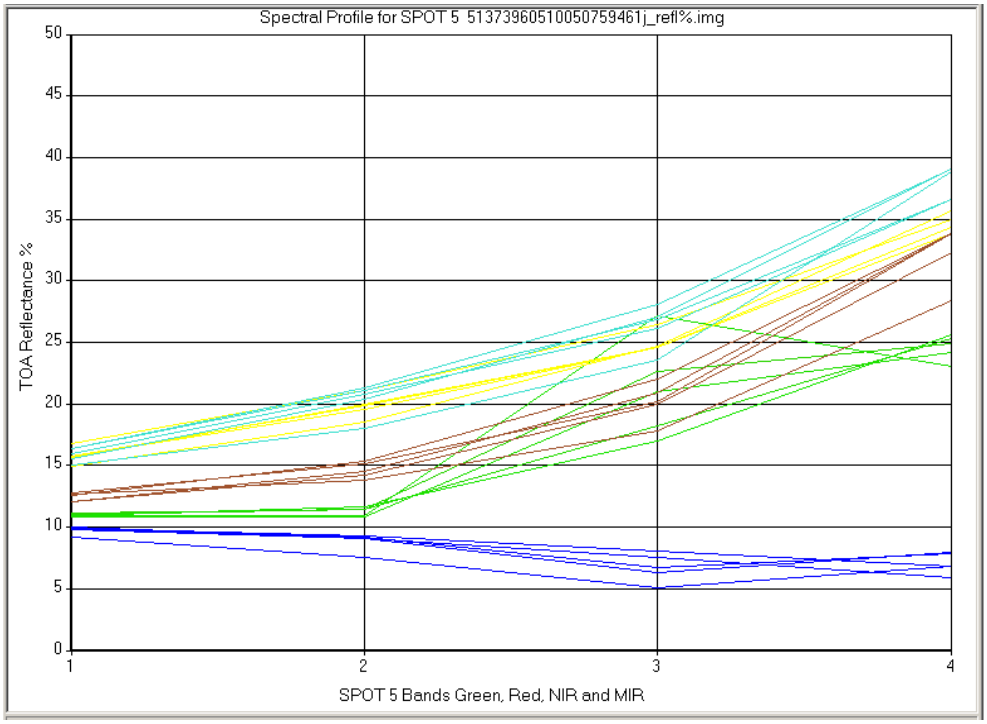
c) The vegetation spectral signatures show the typical higher (or equal) in the green to red band, low in the red band and the red-edge feature of a large difference between the reflectance in the red band and a high reflectance in the near-infra red bands. The varying level of cell moisture content in the mid infra-red bands differentiate between green versus senescent vegetation.

Figure 31 shows the spectral signatures for typical classes for the Landsat 7 ETM+ imagery acquired on 21 May 2001, the early dry season. The season of acquisition for the SPOT 5 imagery was the peak of the dry season (5 October 2005). The spectral signatures of the samples show how the soil signature influences the vegetated samples for the dry season image (Figure 32) and it will be very difficult to distinguish bare sodic patches from other bare soils and senescent vegetation using spectral properties alone.



Bands:Blue Green Red NIR MIR SWIR .
Spectral Signatures: **River Sand** **Sodic sites** **Savanna/Green grass** Trees/Dense foliage Water

Figure 31: Spectral profile for Landsat 7 ETM+ image (north KNP) dated 21 May 2001 plotted from 10 typical sample sites per class.



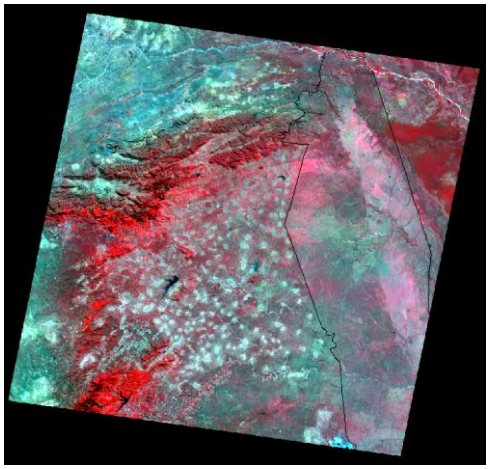
Band: Green Red NIR MIR
Spectral Signatures: **River Sand** **Sodic sites** **Savanna/Dry grass** **Trees/Dense foliage** **Water**

Figure 32: Spectral profile for SPOT 5 image (north KNP) dated 5 October 2005 plotted from 5 typical sample sites per class.

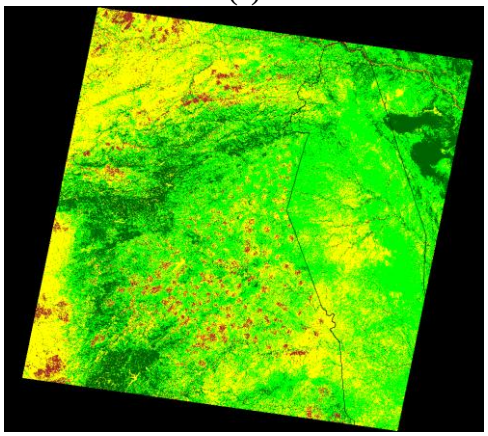
3.1.2 Class separation

To assess whether the multi-spectral imagery selected to classify sodic sites in the KNP will be sufficient using spectral properties only, a clustering of spectral signatures gave the following results.

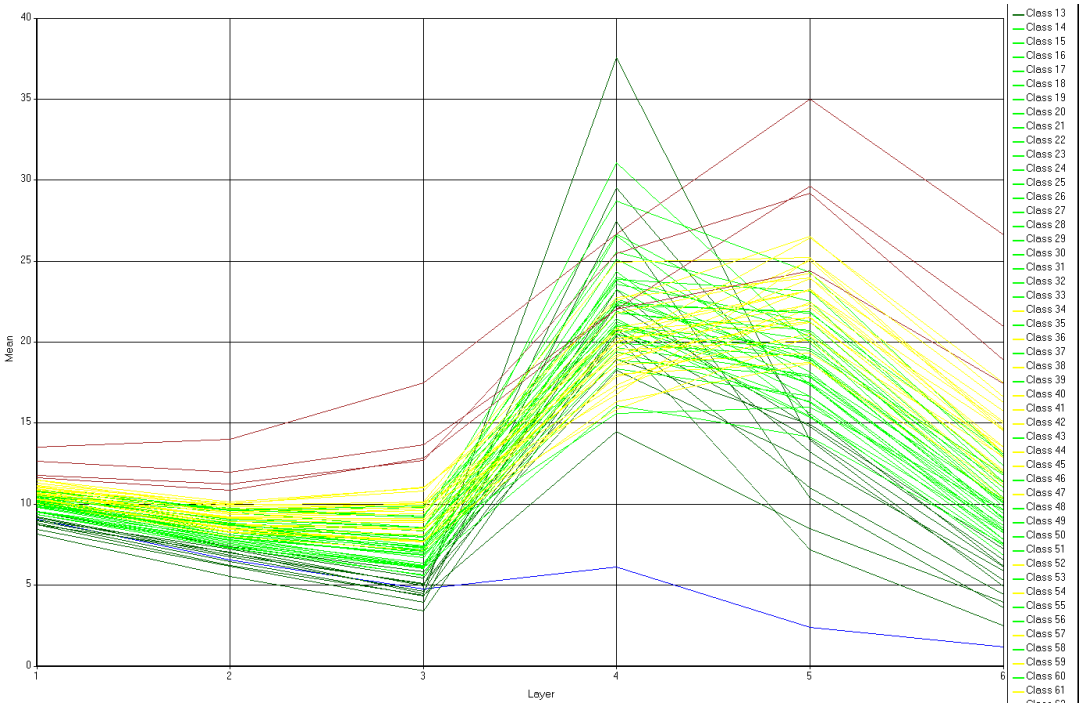
The clustering of spectral signatures for the Landsat 7 ETM+ images for the northern and southern sections of KNP is shown in Figures 33 and 34. The two images were acquired one week apart, so the spectral signatures are highly similar for all classes except the water class. The water spectral signatures show the dominance of deep water in the southern image, but the northern image shows a higher reflectance in the NIR than red bands which indicates vegetation, algae or turbid water. The bare soil class is separated spectrally from green vegetation and indicates that for the Landsat 7 ETM+ imagery (21 and 30 May 2001), bare soils will be classified from spectral signatures but to classify sodic soils, properties such as topographic location and vegetation and soil moisture relationships must be included to improve classification results.



(a)



(b)

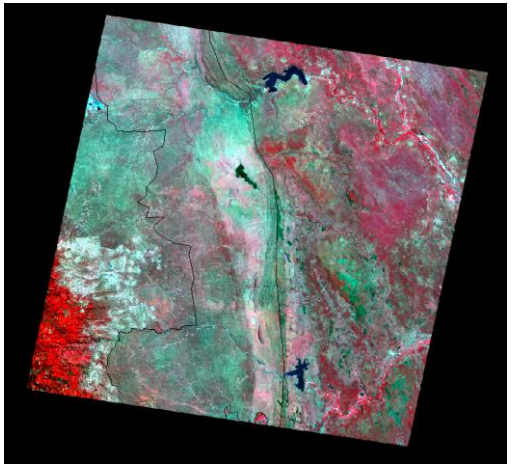


Band: Blue Green Red NIR MIR SWIR

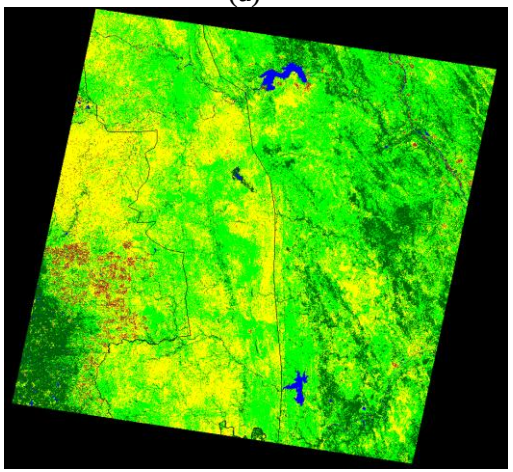
Spectral Signatures: Bare soil Dry Grassland/Soil Savanna/Green grass Trees/Dense foliage Water

(c)

Figure 33: Unsupervised classification of Landsat 7 ETM+ north KNP image dated 21 May 2001 (a) based on 75 classes, grouped into 5 classes (b) using the average spectral signatures (c).



(a)



(b)

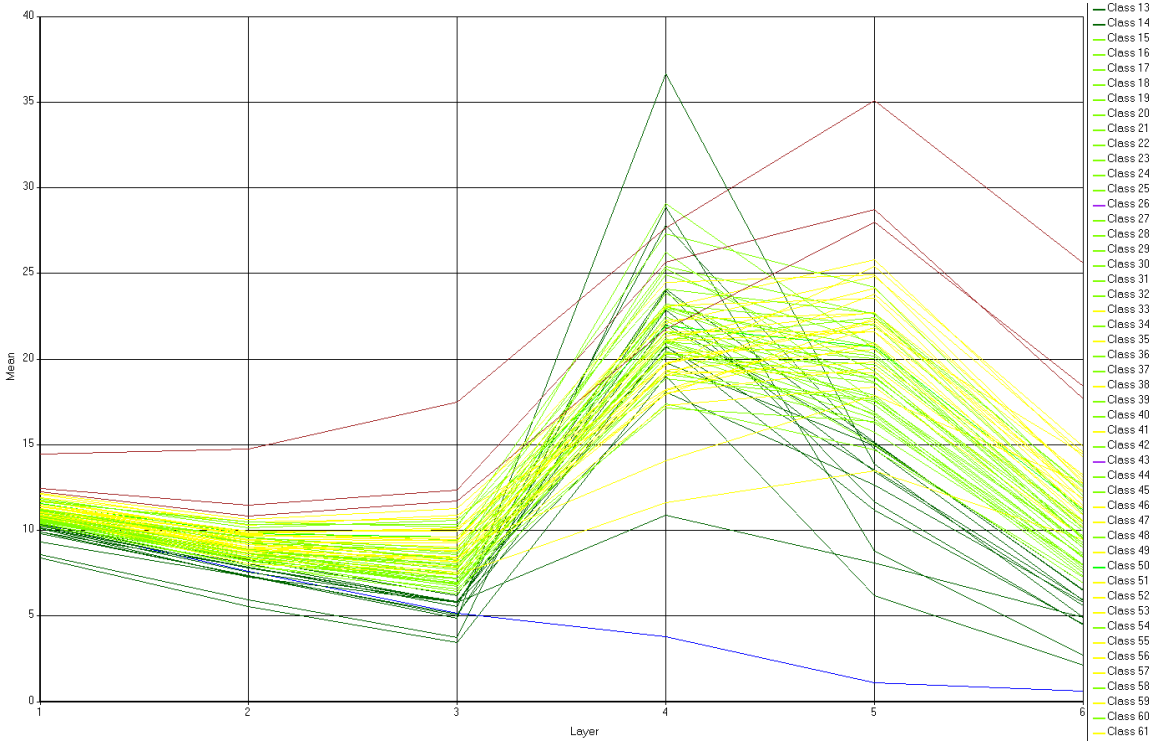


Figure 34: Unsupervised classification of Landsat 7 ETM+ southern KNP image dated 30 May 2001 (a) based on 75 classes, grouped into 5 classes (b) using the average spectral signatures (c).

The clustering of spectral signatures for the SPOT 5 imagery for the northern KNP dated 5 October 2005 (Figure 35), shows that the spectral signatures are highly correlated at the end of the dry the season. A second SPOT 5 image was available for the Shingwedzi River catchment date 12 April 2008, and both scenes were used for classification to investigate the accuracy of the dry season imagery in comparison to the wet season imagery.

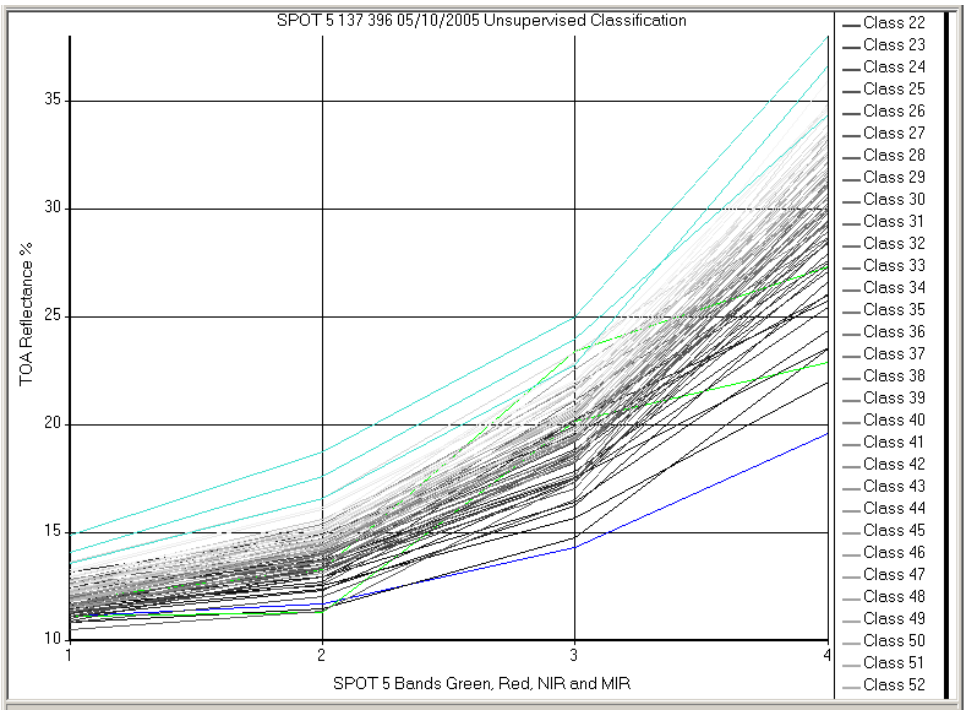


Figure 35: Unsupervised classification of SPOT 5 northern KNP image dated 5 October 2005 (a) based on 75 classes, grouped into 5 classes (b) using the average spectral signatures (c).

The clustering of spectral signatures for the SPOT 5 imagery for the southern KNP, which was acquired in the mid and late wet season showed similar results to the Landsat imagery and that the spectral signatures are distinct and either image is suitable to classify sodic sites.

The hyperspectral imagery was classified into 75 classes shown in Figure 36. One bare soils class (the top blue line) is clearly separated from all other classes across all bands and was spatially found in the centre of the sodic areas (Figure 37).

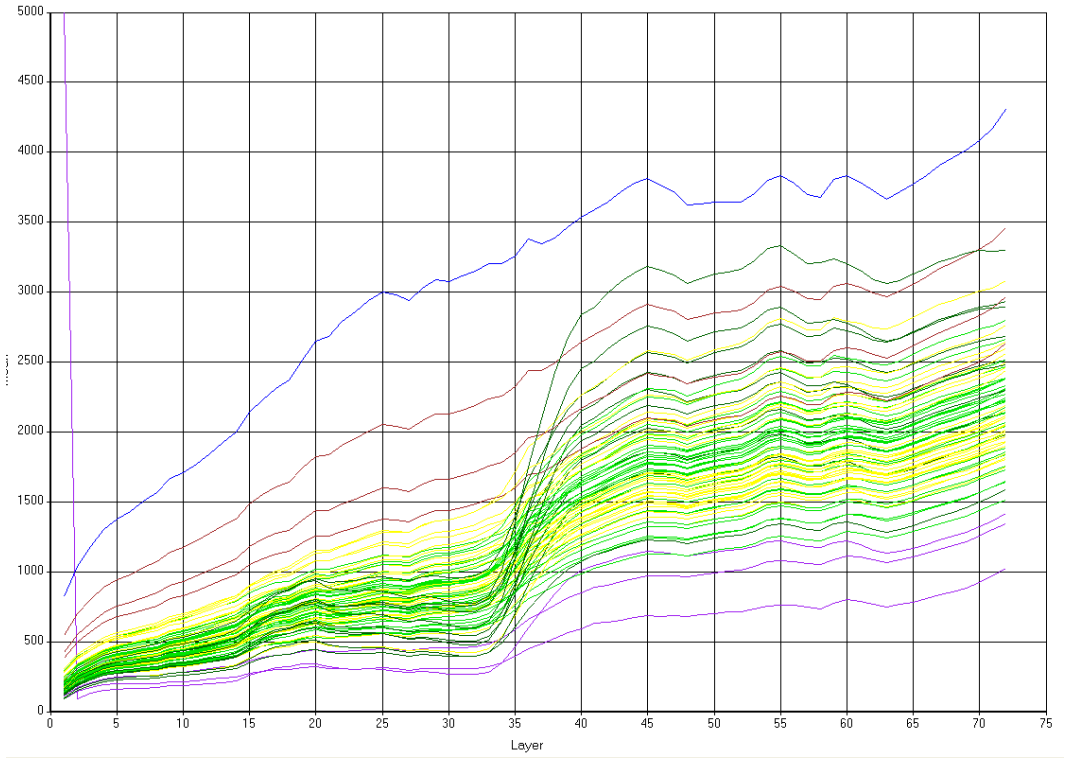


Figure 36: Average spectral profile of the 75 classes determined by an unsupervised classification over all 72 bands using Erdas Imagine 9.2. Blue = sodic; Green = vegetation; Yellow = dry grassland; Brown = bare soil; Purple = shadow.

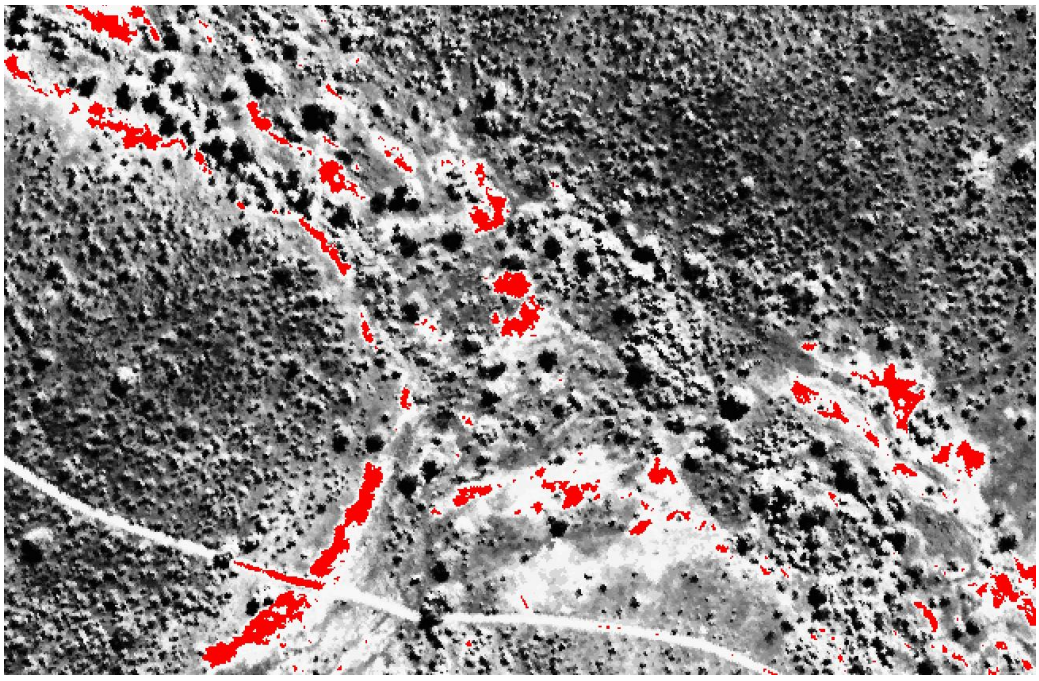


Figure 37: Class 75 (red) of the unsupervised classification image shown in grayscale using Erdas Imagine 9.2 Grouping Tool.

This may be due to the high levels of sodium found in these areas, but will require soil testing at these points to confirm the chemical composition. Other bare soil classes (brown) occur on roads, bare crests, termite mounds and sodic sites over the whole area (Figure 38). The vegetation classes showed a spectral signature with a red edge, while dry grassland and bare soils showed similar signatures but at different absorption in the visible bands. The signatures at the bottom of the graph are vegetation in shadow (Figure 36). The spectral information from this initial investigation will be applied in combination with height classes from the LiDAR, to locate the sodic sites class.

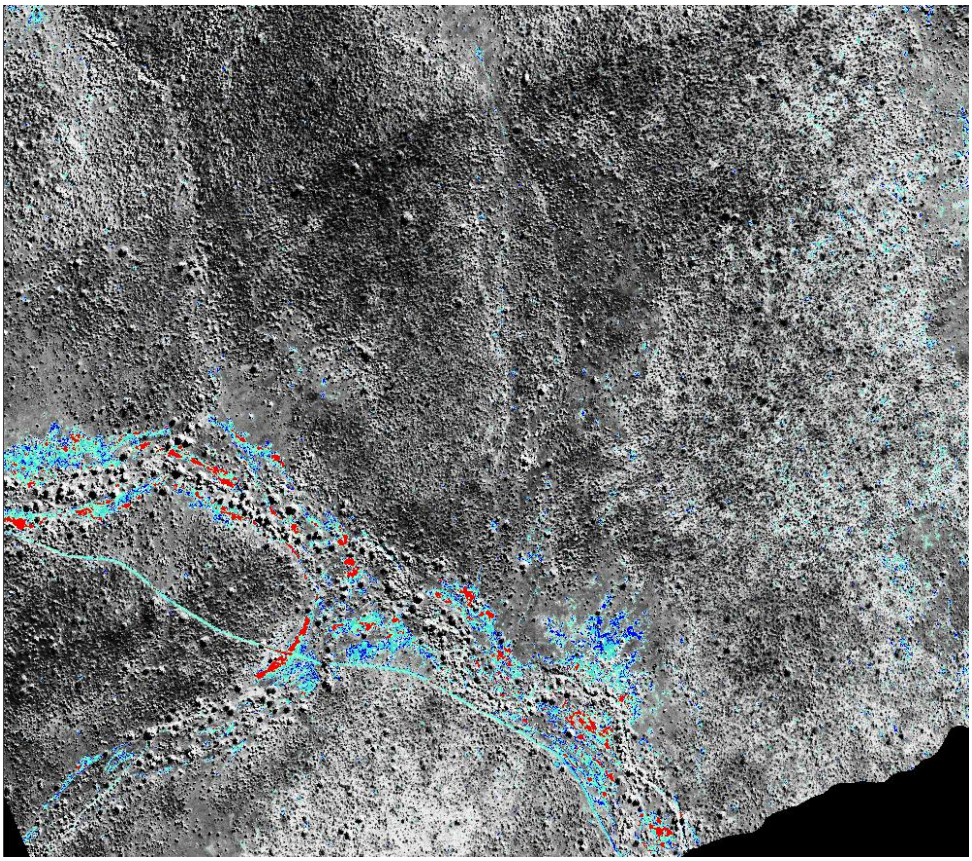


Figure 38: Classes 75 (red), 73 and 72 (turquoise) and 64 (blue), of the unsupervised classification of the hyperspectral imagery using Erdas Imagine 9.2 Grouping Tool.

3.1.3 Seasonal context of imagery

Sodic sites would be best detected from imagery acquired after the peak in the wet season, once the sites have been heavily grazed by herbivores in the early dry season, when the grasses have started to senesce, but before the trees lose their leaves (Grant pers comm., 2008). The mean NDVI values for area covered by each scene of the available

imagery covering the Shingwedzi study site (Figure 39) and the Ripape study site (Figure 40) was plotted using the MODIS 250m NDVI imagery from 2000 to 2008. The seasonal context of each image available for the Shingwedzi and Ripape study sites are summarised in Table 7.

Table 7: Summary of satellite and airborne imagery available for the Shingwedzi River and Ripape River catchment study sites showing acquisition dates and seasonal context.

Study Site	**Satellite Imagery**			***Airborne Imagery***	
	Landsat 7 ETM+	**ASTER**	**SPOT 5**	**Orthophoto (BandW)**	***CAO Hyperspectral and LiDAR***
Shingwedzi	21/05/2001 Late wet season	29/06/2006 Early dry season 01/04/2006 Peak wet season	12/04/2008 Late wet season 05/10/2005 Peak dry season	May 2001 Late wet season	-
Ripape	*30/05/2001* *Mid wet/dry season*	*26/06/2005* *Early dry season*	*12/05/2006* *Early dry season* *26/03/2006* *Peak wet season*	-	*25/04/2008* *Early dry season*

The seasonal context was defined as follows:

- Peak wet season: date of acquisition close to the highest NDVI values in the cycle
- Peak dry season: date of acquisition close to the lowest NDVI in the cycle
- Mid wet/dry season: midway between the peak wet season and peak dry season NDVI value in the cycle
- Late wet season: midway between the peak wet season and the mid wet/dry season NDVI value in the cycle
- Early dry season: midway between the mid wet/dry season and peak dry season NDVI value in the cycle

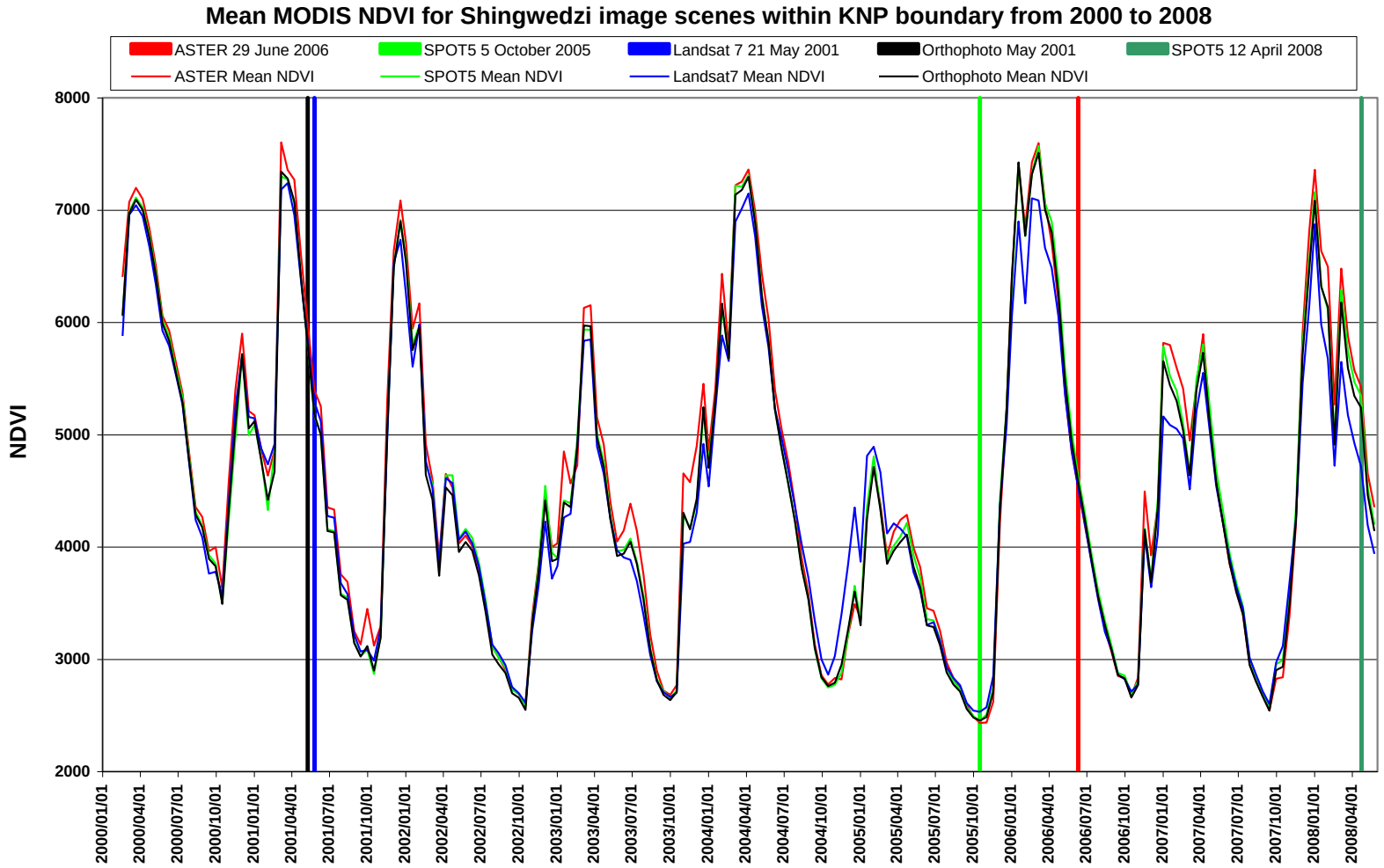


Figure 39: Shingwedzi Study Site MODIS NDVI average for the area of KNP covered by each image over 9 years, depicting the acquisition date of each image as a vertical line.

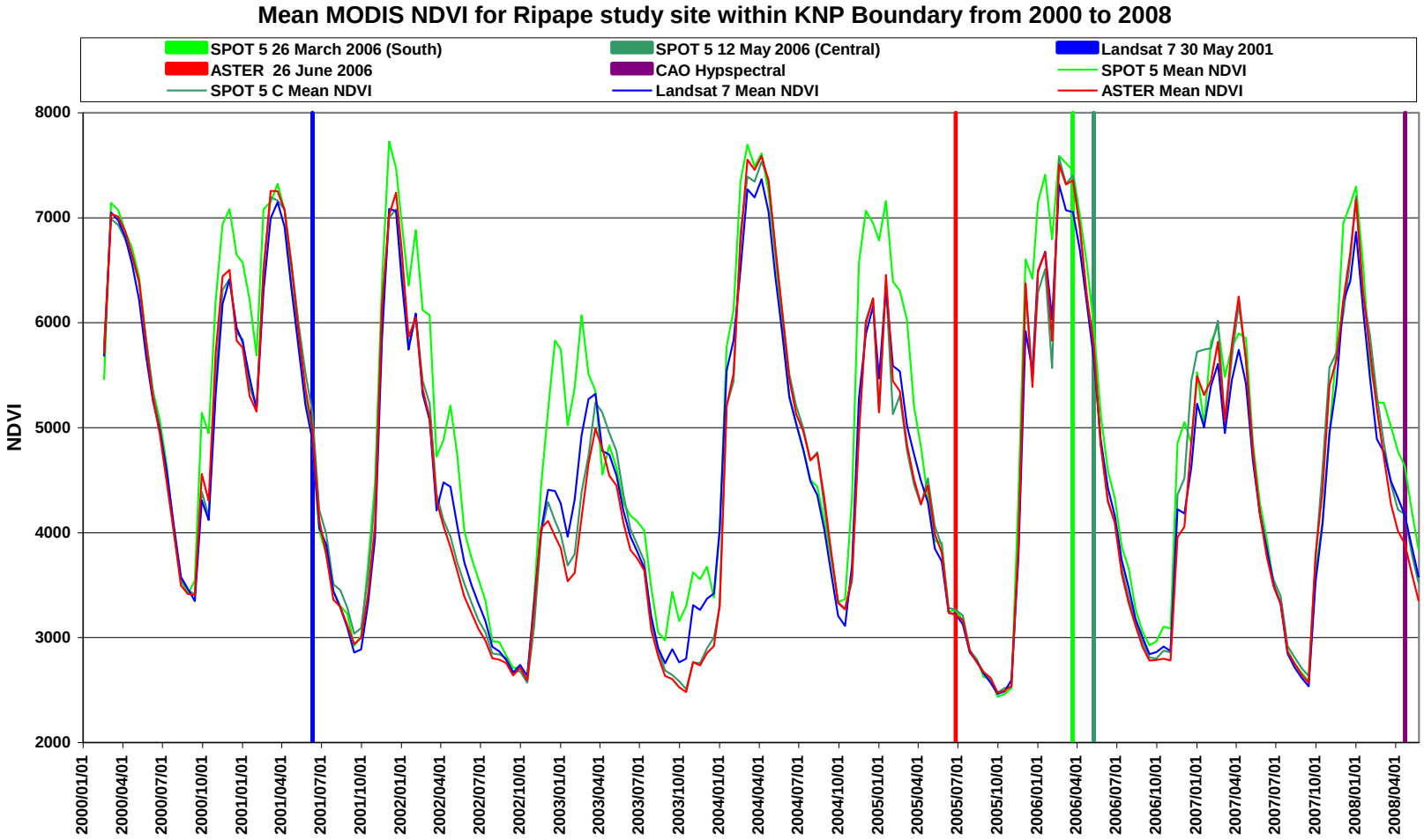


Figure 40: Ripape Study Site MODIS NDVI average for the area of KNP covered by each image over 9 years, depicting the acquisition date of each image as a vertical line.

The most phenologically suitable images for the classification of sodic sites are expected to be images acquired in the late wet season to early dry season. Based on this assumption, Landsat 7, ASTER and SPOT5 imagery dated 21 May 2001, 29 June 2006 and 12 April 2008 respectively, would be most suitable for the classification of sodic sites in the Shingwedzi study site. The orthophotos of May 2001 were taken in a similar phenology stage to the lower resolution Landsat 7, ASTER and SPOT imagery and may be used for accuracy assessment data collection during the iterative classification stage. The SPOT 5 imagery of 5 October 2005 was acquired in the dry season and based on the spectral cluster graph (Figure 35); it will be difficult to distinguish sodic sites from other bare soil as the image was acquired at the height of the dry season. For the Ripape study site, the Landsat 7, ASTER and SPOT 5 imagery is most suitable for classification, acquired after the peak of the wet season. The ASTER imagery acquisition date is during the late dry season, and the CAO hyperspectral imagery is marginal due to the late wet season acquisition date.

The classification algorithm will be developed for the Shingwedzi study site because the ground truth reference data for accuracy assessment was collected for the site. For the algorithm to be successfully applied across the whole of the KNP the sodic sites should be in a similar phenology stage. The mean NDVI values were plotted for the two polygons covered by the Landsat 7 imagery within the KNP boundary (Figure 41). The phenology cycle for the acquisition dates of 21 and 30 May 2001 (the red and green graphs in Figure 41) show a very similar phenological cycle in both the north and south of the park. The results of the classification of the Landsat 7 imagery could be compared to the results of the pixel-based classification by Mathys and Wesssels (2003) as the imagery used for both classification methods have a similar phenology cycle. A similar comparison was made in Figure 42 for the SPOT 5 imagery available for the northern, central and southern KNP. The difference in mean NDVI for the northern, central and southern areas of the KNP in 2003 and 2005 seasons are quite marked, while the 2001, 2004 and 2006 early dry seasons show similar mean NDVI values. The phenologically similar seasons throughout the park would be the best images for a classification algorithm to be applied over the entire park. The anniversary date of the southern SPOT 5 image, shown as vertical dotted lines (Figure 42), illustrates the variable NDVI mean values for each year and which dates would be unsuitable for the classification of sodic sites or change detection analysis.

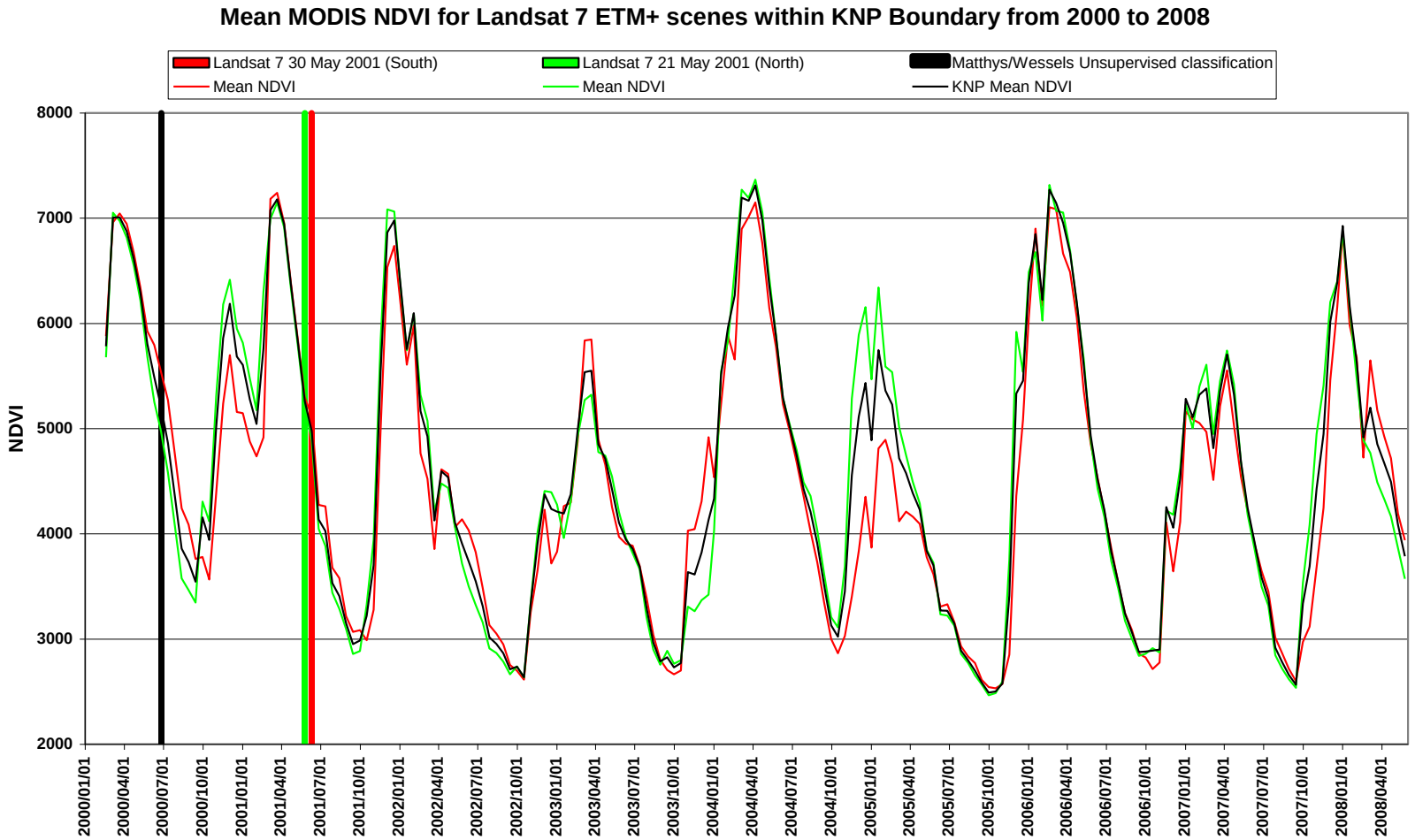


Figure 41: Mean NDVI for each Landsat 7 ETM+ imagery polygon indicating the acquisition date of the Landsat 7 ETM+ images (solid vertical lines).

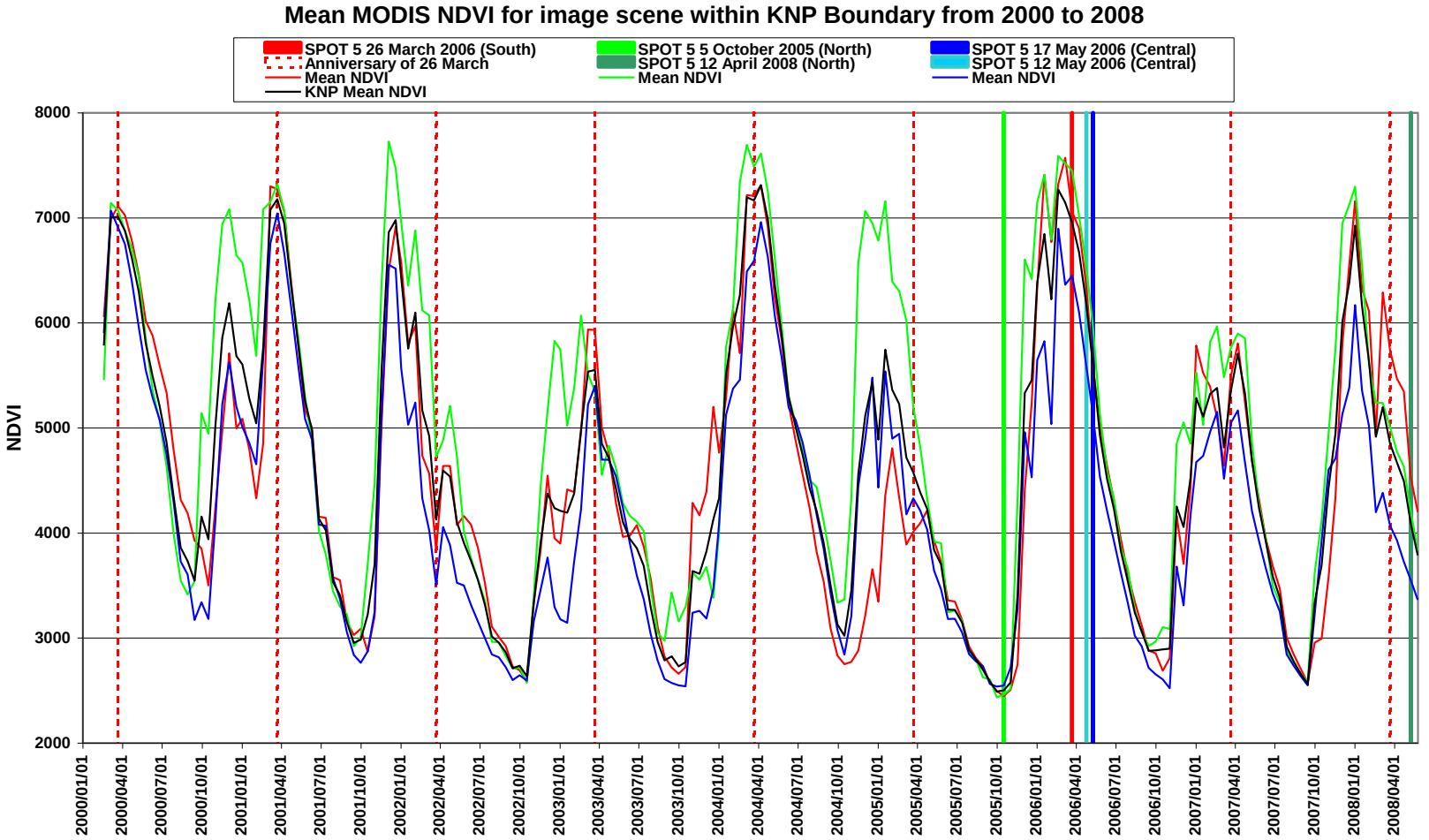


Figure 42: Mean NDVI for each SPOT 5 imagery polygon indicating the acquisition date of the SPOT5 images (solid vertical lines) and the anniversary date of the southern SPOT 5

3.3 Object-based classification

The results of the classifications include the segmentation results per sensor (Landsat 7, ASTER, SPOT 5 and CAO Hyperspectral), the classification algorithm developed for each sensor for the Shingwedzi and the vector layer output (sodic site map). The accuracy assessments resulting from the iterative training process are reported, as well as the final validation accuracy assessment using the stratified random ground truth reference samples. The classification algorithms developed for the Shingwedzi study site are applied to the Ripape study site Landsat 7 and SPOT 5 imagery, and the accuracy results are reported. The classification algorithm for Landsat 7 will be used to classify the whole of the KNP to validate the repeatability of the algorithm across the park.

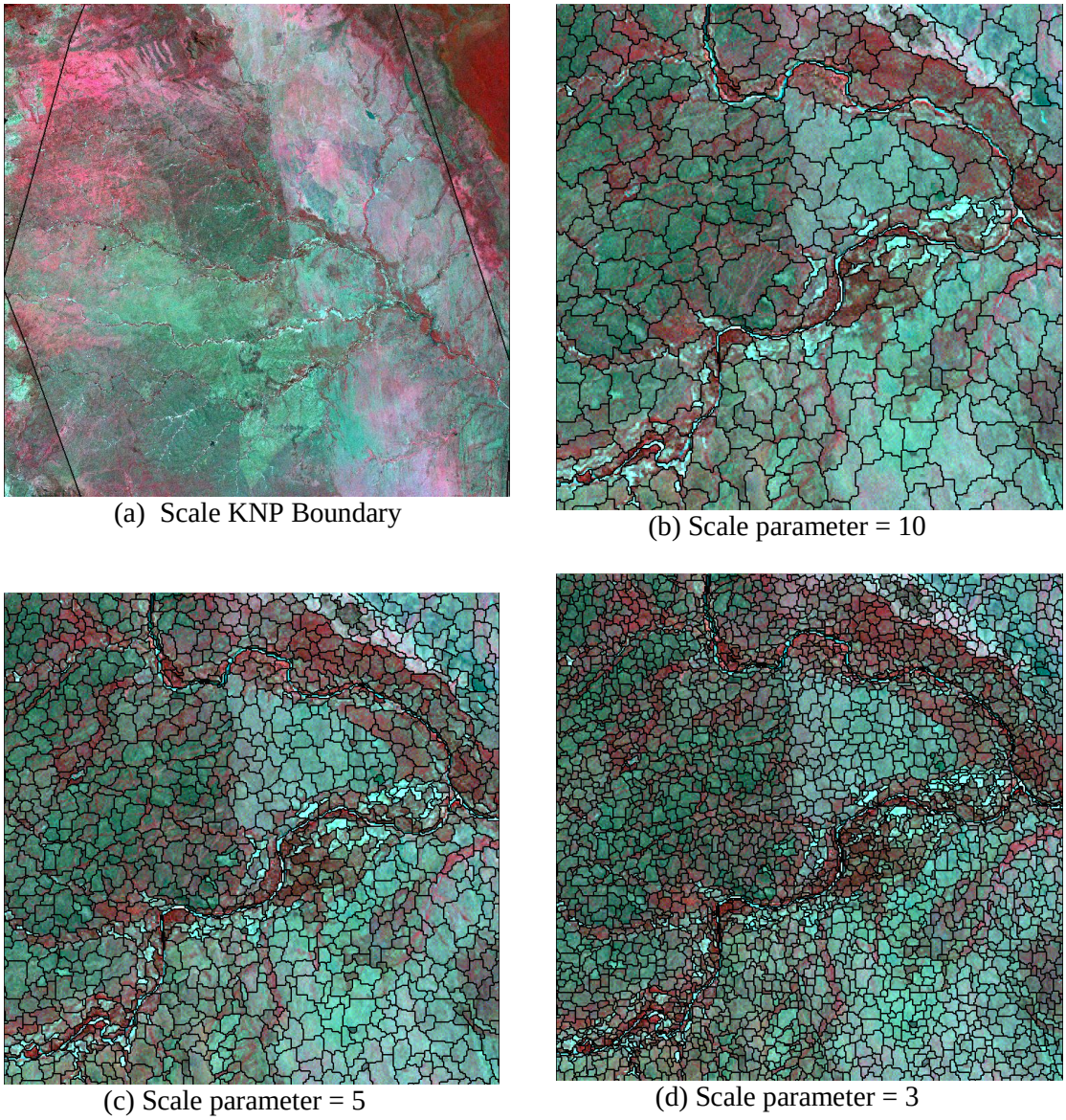
3.3.1 Segmentation

The methods describe the iterative process that is required to determine the best segmentation parameters for each class to obtain meaningful objects. Each sensor has a different spatial resolution which will influence the segmentation parameters. The same segmentation scale, shape and compactness values are applicable to all scenes for the specific sensor, summarised in Table 8. All the multi-spectral and panchromatic input layers are included in the segmentation and each input layer is evenly weighted.

Table 8: Results of the multi-spectral satellite imagery segmentation parameter selection for Landsat 7, ASTER, SPOT 5 and CAO hyperspectral imagery.

Segmentation Level Hierarchy	**Segmentation algorithm and parameters**	**Satellite Imagery (MSS and PAN resolution)**			
		Landsat 7 ETM+ (30m/15m)	**ASTER (15m MSS)**	**SPOT 5 (10m/2.5m)**	**CAO Hyperspectral (1.16m)**
Top: River Level	Multi-spectral Shape = 0.2 Compact = 0.5	Scale =10	Scale =20	Scale =20	Scale =100
Middle: Geology	Multi-spectral Shape = 0.2 Compact = 0.5	Scale = 5	Scale = 10	Scale = 15	Scale = 50
Bottom: Topography Sodic sites	Multi-spectral Shape = 0.2 Compact = 0.5	Scale = 3	Scale = 5	Scale = 10	Scale = 20

The three resulting hierarchical levels from large to small scale for multi-spectral imagery are used to classify the rivers, geology, topography and sodic sites (Figure 43).



(a) Scale KNP Boundary

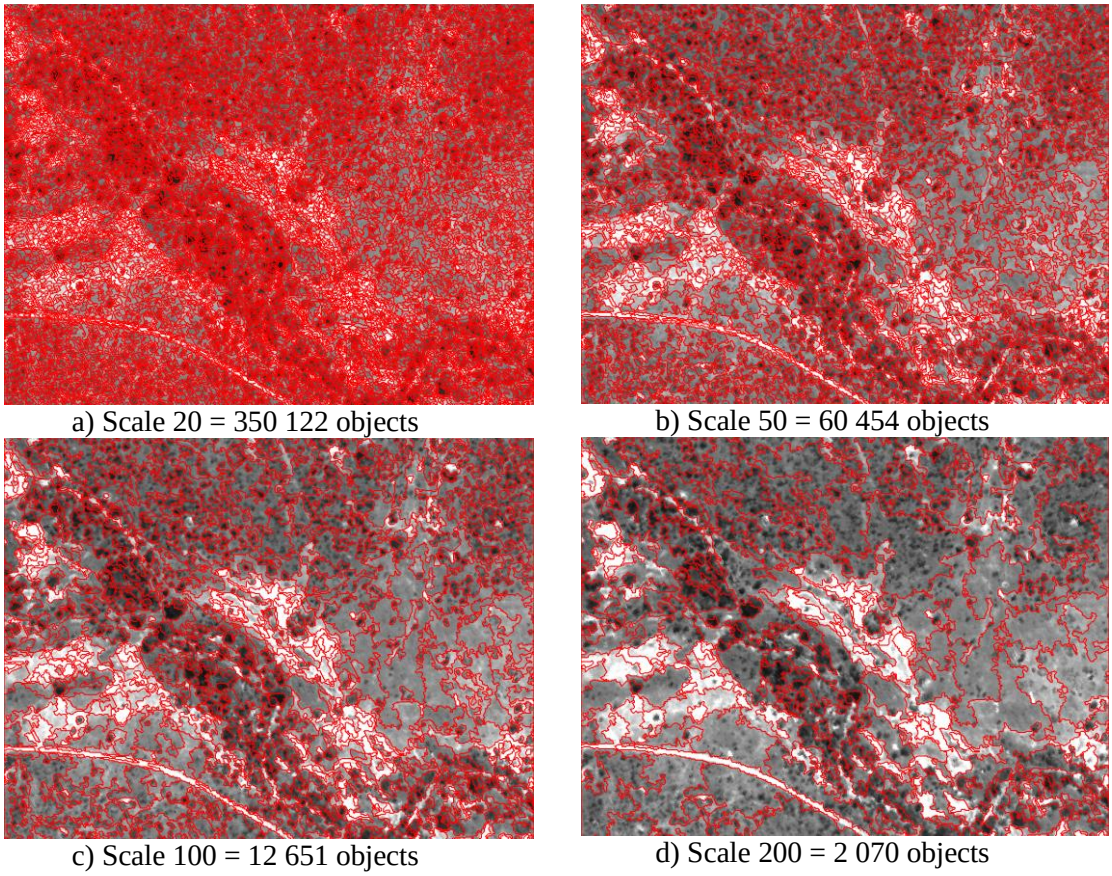
(b) Scale parameter = 10

(c) Scale parameter = 5

(d) Scale parameter = 3

Figure 43: Segmentation of Landsat 7 imagery using chessboard segmentation and the KNP Boundary thematic layer (a) and multispectral segmentation of the visible and infra-red bands at scale parameter of 10 (b), 5 (c) and 3 (d).

After an iterative process of scale parameter selection, a scale parameter of 20 was selected to segment to tree and termite mounds (Figure 44a). Sodic sites divided into sub-objects which show the heterogeneity within sodic sites were best segmented at a scale of 50 and 100 (Figure 44b and 44c). A scale of 200 was used as the largest scale to depict sodic site delineation including the very bare sodic areas, vegetated areas of sparse woody vegetation and the grass layer within the sodic site (Figure 44d). The estimated percentage tree cover was calculated using the standard deviation of height classes within these segments together with tree height classification.



a) Scale 20 = 350 122 objects

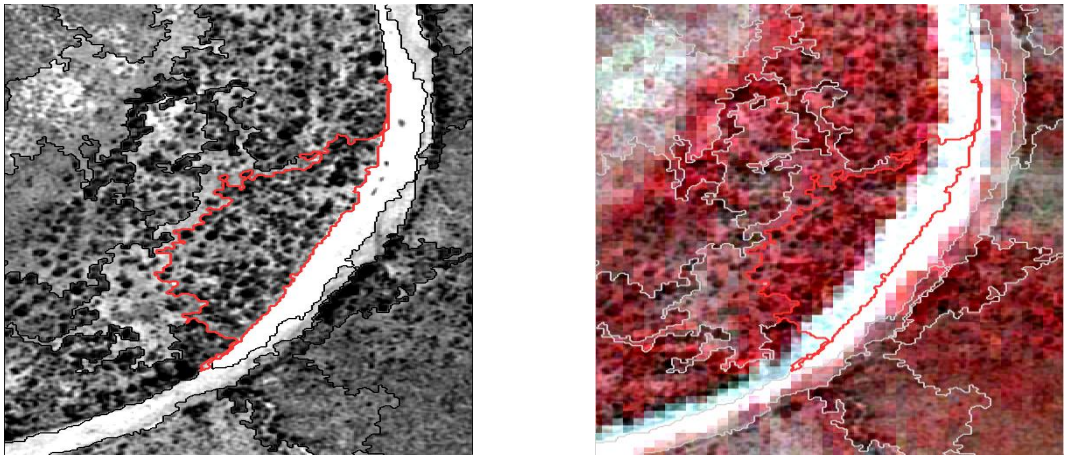
b) Scale 50 = 60 454 objects

c) Scale 100 = 12 651 objects

d) Scale 200 = 2 070 objects

Figure 44: Segmentation of CAO hyperspectral imagery using multispectral segmentation of the visible and infra-red bands at scale parameter of 20 (a), 50 (b), 100 (c) and 200 (d).

As a result of comparisons between segmentation results for the multi-spectral imagery the geo-referencing of the ASTER imagery does not correspond to the SPOT 5 imagery. All vector layers of rivers and roads supplied by the KNP were checked against the SPOT 5 and ASTER imagery and the ASTER imagery was out of alignment with the roads and rivers layers. The SPOT 5 segmentation result along a river in the Shingwedzi study site was overlayed onto ASTER imagery for the same river bed. Figure 45 illustrates an approximately 40m shift of the pixels. The ASTER imagery was resampled to the SPOT 5 panchromatic band and classification methodologies were applied, but the accuracy assessment results interpretation will reflect this geo-referencing shift as inaccuracy.



(a) (b)

Figure 45: SPOT 5 panchromatic imagery segmentation (a) overlayed on ASTER multi-spectral imagery for the same river bed showing the pixel misalignment due to a georeferencing shift of approximately 40m.

3.3.2 Classification algorithm development for Shingwedzi training site

The summary method applied to all multi-spectral imagery is shown in the classification algorithm work flow (Figure 46).

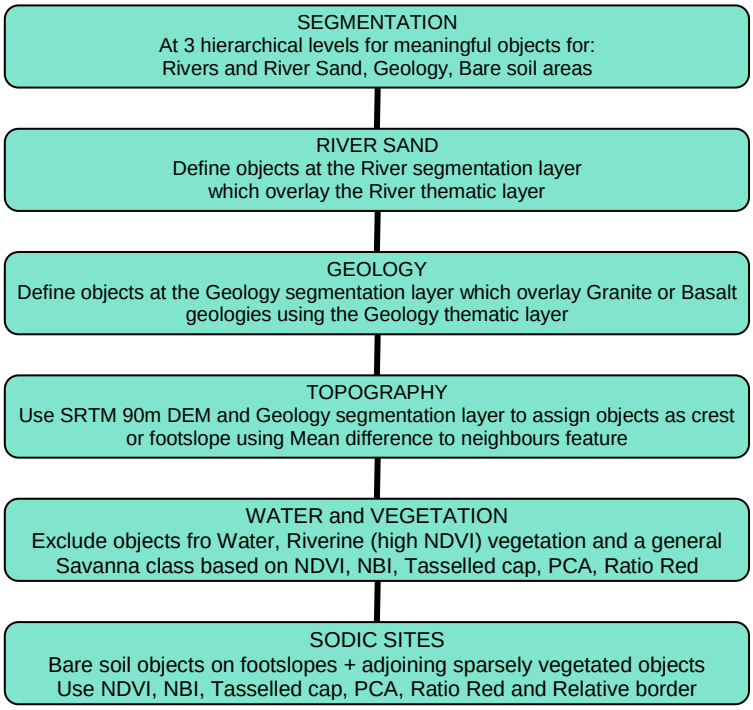
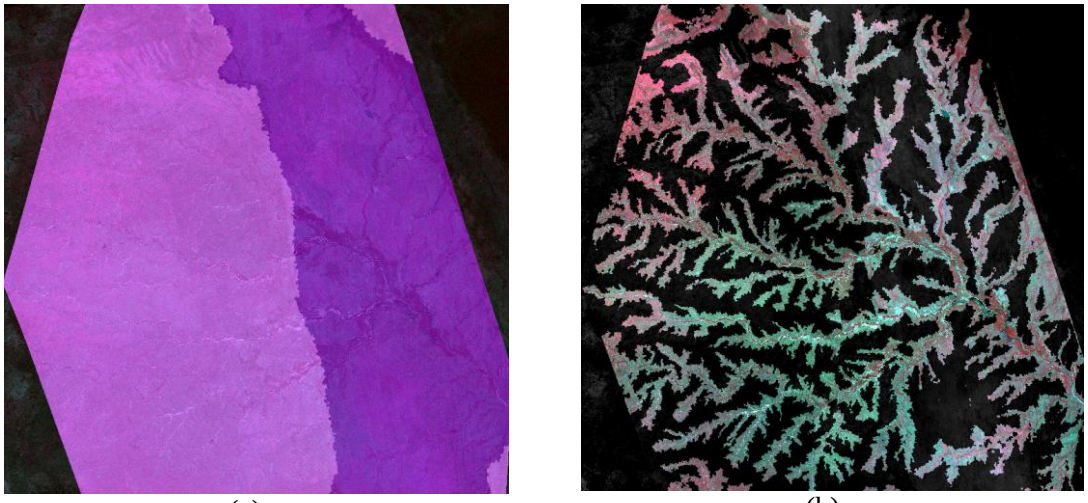


Figure 46: Summary of the classification algorithm work flow applied to all multi-spectral imagery at all study sites.

Before the finest segmentation level is classified for sodic sites, the topography is defined by classification of crests and footslopes. Sodic soils are found on the footslopes of catenas or floodplains according to the literature, which forms the basis for the classification of sodic sites. Figure 47 (b) illustrates the result of the topography classification for the Landsat 7 imagery for the Shingwedzi study site showing crests in black and the drainage lines and footslopes as unclassified objects. The different geologies require a different value for the feature Mean distance to neighbours for the 90m DEM for the algorithm to determine crests and footslopes. The geology layer informs the process tree if objects are granites or basalts (Figure 47a).

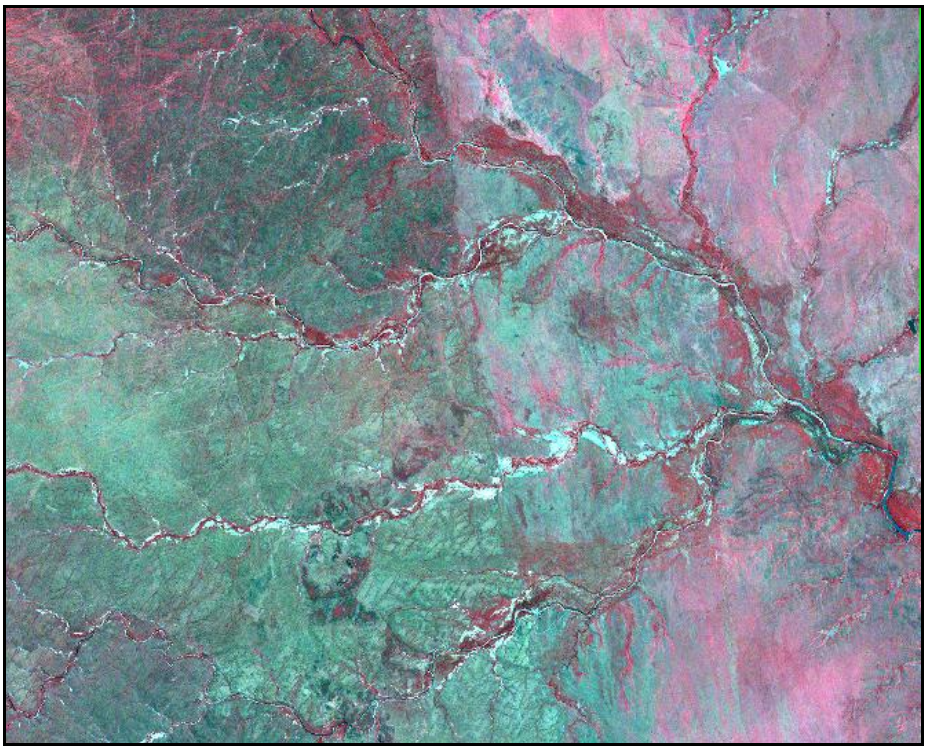


(a) (b)

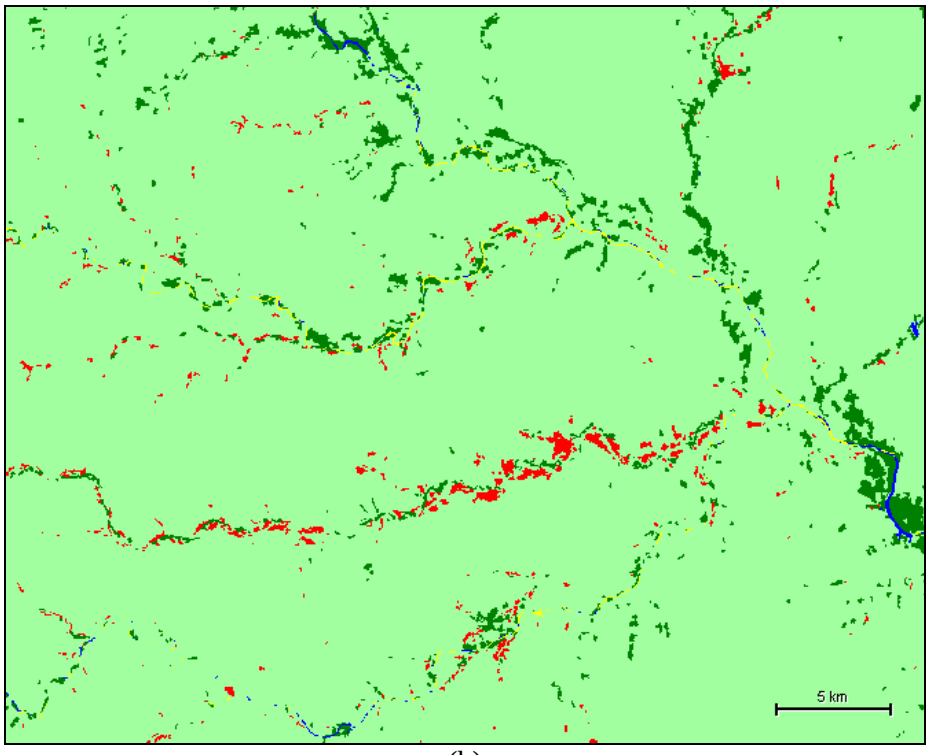
Figure 47: Geology (a) and topography classification (b) showing drainage lines as unclassified and crests as out of the area of interest (AOI) for the Shingwedzi study site using Landsat 7 imagery.

Land cover classification of Landsat imagery

The classification result from the classification algorithm developed for the Shingwedzi study site using the Landsat imagery is shown in Figure 48. The water, river sand, riverine vegetation, savanna and sodic sites are shown to illustrate the relative proportion of sodic sites in the landscape. Figure 49 shows the sodic sites only and includes the main rivers and their tributaries to clearly illustrate the position of sodic sites in the landscape in relation to drainage lines and rivers.



(a)



(b)

Figure 48: Landsat 7 ETM + (21 May 2001) false colour image (a) (RGB = Band 4:3:2) and classification (b) of the Shingwedzi study site showing the classes Water (blue), River Sand (yellow), Riverine vegetation (dark green), Savanna (light green) and Sodic sites (red).

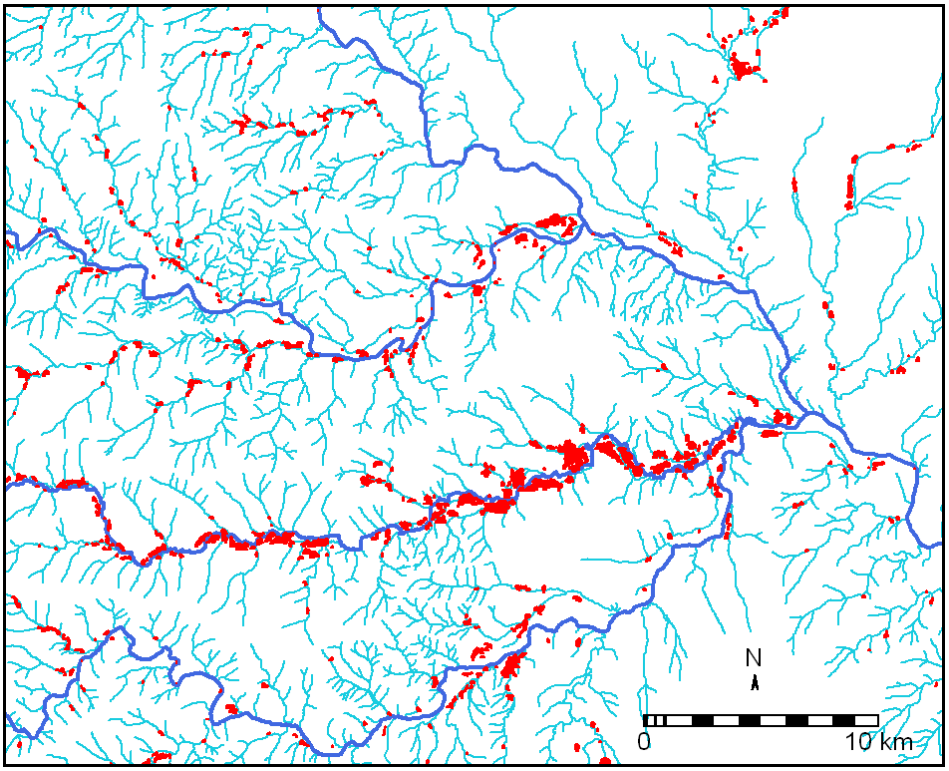


Figure 49: Landsat 7 ETM+ (21 May 2001) classified sodic sites (red) showing the main Shingwedzi catchment rivers (blue) and tributaries (light blue). Area of sodic sites = 15.36 km^2 out of 1316.97 km^2 total area = 1.16 % cover.

The sodic site classification result for the Landsat 7 ETM+ imagery dated 21 May 2001 (Figure 49) gives a sodic site area of 15.36 km^2 out of 1316.97 km^2 total area, which is a 1.16 % sodic site cover. The sodic sites occur along the drainage lines with a higher density in the granite than basalt areas.

Iterative accuracy assessment

The four classes described in Figure 29 are used for the accuracy assessment error matrix: riverine vegetation; savanna; river sand; sodic sites. Virtual random samples from the imagery and black and white orthophotos were identified and classified based on knowledge of the study area from the field sampling exercise. The advantage of this method is that the samples are taken from the same date as the imagery and that random sampling is not restricted by access issues. The training samples collected using visually assessed (virtual) samples are used to test the accuracy of the classification of sodic sites during the training phase (Table 9). However, ground truth validation samples are required to test if the visually assessed samples are sodic according to the decision tree and dispersion tests used in the field.

Table 9: Error matrix of random visually assessed samples (reference class) compared to the classification result (user class) for the Shingwedzi study site based on number of pixels.

User/Reference Class	***River sand***	***Savanna***	***Riverine veg***	***Sodic sites***	***SUM***
Confusion Matrix					
River sand	**331**	0	0	0	*331*
Savanna	0	**3228**	335	124	*3687*
Riverine vegetation	0	100	**2028**	0	*2128*
Sodic sites	10	0	0	**1441**	*1451*
SUM	341	3328	2363	1565	
Accuracy					
Producer	0.97	0.97	0.86	0.92	
User	1.00	0.88	0.95	0.99	
Kappa Index per class	0.97	0.94	0.80	0.90	
Overall Accuracy	**0.93**				
Overall Kappa Index	***0.89***				

The overall accuracy of 0.93 and an overall kappa index of 0.89 is well above the required 85% overall accuracy and over 70% per class. The bold diagonal figures show that most of the pixels selected for the samples were classified in the same class giving a high producers and user's accuracy per class. The sodic sites Producer accuracy is 0.92 and the User accuracy is 0.99 and Kappa Index per class of 0.90, which is a much higher result than using ground truth samples. The confusion between savanna and sodic sites is much lower due to the visual assessment of sodic site samples from the image and not on the ground.

Validation accuracy

The validation samples collected in the field are used to test the accuracy of the classification of sodic sites with an overall accuracy of 0.84 and an overall Kappa Index of 0.61 (Table 10). However, when the sodic sites are assessed on their own, the Producer accuracy is 0.58 with a user accuracy of 0.98 and Kappa Index per class of 0.49.

Table 10: Error matrix of ground truth samples (reference class) compared to the classification result (user class) for the Shingwedzi study site based on pixel numbers.

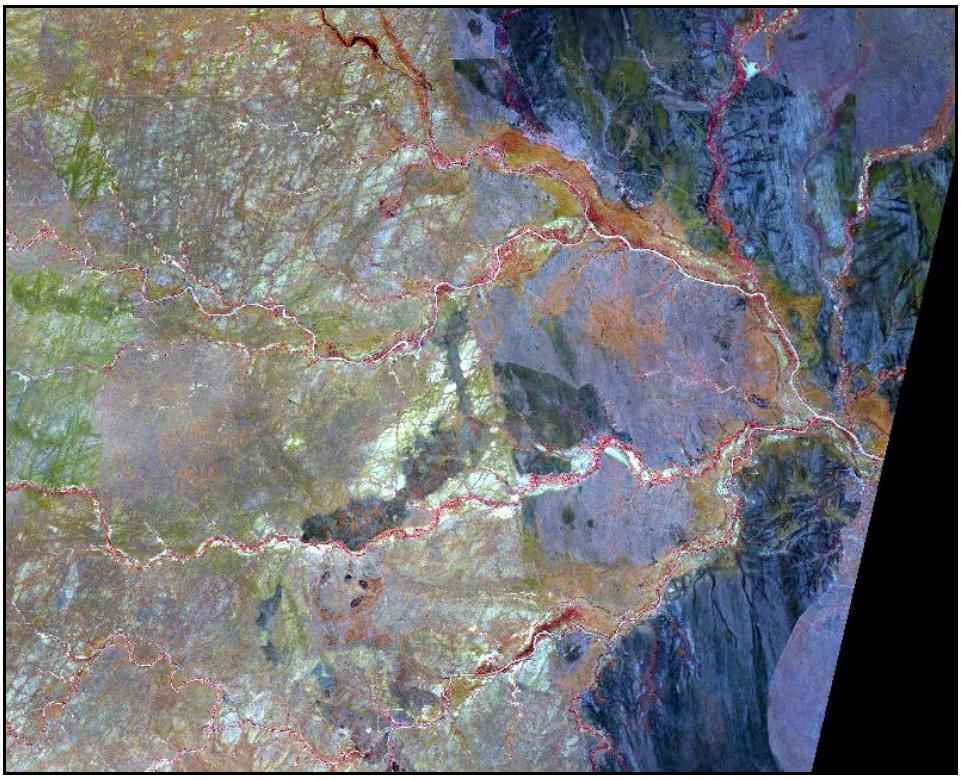
User/Reference Class	***River sand***	***Savanna***	***Riverine veg***	***Sodic sites***	***SUM***
Confusion Matrix					
River sand	**3**	0	2	79	*84*
Savanna	33	**3002**	127	433	*3595*
Riverine vegetation	1	25	**48**	8	*83*
Sodic sites	0	17	0	**705**	*722*
SUM	37	3044	180	1225	
Accuracy					
Producer	0.08	0.99	0.27	0.58	
User	0.04	0.84	0.59	0.98	
Kappa Index per class	0.06	0.93	0.25	0.49	
Overall Accuracy	**0.84**				
Overall Kappa Index	***0.61***				

The user accuracy indicates that out of the 722 pixels classified as sodic sites, 705 (or 98%) were sodic sample sites, which is very accurate. The producer accuracy indicates that of the 1225 pixels sampled as sodic sites in the field, only 705 pixels (58%) were classified as sodic sites with 433 (35%) classified as savanna. This indicates that the field samples included sodic sites that appear to be open woody sites in the field but in the imagery, the sites are difficult to differentiate from other savanna areas. This can be due to the fact that the samples were taken in 2007 or 2008 and the imagery is from 2001. The error matrix also highlights the confusion with riverine vegetation and river sand with savanna classes. This may be due to the mixed pixel effect of Landsat 7 30m data where the one pixel may contain trees and shrubs next to rivers, in combination with sand.

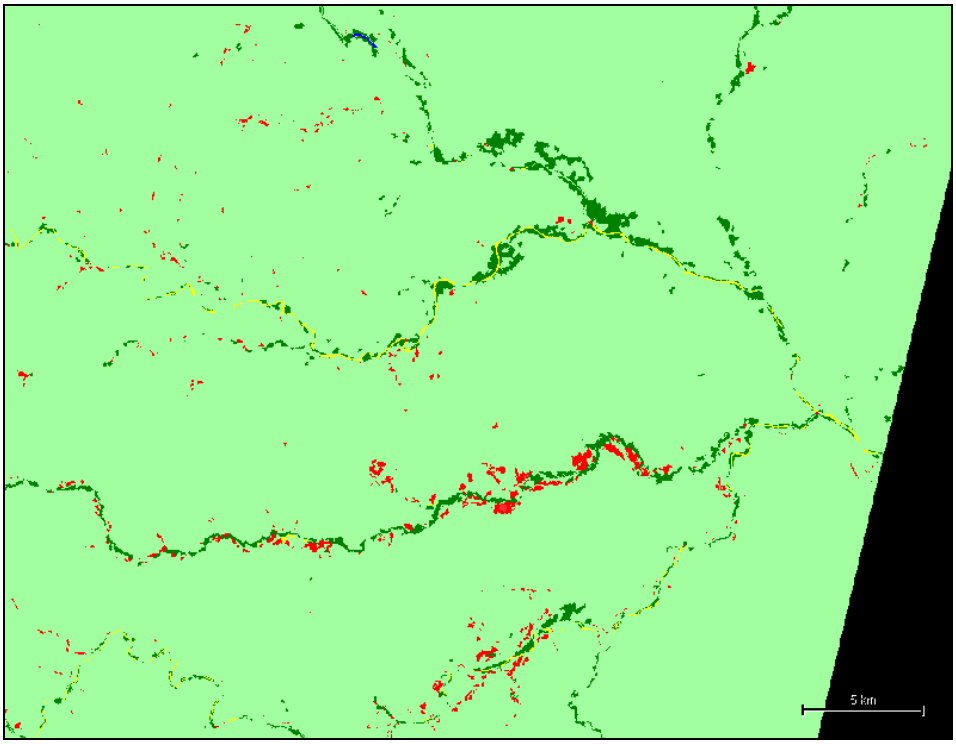
Land cover classification of SPOT 5 imagery

The SPOT 5 imagery was acquired on 5 October 2005 and 12 April 2008. According to the phenology cycle calculated using nine years of MODIS NDVI data as illustrated in Figure 39, the imagery from the 5 October 2005 is the peak of the dry season, and the imagery from 12 April 2008 falls in the late wet season or early dry season, similar to the Landsat 7 ETM+ imagery acquired on 21 May 2001. Both images were classified using different algorithms. The dry season classification was compared to the wet season imagery to determine the best algorithm to repeat on all SPOT 5 imagery for the Ripape study site of similar phenological season.

The classification results for the river sand, riverine vegetation, savanna and sodic site classes of the dry season SPOT 5 image are shown in Figure 50 (b), together with a false colour image of the study site (Figure 50 a). From the bright areas in the image, it can be seen how many areas are bare and devoid of vegetation cover in the dry season, and the sodic sites are easily confused with the other bare soils. The sodic sites class is illustrated in Figure 51 showing only the sodic sites, in relation to the rivers and the different geologies. Although the larger sodic sites appear to be classified, the smaller bare areas have been omitted in an effort to exclude other bare soils from the classification. Only 0.77% of the area was classified as sodic. The error matrix result for training of the classification algorithm (Table 11) was calculated from the visually assessed reference samples to ensure enough samples per class for a robust statistical interpretation. The overall accuracy is 90% with a Kappa Index of 82%.



(a)



(b)

Figure 50: SPOT 5 (5 October 2005) false colour image (a) (RGB = Band 4:3:2) and Classification (b) of the Shingwedzi study site showing four classes: River Sand (yellow), Riverine vegetation (dark green), Savanna (light green) and Sodic sites (red).

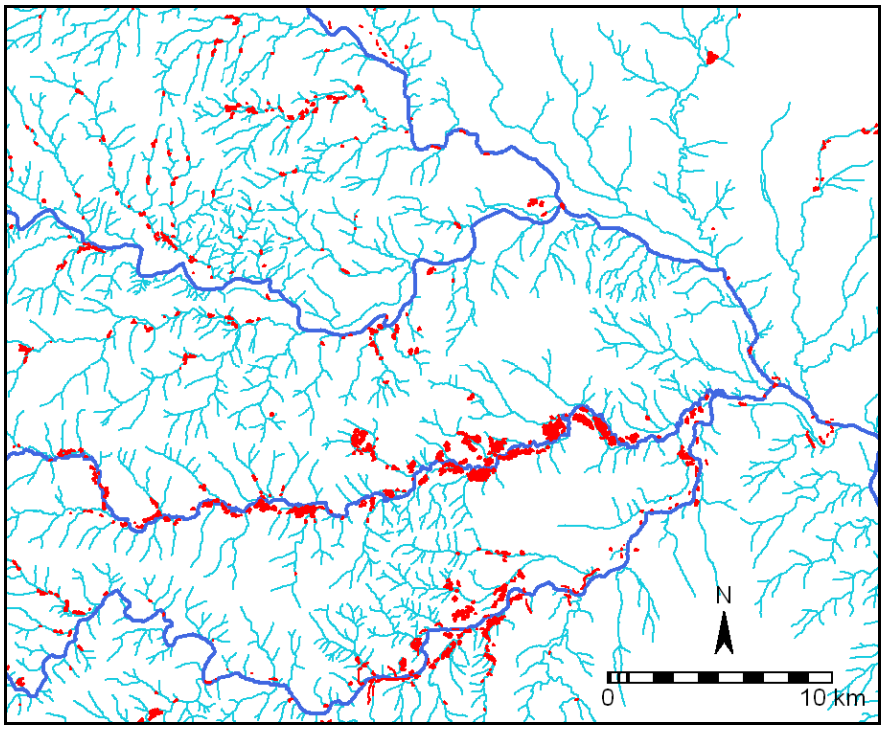


Figure 51: SPOT 5 (5 October 2005) classified sodic sites (red) showing the main Shingwedzi catchment rivers (blue) and tributaries (light blue). Area of sodic sites = 9.28 km^2 out of 1202.86 km^2 total area = 0.77 % cover.

Table 11: Error matrix of random visually assessed samples (reference class) compared to the classification result (user class) for the Shingwedzi study site based on pixel numbers.

User/Reference Class	***River sand***	***Savanna***	***Riverine veg***	***Sodic sites***	***SUM***
Confusion Matrix					
River sand	**2926**	0	30	117	*3073*
Savanna	373	**23779**	835	2155	*27142*
Riverine vegetation	205	368	**4557**	44	*5174*
Sodic sites	18	0	2	**5531**	*5551*
SUM	3522	24147	5424	7847	
Accuracy					
Producer	0.83	0.98	0.84	0.70	
User	0.95	0.88	0.88	1.00	
Kappa Index per class	0.82	0.95	0.82	0.66	
Overall Accuracy	**0.90**				
Overall Kappa Index	***0.82***				

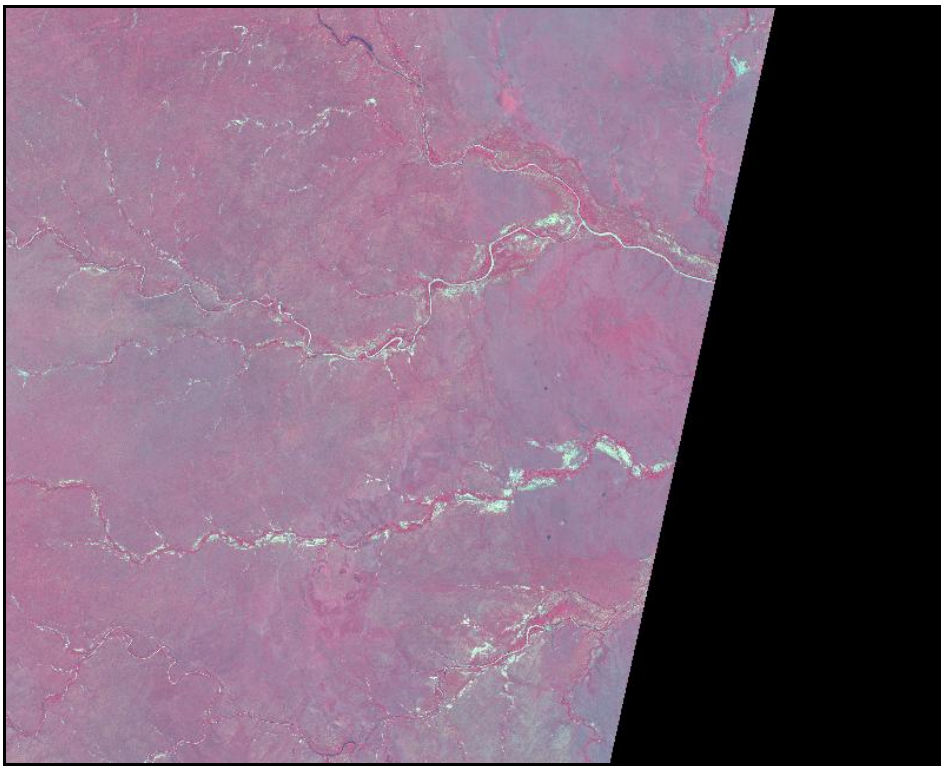
The error matrix (Table 12) calculated using the ground truth samples has a much lower accuracy result. The overall accuracy is only 65%, well below the recommended 85%, and the Kappa Index is 48%. The error matrix highlights where the confusion has occurred between the sodic sites identified in the field and the savanna class. A large number of sodic site sample pixels have been classified as savanna. The classification algorithm has confused dry savanna areas with sodic sites, due to the large proportion of bare soil in the landscape.

Table 12: Error matrix of ground truth samples (reference class) compared to the classification result (user class) for the Shingwedzi study site based on pixel numbers.

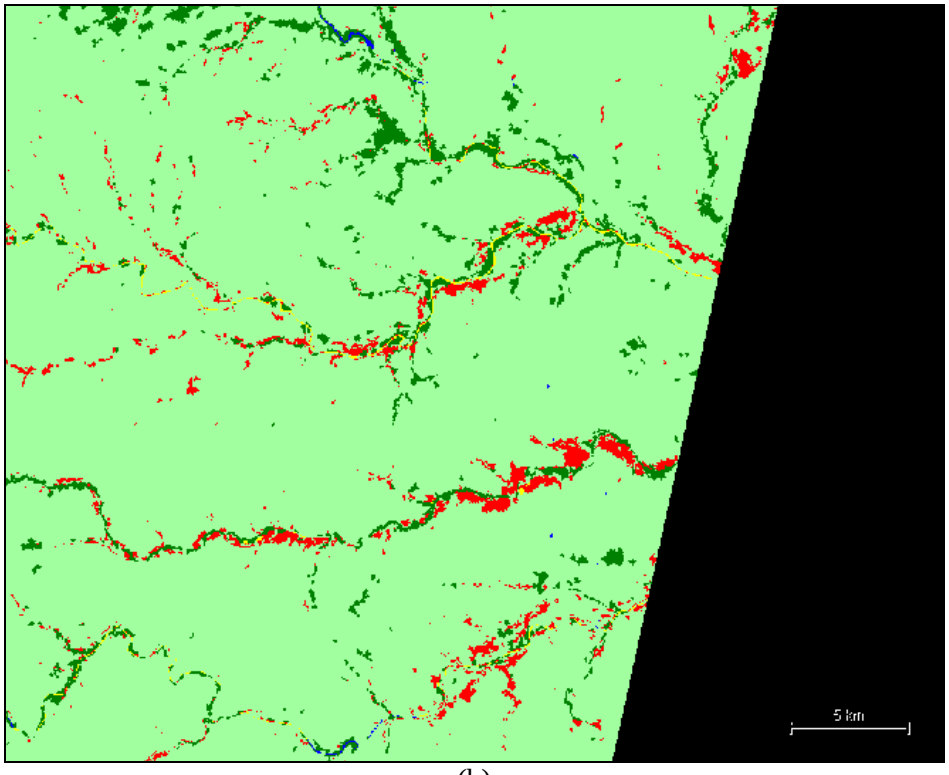
User/Reference Class	***River sand***	***Savanna***	***Riverine veg***	***Sodic sites***	***SUM***
Confusion Matrix					
River sand	**1487**	0	26	95	*1608*
Savanna	234	**13307**	1511	9245	*24297*
Riverine vegetation	103	25	**4381**	631	*5140*
Sodic sites	0	0	5	**3248**	*3253*
SUM	1824	13332	5923	13219	
Accuracy					
Producer	0.82	1.00	0.74	0.25	
User	0.92	0.55	0.85	1.00	
Kappa Index per class	0.81	0.99	0.69	0.17	
Overall Accuracy	**0.65**				
Overall Kappa Index	***0.48***				

The SPOT 5 wet season image was classified by applying an algorithm adapted for the higher vegetation cover and more obvious sodic sites. The classification results for the river sand, riverine vegetation, savanna and sodic site classes of the wet season SPOT 5 image are shown in Figure 52 (b). The false colour image of the study site (Figure 52a) shows the sodic sites clearly defined in comparison with the dry season imagery (Figure 50b). The areas classified as sodic cover 26.74km^2 of the study site which is 2.86%, compared to 0.77% of the dry season image (Figure 53). This indicates that the area covered by sodic sites is greatly under estimated by the dry season imagery. The Landsat 7 classification estimated a 1.16% area of sodic sites, which compared to the wet season SPOT 5 image, may show that smaller sodic sites where included due to the higher resolution of SPOT 5 at 10m compared to 30m for Landsat.

The accuracy assessment using random samples selected from the imagery shows an overall accuracy of 88% and an overall Kappa Index of 78% (Table 13). The sodic site class producer accuracy is 91%, the user accuracy is 93% and Kappa Index of 89%. There is some confusion between riverine vegetation and savanna, possibly due to the high biomass of both vegetation types during the wet season. The validation samples collected in the field (ground truth samples) are used to test the accuracy of the classification of sodic sites with an overall accuracy of 69% and an overall Kappa Index of 52% (Table 14) which is below expected acceptable accuracies in the literature (Thomlinson, Bolstad and Cohen, 1999). The producer accuracy for sodic sites is 52% with a user accuracy of 96% and a Kappa Index of 39%. Again, there is confusion in the matrix between the sodic site samples that have been classified as savanna. The ground truth data includes woody covered sodic sites more than the visually assessed image samples.



(a)



(b)

Figure 52: SPOT 5 (12 April 2008) false colour image (a) (RGB = Band 4:3:2) and Classification (b) of the Shingwedzi study site showing four classes: Water (blue), River Sand (yellow), Riverine vegetation (dark green), Savanna (light green) and Sodic sites (red).

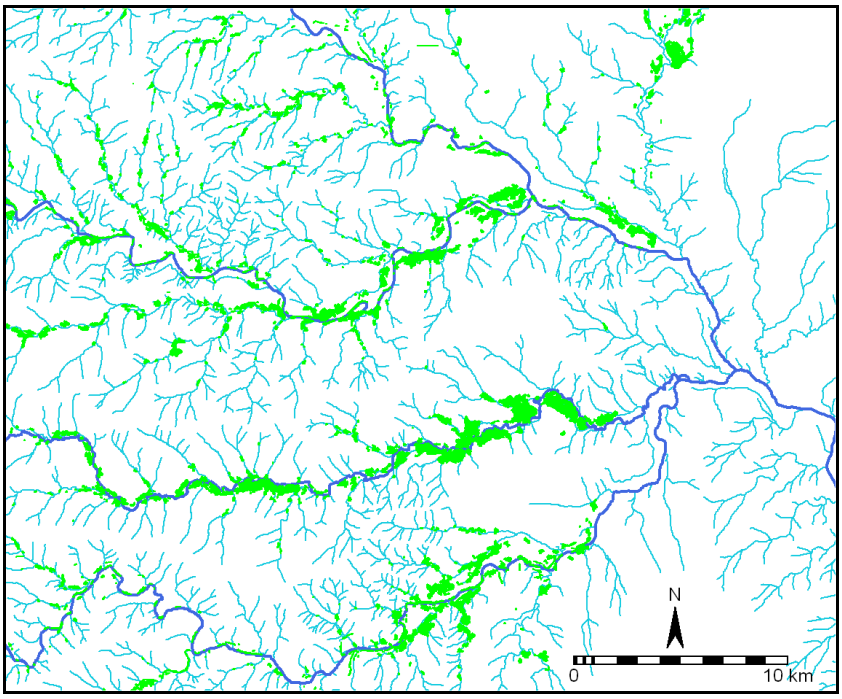


Figure 53: SPOT 5 (12 April 2008) classified sodic sites (green) showing the main Shingwedzi catchment rivers (blue) and tributaries (light blue). Area of sodic sites = 26.74 km^2 out of 935.85 km^2 total area = 2.86 % cover.

Table 13: Error matrix of random visually assessed samples (reference class) compared to the classification result (user class) for the Shingwedzi study site based on pixel numbers.

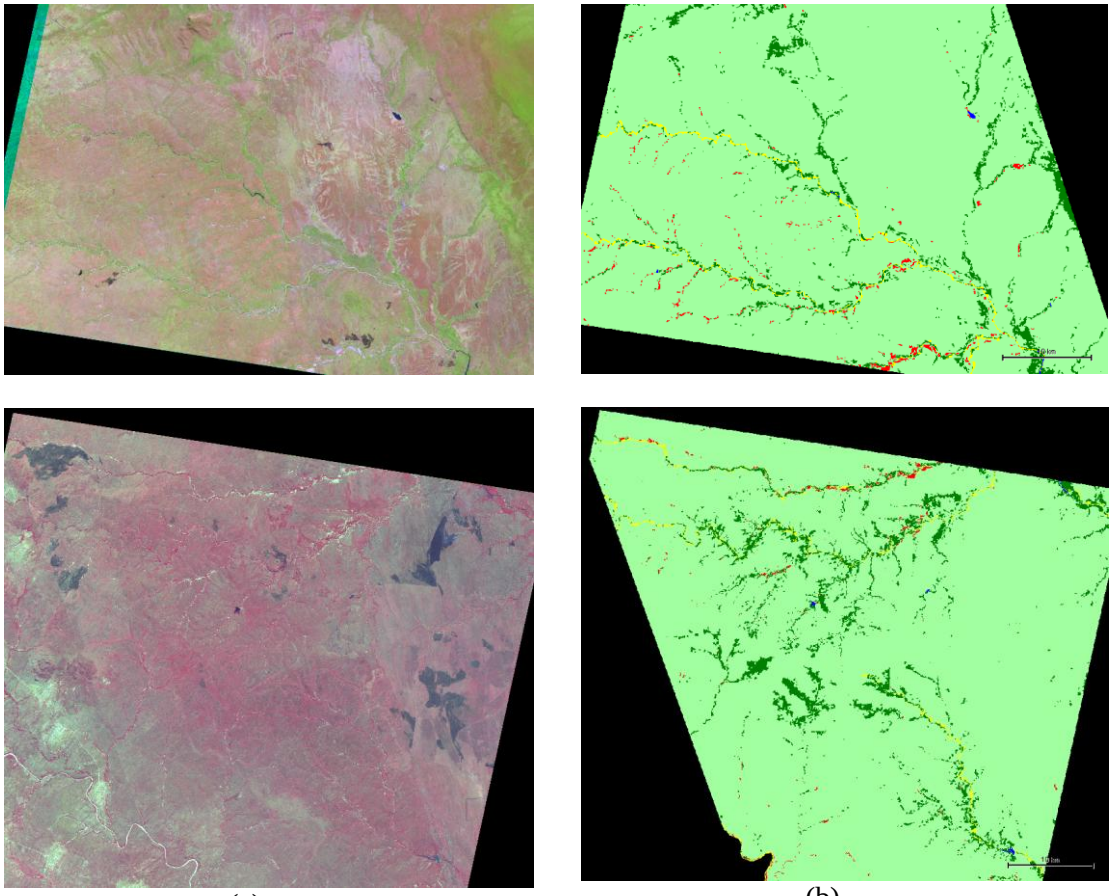
User/Reference Class	***River sand***	***Savanna***	***Riverine veg***	***Sodic sites***	***SUM***
Confusion Matrix					
River sand	**2198**	0	76	0	*2274*
Savanna	348	**23986**	2657	659	*27650*
Riverine vegetation	248	161	**2548**	52	*3009*
Sodic sites	383	0	143	**7136**	*7662*
unclassified	345	0	0	0	*345*
SUM	3522	24147	5424	7847	
Accuracy					
Producer	0.62	0.99	0.47	0.91	
User	0.97	0.87	0.85	0.93	
Kappa Index per class	0.60	0.98	0.43	0.89	
Overall Accuracy	**0.88**				
Overall Kappa Index	***0.78***				

Table 14: Error matrix of ground truth samples (reference class) compared to the classification result (user class) for the Shingwedzi study site based on pixel numbers.

User/Reference Class	***River sand***	***Savanna***	***Riverine veg***	***Sodic sites***	***SUM***
Confusion Matrix					
River sand	**1278**	0	39	89	*1406*
Savanna	176	**13153**	3223	5466	*22018*
Riverine vegetation	47	130	**2427**	764	*3368*
Sodic sites	169	49	101	**6896**	*7215*
unclassified	154	0	133	4	*291*
SUM	1824	13332	5923	13219	
Accuracy					
Producer	0.70	0.99	0.41	0.52	
User	0.91	0.60	0.72	0.96	
Kappa Index per class	0.69	0.96	0.35	0.39	
Overall Accuracy	**0.69**				
Overall Kappa Index	***0.52***				

Land cover classification of ASTER imagery

The ASTER imagery was acquired on 29 June 2006. According to the phenology cycle calculated using nine years of MODIS NDVI data as illustrated in Figure 39, the imagery from the 29 June 2006 falls in the late wet season or early dry season, similar to the Landsat 7 ETM+ imagery acquired on 21 May 2001 and the SPOT 5 imagery acquired on 12 April 2008. The imagery and classification of ASTER imagery is shown in Figure 54 and Figure 55. The accuracy assessments for the random visually assessed samples (Table 15) and ground truth samples (Table 16) illustrate the difference between the samples taken from the imagery and the possible contribution of misregistration of georeferences seen with ASTER imagery to the low accuracies for ground truth samples.



(a) (b)

Figure 54: ASTER (29 June 2006) false colour image (a) (RGB = Band 4:3:2) and Classification (b) of the Shingwedzi study site showing four classes: River Sand (yellow), Riverine vegetation (dark green), Savanna (light green) and Sodic sites (red).

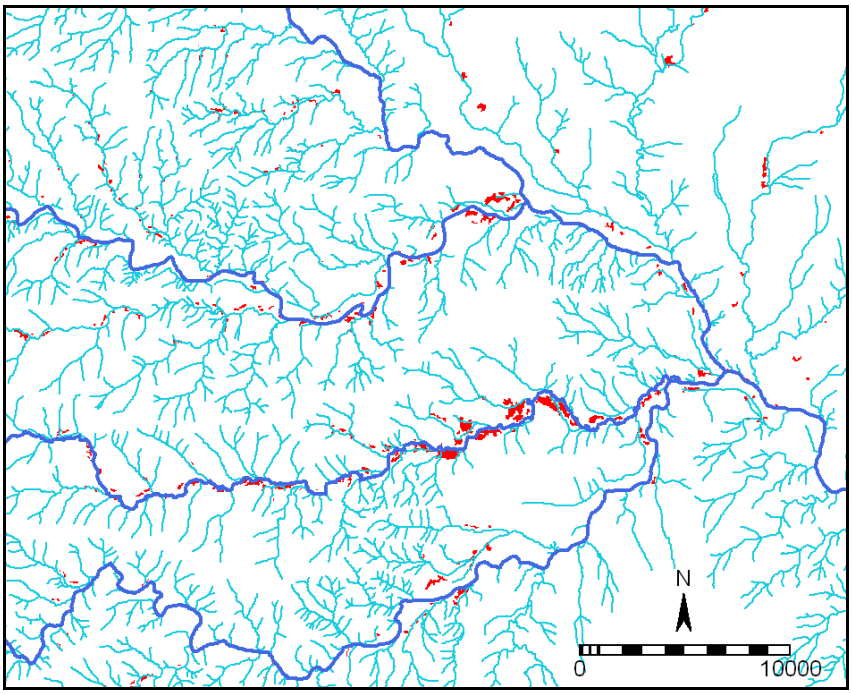


Figure 55: ASTER (29 June 2006) classified sodic sites (red) showing the main Shingwedzi catchment rivers (blue) and tributaries (light blue). Area of sodic sites = 12.03 km^2 out of 1296.6 km^2 total area 0.93 % cover.

Table 15: Error matrix of random visually assessed samples (reference class) compared to the classification result (user class) for the Shingwedzi study site based on pixel numbers.

User/Reference Class	*River sand*	*Savanna*	*Riverine veg*	*Sodic sites*	*SUM*
Confusion Matrix					
River sand	**1074**	0	166	37	*1277*
Savanna	309	**12246**	829	940	*14324*
Riverine vegetation	161	138	**1552**	34	*1885*
Sodic sites	18	0	8	**2823**	*2849*
SUM	1562	12384	2555	3834	
Accuracy					
Producer	0.69	0.99	0.61	0.74	
User	0.84	0.85	0.82	0.99	
Kappa Index per class	0.66	0.97	0.55	0.68	
Overall Accuracy	**0.87**				
Overall Kappa Index	***0.75***				

Table 16: Error matrix of random ground truth samples (reference class) compared to the classification result (user class) for the Shingwedzi study site based on pixel numbers.

User/Reference Class	*River sand*	*Savanna*	*Riverine veg*	*Sodic sites*	*SUM*
Confusion Matrix					
River sand	**501**	38	127	178	*844*
Savanna	214	**6003**	1110	3635	*10962*
Riverine vegetation	76	364	**1456**	376	*2272*
Sodic sites	17	0	2	**2246**	***2265***
SUM	808	6405	2695	6435	*16373*
Accuracy					
Producer	0.62	0.94	0.54	0.35	
User	0.59	0.55	0.64	0.99	
Kappa Index per class	0.60	0.90	0.45	-0.07	
Overall Accuracy	**0.62**				
Overall Kappa Index	***0.42***				

Summary of results: classification algorithm for the Shingwedzi training site

The accuracy assessments of the visually interpreted samples from imagery had consistently higher results than for the ground truth sample data (Table 17). The sodic site ground truth samples were consistently classified as savanna for all images, showing that the classification algorithm is more accurate for bare sodic sites than vegetated sodic sites. The requirement of 85% overall accuracy and over 70% per class is satisfied by the Landsat 7 and SPOT 5 late wet to early dry season imagery using the visual imagery samples. Although the mid dry season SPOT 5 imagery has an overall accuracy of 90% (Kappa Index of 82%), the area of sodic sites is 26% of the sodic area for the growing season image. The ASTER visually assessed image samples were lower than the Landsat or SPOT imagery. The ground truth sample results for ASTER were very low for the Kappa Indices confirming the effect of inaccurate geo-referencing, despite resampling of the imagery to improve geolocation of the pixels.

Table 17: Summary of accuracy assessment results for all imagery classification algorithms for the Shingwedzi study site where the first value is for random visually assessed samples and the value in bold is based on the stratified random ground truth data.

Imagery/ Date	***Season***	***Sampling design***	***Overall Accuracy***	***Overall Kappa Index***	***Sodic Producer***	***Sodic User***	***Sodic Kappa Index***	***% Sodic Cover***
Landsat 7 ETM+								
21/05/2001	Late wet/ Early dry	Visual assess **Ground truth**	0.93 **0.84**	0.89 **0.61**	0.92 **0.58**	0.99 **0.98**	0.90 **0.49**	*1.16*
SPOT 5								
05/10/2005	Mid dry	Visual assess **Ground truth**	0.90 **0.65**	0.82 **0.48**	0.70 **0.25**	1.00 **1.00**	0.66 **0.17**	*0.77*
12/04/2008	Late wet/ Early dry	Visual assess **Ground truth**	0.88 **0.69**	0.78 **0.52**	0.91 **0.52**	0.93 **0.96**	0.89 **0.39**	*2.86*
ASTER								
29/06/2006	*Late wet/ Early dry*	*Visual assess* ***Ground truth***	*0.87* ***0.62***	*0.75* ***0.42***	*0.74* ***0.35***	*0.99* ***0.99***	*0.68* ***-0.07***	*0.93*

Underscore indicates results over 85% overall accuracy and over 70% per class

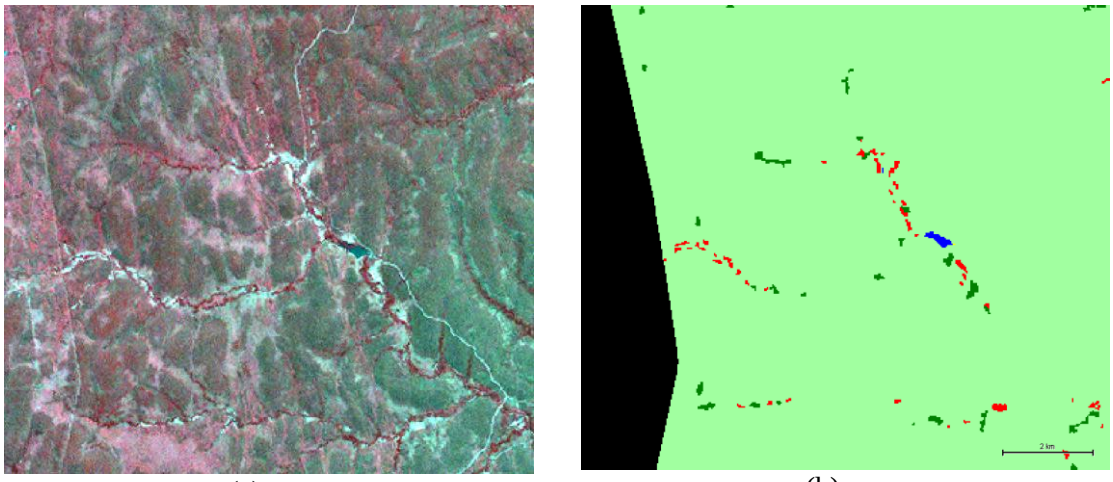
3.3.3 Shingwedzi study site classification algorithm applied to Ripape study site

The algorithms developed for the Shingwedzi study site are applied to Landsat 7 and SPOT 5 imagery on the Ripape site to test the automated repeatablitliy of the eCognition process tree. The ASTER imagery classification algorithm was not tested for the Ripape study site due to the errors of misregistration of the pixels and the lack of spatial coverage to test repeatability of the classification for the entire KNP.

Land cover classificiation of Landsat 7 imagery on the Ripape study site

The classification algorithm developed for the Shingwedzi study site was implemented for the Landsat 7 imagery for the Ripape study site. The results of the classification are shown in Figure 56 and 57 showing the false colour Landsat image, the full classification of four classes and the sodic site classification presented with the rivers and tributraries of the Ripape River.

The error matrix (Table 18) was calculated using the visually assessed samples as there were no ground truth samples taken for the Ripape study site. The statistics will be compared with the same results from the Shingwedzi study site for the visually assessed sample error matrix only.



(a) (b)

Figure 56: Landsat 7 ETM + (30 May 2001) false colour image (a) (RGB = Band 4:3:2) and Classification (b) of the Ripape study site showing four classes: River Sand (yellow), Riverine vegetation (dark green), Savanna (light green) and Sodic sites (red).

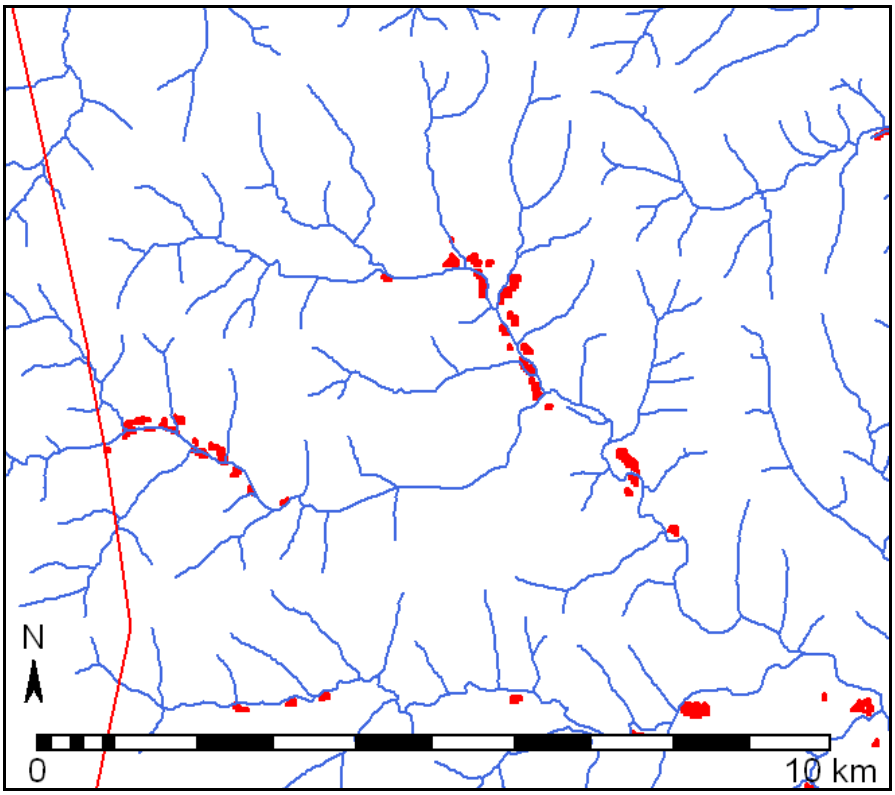


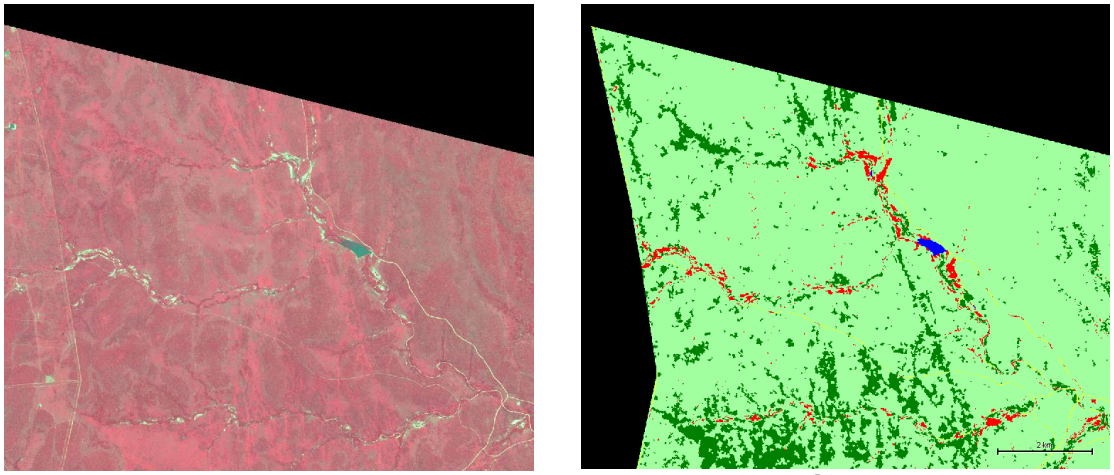
Figure 57: Landsat 7 ETM+ (21 May 2001) classified sodic sites (red) showing the Ripape catchment rivers and tributaries (blue). Area of sodic sites = 0.46 km^2 out of 100.12 km^2 total area = 0.46 % cover.

Table 18: Error matrix of ground truth samples (reference class) compared to the classification result (user class) for the Ripape study site based on pixel numbers.

User/Reference Class	***River sand***	***Savanna***	***Riverine veg***	***Sodic sites***	***SUM***
Confusion Matrix					
River sand	**0**	0	0	0	*0*
Savanna	45	**1378**	300	91	*1814*
Riverine vegetation	0	0	**191**	0	*191*
Sodic sites	6	0	0	**278**	*284*
SUM	51	1378	491	369	
Accuracy					
Producer	0	1.00	0.39	0.75	
User	0	0.76	1.00	0.98	
Kappa Index per class	0	1.00	0.33	0.72	
Overall Accuracy	**0.81**				
Overall Kappa Index	***0.60***				

Land cover classification of SPOT 5 imagery on the Ripape study site

There were two SPOT 5 images suitable for classification of sodic sites for the Ripape study site. The scenes were from the peak wet season and early dry season and the repeatability of the algorithm from Shingwedzi will be tested on both scenes to see if a very high NDVI image is classified as a scene later in the season. The results of the peak wet season image are shown in Figure 58 and 59 with Table 19 giving the accuracy assessment results in the error matrix.



(a) (b)

Figure 58: SPOT 5 (26 March 2006) false colour image (a) (RGB = Band 4:3:2) and Classification (b) of the Ripape study site showing four classes: River Sand (yellow), Riverine vegetation (dark green), Savanna (light green) and Sodic sites (red).

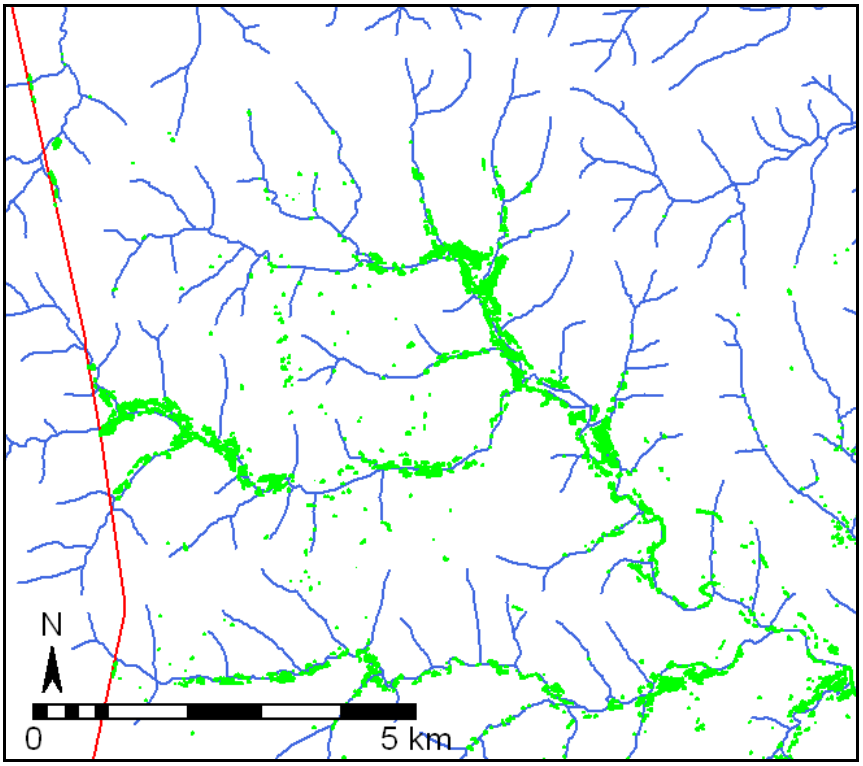
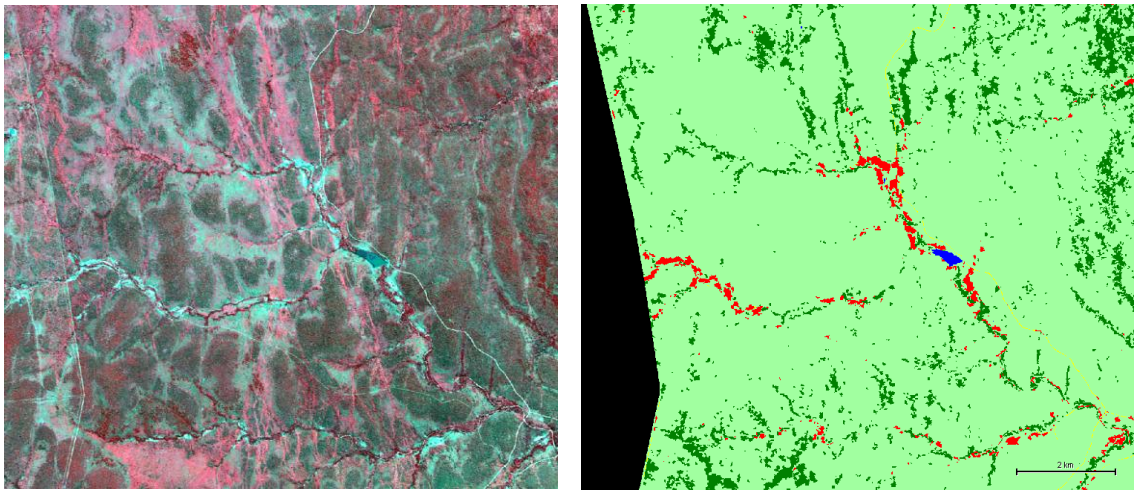


Figure 59: SPOT 5 (26 March 2006) classified sodic sites (green) showing the main Ripape catchment rivers (blue) and tributaries (light blue). Area of sodic sites = 1.44 km^2 out of 79.81 km^2 total area = 1.8 % cover.

Table 19: Error matrix of ground truth samples (reference class) compared to the classification result (user class) for the Ripape study site based on pixel numbers.

User/Reference Class	***River sand***	***Savanna***	***Riverine veg***	***Sodic sites***	***SUM***
Confusion Matrix					
River sand	**56**	0	0	0	*56*
Savanna	0	**23556**	1968	485	*26009*
Riverine vegetation	0	1806	**4373**	0	*6179*
Sodic sites	486	0	0	**7705**	*8191*
SUM	542	25362	6341	8190	
Accuracy					
Producer	0.10	0.93	0.69	0.94	
User	1.00	0.91	0.71	0.94	
Kappa Index per class	0.10	0.80	0.63	0.93	
Overall Accuracy	**0.88**				
Overall Kappa Index	***0.78***				

The second set of SPOT 5 imagery is for early dry season imagery shown in Figure 60 and 61 with the accuracy assessments in Table 20.



(a) (b)

Figure 60: SPOT 5 (12 May 2006**)** false colour image (a) (RGB = Band 4:3:2) and Classification (b) of the Ripape study site showing four classes: River Sand (yellow), Riverine vegetation (dark green), Savanna (light green) and Sodic sites (red).

Table 20: Error matrix of ground truth samples (reference class) compared to the classification result (user class) for the Ripape study site based on pixel numbers.

User/Reference Class	***River sand***	***Savanna***	***Riverine veg***	***Sodic sites***	***SUM***
Confusion Matrix					
River sand	**0**	0	0	0	*0*
Savanna	36	**23789**	1264	1265	*26354*
Riverine vegetation	2	1473	**5415**	0	*6890*
Sodic sites	504	100	61	**6925**	*7590*
SUM	542	25362	6740	8190	
Accuracy					
Producer	0	0.94	0.80	0.85	
User	0	0.90	0.79	0.91	
Kappa Index per class	0	0.83	0.76	0.81	
Overall Accuracy	**0.88**				
Overall Kappa Index	***0.78***				

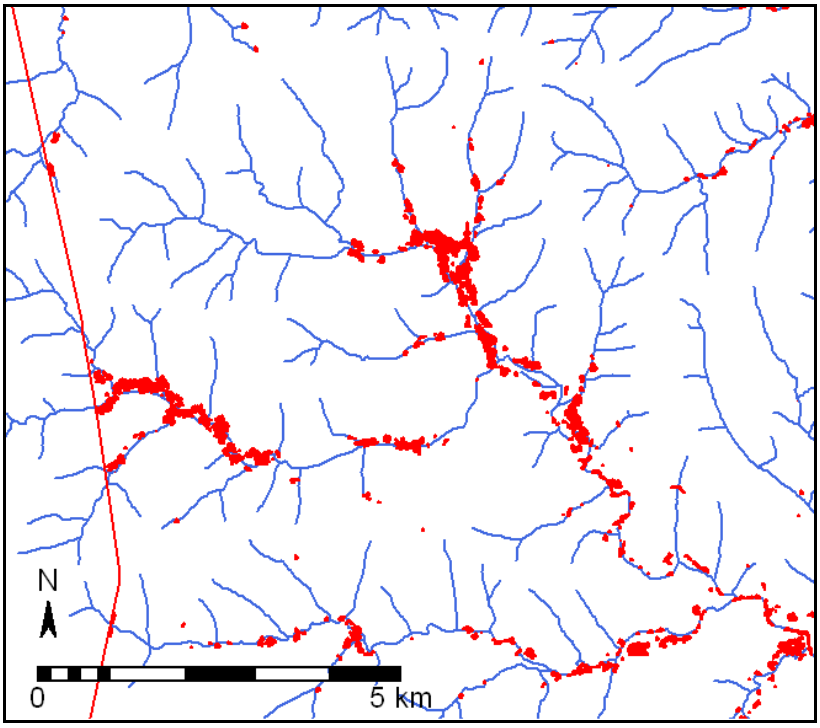


Figure 61: SPOT 5 (12 May 2006) classified sodic sites (green) showing the main Ripape catchment rivers (blue) and tributaries (light blue). Area of sodic sites = 1.495 km2 out of 100.13 km2 total area = 1.49 % cover.

Summary of results: Repeatable classification for the Ripape study site

The classification developed for the Shingwedzi was applied to the Ripape study site Landsat 7 and SPOT 5 imagery. These are the sensors that provide scenes for full coverage of the park. To test the repeatability of the classification algorithm developed in the Shingwedzi study site, scenes of similar phenology status were selected and the results for the Ripape study site are shown together with the Shingwedzi accuracies for comparison (Table 21).

Table 21: Summary of accuracy assessment results for Landsat 7 and SPOT 5 imagery classification algorithms developed on the Shingwedzi study site and applied to the Ripape study site for random visually assessed samples.

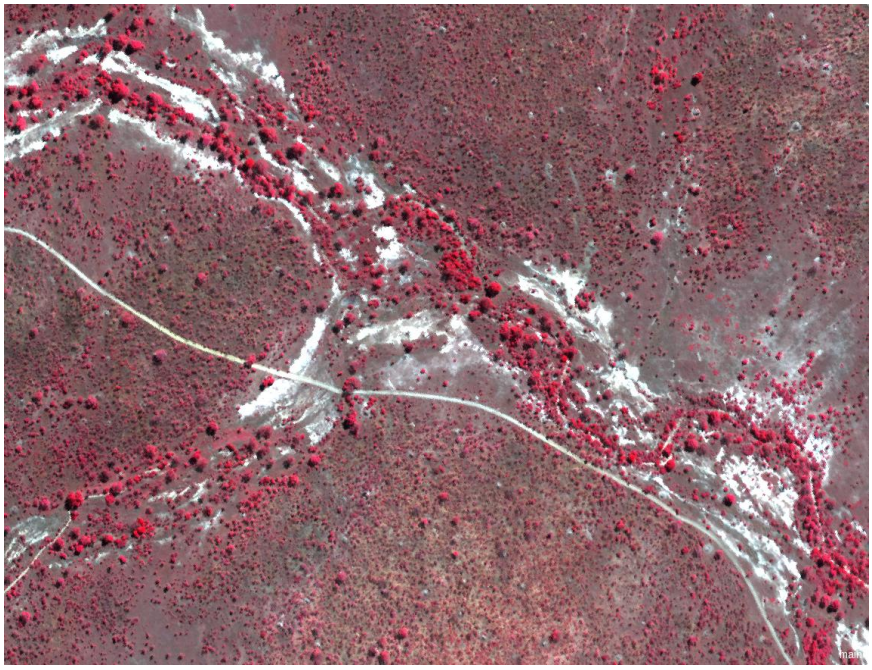
Imagery/ Date	***Study site***	***Season***	***Sampling design***	***Overall Accuracy***	***Overall Kappa Index***	***Sodic Producer***	***Sodic User***	***Sodic Kappa Index***	***% Sodic Cover***
Landsat 7 ETM+									
30/05/2001	**Ripape**	Late wet/ Early dry	Visual assess	**0.79**	**0.56**	**0.64**	**1.00**	**0.6**	***0.46***
21/05/2001	*Shingwedzi*	*Late wet/ Early dry*	*Visual assess*	*0.81*	*0.60*	*0.75*	*0.98*	*0.72*	*1.16*
SPOT 5									
26/03/2006	**Ripape**	Mid wet	Visual assess	**0.88**	**0.78**	**0.94**	**0.94**	**0.93**	***1.8***
12/05/2006	**Ripape**	Late wet	Visual assess	**0.88**	**0.78**	**0.85**	**0.91**	**0.81**	***1.49***
12/04/2008	*Shingwedzi*	*Late wet/ Early dry*	*Visual assess*	*0.88*	*0.78*	*0.91*	*0.93*	*0.89*	*2.86*

Underscore indicates results over 85% overall accuracy and over 70% per class

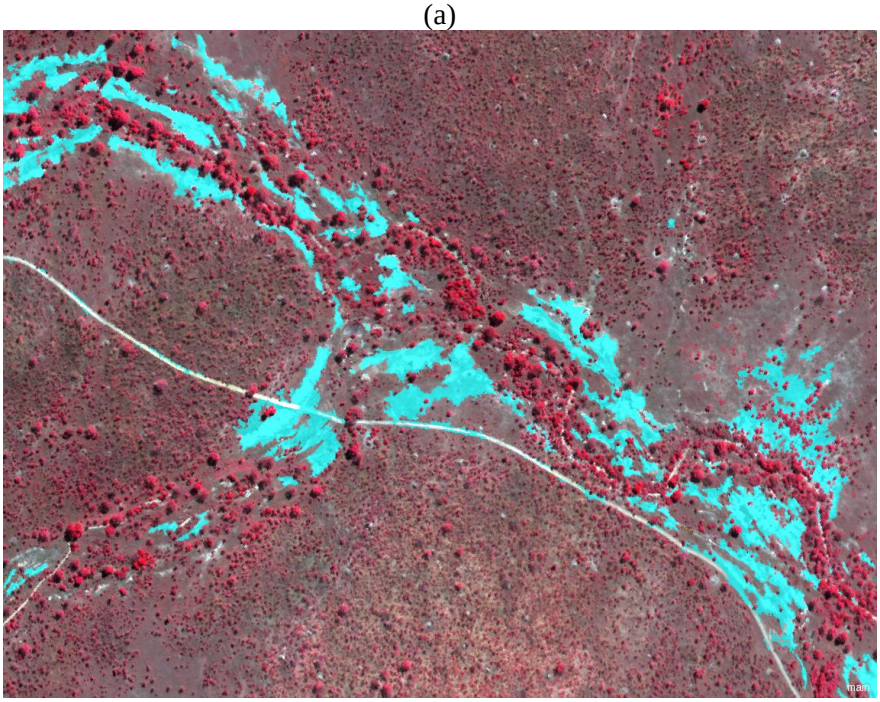
The Landsat 7 overall accuracy and sodic class accuracies for the Ripape study site are lower than the Shingwedzi study site in all cases, and fall below the recommended 85% overall and 70% for each class. The SPOT 5 accuracies are almost identical and the results are above the recommended overall and individual class accuracies. SPOT 5 is therefore recommended as the imagery to develop and apply repeatable classification algorithms for the classification of sodic sites in the KNP.

3.3.4 CAO Hyperspectral and LiDAR imagery for sodic size change classification

Although the CAO Hyperspectral and LiDAR imagery is limited in spatial coverage and cannot be used to classifiy sodic sites over a wide area, the inclusion of height data to help with classification of savanna areas is worth investigating. The classification of sodic sites for change analysis would require higher resolution imagery than Landsat or SPOT 5 and hypespectral may contribute to small scale sodic site monitoring. The scene for the Ripape study site was acquired during April 2008. According to the phenology cycle calculated using nine years of MODIS NDVI data as illustrated in Figure 43, the imagery from the April 2008 is the early dry season. The sodic site classification result is shown in Figure 62.



(a)



(b)

Figure 62: CAO Hyperspectral imagery (25 April 2008) false colour image (a) (RGB = Band 60:45:20) and classification of sodic sites (b) (turquoise) of a subset of the Ripape study site.

The spectral separation of bare soils was found to be most clear in the blue wavelengths. This was used at the largest object level to confirm bare soil for large objects. From the spectral signatures from selected samples, a high infra-red value was seen for sodic bare soils and green or dense vegetation. The distinction between these two classes was found

in the absorption in the red band by green vegetation known as the red edge and the vegetation index NDVI was calculated and used to distinguish between sodic bare soil and green vegetation. Objects with an NDVI similar to dry grass and adjoining an object classified as sodic were included in the sodic class, but potential sodic objects in isolation or without the sodic core identified form the clustering exercise were excluded as small isolated bare areas. The bare areas on crests were removed using the DTM so that only bare areas in drainage lines were classified as sodic (Figure 63).

The classification result for the combination of spectral properties and object heights show a much smaller sodic site area (Figure 63). This method requires further investigation to separate bare sodic areas from other bare ground. No accuracy assessment was applied as no ground truth data was collected at this site. To measure the changes in sodic site size the sodic sites ground truth will require definition of the edge of the sodic site and a recording of the spatial distribution of standing biomass on the sodic soils.

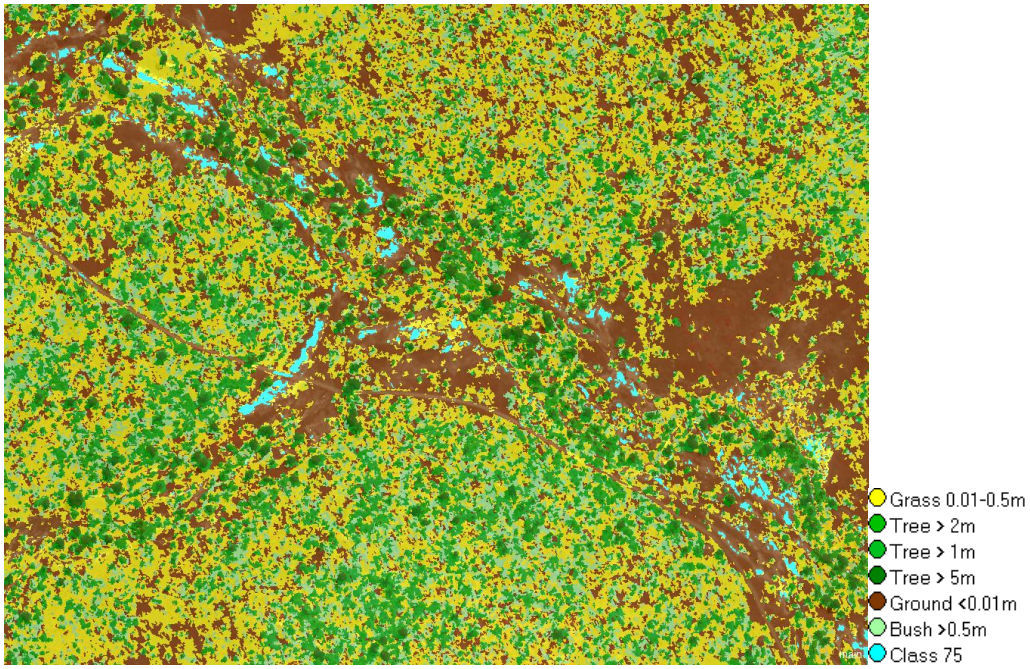


Figure 63: CAO Hyperspectral imagery (25 April 2008) classified by object heights from LiDAR imagery for a subset of the Ripape study site showing ground, grass, bush and tree heights and the sodic core area from the spectral signature clustering result (Class 75 = top blue signature of Figure 38).

3.3.5 Classification of KNP

The classification algorithm developed for the Shingwedzi River catchment site was applied to the KNP Landsat 7 ETM+ imagery. The results are shown in Figure 64. There is no accuracy assessment as the samples only apply to the classification of the Landsat imagery for the Shingwedzi and Ripape study sites.

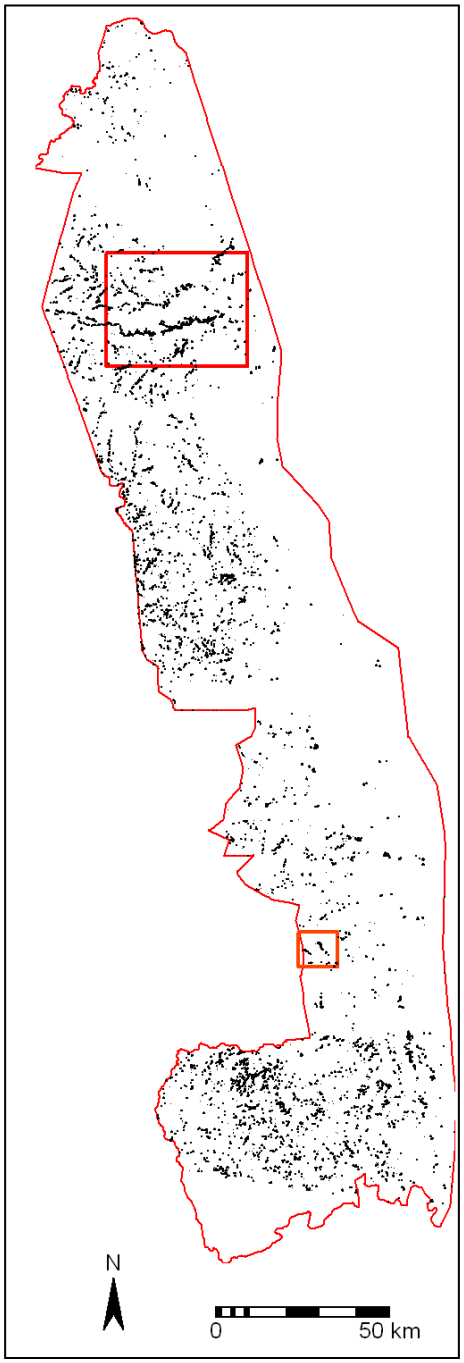


Figure 64: Landsat 7 ETM+ (21 and 30 May 2001) classified sodic sites (black) for the area of the KNP covered by the two images (Path/row: 169/076 and 168/077).

4. DISCUSSION

The classification of sodic sites from multi-spectral satellite imagery with different spatial and spectral resolutions was applied at the Shingwedzi study site using object-based classification methodologies. The most accurate classification method according to the error matrix for each image was applied to the Ripape study site images of similar seasonal phenology and assessed for repeatability for classification of sodic sites for the whole of the KNP.

4.1 Imagery selection

The imagery used for the classification was supplied by the KNP and the study was not able to select alternative sensors. The selection of dates of acquisition was also restricted to what was available, but sufficient input data was available to test the classification of sodic sites for the KNP.

4.1.1 Spatial resolution

Sodic sites can range in size from less than $10m^2$ to very large sodic sites measured in hectares. The spatial resolution of the imagery used to classify sodic sites will determine the smallest size of sodic sites detected on the imagery. Landsat's 30m multi-spectral pixel and 15m panchromatic band will not detect smaller sodic sites, but the SPOT 5 10m multi-spectral pixel and 2.5m panchromatic band has the potential to detect the smaller sodic sites more accurately. The results of the percentage sodic site cover for the Shingwedzi study site of 1.16% for Landsat and 2.86% for SPOT 5, illustrates that Landsat under-estimates the area of sodic sites.

In Figure 66 three areas in the Shingwedzi study site illustrate how the higher resolution imagery classifies a greater area of the sodic site class than the lower resolution imagery. Although computation of the higher resolution imagery is more of a challenge due to the higher number of pixels per scene, the result is a better estimation of the location and percentage cover of sodic sites in the Shingwedzi study site. Figure 65 (a) depicts an area of the Phugwane River where the sodic sites vary from bare and open, to woody and semi-closed canopy. There are many sodic sites that have been omitted from the classification for the Landsat imagery, and river sand has been included as a sodic site in places on the SPOT 5 imagery as a result of spatial resolution differences.

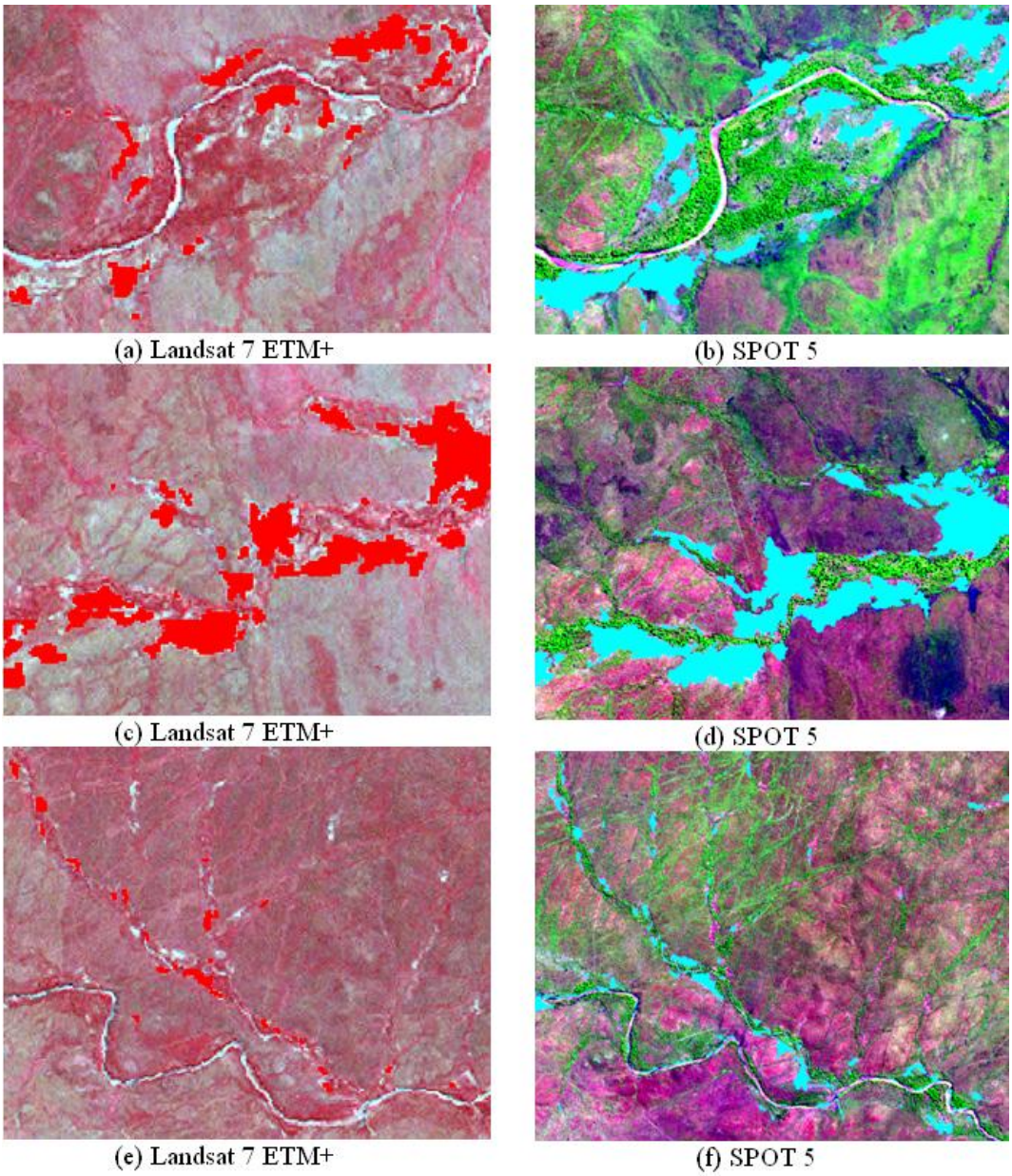


Figure 65: Spatial resolution comparison between the Landsat 7 ETM+ 30m multi-spectral (21 May 2001) and SPOT 5 10m multi-spectral (12 April 2008) late wet season to early dry season object-based classification of sodic sites.

Figure 65 (c) is from the Bububu River which has very large, bare open sodic sites and shows the more accurate classification of large sodic sites based on the visibly "bright" areas in the imagery. Figure 65 (e) is an area of the Bububu River in the upper catchment where the sodic sites are relatively small and are not included in the classification. The pixel size of 30m for Landsat imagery will miss any sodic site less than 60 m x 60 m.

4.1.2 Spectral signature separation

The cluster analysis and spectral signature investigation is necessary to test the reliability of the radiometric normalisation of multi-spectral imagery.

The results also indicate whether the classes selected for classification are spectrally separable from closely related classes. For sodic site classification, other bare soil spectral signatures are similar to the spectral signatures of sodic sites and ancillary data including elevation models and river or road vector layers were able to assist with separating these classes. The effect of the dry season imagery on the amount of bare soil in the image was highlighted for the SPOT 5 mid dry season image using the spectral signature clustering. The study found the spectral signature clustering investigation to be a valuable tool for selecting suitable imagery for the classification of sodic sites in the KNP. The accuracy assessment results of the mid dry season imagery was not suitable for classification of sodic sites.

4.1.3 Geometric accuracy

The ASTER imagery for the Shingwedzi study site consisted of two overlapping scenes. Each scene was classified separately to prevent any changes in the data which may occur when imagery is merged to form a mosaic. The results of the classification where much lower than the Landsat 7 and SPOT 5 accuracies for random visually assessed samples. When the ground truth samples were used for accuracy assessment, it was discovered that the geometric accuracy of the ASTER imagery was between 30-40m different to the SPOT 5 or Landsat 7 imagery. The result was that sample sites did not align with sodic sites in most cases and the accuracy was too poor to report. Based on this geometric inaccuracy, the ASTER results were difficult to quantify for comparison with other imagery. The accuracies were disappointing for ASTER imagery as the spectral resolution of ASTER is much broader than Landsat 7 imagery at similar resolution, and it was expected that these additional SWIR bands of ASTER would contribute to higher accuracy when classifying sodic sites.

4.1.4 Seasonal effects

Two SPOT 5 images were classified for the Shingwedzi study site: a mid dry season image and a late wet season to early dry season image (Figure 66). The accuracy assessment results for the Shingwedzi study area show that both the mid dry season and late wet or early dry season imagery gave accuracies overall of 90% and 88%

respectively for random visually assessed samples, and 65% and 69% over accuracies for the stratified random ground truth samples. The Kappa Index for the sodic class of 66% in the mid dry season imagery and 89% for the late wet or early dry season highlights the difficulty in classification of sodic sites in imagery acquired in the dry season in the KNP. This is due to many areas showing similar spectral signatures to bare ground or sparsely vegetated savanna.

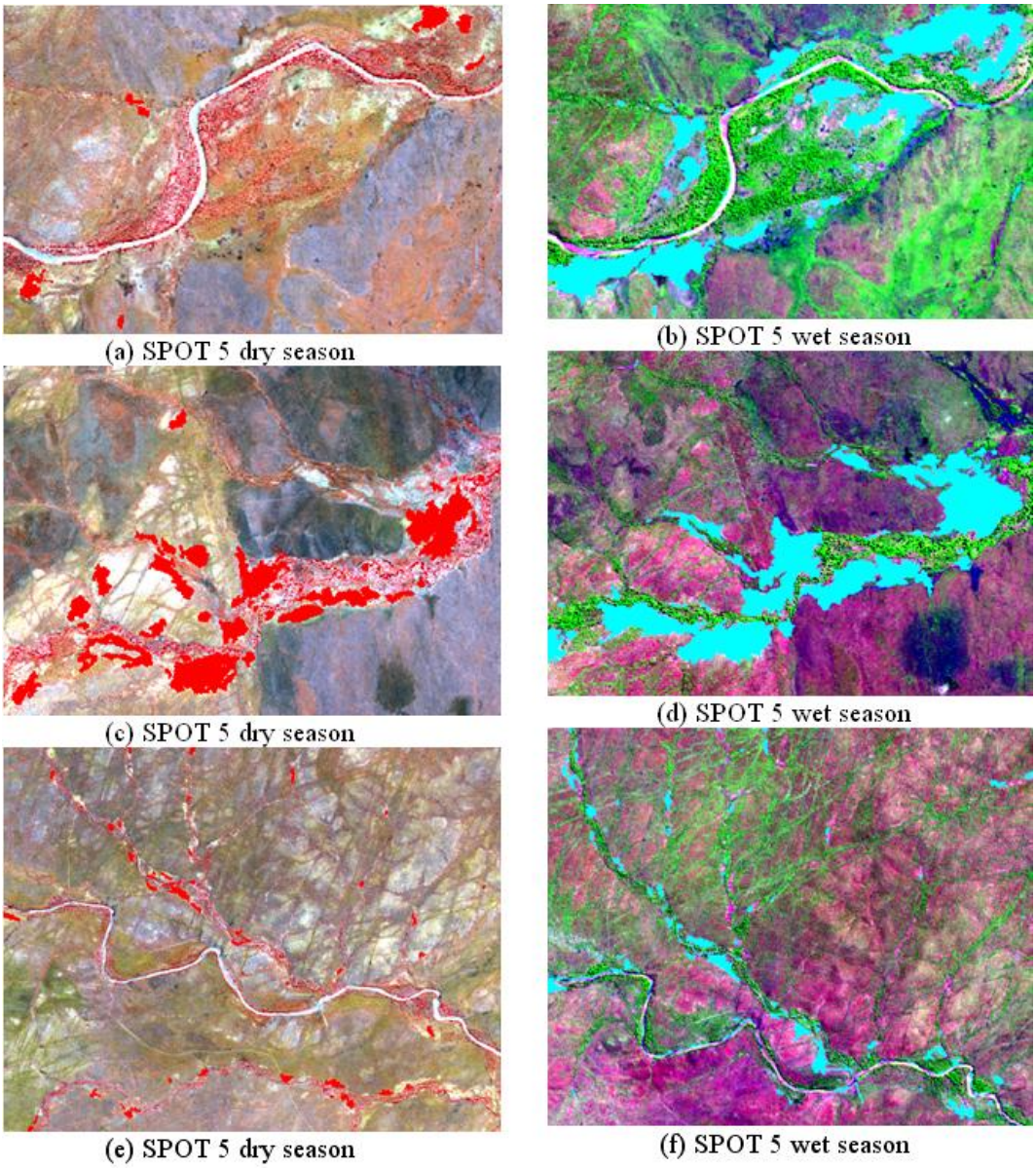


Figure 66: SPOT5 wet and dry season imagery for the Shingwedzi study site where the classification of sodic sites is an underestimation due to the difficulty in separating sodic sites from other bare soils in the dry season. The wet season classification of sodic sites gives a much higher percentage cover because there is less spectral confusion between bare soils.

The difference in the percentage coverage of sodic sites in the study area (0.77% for mid dry season and 2.86% for the late wet or early dry season imagery) illustrates that the classification algorithm for mid dry season imagery severely under estimates sodic site percentage cover. The difference in percentage coverage of classified sodic sites in the Shingwedzi study area is illustrated in Figure 66, when selected areas are magnified, and the shortcomings of using imagery acquired in the mid dry season become evident.

The MODIS NDVI phenology graphs are a useful tool to place the imagery in seasonal context. The accuracy results between the SPOT 5 wet and dry season imagery for the Shingwedzi study site confirm that the late dry to early dry season imagery is most suitable for the classification of sodic sites in the KNP. The repeatability of the classification algorithm on the Ripape study for SPOT 5 imagery of similar season produced comparable accuracies. The study shows that choosing similar seasonal imagery contributes to an accurate classification of sodic sites, and would be relevant to all land cover classifications.

4.2 Classifcation methods

The objective of this study is to classify sodic sites in the KNP using object-based image analysis as opposed to pixel-based classification previously used by Mathys and Wessels (2001). Object-based image analysis groups homogenous pixels into objects which should be a more meaningful ecological unit or patch. The segmentation results show objects can represent sodic sites at different scales or hierarchies. The sodic sites were subset into the bare sodic area components and the surrounding or interspersed vegetated sodic site components.

4.2.1 Object-based classification

The comparison between object-based and pixel-based classification algorithms will be made for the medium and high resolution imagery. Despite the good accuracy results for Landsat 7 in the Shingwedzi study site, when selected areas are magnified in the image, the shortcomings of using 30 m resolution imagery for object-based image analysis become evident. Figure 67 and 68 shows a comparison between the object-based classification of this study and pixel-based classification result from Mathys and Wessels

(2001). A comparison with the results of Saah (2004) was not possible as no shapefile with sodic site results was available for analysis.

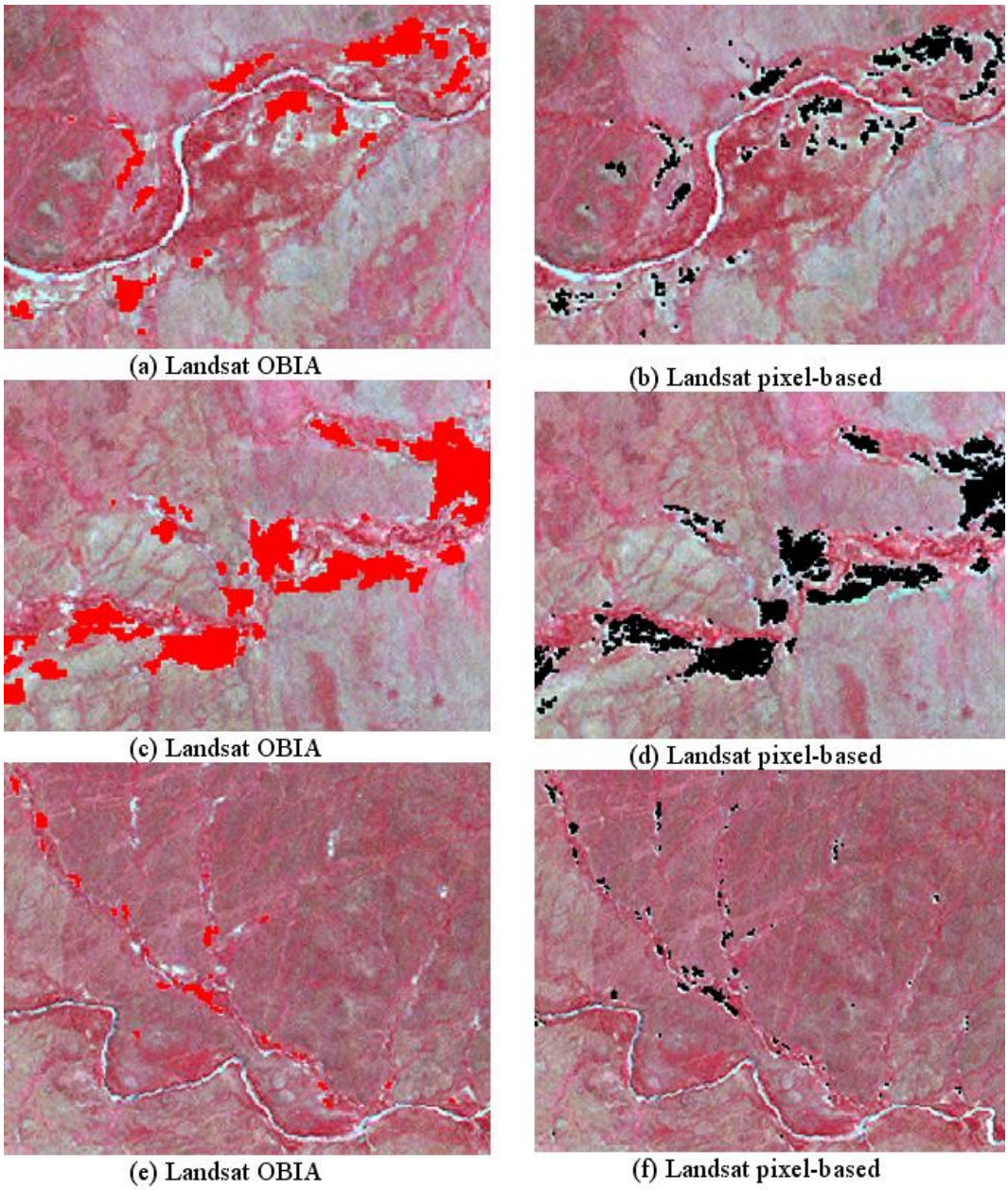


Figure 67: Comparison between the Landsat 7 (21 May 2001) object-based classification and the pixel-based classification of Matthys and Wessels (2001).

In Figure 68 the pixel-based classification of Matthys and Wessels (2001) is compared to the object-based image analysis of SPOT 5 imagery of similar season. The sodic sites for object-based image analysis have more ecological meaning as patches, and the higher resolution of the SPOT 5 imagery has included the smaller sodic sites not included in the Landsat object-based classification.

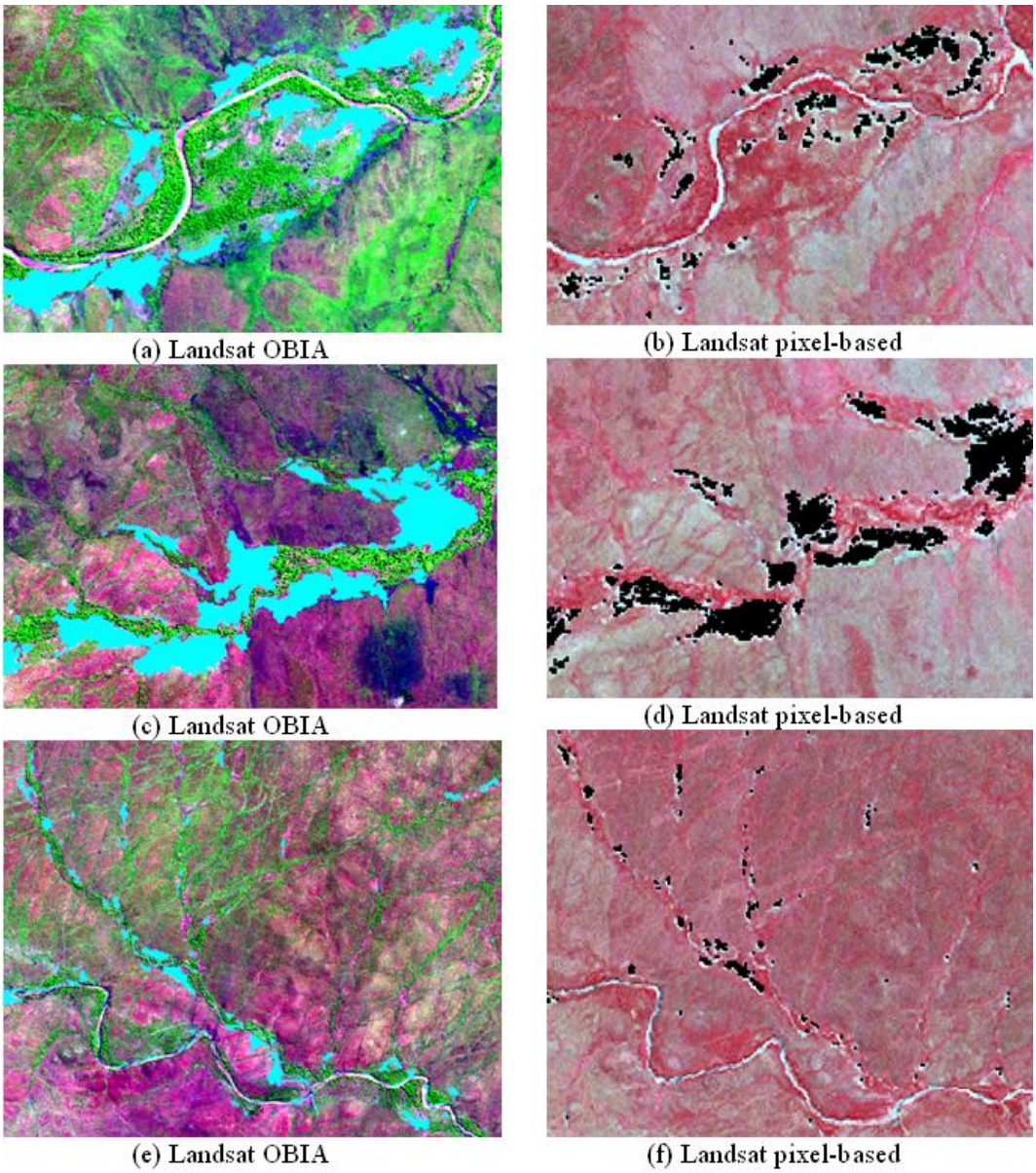


Figure 68: Comparison between the SPOT 5 (12 April 2008) object-based classification and the pixel-based classification of Matthys and Wessels (2001).

The pixel-based classification on Landsat imagery underestimates the area of sodic sites compared to the SPOT 5 imagery. The recommended spatial resolution for object-based image analysis would be the SPOT 5 10m/2.5m imagery. For the medium resolution Landsat 30m/15m imagery, pixel-based classification would classify smaller sodic sites better than object-based image analysis at this scale, but the objects of object-based classification have more ecological meaning than the disassociated pixels of pixel-based classification.

4.2.2 Repeatable classification methodologies

A classification algorithm that is repeatable over other areas of the park is required in order to classify sodic sites for the whole of the KNP. The two different algorithms developed in the Shingwedzi study site for Landsat 7 and SPOT 5 were applied to imagery of similar season in the Ripape study site for the same sensors. The Landsat 7 accuracy was lower for the Ripape study site than for the Shingwedzi results. The SPOT 5 algorithm for the Ripape site had very similar accuracies compared to the Shingwedzi site where the algorithm was developed. The whole of KNP was classified for sodic sites using the Landsat 7 imagery and the results have been visually validated and the map of sodic sites is a promising first attempt. Accuracy assessments have not been performed on this classification as there is no ground truth data for the entire KNP. Future classification of all the available SPOT 5 scenes could now be attempted based on the results obtained for the Shingwedzi and Ripape study sites and validation would use visually assessed image samples.

4.3 Accuracy assessment

The error matrix is used to compare the accuracy of the classification of sodic sites. Both the overall accuracy and accuracy for sodic sites are reported, including the Kappa statistic in each case (Table 18). Two accuracy assessment results are reported for the Shingwedzi study site: training accuracy results based on visually interpreted imagery samples and validation accuracy results based on the ground truth data collected in the field. There are no ground truth field samples collected for the Ripape study site, so it is necessary to use the visually interpreted samples to make comparisons for the repeatability of the algorithm on the Ripape site. There is the added advantage in that the number of ground truth samples is not halved for training and validation datasets thus increasing the number of validation samples per class, which is statistically more robust.

4.4 Change detection

Previous studies have recorded that sodic sites have increased in size over the past 50 years (Chappell 1992; Khomo 2003). Aerial photographs with a very high spatial resolution were used to assess changes in size over time. Change detection using Landsat

7 or SPOT 5 imagery at 15m and 2.5m in the panchromatic bands respectively, will not pick up small changes of under a 1m over a short time span of 10 years. Object-based classifications of high resolution imagery will classifiy small sodic sites compared to pixel-based classification of medium resolution imagery where small sodic sites will be part of mixed pixels. Very high resolution imagery such as colour aerial photographs and hyperspectral images would be more suited to this requirement. The CAO hyperspectral and LiDAR imagery classified for this project over a small subset of the Ripape study site near the sites studied by Chappell (1992). The results show promise for very accurate classification of sodic sites which could then be used to manage sodic sites. Any changes in the size of sodic sites may be linked to changes in the ecosystem and if sodic sites are accurately measured for change, management decisions could be made to mitigate adverse effects on the environment.

5. CONCLUSION

The object-based image analysis was successful in the classification of bare sodic areas to a kappa index over 85%, which is in line with expected results for vegetation classification in the literature (Wulder *et al.*, 2006). Previous classifications of sodic patches using pixel-based classification methods on medium resolution imagery (Landsat 7 ETM+) produced a better result for the inclusion of small sodic patches, but with the expected salt-and-pepper effect of dis-associated sodic pixels as opposed to objects of ecological patches. The object-based segmentation of higher resolution imagery (SPOT 5) classified sodic patches as units with relations to neighbouring objects, allowing for the application of ecological knowledge to improve the classification. Object-based image analysis for each sensor was able to apply one classification method to scenes of similar season.

The spatial resolution of satellite imagery will determine the smallest bare soil area that is measured using object-based image analysis. Spectral resolution and topology contribute to the distinction between classes of segmented objects. However, the date of imagery acquisition is important for vegetation cover percentage estimation of sodic patches, and comparison of accuracy assessments. The season of data acquisition affects the measure of vegetation cover. The most suitable acquisition dates for locating bare sodic sites in different areas of the park are after the peak NDVI (late wet season), and before lowest NDVI for the dry season (early dry season). For a repeatable algorithm to be applied to the entire KNP, the images should be from the same or similar phenological seasonal

cycles. If imagery is not available from a similar season, different classification algorithms must be used.

The recommended methodology for classification of sodic patches is with SPOT 5 imagery acquired after the peak NDVI of the wet season or early dry season. The classification methods can be used to estimate bare sodic patches for the whole park.

The output of this study is a once-off assessment for mapping purposes. For change detection of sodic sites for monitoring or management, any real change can only be measured using very high resolution imagery or hyperspectral products. The seasonal influence on vegetation cover of sodic patches will also affect change detection.

Object-based image analysis is suitable for the classification of sodic sites using high resolution imagery as the objects segmented relate to real patches in the landscape. The relationships between these objects and their neighbours can be interpreted based on expert knowledge about the ecological system and used to classify sodic sites using scientific knowledge and not just spectral properties of the imagery. The season of acquisition plays a major role in the effectiveness of the classification algorithm to classify sodic sites for different imagery scenes in other areas of the park. The algorithm was proved to work on a second scene with similar phenological status, but if imagery was not available for a similar season the thresholds used for the features to classify sodic sites may need to be changed to get an accurate output.

For classification of the entire KNP both Landsat 7 and SPOT 5 may be used, but it depends on the requirements of how the map of sodic sites is used. If the sodic site area estimation is required for a large scale problem, then Landsat 7 imagery would be suitable. For smaller scale requirements, the SPOT 5 imagery would be required. The algorithms were based on a similar work flow, and differed mainly in terms of scale based on their resolution which would affect the segmentation parameters. The classification algorithm for sodic sites is sensor specific based on the spectral resolution differences, but has been shown to be transferable to other scenes of the same sensor, providing the seasonal cycle is from the peak wet season to early dry season.

CHAPTER 4

SPATIAL MODELLING OF SODIC SITES IN THE KRUGER NATIONAL PARK - CONCLUSION

1. THE SODIC TERMINOLOGY DEBATE

The terminology used for patches of sodic soils in the Kruger National Park (KNP) has been widely debated by soil experts when used to describe the functional and visible nature of sodicity in the landscape, without solid evidence that the soils are chemically sodic. Sodic soils are defined by their chemistry and the accepted definition of a sodic patch is based on the chemical definition of a sodic soil. Saline soils are high in neutral soluble salts, which adversely affect plant growth, while sodic soils have a high sodium concentration in relation to calcium and magnesium, which causes alkali hydrolysis.

The term "sodic site" is used by researchers for landscape patches in the KNP that exhibit the characteristics associated with the presence of sodic or saline-sodic soils. Sodic soils are measured by the ESP or SAR, EC and pH (Abrol, Yadav, and Massoud, 1988). However, in this study, in-field measurements of EC and pH were not found to be useful in the identification of sodic soils due to high variability within and between the sample sites, in agreement with results by Teren (2004). Laboratory analyses of large numbers of soil samples for sodium levels are neither practical nor possible for classification studies which require large sample sizes. The level of sodium at which sodic soils cause crusting, cracking, dispersion, erosion and affect plant growth varies within and between sites, so no single level of sodium can be used to define a sodic soil (Qadir and Schubert, 2002). The deflocculation of clay particles occurs when sodium cations are adsorbed by the clay platelets causing swelling and dispersion (McBride, 1999). The Emerson dispersion test was devised to determine dispersion potential (Emerson, 1967) and was successfully tested on known laboratory tested sodic soil sites in the Shingwedzi study site. Therefore, a sodic site in this study is defined by the chemical composition of the soil in terms the presence of sodium which causes dispersion of clay particles, measured

by the Emerson dispersion test, and by the visible signs of sodicity on the site. Alternative descriptions could be "visibly sodic" as opposed to "chemically sodic", "salt-affected hot-spot" or "dispersive hot-spot". For the purposes of this project the term "sodic site" has been used as a functional description of the characteristics of the presence of salts, and in particular, sodium.

2. DECISION TREE DEVELOPED FOR IN FIELD IDENTIFICATION OF SODIC SITES

The field classification of sodic sites showed that it is possible to accurately interpret the visible signs of sodicity, based on sites with a known chemical level of sodium from previous research. The decision tree for the classification of sodic sites (Figure 8) was devised based on the known sodic soil sites and knowledge of the visible characteristics of sodic sites from literature. There is not one single factor which defines a sodic site, but a collection of functional ecological criteria that describe the sodic syndrome which leads to a diagnosis of sodicity. The dispersion test and the identification of *Sporobolus ioclados* are used to confirm the presence of sodium in the soil, but are not used to classify the soil. Confusion with the correct identification of *Sporobolus ioclados* is suspected in previous research due to confusion with similar grass species. Both the inflorescence and the leaf blades must be present for accurate identification. The decision tree, dispersion test and identification of *Sporobolus ioclados* grass species was applied to all ground samples in this study to classify river sand, sodic sites, riverine vegetation and savanna classes. The cluster analysis performed on the attributes recorded at each site confirmed the classification of the decision tree to be an accurate interpretation of the visual properties of sodic sites. This identification tool will be useful to researchers in the park for future studies and may be expanded to more detailed classes.

3. SODIC SITES AND HETEROGENEITY IN THE LANDSCAPE

Sodic sites are nutrient hot spots with high forage quality in comparison to the surrounding crests and therefore have the ability to sustain herbivores through the dry season (Grant and Scholes, 2006). The results of the classification of sodic sites from imagery for the Shingwedzi study site show how the distribution of sodic sites contributes

to heterogeneity in the landscape. Herbivore migrations into the sodic site rich areas can now be mapped using the census data to determine the influence of the nutrient rich areas on animal numbers over time. Researchers could use the map of sodic sites to measure if greater numbers of animals are sustained in areas of higher sodic site density. The seasonal effect of plant growth on sodic sites also contributes to heterogeneity in the landscape. In the field, sodic sites were recorded with visible standing biomass during the wet season, but during the dry season these same sodic sites appeared bare and were completely depleted of biomass by herbivores with only the stolons visible above ground.

4. DYNAMIC PROPERTIES OF SODIC SITE EXTENT

Previous researchers have observed the change in size and shape of sodic sites over time and the results from this study may contribute to this debate. Studies along the Phugwane River in the north of the KNP (Khomo and Rogers, 2005), and along the Ripape River in the south western KNP (Chappell, 1992), have shown that there has been a significant increase in the area of sodic sites on the boundary between riparian and upland systems. These observations are based on the albedo affect of bare soils observed from aerial photographs over a 50 year period from 1942 to 1989. There is no record of the dates of acquisition of the aerial photography or the rainfall pattern prior to acquisition. The phenology changes on sodic sites observed between the wet and dry seasons due to herbivore utilisation of the vegetation will give sodic sites a different albedo appearance on imagery depending on the season of acquisition. Based on the phenology graphs derived from the MODIS NDVI imagery for this project, it is evident that sodic sites appear very much larger in dry periods due to a lack of grass cover and smaller in the wet season before they are heavily grazed. Any change detection of changes in size of sodic site must take the phenology into account and it would be necessary to only compare sodic sites in similar seasonal stages. This also applies to future classification of sodic sites from imagery. For comparable results the phenology stage of the vegetation cover on sodic sites must be similar to the previous classification.

Very high resolution imagery such as aerial photography or hyperspectral imagery used in this project would be suitable to monitor sodic site changes over time or season. New sensors with improved spatial, spectral and temporal resolution are launched every few years. WorldView 2 from Digital Globe (8 band multi-spectral imagery at 1.84m spatial

resolution; panchromatic at 46cm, revisit time 3.7 days)[5] would be worth investigating to monitor individual sodic sites.

The management implications of change detection of sodic sites would be to detect if the change in size or shape of the sodic site may indicate risk of further erosion or some other change in environmental conditions. The objective of mapping sodic sites is to have a base line to work from for future mapping exercises.

5. POSITION IN THE LANDSCAPE

The classification of sodic sites from imagery assumed that sodic soils accumulate at the bottom of a slope and that the catenal theory for the origin of sodic sites applies (Khomo and Rogers, 2005). The map of sodic sites in the Shingwedzi study site confirms that the soils are found along drainage lines, along different categories of rivers and their tributaries, and not only along the large order rivers. Interpretation of these patterns may be of interest to landscape ecologists. Accumulation of clay particles and nutrients appear to concentrate at a point where many slopes converge but what determines the size of the sodic site would be an interesting investigation.

6. INFLUENCE OF GEOLOGY ON CLASSIFICATION OF SODIC SITES

In the field, the geology of the site influences the decisions taken in the sodic site decision tree and therefore the result of the identification of sodic sites. Catenas are clearly defined in the granite landscapes, but in the basalts the footslope of the catena may be incorrectly interpreted due to the gently sloping terrain. The ambiguous attributes may influence the outcome of the classification tree by overestimating sodic sites. The results in this study noted some confusion on a few sites between sodic sites and savanna sites on the basalts which may be as a result of ambiguous attribute criteria for basalt landscapes.

The results for the dispersion test for granite soils were more conclusive than for the basalt soils, highlighted by the cluster analysis on attributes of sodic sites. Basalt soils have a high clay content and the dispersion test may not indicate similar levels of sodium

[5] http://www.digitalglobe.com/index.php/88/WorldView-2 (downloaded 25/02/2011)

at which basalts disperse as in the granites. The effective use of the dispersion test must be further investigated on the basalt soils. The high clay content of the gabbro soils may produce a similar result, and also needs to be tested.

The ground truth sample sites were not divided into the two main geologies for accuracy assessment. The accuracy results of separate geologies may highlight the effect of the basalt geology on the classification algorithm and whether further changes are required to improve the classification of basaltic sodic sites.

7. EROSION AND DEGRADATION OF SODIC SITES

Sodic sites are often associated in the literature with erosion and degradation (Chappell, 1992; Khomo and Rogers 2005). Sodic soils show physical properties of crusting, cracking and water logging which adversely affects plant growth (Mills and Fey, 2004), identified in the KNP as bare soil patches. These bare soil areas appear degraded in terms of over grazing, but the vegetation is adapted to herbivory and recovers in the wet season. Erosion is likely to occur if the sandy A-horizon is eroded, exposing the impervious B-horizon, and the lateral movement of water below the crust causes tunnelling or piping which eventually collapses and forms gulley erosion (Chappell 1992; Barre, Biggs and Sharp, 2004; Raine and Loch, 2003). The KNP would like to implement a monitoring system to prevent soil loss due to erosion. Monitoring sodic sites in terms of erosion potential may be considered based on the map of the location of sodic sites. Although remote sensing techniques may not be applied to monitor the change in gully erosion, the location of sodic sites may be used for modelling erosion risk for management purposes. Field data collected during this study did not find many sites with an eroded B-horizon, and the sites which were affected was due to human interference in the form of a road, bridge or water hole placed in or near a sodic site.

8. GROUND TRUTH SAMPLING

Ground truth sampling design directly affects the validation of image classification. Accuracy assessment is dependant on the data collection in the field and will incorporate errors due to spatial misregistration, photo interpretation errors or changes in land cover

between dates of image acquisition and field data collection (Foody, 2002). The ASTER imagery was an example of spatial misregistration where the ground truth samples did not match with the pixels in the imagery and the resulting accuracy assessment did not represent the true capability of the classification algorithm. Photo interpretation errors may have occurred with the collection of visually assessed samples from the image where the samples were mis-classified and therefore influenced the accuracy assessment. The error due to changes in land cover may be the reason why the accuracy assessments of the ground truth data were much lower than for visually assessed samples. The seasonal aspects will also affect accuracy depending on when the ground truth data was collected in relation to the date of acquisition of the imagery. There was a 3 to 8 year difference between the date of ground truth sample collection and the date of acquisition of the imagery for this project which would contribute to the accuracy assessment of the classification of sodic sites.

The field sample classification key used for the objectives of this study distinguishes between five classes, based on topography and percentage vegetation cover: bare sodic patches, vegetated sodic patches, river sand, dense riparian vegetation and general open or closed savanna. A crisp class definition of each of these classes in the field will ensure a statistically robust validation of the classification of sodic sites. Unfortunately, most of these classes are ambiguous due to environmental gradients and many of the sites are ecotones between two classes. Finding homogenous samples in a heterogeneous landscape is challenging and digital imagery is useful to assist with selection of sample sites that reflect both the landscape and how it is represented digitally. If sample sites are collected at a different time to the date of acquisition of the image, using imagery to select field sample sites would avoid the collection of unrepresentative samples. For this project, both ground truth data and visually assessed imagery data were collected and reported for the classification of the Shingwedzi study site. The advantage of the visually assessed samples is that they are truly random, but only the homogenous, obviously bare sodic sites are selected. The ground truth samples are based on ground based classified sodic sites, but these samples are not purely randomly selected and are heterogeneous, bare or partially vegetated by woody.

Sodic sites samples are difficult to collect in the field as the class is less than 3% of the area of the landscape according to the results from the sodic site maps classified in this

project. Sampling designs need to take this into account when assessing accuracy of small areas.

9. ACCURACY ASSESSMENT

The error matrix is the standard reporting tool for assessing the accuracy of a classification. The statistically robust technique is influenced by the samples used to validate the map and can be manipulated to give better results. During the classification process the accuracy assessment is used to interpret which classes are not accurately classified. The classification algorithm is then changed, the number of training samples increased or the classes merged or divided. Once the accuracy is achieved for the scope of the project, then the validation samples are used for the final accuracy assessment. If the samples are ground truth field samples, the results of this project were less accurate than if visually random samples were selected from the imagery. The reason for this discrepancy is that when selecting samples on the ground, it is difficult to determine whether the sample was homogenous and truly representative of the class. Selecting "virtual" samples from imagery is at a different scale and allows a better interpretation of spectral and textural characteristics to choose the most representative sample of the class. The date discrepancy of time of acquisition of the image and when the samples were taken could also influence the samples. Virtual samples are taken from the image and the classification is performed on the same image, giving much better correlation between sampled and classified classes.

Accuracy assessments are based on the samples selected for the training area and reflect nothing of the rest of the image. Although validation of the map of sodic sites is necessary to assess the different methods, ultimately the user requires a reliable estimation of sodic site coverage with few errors of omission and commission. The best test for the result is its usefulness in the field which is difficult to measure.

Selecting the best result based on accuracy assessment alone is not enough. The size of sodic sites and the spatial resolution of the image determine the classification accuracy. Large size sodic sites are classified at large and small scale imagery, but small sodic sites may not be detected in imagery where the pixel size is larger than the sodic site. The effect of season on sodic sites has the most effect on accuracy of classification. If the

imagery is too late in the dry season other bare soil can also be classified as sodic. The comparison of accuracy can therefore only be made between imagery of similar seasons. If the classification is not accurate, it is not only a reflection of the image analysis, but some of these other factors, and each must be optimal for an accurate map.

When up scaling the classification algorithm to the entire KNP, it is necessary to collect validation samples from the entire area to have an idea of the level of accuracy of the map of sodic sites. The user requires a map that will give as good an estimate of the location and extent of sodic sites that will inform management decisions.

10. CLASSIFICATION RESULTS AND SODIC SITE VARIABLITY

The object-based image analysis was successful in the classification of bare sodic areas to a kappa index of 0.79, which is in line with expected results for vegetation classification in the literature (Wulder *et al*., 2006). Vegetated or woody sodic sites are not easily detectable using remote sensing image analysis as they exhibit similar spectral signatures to open savanna. Previous classifications of sodic patches using pixel-based classification methods on medium resolution imagery (Landsat 7 ETM+) produced a better the inclusion of small sodic patches than object-based image analysis for the same imagery. The object-based segmentation of higher resolution imagery (SPOT 5) classified sodic patches as units with relations to neighbouring objects, allowing for the application of ecological knowledge to improve the classification. Smaller sodic sites were included in this classification.

The recommended methodology for classification of sodic patches is with SPOT 5 imagery acquired after the peak NDVI of the wet season, and before the mid dry season. The spatial resolution of satellite imagery will determine the smallest bare soil area that is measured using object-based image analysis. The date of imagery acquisition is important for vegetation cover percentage estimation of sodic patches, and comparison of accuracy assessments and for an automated and repeatable classification algorithm.

11. FUTURE RESEARCH IDEAS

The map of sodic sites for the whole of the KNP classified with the Landsat 7 imagery is at a medium resolution and underestimates the smaller sodic sites. The first result of this study would be to classify the whole of the KNP with the higher resolution SPOT 5 where suitable imagery was available, for use by researchers in landscape ecology, savanna ecology, nutrient hot-spot research and soil and erosion scientists, and for monitoring programs looking at thresholds of potential concern (TCP).

The identification of sodic sites using the decision tree could be confirmed by using many more georeferenced, laboratory tested sodic soils to improve the number of samples used to further validate this in-field classifier and the effectiveness of the dispersion test. A survey of the differences between basalt, gabbro and granite soils dispersion test results would be of interest, as well as investigating the dispersion test results across transects through sodic sites and into the surrounding savanna to find the edge of the sodic soil patch.

Finding the edge of the sodic site would also be necessary for change detection of individual sodic sites, and together with very high resolution imagery such as hyperspectral or sub 1 metre multi-spectral, would contribute to a monitoring program of sodic sites. The hyperspectral and LiDAR imagery available for small areas of the KNP could assist with the misclassification of savanna and sodic sites using woody structure and cover attributes.

The phenology cycles of sodic sites needs investigation as well as the grass species composition and possible changes over time, which may indicate environmental changes on sodic sites.

The patterns of where sodic sites occur in the landscape could be analysed using the map of sodic sites to assist in determining where and why sodic sites occur where they are currently located, and to predict how and where they will change in the landscape.

Mapping of sodic sites must be an ongoing endeavour as new imagery becomes available and the methodologies and should be extended to other environmental classifications.

REFERENCES

Abrams, M., and Hook, S. (2001). *ASTER User Handbook - Advanced Spaceborne Thermal Emission and Reflection Radiometer* (pp. 1-135). Californina, USA.

Abrol, I. P., Yadav, J. S. P., and Massoud, F. I. (1988). Salt-affected soils and their management. *FAO Soils Bulletin 39*.

Archibald, S., and Scholes, R. J. (2007). Leaf green-up in a semi-arid African savanna – separating tree and grass responses to environmental cues. *Journal of Vegetation Science*, 18, 583-594.

Asner, G. P., Knapp, D. E., Kennedy-Bowdoin, T., Jones, M. O., Martin, R. E., Boardman, J. and Field, C.B. (2007). Carnegie Airborne Observatory: in-flight fusion of hyperspectral imaging and waveform light detection and ranging (wLiDAR) for three-dimensional studies of ecosystems. *Journal of Applied Remote Sensing*, Vol. 1 (013536), 1-21.

Baatz, M., and Schäpe, A. (2000). Multiresolution segmentation: An optimization approach for high quality multi-scale image segmentation. In Angewandte Geographische Informationsverarbeitung XII. Beiträge zum AGIT-Symposium Salzburg 2000, Karlsruhe, Herbert Wichmann Verlag (2000), pp. 12-23.

Bannari, A., Guedon, A. M., El-Harti, A., Cherkaoui, F. Z., El-Ghmari, A., and Saquaque, A. (2008). Slight and moderate saline and sodic soils characterization in irrigated agricultural land using multispectral remote sensing. *International Archives of the Photogrammetry, Remote Sensing and Spatial Information Sciences*, 34, Part XXX.

Baraldi, A., Puzzolo, V., Blonda, P., Bruzzone, L., and Tarantino, C. (2006). Automatic Spectral Rule-Based Preliminary Mapping of Calibrated Landsat TM and ETM+ Images. *IEEE Transactions on Geoscience and Remote Sensing*, 44(9), 2563-2586.

Barichievy, C. (2005). *Interactions between Soil Patchiness, Water and Salts on a Sodic Site*. Unpublished B.Sc. Honours report. University of the Witwatersrand, South Africa.

Barre, D. A., Biggs, A. J. W., and Sharp, G. C. (2004). Sodicity and dispersion relations in some Darling Downs subsoils. *SuperSoil 2004: 3rd Australian New Zealand Soils Conference*. Sydney, Australia. Retrieved from: http://www.regional.org.au/au/asssi/supersoil2004/s14/poster/1499_biggsa.htm

Benz, U. C., Hofmann, P., Willhauck, G., Lingenfelder, I., and Heynen, M. (2004). Multi-resolution, object-oriented fuzzy analysis of remote sensing data for GIS-ready information. *ISPRS Journal of Photogrammetry and Remote Sensing*, 58, 239-258.

Blaschke, T., and Hay, G. J. (2001). Object-oriented image analysis and scale-space: theory and methods for modelling and evaluating multi-scale landscape structure. *Proceedings of the International Archives of Photogrammetry and Remote Sensing*, vol. 34, part 4/W5, 22-29. *Challenges in Geospatial Analysis, Integration and Visualization*. University of Georgia. Athens, Georgia.

Bohensky, E. (2006). *Creation of Orthorectified Aerial Photography Mosaics for the Sabie and Shingwedzi Rivers, Kruger National Park*. Unpublished report. River/Savanna Boundaries Programme. University of California, Berkeley.

Brady, N. C., and Weil, R. R. (2001). *The Nature and Properties of Soil* (13th edition, pages 960). Prentice Hall.

Brodsky, L., and Boruvka, L. (2006). Object-oriented Fuzzy Analysis of Remote Sensing Data for Bare Soil Brightness Mapping. *Soil and Water Research*, 1(3), 79-84.

Bui, E. N., Krogh, L., Lavado, R. S., Nachtergaele, F. O., Toth, T., and Fitzpatrick, R. W. (1998). Distribution of sodic soils: the world scene. In M. E. Sumner and R. Naidu (Eds.), (pp. 19-33). New York: Oxford University Press.

Cadenasso, M. L., Pickett, S. T. A., Weathers, K. C., Bell, S. S., Benning, T. L., Carreiro, M. M., et al. (2003). An Interdisciplinary and Synthetic Approach to Ecological Boundaries. *BioScience*, 53(8), 717-722.

Campbell, J. B. (2002). *Introduction to Remote Sensing* (3rd ed., p. 620). London: Taylor and Francis.

Chander, G., and Markham, B. (2003). Revised Landsat-5 TM Radiometric Calibration Procedures and Postcalibration Dynamic Ranges, *IEEE Transactions on Geoscience and Remote Sensing*, 41(11), 2674-2677.

Chappell, C. (1992). *The ecology of sodic sites in the Eastern Transvaal Lowveld*. Unpublished M.Sc. dissertation. University of the Witwatersrand, South Africa.

Chappell, C. A. and Brown, M. A. 1993. The use of remote sensing in quantifying raes fo soil erosion. *Koedoe*, 36(1), 1-14.

Chavez, P. S. (1996). Image-based atmospheric corrections - revisited and improved. *Photogrammetric Engineering and Remote Sensing*, 62(9), 1025-1036.

Congalton, R. G. (1991). A review of assessing the accuracy of classifications of remotely sensed data. *Remote Sensing of the Environment*, 37, 35-46.

Congalton, R. G., and Greene, K. (2008). *Assessing the Accuracy of Remotely Sensed Data: Principles and Practices - Mapping Science Series* (2nd ed., p. 200). CRC Press.

Corcoran, P., and Winstanley, A. (2006). Using texture to tackle the problem of scale in land-cover classification. *1st International Conference on Object-based Image Analysis (OBIA 2006)*. Salzburg University, Austria.

Crist, E. P., and Kauth, R. J. (1986). The tasseled cap de-mystefied. *Photogrammetric Engineering and Remote Sensing*, 52(1), 81-86.

Definiens Version 5. (2006). *Definiens Professional 5 User Guide* (5.0.6.2 ed.). Munich, Germany: Definiens AG.

de Kok, R. (2006). Sequential processing of image objects and it□ s consequences for automatic analysis. *1st International Conference on Object-based Image Analysis (OBIA 2006)*. Salzburg University, Austria: ISPRS Volume No.XXXVI -4/C42.

de Kok, R., Buck, A., Schneider, T., and Ammer, U. (2000). Analysis of image objects from VHR imagery for forest GIS updating in the Bavarian Aps. *ISPRS Vol XXXIII* (Vol. XXXIII). Amsterdam, the Netherlands.

de Villiers, M. C., Nell, J. P., Barnard, R. O., and Henning, A. (2003). *Salt-affected soils: South Africa*. Paper for FAO contract No. PR 26897. ISCW Project GW 56/003/20.

Dobermann, A., and Fairhurst, T. (2008). *Rice. Nutrient disorders and nutrient management. Handbook series.* Potash and Phosphate Institute of Canada (PPIC) and International Rice Research Institute.

Dye, P. J., and Walker, B. H. (1980). Vegetation-environment relations on sodic soils of Zimbabwe Rhodesia. *Journal of Ecology*, 68, 589-606.

Eastman, J. R. (2003). *IDRISI Kilimanjaro Guide to GIS and Image Processing. Production* (p. 328). Worcester, USA: Clark Labs.

Eldiery, A., Garcia, L. A., and Reich, R. M. (2005). Estimating Soil Salinity from Remote Sensing Data in Corn Fields. *Hydrology Days*, (970), 31-42.

Emerson, W. W. (1967). A classification of soil aggregates based on their coherence in water. *Australian Journal of Soil Research*, 5, 47-57.

Farifteh, J., Farshad, A., and George, R. J. (2006). Assessing salt-affected soils using remote sensing, solute modelling, and geophysics. *Geoderma*, 130, 191 - 206.

Foody, G. M. (2002). Status of land cover classification accuracy assessment. *Remote Sensing of the Environment*, 80, 185-201.

Fox, G. A., and Sabbagh, G. J. (2002). Estimation of soil organic matter from red and near-infrared remotely sensed data using a soil line euclidean distance technique. *Soil Science Society of America Journal*, 66(2), 1922-1929.

Fox, G. A., Sabbagh, G. J., Searcy, S. W., and Yang, C. (2004). An Automated Soil Line Identification Routine for Remotely Sensed Images. *Soil Science Society of America Journal*, 68, 1326-1331.

French, A. N., Schmugge, T. J., Ritchie, J. C., Hsu, A., Jacob, F., and Ogawa, K. (2008). Detecting land cover change at the jornada Experimental Range, New Mexico with ASTER emissivities. *Remote Sensing of Environment*, 112, 1730-1748.

Fritz, S., and See, L. (2004). Improving quality and minimising uncertainty of land cover maps using fuzzy logic. *GIS UK Research ConferenceGISRUK 2004*. Norwich: University of East Anglia.

Gertenbach, W. P. D. (1983). Landscapes of the Kruger National Park. *Koedoe*, 29, 45-58.

Geosystems (2006). *ATCOR Calibration files - A mystery? Earth* (pp. 1-7). Germering, Germany. Retrieved from www.atcor.de.

Grant, C. C., and Scholes, M. C. (2006). The importance of nutrient hot-spots in the conservation and management of large wild mammalian herbivores in semi-arid savannas. *Biological Conservation*, 130, 426-437.

Hajek, F. (2006). Object-oriented classification of Ikonos satellite data for the identification of tree species composition. *Journal of Forest Science*, 52(4), 181-187.

Hajek, F. (2008). Process-based approach to automated classification of forest structures using medium format digital aerial photos and ancillary GIS information. *European Journal of Forest Research*, 127, 115-124.

Hoare, D., and Frost, P. E. (2004). Phenological description of natural vegetation in southern Africa using remotely-sensed vegetation data. *Applied Vegetation Science*, 7, 19-28.

Howari, F. M., Goodell, P. C., and Miyamoto, S. (2002). Spectral Properties of Salt Crusts Formed on Saline Soils. *Journal of Environment Quality*, 31, 1453-1461.

Huang, C., Wylie, B., Yang, L., Homer, C., and Zylstra, G. (2002). Derivation of a tasselled cap transformation based on Landsat 7 at-satellite reflectance. *International Journal of Remote Sensing*, 23(8), 1741-1748.

Huang, C., Yang, L., Homer, C., Wylie, B., Vogelmann, J. E., and DeFelice, T. (2002). *At-satellite reflectance: a first order normalization of Landsat 7 ETM+ images*. *Science*. Unpublished U.S. Geological Survey report. Raytheon ITSS, EROS Data Center, Sioux Falls, USA.

Huete, A. R. (1988). A soil-adjusted vegetation index (SAVI). *Remote Sensing of Environment*, 25, 295-309.

Huete, A. R. (2004). Remote Sensing of Terrestrial Ecosystems: Part 1. *Remote Sensing of Soils and Soil Porcesses*. Wiley.

Jacobs, S. M., Bechtold, J. S., Biggs, H. C., Grimm, N. B., Lorentz, S., McClain, M. E., Naiman, R.J., Pinay, G. and Scholes, M.C. (2007). Nutrient vectors and riparian processing: A review with special reference to African semiarid savanna ecosystems. *Ecosystems*, 10, 1231-1249.

Jamalabad, M. S., and Abkar, A. A. (2004). Forest canopy density monitoring, using satellite images. *ISPRS*. Istanbul, Turkey.

Janssen, L. L. F., and van der Wel, F. J. M. (1994). Accuracy assessment of satellite derived land cover data: A review. *Photogrammetric Engineering and Remote Sensing*, 60(4), 419-426.

Jenness, J., and Wynne, J. J. (2007). Cohen's Kappa and Clasificaiton Table Metrics 2.1a: An ArcView 3x Extension for Accuracy Assessment of Spatially-Explicit Models. Retreived from internet: http://www.jennessent.com/arcview/kappa_stats.htm.

Jensen, J. R. (2006). *Remote Sensing of the Environment: An Earth Resource Perspective* (2nd ed., p. 608). Prentice Hall.

Jindal, S., and Josan, G. (2007). Neural Network and Fuzzy Logic Approach for Satellite Image Classification: A Review. *National Conference on Challenges and Opportunites in Information Technology*. Punjab, India: COIT2007.

Karnieli, A., Kaufman, Y. T., Rener, L., and Wald, A. (2001). AFRI - aerosol free vegetation. *index, Remote Sensing of Environment*, 77, 10-21.

Kerle, N., Janssen, L. L. F., and Huurneman, G. C. (2004). *Principles of Remote Sensing* (p. 250). ITC, Enschede, The Netherlands.

Khan, M. A., and Gulzarw, S. (2003). Germination of responses of Sporobolus ioclados: a saline desert grass. *Journal of Arid Environments*, 53, 387-394.

Khomo, L. M. (2003). The influence of geomorphic gradients on physical and vegetation hetergoneity in a savanna drainage network. Unpublished M.Sc. dissertation. University of the Witwatersrand, South Africa.

Khomo, L. M., and Rogers, K. H. (2005). Proposed mechanism for the origin of sodic patches in Kruger National Park, South Africa. *African Journal of Ecology*, 43, 29-34.

Kimani, J. N., Hussin, Y. A., Lubczynski, D., Chavarro, D., and Obakeng, O. T. (2007). Mapping savannah trees in Kalahari using high resolution remotely sensed images and object-oriented classification. *International Journal of Geoinformatics*, 3(2), 29-39.

Kotze, I. J. D. F., and Fairall, N. (2006). Using Landsat TM imagery to map fynbos plant communities: a case study. *South African Journal of Wildlife Research*, 36(1), 75-87.

Kroger, R., and Rogers, K. H. (2005). Roan (*Hippotragus equinus*) population decline in Kruger National Park, South Africa: influence of a wetland boundary. *European Journal of Widlife Reserves*, 51, 25-30.

Laliberte, A. S., Rango, A., and Fredrickson, E. L. (2006). Separating green and senescent vegetation in very high resolution photography using an intensity-hue-saturation transformation and object based classification. *ASPRS Annual Conference*. Reno, Nevada.

Leske, T., and Buckley, C. (2003). Towards the development of a salinity impact category for South African environmental life-cycle assessments: Part 1 – A new impact category. *Water SA*, 29(3), 289-296.

Levick, S. R. (2008). *A scaled, contextual perspective of woody structure and dynamics across a savanna riparian landscape*. Unpublished Ph. D. thesis. University of the Witwatersrand, South Africa.

Levy, G. J. (1999). Interdisciplinary Aspects of Soil Science: Sodicity. In M. E. Sumner (Ed.), *Handbook of Soil Science* (p. G27-G64). CRC Press LLC.

Lhermitte, S., Verbesselt, J., Jonckheere, I., Nackaerts, K., Verstraeten, W. W., and Coppin, P. (2008). Hierarchical image segmentation based on similarity of NDVI time series. *Remote Sensing of Environment*, 112, 506-521.

Lillesand, T. M., Kiefer, R. W., and Chipman, J. W. (2004). *Remote Sensing and Image Interpretation* (5th ed., Vol. 5, p. 784). New York: Wiley.

Lucas, R., Lee, A., Armston, J., Breyer, J., Bunting, P., and Carreiras, J. (2008). Advances in forest characterisation, mapping and monitoring through integration of LiDAR and other remote sensing datasets. *SilviLaser* (Vol. 4, pp. 2-12).

Manakos, I., Schneider, T., and Ammer, U. (2000). A comparison between the ISODATA and the eCognition classification methods on basis of field data. *ISPRS2000* (Vol. XXXIII). Amsterdam, the Netherlands.

Mathew, T. R., Aplin, P., and Field, R. (2005). A multiscale remote sensing approach to analyse the spatial dynamics of savanna in Kruger National Park, South Africa. *Proceedings of the 31st International Symposium on Remote Sensing of Environment: global Monitoring for Sustainability and Security*. Columbia.

Mathys, L., and Wessels, K. J. (2001). *Procedure - Landcover mapping for the northern Kruger National Park*. Unpublished report (pp. 1-2). Skukuza, Kruger National Park Scientific Services, South Africa.

McBride, M. B. (1999). Soil Chemistry: Chemisorption and Precipitation reactions. In M. E. Sumner (Ed.), *Handbook of Soil Science* (p. B265-B302). CRC Press LLC.

McCarthy, T. S., and Ellery, W. N. (1994). The effect of vegetation on soil and ground water chemistry and hydrology of islands in the seasonal swamps of the Okavango Fan, Botswana. *Journal of Hydrology*, 154, 169-193.

Mills, A. J., and Fey, M. V. (2004). Effects of vegetation cover on the tendency of soil to crust in South Africa. *Soil Use and Management, 20*, 308-317.

Moran, M. S., Bryant, R., Thome, K., Ni, W., Nouvellon, Y., Gonzalez-Dugo, M. P.,Qi, J. and Clarke, T. R. (2001). A refined empirical line approach for reflectance factor retrieval from Landsat-5 TM and Landsat-7 ETM+. *Remote Sensing of Environment*, 78, 71-82.

Moran, M. S., Hymer, D. C., Qi, Jiaguo, and Kerr, Y. (2002). Comparison of ERS-2 SAR and Landsat TM imagery for monitoring agricultural crop and soil conditions. *Remote Sensing of Environment*, 79, 243 - 252.

Murwira, A., and Skidmore, A. K. (2006). Monitoring change in the spatial hetereogeneity of vegetation cover in an African savanna. *International Journal of Remote Sensing*, 27(11), 2255-2269.

Mutanga, O. (2004). *Hyperspectral remote sensing of tropical grass quality and quantity*. Unpublished Ph. D. thesis. Univeristy of Wageningen and ITC, Enschede, Netherlands.

Naiman, R. J., Braack, L., Grant, C. C., Kemp, A. C., du Toit, J. T. and Venter, F. J. (2003). Interactions between Species and Ecosystem Characteristics. In J. T. du Toit, K. H. Rogers, and H. C. Biggs (Eds.), *The Kruger Experience: Ecology and management of savanna heterogeneity* (pp. 221-241). Washington: Island Press.

Onkware, A. O. (2000). Effect of soil salinity on plant distribution and production at Loburu delta, Lake Bogoria National Reserve, Kenya. *Austral Ecology*, 25, 140-149.

Palmer, A. R., and Fortescue, A. (2003). Remote Sensing and change detection in rangelands. *Proceedings of the VIIth International Rangelands Congress*. Durban , South Africa.

Pannell, D. J., and Ewing, M. A. (2004). Managing secondary dryland salinity: Options and challenges. *Proceedings of the 4th International Crop Science Congress*. Brisbane, Australia.

Pickett, S. T. A., Cadenasso, M. L., and Benning, T. L. (2003). Biotic and abiotic Variabliltiy as Key Determintants of Savanna Heterogeneity at Multiple Spatiotemporal Scales. In J. T. du Toit, K. H. Rogers, and H. C. Biggs (Eds.), *The Kruger Experience: Ecology and management of savanna heterogeneity* (pp. 22-40). Washington: Island Press.

Pidwirny, M. (2006). Introduction to the Lithosphere: Characteristics of Igneous Rocks. *Fundamentals of Physical Geography* (2nd ed.). eBook Viewed: September 2009. Retrieved from http://www.physicalgeography.net/fundamentals/10e.html.

Qadir, M., and Schubert, S. (2002). Degradation processes and nutrient constraints in sodic soils. *Land Degradation and Development*, 13, 275-294.

Qi, J, Chehbouni, A., Huete, A. R., Kerr, Y. H., and Sorooshian, S. (1994). A modified soil adjusted vegetation index. *Remote Sensing of Environment*, 48, 119-126.

Quirk, J. P. (2001). The significance of the threshold and turbidity concentrations in relation to sodicity and microstructure. *Australian Journal of Soil Research*, 39, 1185-1217.

Raine, S. R., and Loch, R. J. (2003). What is a sodic soil? Identification and managment options for construction sites and disturbed lands. *Roads, Structures and Soils in*

Rural Queensland (p. 14). Brisbane: Queensland Department of Main Roads. Retrieved from http://www.usq.edu.au/users/raine/index_files/RaineandLoch_WhatIsASodicSoil_2003.pdf.

Ratnam, J., Sankaran, M., Hanan, N. P., Grant, C. C. and Zambatis, N, (2008). Nutrient resorption patterns of plant functional groups in a tropical savanna: variation and functional significance. *Oecologia*, 157, 141-151.

Rengasamy, P., and Bourne, J. (1997). *Managing sodic, acidic and saline soils*. CRC Soil and Land Management.

Rocchini, D., and Ricotta, C. (2007). Are landscapes as crisp as we may think? *Ecological Modelling*, 204, 535-539.

Rowlinson, L. C., Summerton, M., and Ahmed, F. (1999). Comparison of remote sensing data sources and techniques for identifying and classifying alien invasive vegetation in riparian zones. *Water SA*, 25(4), 497-500.

Saah, D. S. (2004). *Partitioning of spatial heterogeneity in an object-oriented riparian boundaries classification system for a South African savanna*. Unpublished Ph. D. thesis. University of California, Berkeley.

Sanderson, R. (2008). *Introduction to remote sensing* (p. Downloaded Sept 2008). Retrieved from http://spacegrant.nmsu.edu/statewide/projects/remote_sensing.pdf.

Scanlon, T. M., Albertson, J. D., Caylor, K. K., and Williams, C. A. (2002). Determining land surface fractional cover from NDVI and rainfall time series for a savanna ecosystem. *Remote Sensing of Environment*, 82, 376 - 388.

Schiewe, J. (2002). Segmentation of high-resolution remotely sensed data - concepts, applications and problems. *Symposium on Geospatial Theory, Processing and Applications*. Ottawa, Canada.

Scholes, R. J., and Walker, B. H. (1993). *An African savanna: Synthesis of the Nylsvley Study* (p. 320). Cambridge University Press.

Sethi, M., Dasog, G. S., Lieshout, A. van, and Salimath, S. B. (2006). Salinity appraisal using IRS images in Shorapur Taluka, Upper Krishna Irrigation Project, Phase I, Gulbarga District, Karnataka, India. *International Journal of Remote Sensing*, 27(14), 2917-2926.

Siebert, S. J., Matthee, M. and van Wyk, A. E. (2003). Semi-arid savanna of the Potlake Nature Reserve and surrounding areas in Sekhukhuneland, South Africa. *Koedoe*, 46,1.

Skidmore, A. K., Mutanga, O., Schmidt, K. S., and Ferwerda, J. (2005). Modelling herbivore grazing resources using hyperspectral remote sensing and GIS. *8th Association of Geographic Laboratories in Europe Conference, Portugal*. Retrieved from http://plone.itc.nl/agile_old/Conference/estoril/papers/20_Andrew Skidmore.pdf.

Slattery, W. J., Conyers, M. K., and Aitken, R. I. (1999). Soil pH, aluminium, manganese and lime requirement. In K. I. Peverill, L. A. Sparrow, and D. J. Reuter (Eds.), *Soil Analysis: an interpretation manual* (illustrated, reprint., p. 369). Collingwood, Victoria: CSIRO Publishing.

Smith, J. H., Wickham, J. D., Stehman, Steven V, and Yang, L. (2002). Impacts of Patch Size and Land-Cover Heterogeneity on Thematic Image Classification Accuracy. *Photogrammetric Engineering and Remote Sensing*, 68(1), 65-70.

Song, C., Woodcock, C. E., Seto, K. C., Lenney, M. P., and Macomber, S. A. (2001). Classification and Change Detection Using Landsat TM Data: When and How to Correct Atmospheric Effects? *Remote Sensing of Environment*, 75, 230-244.

Stehman, S V, and Czaplewski, R. L. (1998). Design and analysis for thematic map accuracy assessment: Fundamental principles. *Remote Sensing of the Environment*, 64, 331-344.

Steinnocher, K. (1999). Adaptive fusion of multisource raster data applying filter techniques. *Inernational Archives of Photogrammetry and Remote Sensing*, 32(743).

Stow, D., Hamada, Y., Coulter, L., and Anguelova, Z. (2007). Monitoring shrubland habitat changes through object-based change identification with airborne multispectral imagery. *Remote Sensing of Environment*, 112, 1051-1061.

Tanser, F., and Palmer, A. R. (2000). Vegetation mapping of the Great Fish River basin, South Africa: Integrating spatial and multi-spectral remote sensing techniques. *Applied Vegetation Science*, 3, 197-204.

Taruvinga, K. (2008). *Gully mapping using remote sensing: case study in KwaZulu-Natal, South Africa*. Unpublished Master of Environmental Science dissertation. University of Waterloo, Ontario, Canada.

Teren, G. (2004). *Salvadora australis as an ecosystem engineer of sodic sites in the northern Kruger National Park*. Unpublished B. Sc. Honour's report. University of the Witwatersrand, South Africa.

Thien, S. J. (1979). A flow diagram for teaching texture-by-feel analysis. *Journal of Agronomy Education*, 8, 54-55.

Thomlinson, J. R., Bolstad, P. V., and Cohen, W. B. (1999). Coordinating Methodologies for Scaling Landcover Classifications from Site-Specific to Global: Steps toward Validating Global Map Products. *Remote Sensing of Environment*, 70, 16-28.

Thorne, K., Biffar, S., and Takashima, T. (1999). *Algorithm Theoretical Basis Document for ASTER Level 2B1 - Surface Radiance and ASTER Level 2B5 - Surface Reflectance*. *Imaging* (pp. 1-45). Tucson, Arizona.

Thrash, I. (1998). Impact of large herbivores at artificial watering points compared to that at natural watering points in Kruger National Park, South Africa. *Journal of Arid Environments*, 38, 315-324.

Tongway, D. J., and Hindley, N. L. (2005). *Landscape function analysis: Porcedures for mointoring and assessing landscapes*. *Landscape* (Updated., p. 80). Canberra, Australia: CSIRO Publishing.

Tucker, C. J. (1979). Red and Photographic Infrared Linear Combinations for Monitoring Vegetation. *Remote Sensing of Environment*, 8, 127-150.

Vance, W. H., McKenzie, B. M., and Tisdall, J. M. (2002). The stabilityof soils used for cropping in northern Victoria and southern New South Wales. *Australian Journal of Soil Research*, 40, 615-624.

van de Graaff, R., and Patterson, R. A. (2001). Explaining the mysteries of salinity, sodicity, SAR and ESP in on-site practice. In R. van de Graaff and R A Patterson (Eds.), *Proceedings of On-site '01 Conference: Advancing On-site Wastewater Systems* (pp. 361-368). Armidale: Lanfax Laboratories.

van Oudtshoorn, F., and van Wyk, E. (1999). *Guide to the grasses of southern Africa* (First edition., p. 288). Pretoria, South Africa: Briza Publications.

Venter, F. J. (1990). *A classification of land for management planning in the Kruger National Park*. Unpublished Ph. D. thesis. University of South Africa, Pretoria, South Africa.

Venter, F. J., Scholes, R. J., and Eckhardt, H. C. (2003). The abiotic template and its associated vegetation pattern. In J T du Toit, K. H. Rogers, and H. C. Biggs (Eds.), *The Kruger Experience: Ecology and management of savanna heterogeneity* (pp. 83-129). Washington: Island Press.

Verbyla, D. L., and Hammond, T. O. (1996). *How to lie with an error matrix*. Unpublished report. Department of Forest Sciences, University of Alsaka Fairbanks. Email:D.Verbyla@uaf.edu.

Vogelmann, J. E., Helder, D., Morfitt, R., Choate, M. J., Merchant, J. W., and Bulley, H. (2001). Effects of Landsat 5 Thematic Mapper and Landsat 7 Enhanced Thematic Mapper Plus radiometric and geometric calibrations and corrections on landscape characterization. *Remote Sensing of Environment*, 78, 55 - 70.

Wang, C., Qi, Jiaguo, Moran, M. S., and Marsett, R. C. (2004). Soil moisture estimation in a semi-arid rangeland using ERS-2 and TM imagery. *Remote Sensing of Environment*, 90, 178 - 189.

Wei, H., and Chen, D. (2004). The effect of spatial autocorrelation on the sampling design in accuracy assessment: a case study with simulated data. *Environmental Informatics Archives*, 2, 910-919. International Society for Environmental Information Sciences.

Wessels, K. J., Prince, S. D., Frost, P. E., and van Zyl, D. (2004). Assessing the effects of human-induced land degradation in the former homelands of northern South Africa with a 1 km AVHRR NDVI time-series. *Remote Sensing of the Environment*, 91, 47-67.

Wulder, M. A., Franklin, S. E., White, J. C., Linke, J., and Magnussen, S. (2006). An accuracy assessment framework for large-area land cover classification products derived from medium-resolution satellite data. *International Journal of Remote Sensing*, 20(4), 663-683.

Yu, J. B., and Meixner, F. X. (2007). Biogenic nitric oxide emmissions from saline sodic soil. *Geophysical Research Abstracts*, 9, 1-2. European Research Abstracts.

Yu, Q., Gong, P., Clinton, N., Biging, G., Kelly, M., and Schirokauer, D. (2006). Object-based detailed vegetation classification with airborne high spatial resolution remote sensing imagery. *Photogrammetric Engineering and Remote Sensing*, 72(7), 799-811.

Yuksel, A., Akay, A. E., and Gundogan, R. (2008). Using ASTER Imagery in Land Use/cover Classification of Eastern Mediterranean Landscapes According to CORINE Land Cover Project. *Sensors*, 8, 1237-1251.

Zhang, H., Schroder, J. L., Pittman, J. J., Wang, J. J., and Payton, M. E. (2005). Soil Salinity Using Saturated Paste and 1:1 Soil to Water Extracts. *Soil Science Society of America Journal*, 69, 1146-1151.

Zhang, Y. (2004). Understanding Image Fusion. *Photogrammetric Engineering and Remote Sensing*, (June), 657-661.

Zhang, Y., Guindon, B., and Cihlar, J. (2002). An image transform to characterize and compensate for spatial variations in thin cloud contamination of Landsat images. *Remote Sensing of Environment*, 82, 173 - 187.

Zhang, Y., and Maxwell, T. (2006). A trained segmentation technique for optimization of object-oriented classification. *ISPRS Commission VII Mid-term Symposium "Remote Sensing: From Pixels to Processes"*. Enschede, the Netherlands.

APPENDIX I: Published laboratory chemical analyses of sodic soils in the Shingwedzi and Ripape River catchments of the KNP

Catchment/ Researcher	Sample Code	UTM co-ordinates	EC (dS/m)	CEC (me/kg)	ESP	Ca (me/kg)	Mg (me/kg)	Na (me/kg)	SAR (calc)	pH	Visible on imagery	Sodic Class
Shingwedzi: Venter(1990) A or B horizon	1736b	(350687.1,7410285.1)	3.1	226	**38**	189	67	86	8	8.0	Yes	V Sodic
	1765a	(342799.9,7437503.2)	1.5	306	**33**	202	28	100	9	9.0	Yes	V Sodic
	1824b	(298896.1,7433666.3)	3.0	188	**41**	147	59	77	8	9.0	Yes	V Sodic
	1844a	(306295.9,7442309.4)	8.6	220	**124**	39	4	272	59	11.0	Yes	V Saline/V Sodic
	1844b	(306295.9,7442309.4)	0.4	51	**42**	8	4	21	9	9.0	Yes	V Sodic
	1893a	(328623.5,7444550.7)	2.5	440	**25**	254	54	109	9	9.0	Yes	V Sodic
	1913a	(296824.1,7437952.8)	6.8	285	**39**	296	38	112	9	7.0	Yes	Saline/V Sodic
	1913b	(296824.1,7437952.8)	2.0	109	**15**	83	20	16	2	7.0	Yes	Sodic
	1923a	(291155.2,7455594.1)	4.7	123	**64**	257	19	79	7	10.0	Yes	Saline/V Sodic
	1923b	(291155.2,7455594.1)	0.1	27	**18**	11	3	5	2	7.0	Yes	V Sodic
	1960b	(302118.2,7468308.5)	4.0	411	**9**	323	83	38	3	8.0	Yes	Sodic
	1967a	(325658.6,7466707.7)	4.9	467	**20**	273	104	95	7	9.0	Yes	Saline/V Sodic
	2022ac	(307950.0,7476677.0)	1.8	149	**15**	263	55	22	2	9.0	No	Sodic
	2031a	(294797.9,7478641.0)	4.0	477	**15**	258	138	72	5	9.0	Yes	Sodic
	2031b	(294797.9,7478641.0)	0.2	155	**7**	102	36	11	1	7.0	Yes	Sodic
	2081a	(330857.5,7490770.0)	4.1	89	**94**	30	32	26	5	8.0	No	Saline/V Sodic
	2081c	(330857.5,7490770.0)	0.1	27	**6**	8	3	2	1	6.0	No	Sodic
	2085a	(318292.0,7488573.3)	10.0	188	**7**	158	44	14	1	9.0	Yes	V Saline-sodic
	2085b	(318292.0,7488573.3)	0.9	50	**28**	46	28	14	2	8.0	Yes	V Sodic
Shingwedzi: Teren (2004) Depth 0-20cm	44	(321178.1,7451219.1)	4.3	-	-	-	-	-	-	7.4	Yes	Saline-sodic
	68	(324455.1,7453125.1)	9.8	-	-	-	-	-	-	7.3	Yes	Saline-sodic
	83	(327349.1,7453583.1)	7.0	244	-	173	81	163	**15**	7.3	Yes	Saline-sodic
Ripape: Chappeil (1992) B horizon	I	(359212.2,7264231.7)	-	536	-	41	265	118	**10**	7.97	Yes	Marginally Sodic
	II	(359623.2,7263856.1)	-	668	-	31	256	341	**28**	6.07	Yes	Sodic

1me/100kg = 1 cmol/kg 10me/kg = 1 cmol/kg

APPENDIX II: Landsat 7 ETM+

The Landsat Program has been in operation since 1972 and is the longest running imagery acquisition program of the earth from space (Figure 69). The Landsat program therefore provides imagery for observing the earth's surface over an extended period of time and is the most common source of imagery for environmental research and monitoring.

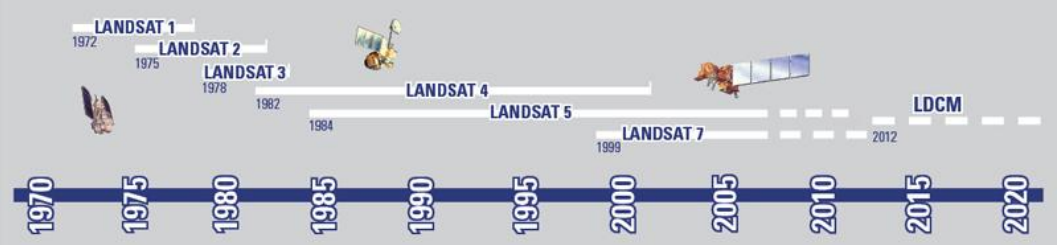


Figure 69: Time line of the Landsat missions showing the currently operational Landsat 5 and 7 satellites and the planned Landsat Data Continuity Mission (LDCM) to be launched in 2012[6]

The multispectral sensor (MSS) was carried on Landsat 1 to 5 and the Thematic Mapper (TM) sensor was carried on Landsat 4 and 5. The Landsat Enhanced Thematic Mapper Plus (ETM+) sensor was launched on the Landsat 7 satellite in April 1999. Landsat 5 is still in circulation (in 2010) and recording, but the quality of the sensor has deteriorated and corrections are required to the imagery if the year of acquisition is after 1988 (Vogelmann, Helder, Morfitt, Choate, Merchant and Bulley, 2001). Landsat 5 has more instrument-related artefacts than Landsat 7, but after radiometric and geometric corrections (see Appendix IX), the image products are highly similar, and similar enough to continue with monitoring programs started with Landsat 5, provided the appropriate calibration corrections are applied (Vogelmann *et al*., 2001).

There were high expectations that Landsat 7 would continue to supply data for long-term studies as supplied by other Landsat satellites since 1982 (Landsat 4 TM), but on 31 May 2003 the scan line corrector (SLC) malfunctioned and since this date all imagery has been supplied as SLC-off mode. The middle 22 km strip of the scene is unaffected and has similar reliability as the SLC-on mode images prior to 31 May 2003. There are algorithms available to fill the gaps in the latest Landsat 7 images, but these are more costly to obtain.

The future of the Landsat Program as a continuous, long-term imagery resource of the earth's surface is planned with the launch of the Landsat Data Continuity Mission (LDCM) in late 2012. The Operational Land Imager (OLI) sensor carried on this satellite will collect and archive data consistent with the previous Landsat multispectral bands, although the band widths have been refined as shown in Figure 70. There will be two additional spectral bands: Band 9 for detecting cirrus clouds and Band 1 for coastal zone observation. No thermal infrared bands will be recorded.

[6] http://landsat.usgs.gov/about_mission_history.php (downloaded on 6 October 2009)

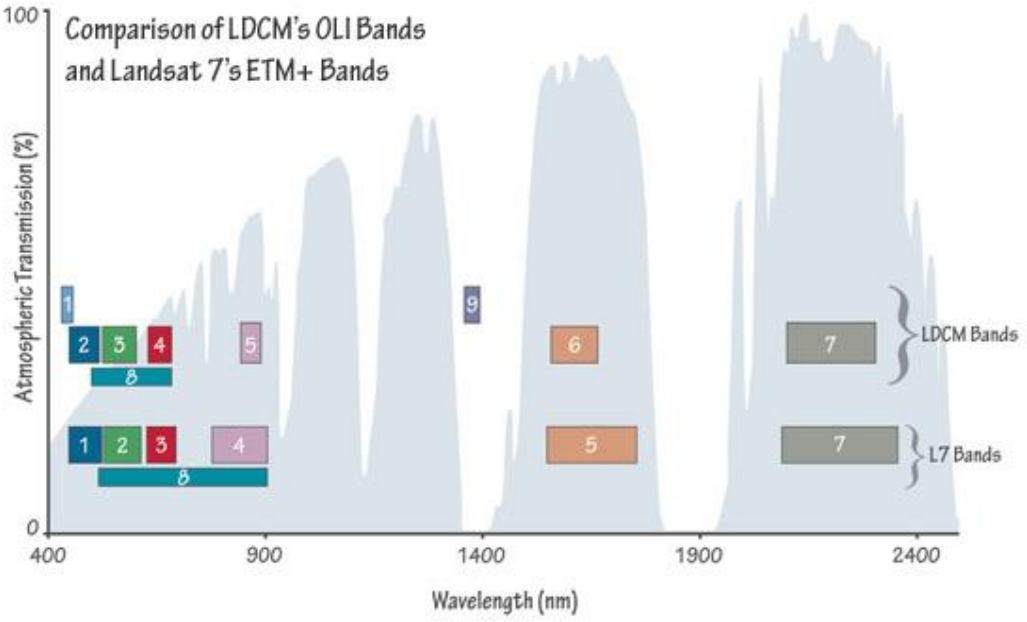


Figure 70: The new Landsat LDCM satellite's OLI sensor bands compared to Landsat 7 bands created by L.Rocchio and J.Barsi [7]

Technical details

The Landsat satellites follow a repetitive, circular, sun-synchronous, near earth orbit at an altitude of 705 km measured at the equator. The return interval is 16 days for Landsat-7 and 18 days for Landsat-5, and a wisk-broom (side to side) action covers a swath of 185 km giving a scene size of 183 km x 170 km. The bands are shown in Table 22.

Table 22: Landsat 7 ETM+ bands and band widths[8]

	Name	Wavelength (µm)	*Description*
VNIR (30 metres)		$W/m^2/sr/\mu m$	
Band 1	Blue	0.45-0.52	*Useful for bathymetric mapping and distinguishing soil from vegetation and deciduous from coniferous vegetation.*
Band 2	Green	0.52-0.60	*Emphasizes peak vegetation, which is useful for assessing plant vigor.*
Band 3	Red	0.63-0.69	*Discriminates vegetation slopes*
Band 4	NIR	0.77-0.90	*Emphasizes biomass content and shorelines.*
Band 5	$MIR/SWIR_{1.6}$	1.55-1.75	*Discriminates moisture content of soil and vegetation; penetrates thin clouds.*
Band 7	$SWIR/SWIR_{2.235}$	2.09-2.35	*Useful for mapping hydrothermally altered rocks associated with mineral deposits*
TIR (60 metres)		$W/m^2/sr/\mu m$	
Band 6	TIR	10.40-12.50	*Useful for thermal mapping and estimated soil moisture.*
PAN (15 Metres)		$W/m^2/sr/\mu m$	
Band 8	*PAN/PANir*	*0.52-0.90*	*Used for "sharpening" of multispectral images.*

The Worldwide Reference System (WRS)[9] is a global notation system for Landsat data. The path and row grid system uniquely identifies the scene centre and is used to identify

[7] http://landsat.gsfc.nasa.gov/about/ldcm.html (downloaded 9 October 2009)
[8] http://landsathandbook.gsfc.nasa.gov/handbook.html (downloaded 9 October 2009)

[9] http://landsat.usgs.gov/worldwide_reference_system_WRS.php (downloaded 9 October 2009)

imagery transmitted from the Landsat satellites. The satellites stay on the same orbit for each pass over an area on the earth's surface giving repeatable scene identification. This system has been adopted by other satellites as an industry standard. WRS-1 applied to Landsat 1, 2 and 3 and WRS-2 for Landsat 4, 5 and 7 due to the difference in altitude of the satellite.

The naming convention for Landsat files is as follows, but may differ between data suppliers:

L71015033_03320000409_B10

where

L7 = satellite Landsat 7
1 = sensor ETM+
015 = WRS-2 path
033 = WRS-2 starting row
033 = WRS-2 ending row
20000409 = Acquisition date YYYYMMDD
B10 = Band 1

APPENDIX III: Advanced Airborne Thermal Emission and Reflections Radiometer (ASTER)

The ASTER satellite was launched in December 1999 on the NASA Terra multi-sensor spacecraft, as a joint US-Japanese venture. This is the same spacecraft which carries the MODIS sensor, amongst other instruments.

The ASTER imagery is comparable to the Landsat program in that the orbit it follows is the same and the spectral range recorded is very simlar, as illustrated in Figure 71. The ASTER imagery is acquired at a higher spatial and spectral resolution, but does not have a panchromatic sensor. The revisit time of the two satellites is the same, at 16 days, but the swath of the ASTER sensor is 60 km (one third of the Landsat sensor) and will record on demand at nadir or pointed to either side, but cannot cover the 180 km of Landsat, at one overpass. ASTER is only acquired on request and is not a continuous record of the earth's surface, as with Landsat.

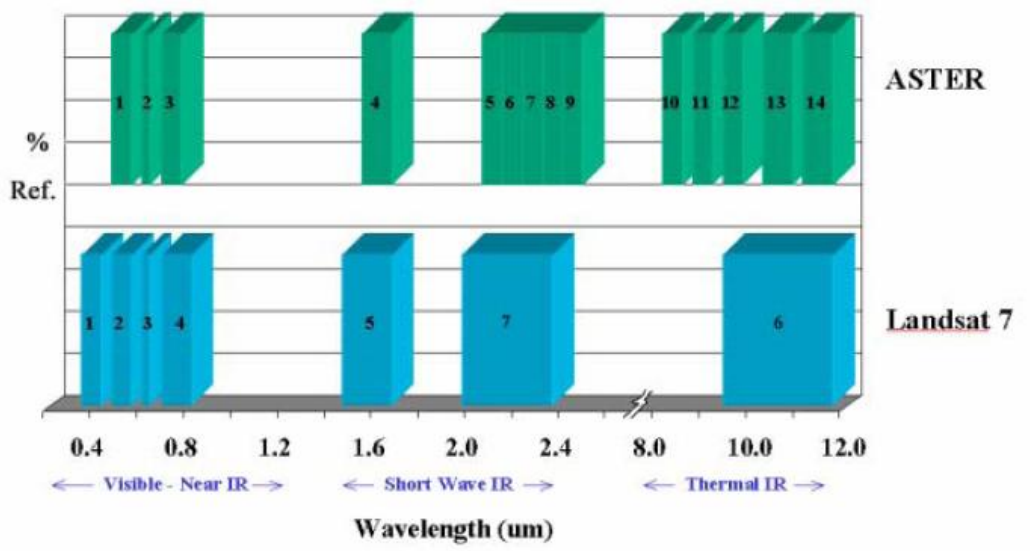


Figure 71: Comparison of Spectral Bands between ASTER and Landsat 7 ETM+ showing percentage reflectance per wavelength.[10]

There are three separate instruments recording the Visible and Near-Infrared (VNIR), Short Wave Infrared (SWIR) and Thermal Infrared band widths. Band 3N (NIR) records at nadir and Band 3B is a backward pointing sensor giving stereoscopic pairs of images used to calculate DEMs (Abrams and Hook, 2001) described in detail in Table 23.

Technical details

The high resolution multi-spectral sensors on board record 14 bands across the visible and infra-red electromagnetic spectrum. The instrument is a pointable, stereoscopic sensor with a 16-day revisit following a sun-synchronous polar orbit, approximately 30 minutes behind the Landsat-7 satellite, at an altitude of 705 km. The ASTER images cover approximately 60 km by 60 km and images are referenced according to the World

[10] http://asterweb.jpl.nasa.gov/content/03_data/04_Documents/aster_user_guide_v2.pdf (downloaded 9 October 2009)

Reference System (WRS-2) used for Landsat images, although it is not tiled the same as Landsat due to the smaller swath.

Table 23: ASTER band and band widths

	Name	Spectral range(μm)	*Units*
VNIR(15 metres)			
Band 1	Green	0.52-0.60	$W/m^2/sr/\mu m$
Band 2	Red	0.63-0.69	$W/m^2/sr/\mu m$
Band 3N	NIR	0.78-0.86	$W/m^2/sr/\mu m$
Band 3B	NIR	0.78-0.86	$W/m^2/sr/\mu m$
SWIR(30 metres)			
Band 4	$MIR/SWIR_{1.6}$	1.600-1.700	$W/m^2/sr/\mu m$
Band 5	$SWIR5/SWIR_{2.145}$	2.145-2.185	$W/m^2/sr/\mu m$
Band 6	$SWIR6/SWIR_{2.185}$	2.185-2.225	$W/m^2/sr/\mu m$
Band 7	$SWIR7/SWIR_{2.235}$	2.235-2.285	$W/m^2/sr/\mu m$
Band 8	$SWIR8/SWIR_{2.295}$	2.295-2.365	$W/m^2/sr/\mu m$
Band 9	$SWIR9/SWIR_{2.360}$	2.360-2.430	$W/m^2/sr/\mu m$
TIR(90 metres)			
Band 10	TIR10	8.125-8.475	$W/m^2/sr/\mu m$
Band 11	TIR11	8.475-8.825	$W/m^2/sr/\mu m$
Band 12	TIR12	8.925-9.275	$W/m^2/sr/\mu m$
Band 13	TIR13	10.25-10.95	$W/m^2/sr/\mu m$
Band 14	*TIR14*	*10.95-11.65*	$W/m^2/sr/\mu m$

The naming convention for ASTER files is as follows:

ASTL1A YYMMDDHHMMSSyymmddNNNN

where

AST = ASTER sensor
L1A = Level of pre-processing applied by supplier
YYMMDD = observation date /date of acquisition
HHMMSS = observation time / time of acquisition
yymmdd = the data granule generation date / date processed
NNNN = the data granule sequential number per day

APPENDIX IV: SPOT 5

The SPOT earth observation satellite program was developed by the French space agency, CNES, in collaboration with Belgium and Sweden. The first satellite was launched in 1986 and the latest satellite, SPOT 5, was launched in May 2002. On 30 June 2009, SPOT 2 began de-orbiting to burn up in the earth's atmosphere, ending 14 years of service, and leaving SPOT 4 and SPOT 5 to continue with data acquisition of the earth's surface.

SPOT 5 carries two High Geometric Resolution instruments (HRG) which record two panchromatic bands at 5m resolution (combined to give 2.5m), three multi-spectral bands at 10 m resolution, and one short wave band at 20 m resolution (Figure 72). This 20 m band is re-sampled to 10 m. The High Resolution Stereoscopic (HRS) instrument acquires two images at the same time, one forward and one back, creating stereo pairs used to create highly accurate digital elevation models. The VEGETATION2 instrument records daily at a spatial resolution of 1 km for environmental and biosphere monitoring of global change.[11]

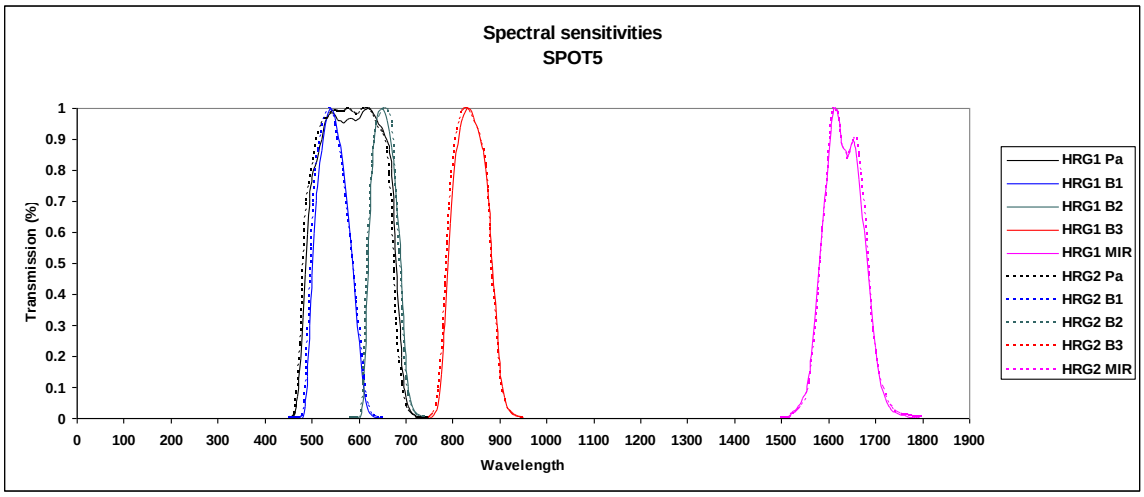


Figure 72: Spectral sensitivities for the four multi-spectral and panchormaitc bands for SPOT 5[12]

Although the satellite has a 26-day revisit interval, it only acquires imagery over a 60 km x 60 km swathe on request and has a cloud detection algorithm which prevents acquisition if cloud cover is above a customer specified level.

The CSIR Satellite Applications Centre (SAC) at Hartbeeshoek is one of 22 SPOT direct receiving stations (DRS) around the world. In April 2007, a set of SPOT-5 images covering the whole of South Africa was made available from Spot Image, France, for use

[11] http://www.spotimage.fr/web/en/229-the-spot-satellites.php (downloaded 9 October 2008)

[12] http://www.spotimage.fr/automne_modules_files/standard/public/p445_fileLINKEDFILE_spectral-sensitivity.xls (downloaded 9 October 2008)

by South African research institutions. The KNP received a set of images covering the entire Kruger National Park for the dates between 5 September 2005 and December 2006. The future of the SPOT program includes the expected launch of Astroterra/SPOT 6 in 2012 and SPOT 7 in 2014. The SPOT 6 spatial resolution will be 2m for the panchromatic and 8m colour (RGB and NIR only). Although a blue band has been included, the mid infra-red band of SPOT 5 will be missing. SPOT have developed a very high resolution satellite, Pleiades 1, which will supply natural colour (RGB and NIR), 50 cm orthorectified imagery from early 2010[13].

Technical details

The SPOT orbit is polar, circular, sun-synchronous and phased and has an oblique viewing capacity within a 900 km swath, allowing more frequent viewing of a point on the earth during a single 26-day cycle. A single point is recorded up to 7 times during one cycle at the equator and up to 11 times at latitude 45 degrees. The two High Geometric Resolution Instruments (HRG) record two panchromatic bands at 5m resolution (combined to give 2.5m), three multi-spectral bands at 10 m resolution, and one short wave band at 20 m resolution (Table 24). This 20 m band is re-sampled to 10 m. The High Resolution Stereoscopic (HRS) instrument acquires two images at the same time, one forward and on back, creating stereo pairs used to create highly accurate digital elevation. The images cover a 60 km x 60 km swathe and are referenced using the grid reference system (GRS) where the centre of a scene is named according to the nearest intersection of the column (K) and row (J) of the grid. [14]

Table 24: Spectral Bands and band widths for SPOT 5 satellite imagery

Band	**Name**	***Spectral range(µm)***
PAN 2.5m (from 5m)	PAN	*0.49-0.69*
B1	Green	*0.49-0.61*
B2	Red	*0.61-0.68*
B3	NIR	*0.78-0.89*
B4	*MIR/SWIR$_{1.6}$*	*1.580-1.750*

[13] http://www.spotimage.com/web/en/1663-pleiades-very-high-resolution-satellite-imagery.php
[14] http://www.spotimage.fr/web/en/229-the-spot-satellites.php

APPENDIX V: Carnegie Airborne Observatory (CAO) Hyperspectral images and waveform LiDAR data

The CAO sensor was developed to scan data to specifically measure the structural and biochemical diversity of ecosystems to facilitate research and management of conservation areas (Asner *et al*., 2007). The instrument was developed by the Carnegie Institution, Department of Global Ecology. The product is a fusion of imaging spectroscopy (hyperspectral imaging) in the visible and near-infrared bands, and waveform light detection and ranging (wLiDAR), giving a geo-orthorectified image of vegetation structure, physiology and biochemistry, as well as the surface water, soils and underlying topography (Asner *et al*., 2007).

Selected areas of the KNP were flown using this technology during April and May 2008. The combination of vegetation structure, topography and hyperspectral imagery (between 400-1050 nm) gives a unique opportunity to investigate the location of sodic soils at a high resolution based on their chemical composition compared to the albedo effect of sodic bare areas.

Table 25: The CAO Alpha System design specifications (Asner *et al*., 2007)

Table 4. The CAO Alpha System design specifications.

Component	Description
Spectrometer	Pushbroom array, diffraction grating, Offner design
	373-1052 nm spectral range
	1500 cross-track pixels; 40 degree field-of-view
	Fully programmable, up to 2.4 nm spectral resolution (288 bands)
	14-bit dynamic range
	Spectral smile = 0.1 pixels across the entire 1500 pixel array
	Spectral keystone = 0.02 from 365 to 1050 nm
	SNR at nadir = ~400 @ 550 nm on 10% reflectance target
	SNR at nadir = ~400 @ 850 nm on 30% reflectance target
	Coincident downwelling radiance sensor (200-1100 nm; 2048 bands)
	Instantaneous field-of-view = 0.56 mrad to match wLiDAR
	Compatible with same GPS/IMU data stream as wLiDAR
wLiDAR	Wavelength = 1064 nm
	12-bit dynamic range for LiDAR intensities
	Waveform digitization; nanosecond temporal resolution; up to 440 slices or elevations per laser shot
	Laser repetition programmable up to 100 kHz
	Scan angle programmable up to 44 degrees
	Scan frequency programmable up to 70 Hz
	Laser beam divergence of 0.56 mrad (1/e) to match spectrometer
	Compatible with same GPS/IMU data stream as spectrometer
IMU	200 Hz high-performance FOG gyros; silicon accelerometers
	Performance: velocity = 0.005 m/s; roll and pitch = 0.005 deg; heading = 0.008 deg
GPS	L1/L2 compatible; 43 db
	12 channel dual frequency; 10 Hz raw data rate
Sensor Mount	Floating-plate design with six pneumatic mounts for vibration dampening
Pilot Controls	Navigation display controlled by instrument operator from rear of aircraft

Table 26: Spectral bands and band widths for CAO Hyperspectral data giving Landsat equivalent names for common wavelegths for comparison.

Band	Landsat equivalent name	Spectral Band (nm)		Band	Landsat equivalent name	Spectral Band (nm)
Band 1		384.8		Band 37		724.9
Band 2		394.3		Band 38		734.4
Band 3		403.7		Band 39		743.8
Band 4		413.1		Band 40		753.3
Band 5		422.6		Band 41		762.7
Band 6		432.0		Band 42	NIR	772.1
Band 7		441.4		Band 43	NIR	781.6
Band 8	Blue	450.9		Band 44	NIR	791.0
Band 9	Blue	460.3		Band 45	NIR	800.5
Band 10	Blue	469.7		Band 46	NIR	809.9
Band 11	Blue	479.2		Band 47	NIR	819.3
Band 12	Blue	488.6		Band 48	NIR	828.8
Band 13	Blue	498.1		Band 49	NIR	838.2
Band 14	Blue	507.5		Band 50	NIR	847.6
Band 15	Green	517.0		Band 51	NIR	857.0
Band 16	Green	526.4		Band 52	NIR	866.5
Band 17	Green	535.9		Band 53	NIR	875.9
Band 18	Green	545.3		Band 54	NIR	885.3
Band 19	Green	554.8		Band 55	NIR	894.7
Band 20	Green	564.2		Band 56		904.1
Band 21	Green	573.7		Band 57		913.5
Band 22	Green	583.1		Band 58		922.9
Band 23	Green	592.6		Band 59		932.3
Band 24		602.0		Band 60		941.7
Band 25		611.5		Band 61		951.1
Band 26		620.9		Band 62		960.5
Band 27		630.4		Band 63		969.9
Band 28	Red	639.9		Band 64		979.3
Band 29	Red	649.3		Band 65		988.7
Band 30	Red	658.8		Band 66		998.1
Band 31	Red	668.2		Band 67		1007.4
Band 32	Red	677.7		Band 68		1016.8
Band 33	Red	687.1		Band 69		1026.2
Band 34		696.6		Band 70		1035.6
Band 35		706.0		Band 71		1044.9
Band 36		715.5		Band 72		1054.3

APPENDIX VI: Orthorectified aerial photographs

Panchromatic (black and white) orthorectified aerial photograph mosaics were created by Bohensky (2006) for the Shingwedzi and Sabi River systems using aerial photographs flown in May 2001. This included over 1000 1:20000 aerial photographs; approximately 200 in the south and 800 in the north. A complete description of the methods used for orthorectification is available as a KNP internal report (Bohensky, 2006). The accuracy of these mosaics has been tested against the KNP road and rivers GIS layers and found to be acceptable.

Georeferencing was done using ground control points measured using a hand-held GPS as well as points identified from the 1:50000 topographical map series of the area. Orthorectification included elevation values from a 20 m digital terrain model (DTM) (Bohensky, 2006)

The orthophotographs are high resolution (0.86m) panchromatic radiometrically adjusted images useful for landscape or small-scale studies of the Shingwedzi and Sabi River catchments. Sodic sites are visually identified using the albedo effect of bare soil at the footslopes of catenas near rivers. A disadvantage of using orthophotographs in a semi-automated classification system is that the files are very large and can be 46000 x 12000 pixels. Definiens Developer (eCognition V7) is able to divide this mosaic into tiles, run the analysis and re-stitch after classification for post-classification purposes.

APPENDIX VII: Shuttle Radar Topography Mission (SRTM) 90 m digital elevation model (DEM)

The shuttle radar topography mission was a joint venture between NASA, the NGA and the USGS and was flown by the NASA Space Shuttle Endeavour between 11 and 22 February, 2000. The result of this mission was a three-dimensional map of the earth's surface, suppied to the US at 30m resolution and to the rest of the world at 90 m resolution. A technique known as single pass interferometry was used to collect this data. Two radar antennae record two images from slightly different locations which are then used to calculate ground heights[15]. This DEM is freely available from the USGS EROS Data Centre or on the internet[16].

APPENDIX VIII: Moderate Resolution Imaging Spectroradiometer (MODIS)

The MODIS sensor is carried aboard the Terra (EOS AM) and Aqua (EOS PM) satellite which travels in the same orbit as the Landsat 7 satellite, about 15 minutes behind (Landsat 7 User Handbook). This means that the imagery from Landsat-7 and MODIS have similar atmospheric and vegetation physiological conditions. This sensor covers the entire Earth's surface in 1 to 2 days with a swath of 2330 km, scene size of approximately 10 km by 10 km and a return time of 16 days. The instrument supplies hyper-temporal images for 36 spectral bands. MODIS data are used for vegetation, atmospheric and oceanic research. The MODIS NDVI vegetation index product is a 16-day composite at a resolution of 250 m expressed as surface reflectance scaled by 10000, with valid values between -2000 and 10000[17].

[15] http://mac.usgs.gov/isb/pubs/factsheets/fs07103.html (downloaded 21October 2008)
[16] http://srtm.csi.cgiar.org/SELECTION/inputCoord.asp (downloaded 21October 2008)
[17] http://lpdaac.usgs.gov/modis/mod13q1.asp (downloaded 18 October 2008)

APPENDIX IX: Radiometric normalisation: pre-processing methods for conversion from DN to reflectance values for Landsat 7 ETM+, ASTER and SPOT 5 imagery.

Background

Satellite imagery received from any supplier is supplied in the format ordered by the user. For land cover classification of imagery the data must be converted from the supplied units (DN or radiance) into the unitless top of atmosphere reflectance, expressed as a value between 0 and 1. The following sections will describe this process in detail to ensure that the classification result is derived from robustly pre-processed imagery.

Data suppliers process the data into a usable format using pre-processing algorithms developed for each satellite, and scale these values to an 8-bit or 16-bit image for each band separately, storing 256 and 65536 unique values respectively. The file sizes of the scaled data are smaller than the original file (floating point) and therefore more easily transferable. Classification results based on unprocessed or incorrectly processed imagery are not robust and cannot be compared with other research results.

Radiometric corrections involve the value of the pixel influenced by the sensor itself or the angle of the sun and atmospheric effects. The geometric corrections involve the position of the pixel in the image influenced by the problems of expressing a three dimensional object in two dimensions in the correct geographic location. The first radiometric and geometric corrections are made by the image supplier and take into account the satellite internal and external radiometric and geometric factors. The general format of pre-processing of raw imagery by data suppliers is as follows:

- Radiometric corrections due to the differences in sensitivity of the sensors
- Geometric corrections due to satellite internal and external orientations or errors
- Geometric corrections to a standard projection without ground control points
- Geometric correction and re-sampling to a standard projection using ground control points (X and Y coordinates).
- Orthorectification using a digital elevation model or topography model (X, Y and Z coordinates)

The second series of radiometric and geometric corrections are made by the user on receipt of the imagery and before analysis of the data.

A summary of pre-processing by the user for all sensors is as follows:

- Radiometric correction (unscaling): The top of atmosphere (TOA) or radiation at sensor is calculated using bias and gains for each sensor to rescale the 8-bit or 16-bit values to radiance expressed as $W/m^2/sr/\mu m$, and saved in non-scaled floating point format.
- Geometric correction (sun-earth geometry): The reflectance at sensor is calculated taking solar elevation angle of the sun, the distance between earth and sun (d) and the ESUN value (mean solar exo-atmospheric irradiance), and is expressed as the ratio of radiance to possible radiance expressed as a percentage.
- Atmospheric corrections to the radiance or reflectance values will give surface radiation or reflectance values. There are various methods used to correct for atmospheric effects and this is the area which is avoided by most researchers, as it is the most difficult task to perform accurately

Orthorectification, where the location of the pixel is also corrected for altitude, may also be performed by the user if the images are not supplied in this format. The result of this

pre-processing by the supplier is a general Level 1 pre-processing in LANDSAT and ASTER, or Level 2 in SPOT5. The Level 1G Landsat and Level 1B ASTER images are not orthorectified and the value of the scaled DN number is the top of atmosphere (TOA) or "at sensor" radiance, not reflectance. At this point, the imagery is useful for photogrammetric measurements and road mapping exercises as it has been radiometrically and geometrically corrected as well as geo-referenced. Further radiometric and geometric correction is required by the user before vegetation analysis is performed.

Before a sensor is launched the relationship between the spectral radiance and the DN value are measured, called the sensor calibration. These scaling coefficients, namely gains (or slope) and biases (or offset), are calculated from pre- and post-launch calibrations (Abrams and Hook, 2001). The gain is the gradient of the calibration function and the bias defines the spectral radiance for DN = 0 (the Y-axis intercept). The accuracy of these sensor coefficients deteriorate over time and re-calibrations may be published by the image suppliers from time to time (Geosystems, 2006). The scaling coefficients are supplied in the header file or metadata of the imagery and are used to convert the scaled DN value to "unscaled" DN and to calculate the radiance "at sensor" for each band.

Pre-processing methods

The header file or metadata file supplied with the image data contains all the information required for further pre-processing of imagery into reflectance values. It must therefore be supplied with the imagery to perform further processing. All imagery must be converted to at sensor (TOA) reflectance values before image analysis is performed (Step1 and Step 2).

Step 1: Convert DN to radiance at sensor

Each satellite sensor has a unique set of co-efficients that are made available in the header file for each satellite or available in reference documentws. The specific formulae for calculating the radiance at the sensor from digital numbers (DN) are shown as follows:

a) Landsat DN to radiance at sensor

$$L_{rad} = (DN \times Gain) + Bias \qquad [8]$$

OR

$$L_{rad} = ((L_{max} - L_{min})/(QCAL_{max} - QCAL_{min})) * (QCAL-QCAL_{min}) + L_{min} \qquad [9]$$

where

L_{rad} = the equivalent radiance at the input of the instrument ($W/m^2/sr/\mu m$)

DN = the count (0 to 255)

Gain (slope) = $(L_{max} – L_{min}) / DN_{max}$

Bias (offset) = L_{min}

L_{max} = maximum detectable radiance

L_{min} = lowest detectable radiance

DN_{max} = maximum DN recorded (255 for 8-bit)

$QCAL_{min} = 1$

$QCAL_{max} = 255$

QCAL = Digital Number (DN)

(Chander and Markham, 2003)

b) ASTER DN to radiance at sensor

$$L_{rad} = (DN - 1) \times Gain \quad [10]$$

where DN = 0 is a no data pixel
DN = 1 is the lowest detectable radiance
(Thorne, Biffar and Takashima, 1999)

Table 27: Gain coefficients for ASTER images (Thorne, Biffar and Takashima, 1999)

Band	***Coefficient (W/m²/sr/µm)/DN)***			
	High Gain	**Normal**	**Low Gain 1**	***Low Gain 2***
1	0.676	1.688	2.25	
2	0.708	1.415	1.89	
3N	0.423	0.862	1.15	
3B	0.423	0.862	1.15	
4	0.1087	0.2174	0.2900	*0.2900*
5	0.0348	0.0696	0.0925	*0.4090*
6	0.0313	0.0625	0.0830	*0.3900*
7	0.0299	0.0597	0.0795	*0.3320*
8	0.0209	0.0417	0.0556	*0.2450*
9	*0.0159*	*0.0318*	*0.0424*	*0.2650*

c) SPOT 5 DN to radiance at sensor

$$L_{rad} = (DN/Gain) + Bias \quad [11][18]$$

where
L_{rad} = the equivalent radiance at the input of the instrument ($W/m^2/sr/\mu m$)
DN = the count (0 to 255),
Gain = absolute calibration gain, for the considered spectral band
Bias = absolute calibration offset, for the considered spectral band.

Step 2: Convert spectral radiance to reflectance:
This is a standard formula for all imagery and incorporates the sun-earth geometry at the time of acquisition of the imagery[19]. Each sensor has a different ESUN value (see Table 28, Table 29 and Table 30), and the day and solar elevation angle data obtained from the header data of the imagery, are unique for each image.

[18] http://gmesdata.esa.int/c/document_library/get_file?uuid=6a2899a7-1a7a-4b65-b1b6-3291781d55c0andgroupId=10725 (downloaded 9 October 2008)

[19] http://landsathandbook.gsfc.nasa.gov/handbook/handbook_htmls/chapter11/chapter11.html (downloaded 1 October 2008)

$$\rho_\lambda = \frac{(\pi \times d^2 \times L_{rad})}{(ESUN \times Cos(z))} \quad [12]$$

where

ρ_λ = unitless planetary reflectance
π = pi = 3.14159
d = earth-sun distance in astronomical units
= (1 - 0.01672 x COS(RADIANS(0.9856 x (Julian Day-4))))
L_{rad} = the spectral radiance at the sensor ($W/m^2/sr/\mu m$)
ESUN = mean solar exoatmospheric irradiance ($W/m^2/sr/\mu m$)
z = solar zenith angle in degrees = 90 – solar elevation angle

Table 28: Landsat ESUN values for the conversion from spectral radiance to reflectance (Chander and Markham, 2003)

Band	***Irradiance($W/m^2/\mu m$)***		
	Landsat4	Landsat5	*Landsat 7 ETM*
1	1957.000	1957.000	*1969.000*
2	1825.000	1826.000	*1840.000*
3	1557.000	1554.000	*1551.000*
4	1033.000	1036.000	*1044.000*
5	214.900	215.000	*225.700*
7	80.720	80.670	*82.070*
8	-	-	*1368.000*

Table 29: ASTER ESUN values for the conversion from spectral radiance to reflectance (Smith[20])

Band	***Irradiance($W/m^2/\mu m$)***		
	Smith [a]	Thome et al [b]	*Thome et al [c]*
1	1845.99	1847	*1848*
2	1555.74	1553	*1549*
3N	1119.47	1118	*1114*
4	231.25	232.5	*225.4*
5	79.81	80.32	*86.63*
6	74.99	74.92	*81.85*
7	68.66	69.20	*74.85*
8	59.74	59.82	*66.49*
9	*56.92*	*57.32*	*59.85*

[a] Smith: Calculated by interpolating the ASTER spectral response functions to 1nm and convolving them with the 1nm step WRC data
[b] Thorne et al., 1999: Calculated by convolving the ASTER spectral response functions them with the WRC data [Unknown whether these where both interpolated to 1nm or whether a subsample of WRC data values at the ASTER spectral response function step intervals were used in the convolution]
[c] Thome et al: Calculated using spectral irradiance values derived using MODTRAN.

[20] http://www.cnrhome.uidaho.edu/default.aspx?pid=85984
(downloaded 9 October 2008)

Table 30: SPOT 5 ESUN values for the conversion from spectral radiance to reflectance[21]

Band	***Irradiance(W/m²/µm)***	
	HRG1	*HRG2*
HMA/HMB	1762	*1773*
B1	1858	*1858*
B2	1573	*1575*
B3	1043	*1047*
MIR	*236*	*234*

Step 1 and 2 in one step

Radiometric and earth-sun geometric corrections (Steps 1 and 2) can be applied in one step using formula substitution into the equations. Models are available in ERDAS 9.2 for many of these corrections and are applied after changes to the variables are made according to the metadata of the imagery.

Step 3: Atmospheric correction

Atmospheric correction is dependant on the data available and the methods used. Absolute corrections are either empirical, making generalised assumptions, or physical, also called Radiative Transfer Models (RTMs). Relative atmospheric correction is based on the assumption of a linear relationship between image bands across time determined from radiometric measurements of pseudo-invariants in the images (Song *et al.*, 2000).

Relative atmospheric corrections use reference images, histogram matching or calibrations using pseudo-invariants.

Absolute atmospheric corrections include the following methods:

- Empirical: Dark object subtraction (DOS) (Moran, Bryant, Thorne, Ni., Nouvellon, Gonzalez-Dugo, Qi and Clarke, 2001), COST model (Chavez, 1996), Empirical Line method (Moran *et al.*, 2001), Haze optimisation transformation (HOT) (Zhang, Guindon and Cihlar, 2002).
- Physical: Radiative Transfer Model: ATCOR 2 and 3, 6S model

The preferred method is the radiative transfer model 6S implemented by the ATCOR 2 and 3 programs as stand alone software, or included in PCI Geomatica and GRASS.

Step 1 to 3: One-step atmospheric and radiometrically corrected using the COST formula (Chavez, 1996) by inclusion of a haze correction[22]:

$$\rho_{\lambda} = \frac{(\pi \times d^2 \times (L_{\lambda sat} - (L_{\lambda lowest_value} - L_{\lambda black_object})))}{(Esun \times Cos^2\theta)}$$

To check the result of reflectance calculations, compare the spectral signatures of invariant objects such as deep water, roads or runways (Geosystems, 2006).

21 http://www.spotimage.com/automne_modules_files/standard/public/p2751_fileLINKEDFILE_luminances-F.pdf (downloaded 12 October 2008)

22 http://arsc.arid.arizona.edu/resources/image_processing/landsat/ls5-atmo.html (downloaded 17 October 2008)

APPENDIX X: Classification algorithm process tree for object-based image analysis of Landsat 7 and SPOT 5 imagery using eCongnition (Definiens Professional V 5).

Classes:

Bare Soil sodic patches
Basalt
Burn scar
Closed Savanna
Crest
Drainage line
Geology
Granite
KNP Boundary
Landcover
No veg
Not AIO
Open Savanna
River sand
Riverine vegetation
Savanna
Sparse veg
Topography
Vegetated sodic patches
Vegetation
Water

(A) Landsat 7 ETM+ - Shingwedzi full algorithm

Process: Main:

```
do
    Define KNP Boundary Mask
        chessboard segmentation: chess board: 1000000 creating 'Boundary Mask'
        assign class: with Thematic object ID: KNP_BOUNDARY = 0  at  Boundary Mask: KNP Boundary
    Segmentation
        multiresolution segmentation: KNP Boundary at  Boundary Mask: 3 [shape:0.2 compct.:0.5] creating
            'Level 3'
        multiresolution segmentation: KNP Boundary at  Boundary Mask: 5 [shape:0.2 compct.:0.5] creating
            'Level 5'
        multiresolution segmentation: KNP Boundary at  Boundary Mask: 10 [shape:0.2 compct.:0.5] creating
            'Level 10'
    [Add samples from GPS data]
        assign class: with VEGCLASS_C: KNP_SAMPLE_WAYPOINTS = 1  at  Level 3: River sand
        assign class: with VEGCLASS_C: KNP_SAMPLE_WAYPOINTS = 2  at  Level 3: Riverine vegetation
        assign class: with VEGCLASS_C: KNP_SAMPLE_WAYPOINTS = 3  at  Level 3: Savanna
        assign class: with VEGCLASS_C: KNP_SAMPLE_WAYPOINTS = 4  at  Level 3: Bare Soil sodic
            patches
        assign class: with VEGCLASS_C: KNP_SAMPLE_WAYPOINTS = 5  at  Level 3: Vegetated sodic
            patches
        classified image objects to samples: at  Level 3: classified image objects to samples
        assign class: Bare Soil sodic patches, Burn scar, Closed Savanna, No veg, Savanna, River sand,
            Riverine vegetation, Vegetation, Water, Open Savanna at  Level 3: unclassified
    Add virtual samples manually
    Classification
        Exclude Areas not of Interest
            assign class: unclassified with Existence of super objects KNP Boundary (3) <> 1  at  Level 3: Not
                AIO
            assign class: with Mean Green < 4  at  Level 5: Not AIO
            assign class: with Existence of sub objects Not AIO (1) <> 0  at  Level 5: Not AIO
            assign class: with Existence of sub objects Not AIO (1) <> 0  at  Level 10: Not AIO
        Classify Level 10: River Sand
            assign class: with OBJECTID: Thematic Layer 4 >= 0  at  Level 10: Drainage line
            assign class: Drainage line with Mean TasCap2 <= 0  at  Level 10: River sand
            assign class: with Length\Width <= 3  at  Level 10: unclassified
        Classify Level 5: Geology
            assign class: with Membership to Not AIO = 0  at  Level 5: Basalt
            assign class: Basalt with OBJECTID: Thematic Layer 5 = 2  at  Level 5: Granite
        Classify Level 3: Topography
            assign class: with Existence of super objects Granite (1) = 1  at  Level 3: Granite
            assign class: with Existence of super objects Basalt (1) = 1  at  Level 3: Basalt
```

assign class: Granite with Mean Diff. to neighbors DEM90m (75) < -2 at Level 3: Drainage line
assign class: Basalt with Mean Diff. to neighbors DEM90m (75) < -1 at Level 3: Drainage line
assign class: Basalt, Granite at Level 3: Crest
assign class: Drainage line at Level 3: unclassified
Classify Level 3: Landcover
assign class: unclassified with Mean MIR < 10 at Level 3: Water
assign class: unclassified with Mean TasCap1 >= 37 at Level 3: No veg
assign class: unclassified with Mean TasCap2 <= -1 at Level 3: Sparse veg
assign class: unclassified with Ratio Red >= 0.11 at Level 3: No veg
assign class: unclassified with Mean PCA1 >= 35 at Level 3: No veg
assign class: unclassified with Mean MIR >= 26 at Level 3: No veg
assign class: unclassified with Mean NDVI <= 29 at Level 3: No veg
assign class: unclassified with Mean NDVI <= 38 at Level 3: Sparse veg
Vegetation
assign class: unclassified with Mean NDVI >= 53 at Level 3: Riverine vegetation
assign class: unclassified with Mean NDVI >= 32 at Level 3: Savanna
assign class: No veg with Mean NDVI > 40 at Level 3: Savanna
assign class: Sparse veg with Mean NDVI > 38 at Level 3: Savanna
assign class: unclassified at Level 3: Savanna
River sand
assign class: No veg with OBJECTID: Thematic Layer 4 > 0 at Level 3: River sand
assign class: No veg at Level 3: Bare Soil sodic patches
assign class: River sand with Rel. border to Bare Soil sodic patches >= 0.3 at Level 3: Bare Soil sodic patches
assign class: Bare Soil sodic patches with Existence of super objects River sand (2) = 1 at Level 3: River sand
assign class: with Existence of sub objects River sand (2) = 1 at Level 10: River sand
assign class: Bare Soil sodic patches with Existence of super objects River sand (2) = 1 at Level 3: River sand
Sodic areas
assign class: Sparse veg with Rel. border to Bare Soil sodic patches >= 0.4 at Level 3: Bare Soil sodic patches
assign class: Bare Soil sodic patches with Mean NDVI >= 38 at Level 3: Savanna
assign class: Sparse veg with Mean NDVI > 38 at Level 3: Savanna
assign class: Sparse veg with Mean NDVI <= 33 at Level 3: Bare Soil sodic patches
assign class: Bare Soil sodic patches with Existence of super objects Basalt (1) >= 1 at Level 3: Vegetated sodic patches
assign class: Vegetated sodic patches with Mean NDVI >= 30 at Level 3: Savanna
assign class: Vegetated sodic patches with Mean NDVI < 30 at Level 3: Bare Soil sodic patches
assign class: Crest at Level 3: Savanna
Export Sodic Sites
create polygons: create polygons [base: 1.25 slivers: yes shape: 1]
export vector layers: Bare Soil sodic patches, River sand, Riverine vegetation, Savanna, Sparse veg, Water at Level 3: export object shapes to Landsat7_168077_20010530_Classification
export vector layers: Bare Soil sodic patches at Level 3: export object shapes to Landsat7_168077_20010530_Sodics

(B) SPOT 5 - Shingwedzi full algorithm

Process: Main:

do
Define KNP Boundary Mask
chessboard segmentation: chess board: 1000000 creating 'Boundary Mask'
assign class: with Thematic object ID: KNP_BOUNDARY = 0 at Boundary Mask: KNP Boundary
Segmentation
multiresolution segmentation: KNP Boundary at Boundary Mask: 10 [shape:0.2 compct.:0.5] creating 'Level 10'
multiresolution segmentation: KNP Boundary at Boundary Mask: 15 [shape:0.2 compct.:0.5] creating 'Level 15'
multiresolution segmentation: KNP Boundary at Boundary Mask: 20 [shape:0.2 compct.:0.5] creating 'Level 20'
Add virtual samples manually
[Add samples from GPS data]
assign class: at Level 3: River sand
assign class: at Level 3: Riverine vegetation
assign class: at Level 3: Savanna
assign class: at Level 3: Bare Soil sodic patches
assign class: at Level 3: Vegetated sodic patches
classified image objects to samples: at Level 3: classified image objects to samples
assign class: Bare Soil sodic patches, Burn scar, Closed Savanna, No veg, Savanna, River sand, Riverine vegetation, Vegetation, Water, Open Savanna at Level 3: unclassified
Classification
Exclude Areas not of Interest

assign class: unclassified with Existence of super objects KNP Boundary (4) <> 1 at Level 10: Not AIO
assign class: with Mean Green < 4 at Level 10: Not AIO
assign class: with Existence of sub objects Not AIO (1) <> 0 at Level 15: Not AIO
assign class: with Existence of sub objects Not AIO (1) <> 0 at Level 20: Not AIO
Classify Level 20: River Sand or Roads
assign class: with OBJECTID: KNP_RIVERS_MAIN >= 0 at Level 20: Drainage line
assign class: unclassified with Mean PAN > 150 at Level 20: No veg
assign class: No veg with Shape index > 2.8 at Level 20: River sand
assign class: River sand with Rel. border to No veg >= 0.2 at Level 20: No veg
assign class: No veg at Level 20: unclassified
Classify Level 15: Geology
assign class: with Membership to Not AIO = 0 at Level 15: Basalt
assign class: Basalt with Thematic object ID: KNP_GEOLOGY = 1 at Level 15: Granite
Classify Level 10: Topography
assign class: with Existence of super objects Granite (1) = 1 at Level 10: Granite
assign class: with Existence of super objects Basalt (1) = 1 at Level 10: Basalt
assign class: Granite with Mean Diff. to neighbors DEM90m (150) < -1 at Level 10: Drainage line
assign class: Basalt with Mean Diff. to neighbors DEM90m (150) < 0 at Level 10: Drainage line
assign class: Basalt, Granite at Level 10: Crest
export vector layers: Crest, Drainage line at Level 10: export object shapes to 5_140400_20060326_Topography
assign class: Drainage line at Level 10: unclassified
Classify Level 10: Landcover
assign class: Crest, unclassified with Mean MIR < 13 at Level 10: Water
assign class: unclassified with Mean PAN > 150 at Level 10: No veg
assign class: No veg with OBJECTID: KNP_RIVERS_MAIN >= 0 at Level 10: River sand
assign class: unclassified with Ratio Red > 0.043 at Level 10: Vegetated sodic patches
assign class: unclassified with Mean NDVI <= 36 at Level 10: Sparse veg
assign class: Sparse veg with Rel. border to No veg >= 0.4 at Level 10: No veg
assign class: Sparse veg with Rel. border to No veg <= 0.2 at Level 10: unclassified Vegetation
assign class: unclassified with Mean NDVI >= 46 at Level 10: Riverine vegetation
assign class: unclassified at Level 10: Savanna
assign class: Crest at Level 10: Savanna
Sodic areas
assign class: No veg, Sparse veg at Level 10: Bare Soil sodic patches
assign class: Bare Soil sodic patches with OBJECTID: KNP_RIVERS_MAIN >= 0 at Level 10: River sand
assign class: Vegetated sodic patches at Level 10: Bare Soil sodic patches
Export Sodic Sites
create polygons: create polygons [base: 1.25 slivers: yes shape: 1]
export vector layers: Bare Soil sodic patches, River sand, Riverine vegetation, Savanna, Water at Level 10: export object shapes to Shingwedzi_SPOT5_137396_20080412_Classification.shp
export vector layers: Bare Soil sodic patches at Level 10: export object shapes to Shingwedzi_SPOT5_137396_20080412_Sodic.shp